DISS. ETH NO. 19508

SPATIAL EFFECTS IN TUNNELLING THROUGH SQUEEZING GROUND

A dissertation submitted to

ETH ZURICH

for the degree of

Doctor of Sciences

presented by

LINARD CANTIENI

MSc ETH Zurich

10.05.1979

citizen of DONAT GR

accepted on the recommendation of

Prof. Dr. Georgios Anagnostou
Prof. Dr. Giovanni Barla
Prof. Dr. Frédéric Pellet

2011

Spatial effects in tunnelling through squeezing ground

Linard Cantieni

Keywords

Squeezing, Tunnelling, Stress history, Stress path, Convergence-confinement, Yielding support, Design, Tunnel analysis, Ground response, Elasto-plastic behaviour, Stress relief, Core extrusion, Variability, Prediction, Fault zone, Gotthard Base Tunnel

Acknowledgments

I am deeply grateful to my supervisor Prof. Dr. Georgios Anagnostou (ETH Zürich) for his important guidance and support throughout this work and for his detailed and constructive comments. I would also like to thank him for giving me the opportunity to work together with him in teaching and consulting.

I am also deeply grateful to Prof. Dr. Giovanni Barla (Politecnico di Torino) and Prof. Dr. Frédéric Pellet (INSA - University of Lyon) for agreeing to be co-examiner of this PhD thesis. Their detailed and constructive comments were of great value.

I acknowledge the AlpTransit Gotthard AG for the high quality data provided from the tunnel advance of the Sedrun Lot of the Gotthard Base Tunnel and for the permission to use the data for this research. In this context, I want especially to thank Heinz Ehrbar, Dr. Peter Guntli, Robert Meier and Tobias Wilmer.

During this work at the ETH Zürich I have collaborated with many colleagues for whom I have great regard, and I wish to extend my warmest thanks to all those who have supported me professionally and privately during my engagement. I offer my cordial thanks for the interesting discussions and the pleasant working atmosphere over the years.

Last but not least, I owe my loving thanks to my wife Annamarie, for her continuous support, encouragement and understanding.

Zurich, March 2011

Linard Cantieni

Summary

The term “squeezing” refers to the phenomenon of large time-dependent deformations that develop when tunnelling through weak rocks. If an attempt is made to stop the deformations with a lining, a so-called ‘‘genuine rock pressure” builds up, which may reach values beyond the structurally manageable range. Often, the only feasible solution in heavily squeezing ground is a tunnel support that is able to deform without becoming damaged, in combination with a certain amount of overexcavation in order to accommodate the deformations.

Although the interaction between the ground and the support is well understood and considerable experience has been built up with different construction methods in recent years, the prediction of ground response to tunnelling under squeezing conditions still remains one of the most demanding tasks in tunnelling, during both design and construction.

The interaction between support systems and the rock when tunnelling under squeezing conditions is normally studied by means of two-dimensional analyses. Part I (of five) shows that the plane strain assumption underlying two-dimensional analyses may lead, under certain conditions, to ground pressure and deformation values that are considerably lower than those produced by stress analyses that take into account spatial effects in the vicinity of the tunnel face. The differences are due to the stress path dependency in the elasto-plastic behaviour of the ground and, more specifically, to the inability of the plane strain model to map the actual radial stress history, which involves a complete radial unloading (and, later, a re-loading) of the tunnel boundary over the unsupported span. This inherent weakness of any plane strain analysis is relevant from the design standpoint, particularly for heavily squeezing conditions that require a yielding support.

Part II investigates an important practical consequence of the Part I results. Specifically, it shows the effects of stress-path dependency on the interaction between yielding supports and squeezing ground. The idea behind yielding supports is that squeezing pressure will decrease by allowing the ground to deform. When estimating the amount of deformation required, one normally considers the characteristic line of the ground, i.e. the relationship between the ground pressure and the radial displacement of the tunnel wall under plane strain conditions. The computation of the characteristic line assumes a monotonic decrease of radial stress at the excavation boundary, while the actual tunnel excavation and subsequent support installation involve a temporary complete radial unloading of the tunnel wall. This difference, in combination with the stress path dependency of the ground behaviour, is responsible for the fact that the results obtained by spatial analysis are not only quantitatively, but also qualitatively different from those obtained by plane strain analysis. More specifically, the relationship between ground pressure and deformation at the final state prevailing far behind the face is not unique, but depends on the support characteristics, because these affect the stress history of the ground surrounding the tunnel. The yield pressure of the support, i.e. its resistance during the deformation phase, therefore proves to be an extremely important parameter. The higher the yield pressure of the support, the lower will be the final ground pressure. A targeted reduction in ground pressure can be achieved not only by installing a support that is able to accommodate a larger deformation (which is a well-known principle), but also by selecting a support that yields at a higher pressure. Part II presents design nomograms, which enable the rapid assessment of yielding supports.

Part III presents a systematic and in-depth study of a paradox of elasto-plastic tunnel analysis which is occasionally mentioned in the literature. The elasto-plastic tunnel analysis may produce a paradox in the calculation of ground pressure whereby ground pressures appear to increase in relation to higher ground quality. More specifically, for an overstressed ground in combination with a stiff support, analysis may indicate greater loading of the support with a ground of high strength than with a ground of low strength (all of the other parameters being equal). This counter-intuitive outcome appears in all of the common calculation models (analytical plane strain analysis, numerical plane strain analysis and numerical axisymmetric analysis), although it does not correspond either to the ground behaviour that is intuitively expected or to ground behaviour observed in the field, thus raising doubts over the predictive power of common tunnel design calculations. Part III discusses the assumptions made in the models that are responsible for the paradox: the assumption that ground behaviour is time-independent (whereas in reality over-stressed ground generally creeps) and the assumption that the support operates with full stiffness close to the face (which is not feasible in reality due to the nature of the construction procedures). When proper account is taken of either or both of these assumptions in more advanced models, the paradox disappears. As the models which generate the paradox are very commonly used in engineering and scientific practice, the investigations of Part III may be of value, helping the engineer to understand the uncertainties inherent in the models and to arrive at a better interpretation of the results they produce.

Part IV shows some of the reasons for the frequently observed variability of squeezing intensity over short distances along the tunnel alignment. The variability of squeezing can be traced back to heterogeneities of the ground at different scales and with respect both to its mechanical and to its hydraulic characteristics. Often the cause of this phenomenon is an advance through a sequence of rock zones with different degrees of crushing or shearing. The results of numerical calculations indicate that even relatively thin competent rock interlayers may have a pronounced stabilizing effect. However, even in a macroscopically homogeneous rock mass, a large variation of deformations may be observed. This can be explained theoretically by the fact that the results of ground response analyses are highly sensitive to minor changes in rock properties.

The variability of squeezing intensity makes tunnelling in squeezing ground very demanding as it decreases the predictability of the ground response even after experience has been built up with a specific geological formation during excavation. Reliable predictions of the ground conditions ahead of the face are thus essential in order to avoid project setbacks. Such predictions would enable adaptations to be made during construction to the temporary support, to the excavation diameter and also to the final lining. The assessment of the behaviour of the core ahead of the face, as observed by means of extrusion measurements, provides some indications as to the mechanical characteristics of the ground. Part V investigates whether it is possible to predict the ground response to tunnelling by assessing the axial extrusion of the core ahead of the face. Part V shows that if the ground exhibits a moderate time-dependent behaviour, a prediction of the convergences is feasible, provided that the interpretation of the core extrusion takes into account the effects of the support measures. If the ground behaviour is pronouncedly time-dependent, however, convergence predictions become very difficult, because the extrusion of the core depends on the short-term characteristics of the ground, which may be different from the long-term properties that govern the final convergences. The case histories of the Gotthard Base Tunnel and of the Vasto tunnel show that there is a weak correlation between the axial extrusions and the convergences of the tunnel. In order to identify potentially weak zones on the basis of extrusion measurements, careful

processing of the monitoring data is essential, in order to take account of the effects of tunnel support and time, and to eliminate errors caused by the monitoring process.

Zusammenfassung

Der Ausdruck „druckhaftes Gebirge“ bezeichnet das Phänomen von grossen, langanhaltenden Gebirgsverformungen, die beim Vortrieb im gering festen und hoch verformbaren Gebirge auftreten. Beim Versuch, die Verformungen mit einem Ausbau zu stoppen, baut sich der sogenannte „echte Gebirgsdruck“ auf diesen auf. Die dadurch entstehenden Gebirgsdrücke können Werte erreichen, welche die technische Machbarkeit solcher Ausbauten überschreiten können. In stark druckhaftem Gebirge besteht die einzige machbare Lösung oft aus einem nachgiebigen Ausbau, welcher sich verformen kann, ohne dabei zerstört zu werden.

Obwohl das Zusammenspiel von Gebirge und Ausbau heute gut erforscht ist und in den letzten Jahren viele Erfahrungen mit verschiedenen Vortriebskonzepten gemacht wurden, ist die Voraussage des Gebirgsverhaltens in druckhaftem Gebirge immer noch eine der anspruchsvollsten Aufgaben des Tunnelbaus – sowohl während der Projektierung als auch während des Baus.

Die Interaktion zwischen Ausbau und Gebirge beim Vortrieb eines Tunnels in druckhaftem Gebirge wird häufig mit Hilfe von Modellen im ebenen Verformungszustand untersucht. Teil I (von fünf) zeigt, dass die Annahme des ebenen Verformungszustandes unter bestimmten Bedingungen zu Gebirgsdrücken und Verformungen führen kann, welche deutlich niedriger sind als jene, die mit räumlichen Spannungsanalysen bestimmt wurden. Der Unterschied besteht in der Spannungspfadabhängigkeit des elasto-plastischen Baugrundverhaltens, beziehungsweise im Unvermögen ebener Modelle die wirkliche Spannungsgeschichte zu reproduzieren. Der Vortrieb mit anschliessender Sicherung des Ausbruchrandes führt zu einer Spannungsgeschichte, welche eine vollständige Entlastung (und eine spätere Wiederbelastung) des Ausbruchrandes über der ungesicherten Länge beinhaltet. Diese inhärente Schwäche aller Modelle im ebenen Verformungszustand ist betreffend des Entwurfs und der Dimensionierung besonders im Fall von stark druckhaftem Gebirge, welches den Einsatz eines nachgiebigen Ausbaus erfordert, relevant.

Teil II behandelt eine wichtige praktische Folge der Ergebnisse von Teil I. Die Interaktion zwischen nachgiebigen Ausbauten und druckhaftem Gebirge wird mittels räumlichen Berechnungen, welche die wirkliche Spannungsgeschichte des Baugrunds während des Vortriebs berücksichtigen, untersucht. Die Idee des nachgiebigen Ausbaus entstand aufgrund der Beobachtung, dass der Gebirgsdruck abnimmt, wenn Verformungen des Gebirges zugelassen werden. Bei der Bestimmung des erforderlichen Mehrausbruchs wird in der Regel die Gebirgskennlinie angewendet. Die Gebirgskennlinie stellt die Beziehung zwischen dem Gebirgsdruck und der radialen Verschiebung des Ausbruchsrandes unter der Annahme des ebenen Verformungszustandes dar. Die Bestimmung der Gebirgskennlinie geht von einem monotonen Abfall der radialen Spannungen am Ausbruchsrand aus. Der wirkliche Vortrieb mit dem anschliessenden Aufbringen der Sicherung beinhaltet jedoch eine vollständige Entlastung des Ausbruchrandes. Dieser Unterschied in Kombination mit dem spannungspfadabhängigen Baugrundverhalten ist dafür verantwortlich, dass die Ergebnisse, die mit räumlichen Modellen ermittelt werden, sich nicht nur quantitativ, sondern auch qualitativ von den Resultaten unterscheiden, die mit ebenen Berechnungen ermittelt werden. Die Beziehung zwischen Gebirgsdruck und Gebirgsverformung im Endzustand weit hinter der Ortsbrust ist nicht eindeutig, sondern hängt auch von der Kennlinie des Ausbaus ab, welche die Spannungsgeschichte des Baugrunds im Bereich des Tunnels beeinflusst. Der Widerstand des nachgiebigen Ausbaus

während der Deformationsphase (die sogenannte Fliessspannung des nachgiebigen Ausbaus) stellt aus diesem Grund einen sehr wichtigen Parameter des Ausbaus dar. Je höher dieser gewählt wird, umso kleiner wird die Endbelastung des Ausbaus. Eine angestrebte Verminderung des Gebirgsdrucks kann demzufolge nicht nur mit einem grösseren Mehrausbruch, sondern auch mit einer höheren Fliessspannung des Ausbaus erreicht werden. Für die Vordimensionierung des nachgiebigen Ausbaus werden in Teil II Nomogramme bereitgestellt.

Teil III untersucht systematisch und ausführlich ein Paradox der elasto-plastischen Tunnelanalyse, welches fallweise in der Literatur zu finden ist. Die Analyse eines Tunnelvortriebs in einem Baugrund mit einem elasto-plastischen Verhalten kann zu paradoxen Resultaten führen, die besagen, dass der Gebirgsdruck im Fall einer höheren Baugrundqualität höher ist, als für eine niedrige Baugrundqualität. Ein überbeanspruchter Baugrund in Kombination mit einem steifen Ausbau führt zu höheren Belastungen des Ausbaus im Falle eines Baugrundes mit einer hohen Festigkeit als im Falle eines Baugrundes mit einer niedrigen Festigkeit (wobei alle anderen Parameter konstant gehalten werden). Dieses Verhalten tritt bei allen gebräuchlichen Berechnungsmodellen (analytische und numerische Lösung unter der Annahme des ebenen Verformungszustandes und numerische Lösung eines axialsymmetrischen Modells) auf, obwohl es sowohl der Intuition wie auch der Erfahrung widerspricht. Ein solches Verhalten lässt an der Zuverlässigkeit der Voraussagen aller gängigen Berechnungsmethoden zweifeln. Teil III diskutiert die Modellannahmen, die für das Paradox verantwortlich sind: Einerseits die Annahme, dass das Baugrundverhalten zeitunabhängig ist (obwohl ein überbeanspruchter Baugrund in Wirklichkeit kriecht) und anderseits die Annahme eines steifen Ausbaus nahe an der Ortsbrust (was in Wirklichkeit wegen des Bauablaufs nicht möglich ist). Wenn eine oder beide dieser Annahmen korrekt mit erweiterten Modellen berücksichtigt werden, verschwindet das Paradox. Da die Modelle, die das Paradox zeigen sowohl in der Tunnelbaupraxis als auch in der Forschung sehr verbreitet sind, sollen die Untersuchungen von Teil III dem Ingenieur beziehungsweise dem Wissenschaftler helfen, die modellinhärenten Unsicherheiten zu verstehen und dadurch zu einer besseren Interpretation der Ergebnisse führen.

Teil IV zeigt einige Gründe für die häufig beobachtete und über kurze Distanzen auftretende Variabilität der Intensität der Druckhaftigkeit entlang der Linienführung eines Tunnels im druckhaften Gebirge. Die Variabilität kann auf die Heterogenität des Baugrundes in verscheiden Massstäben und bezüglich den mechanischen und auch hydraulischen Eigenschaften zurückgeführt werden. Der Grund für dieses Phänomen ist häufig ein Vortrieb durch eine Abfolge von Gebirgsabschnitten von unterschiedlicher Zerscherung und Zerdrückung. Die Ergebnisse von numerischen Berechnungen zeigen, dass schon dünne Zwischenschichten von intaktem Fels einen ausgeprägten Stabilisierungseffekt haben. Jedoch auch im makroskopisch homogenen Fels kann eine grosse Variation der Gebirgsverformungen beobachtet werden. Dies kann theoretisch durch die hohe Sensitivität des Gebirgsverhaltens bezüglich kleiner Änderungen der Gebirgseigenschaften erklärt werden.

Die Variabilität der Intensität der Druckhaftigkeit erschwert die Voraussage des Gebirgsverhaltens, auch wenn schon Erfahrungen mit bestimmten geologischen Verhältnissen während des Vortriebs gemacht wurden. Eine zuverlässige Voraussage der Baugrundverhältnisse vor der Ortsbrust ist unverzichtbar, um Rückschläge vermeiden zu können. Solche Voraussagen ermöglichen es, die Ausbruchsicherung, den Ausbruchsquerschnitt und den Endausbau während des Vortriebs anzupassen. Die Verformungen des Gebirgskerns vor der Ortsbrust, welche mittels Messung der Extrusion des Kerns erfasst werden können, liefern Hinweise auf die mechanischen Eigenschaften des Gebirges. Teil V untersucht, ob es möglich ist, das Gebirgsverhalten mit Hilfe der Messungen der axialen Extrusion des Gebirgskerns vorauszusagen. Es wird gezeigt, dass eine Voraussage der Konvergenzen im Falle von mässig zeitabhängigem Gebirgsverhalten machbar ist, wenn bei der Interpretation der Extrusion die Effekte der Sicherung miteinbezogen werden. Bei einem ausgeprägt zeitabhängigen Gebirgsverhalten gestaltet sich die Voraussage der Konvergenzen jedoch schwieriger: Die kurzfristigen Gebirgseigenschaften, welche die Extrusion bestimmen, können ungleich den langfristigen Eigenschaften sein, welche die Konvergenzen bestimmen. Bei den Fallbeispielen des Gotthard Basistunnels und des Tunnels „Vasto" ist eine schwache Korrelation der axialen Extrusionen und der Konvergenzen zu erkennen. Teil V zeigt weiter, dass eine sorgfältige Auswertung der Messdaten von grosser Bedeutung ist, wenn potentielle Bereiche niedriger Gebirgsqualität vor der Ortsbrust mittels der Extrusionen erkannt werden sollen. Die Auswertung muss die Einflüsse der Ausbruchsicherung und der Zeit berücksichtigen sowie möglich Fehler, welche durch den Messprozess verursacht werden können, eliminieren.

Table of contents

INTRODUCTION

Introduction

The term “squeezing” refers to the phenomenon of large time-dependent deformations that develop when tunnelling through weak rocks. If an attempt is made to stop the deformations with a lining, a so-called ‘‘genuine rock pressure” builds up, which may reach values beyond the structurally manageable range. Often, the only feasible solution in heavily squeezing ground is a tunnel support that is able to deform without becoming damaged, in combination with a certain amount of over-excavation in order to accommodate the deformations.

The interaction between the ground and the support is well understood in principle. In the initial state prevailing before tunnel construction, an equilibrium exists between the core ahead of the tunnel face and the surrounding ground. The ground around the future opening exerts a load upon the core and, vice versa, the core supports the surrounding ground. As the support effect of the core disappears with its excavation, a spatial stress redistribution accompanied by deformations occurs around the working face, and a pressure develops upon the lining, because the latter partially hinders the convergence of the tunnel walls.

Although the interaction between the core and the support is well understood and considerable experience has been built up with different construction methods in recent years, the prediction of ground response to tunnelling under squeezing conditions still remains one of the most demanding tasks in tunnelling, during both design and construction.

Besides the numerous uncertainties caused by the lack of available information in the design stage (in respect of the initial stress field and the material constants of the ground), the constitutive model and the static system represent additional sources of uncertainty. Several computational models in one, two or three spatial dimensions are available today. The one-dimensional ground response in the rotational-symmetric problem of a deep tunnel can be expressed by a closed-form solution of the so-called “ground response curve”. The ground response curve relates the radial displacement of the rock at the excavation boundary to the support pressure. Numerical two-dimensional plane strain models consider a tunnel cross section far behind the face and can be applied for arbitrary geometries and initial conditions. Spatial effects can be handled numerically only with axially symmetric or three-dimensional models, which take into account the sequence of lining installation and excavation works. Due to the high cost of such spatial analyses, however, tunnel design calculations are based, in most cases, upon plane strain models. The present thesis analyses certain spatial effects in tunnelling associated with the advancing tunnel heading and investigates whether and to which extent the uncertainties of the simplified computational models limit the value of their predictions.

One of the main difficulties encountered during the construction of tunnels in squeezing ground is the variability of squeezing intensity, which decreases the predictability of the conditions ahead of the face, even after experience has been acquired with a specific geological formation. Squeezing variability therefore introduces major uncertainties concerning the prediction of the ground response during construction. The thesis discusses some of the reasons for squeezing variability and analyses in-depth the spatial variation in ground response in the specific case of heterogeneous rock structures. Furthermore, the thesis investigates whether it is possible to predict the ground response (including all spatial effects) on the basis of the monitored extrusions of the core ahead of the face. Such prediction would considerably reduce the uncertainties during construction.

The thesis is structured in five parts. Parts I to IV have been published in 4 scientific papers.

Part I (Cantieni and Anagnostou 2009a) shows that the plane strain assumption underlying two-dimensional analyses may lead, under certain conditions, to ground pressure and deformation values that are considerably lower than those produced by stress analyses that take into account spatial effects in the vicinity of the tunnel face. More specifically, the relationship between ground pressure and deformation at the final state prevailing far behind the face is not unique (as we might expect from the plane strain ground response curve), but depends on the support characteristics, as these affect the stress history of the ground surrounding the tunnel. Part I emphasises the influence of the stress path on the deformations and pressures developing in tunnels crossing weak rocks that are prone to squeezing and exhibit important plastic flow. More specifically, it is the purpose of Part I to show, by comparative computations, how greatly the ground response calculated using a more realistic spatial model may deviate from the response predicted through plane strain analyses, to show the limitations and nature of the simplifications involved in even the most sophisticated methods of pre-deformation estimation, and to improve our understanding of the reasons for these deviations.

Part II (Cantieni and Anagnostou 2009b) investigates an important practical consequence of the Part I results. Specifically, it shows the effects of stress-path dependency on the interaction between yielding supports and squeezing ground. Yielding supports which yield under high ground pressures lead to lower final pressures on the shotcrete lining than supports which yield under low ground pressures. Such results cannot be reproduced with plane strain models. This is due to the different stress histories of the stress-path dependent ground during the advance of the face. Part II provides a new insight into the problem of ground-support interaction, and investigates in detail the influence of the main design parameters of the yielding support (yield pressure and deformation capacity). Part II also presents design nomograms which enable a rapid assessment to be made of yielding supports.

Part III (Cantieni and Anagnostou 2010) presents a systematic and in-depth study of a paradox of elasto-plastic tunnel analysis which is occasionally mentioned in the literature. The paradox is that the commonly-used elasto-plastic computational models predict that pressures may increase with better ground quality (the higher the ground strength, the higher the loading will be). This is clearly contrary to the behaviour that might be expected both intuitively and on the basis of tunnelling experience, which is that overstressing of the lining or severe convergences are associated with ground of poor quality. Part III illustrates the paradox by means of results obtained from the application of commonly used computational methods, investigates the conditions under which the paradox occurs and explains why the paradox occurs. It shows that the paradox can be traced back to a combination of large deformations ahead of the face and small deformations of the support system. Even if the reason for the paradox is understood, a question remains as to why such behaviour is not exhibited in nature or, in other words: what are the specific modelling assumptions that lead to the paradoxical model behaviour. Part III discusses possible reasons for the discrepancy between model behaviour and actual behaviour.

Part IV (Cantieni and Anagnostou 2007) shows some of the reasons for the frequently observed variability of squeezing intensity along the tunnel alignment (which can be observed for one and the same excavation method, type of temporary support, depth of cover and lithology). The variability of squeezing can be traced back to heterogeneities of the ground at different scales and with respect both to its mechanical and its hydraulic characteristics. Part IV discusses the sensitivity of ground response to small variations in rock mass properties by means of computational results and with reference to tunnelling experience. Furthermore it deals with the case of a heterogeneous rock mass consisting of alternating weak and hard rock zones.

Part V investigates whether it is possible to predict the ground response to tunnelling by assessing the axial extrusion of the core ahead of the face. Such a prediction would enable adaptations to be made, during construction, to the temporary support, to the excavation diameter and also to the final lining. Part V analyses the behaviour of the core ahead of the face on the basis of extrusion measurements from a number of case histories and by means of numerical computations which consider the effect of the support measures and of the ground properties (such as strength, rheology and heterogeneity). Part V shows that a prediction is very difficult in ground with a pronounced time-dependent behaviour because the extrusion of the core depends on the short-term ground properties, while the final convergences depend on the long-term ground properties. In the light of the results of the numerical computations, Part V discusses the predictability of the convergences by means of case histories.

References

Cantieni, L., Anagnostou, G. 2007. On the variability of squeezing in tunneling. In: Ribeiro e Sousa L, Olalla C, Grossmann NF (eds). 11th Congress of the International Society for Rock Mechanics, Lisbon, pp 983-986.

Cantieni, L., Anagnostou, G. 2009. The effect of the stress path on squeezing behaviour in tunnelling. Rock Mechanics and Rock Engineering 42 (2): 289–318.

Cantieni, L., Anagnostou, G. 2009b. The interaction between yielding supports and squeezing ground. Tunneling and Underground Space Technology 24 (3): 309-322.

Cantieni, L., Anagnostou, G. 2011. On a Paradox of Elasto-Plastic Tunnel Analysis. Rock Mechanics and Rock Engineering 44: 289–318.

PART I

THE EFFECT OF THE STRESS PATH ON SQUEEZING BEHAVIOUR IN TUNNELLING

Abstract: The interplay between support systems and the rock when tunnelling under squeezing conditions is normally studied by means of two-dimensional analyses. The present paper shows that the underlying plane strain assumption involved in a two-dimensional analysis may lead under certain conditions to ground pressure and deformation values that are considerably lower than the ones produced by stress analyses that take into account spatial effects in the vicinity of the tunnel face. The differences are due to the stress path dependency in the elasto-plastic behaviour of the ground and, more specifically, to the inability of the plane strain model to map the actual radial stress history, which involves a complete radial unloading (and, later, a re-loading) of the tunnel boundary over the unsupported span. This inherent weakness of any plane strain analysis is relevant from the design standpoint particularly for heavily squeezing conditions that require a yielding support. For the majority of tunnelling conditions and methods, however, involving as they do completion of a stiff support within a few meters of the face, the errors introduced by the plane strain assumption are not important from a practical point of view.

Notation:

a	Tunnel radius
c	Ground cohesion
d	Lining thickness
$d\lambda_{1,2}$	Plastic multipliers
E	Young's modulus of the ground
E_L	Young's modulus of the lining
e	Unsupported span
f_c	Uniaxial compressive strength
F	Function defined by Eq. (6)
$g_{1,2}$	Plastic potential functions
k	Lining stiffness
m	Material constant defined by Eq. (4)
p	Radial pressure acting upon the lining
p_∞	Final radial pressure acting upon the lining
r	Radial co-ordinate (distance from tunnel axis)
s	Round length in the step-by-step calculations
u	Radial displacement
$\bar{u}$	Radial displacement (unsupported opening)
$\bar{u}_E$	Radial displacement (unsupported opening, elastic ground)
y	Axial co-ordinate (distance behind the tunnel face)
$\delta_{1,2,\ldots}$	Material constants defined by Eq. (4)
ε_{yy}	Axial strain
ε_{rr}	Radial strain
ε_{tt}	Tangential strain
ε_{ry}	Shear strain
$\varepsilon_{\ldots,el}$	Elastic strain
$\varepsilon_{\ldots,pl}$	Plastic strain
$\eta_{1,2,3}$	Material constants defined by Eq. (A32)
η_4	Material constants defined by Eq. (A14)
$\eta_{5,6}$	Material constants defined by Eq. (A29)
κ	Material constant defined by Eq. (4)
ν	Poisson's ratio of the ground
ρ	Radius of plastic zone
ρ'	Radius of the inner part of the plastic zone

ρ_{2D} Radius of plastic zone under plane strain conditions

ρ_{pl} Radius of plastic zone

ρ_{py} Radius of zone yielding in the past

$\bar{\sigma}_{...}$ Transformation of stress $\sigma_{...}$ (Eq. A3)

σ_1 Maximum principal stress

σ_3 Minimum principal stress

σ_a Radial support pressure

σ_o Initial stress

σ_{yy} Axial stress

σ_{rr} Radial stress

σ_{tt} Tangential stress

σ_{ry} Shear stress

$\sigma_{\rho'}$ Radial stress at $r = \rho'$

ϕ Angle of internal friction of the ground

Φ Function defined by Eq. (12)

ψ Dilatancy angle of the ground

1 Introduction

The interaction between the ground and the tunnel lining is well understood in principle (cf. Lombardi 1971 & 1981, Panet & Guellec 1974). In the initial state prevailing before tunnel construction, an equilibrium exists between the core ahead of the tunnel face and the surrounding ground. The ground around the future opening exerts a load upon the core and, vice versa, the core supports the surrounding ground. As the support effect of the core disappears with its excavation, a spatial stress redistribution accompanied by deformations occurs around the working face, and a pressure develops upon the lining, because the latter partially hinders the convergence of the tunnel walls. The magnitude of the loading depends on the magnitude of the deformations constrained by the lining (i.e. on the magnitude of the deformations that would occur in the absence of a lining) and thus on the distance between the working face and the location of the lining installation (*e* in Fig. 1a). The smaller this distance, the higher will be the load that develops with the progress of excavation. Furthermore, as in any statically undetermined system, the magnitude of the ground pressure depends on the load-deformation characteristics both of the lining and of the ground.

The deformations and rock pressures can be estimated by means of three-dimensional numerical models that take into account the sequence of lining installation and excavation works. Due to the high cost of such three-dimensional analyses, however, tunnel design calculations are based in most cases upon plane strain models that consider a tunnel cross section. The principle of such two-dimensional calculations can be illustrated best by considering the axisymmetric case of a

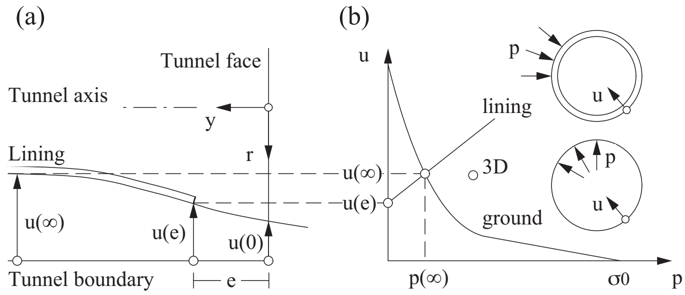

Fig. 1 (a) Radial displacement of the tunnel wall; (b) Characteristic lines of the ground and of the lining

deep cylindrical tunnel. Figure 1b shows the characteristic lines of the ground and of the lining. The characteristic line of the rock (the so-called "ground response curve") relates the radial displacement of the rock at the excavation boundary to the support pressure, while the characteristic line of the lining relates the radial displacement of the lining to the pressure exerted by the rock. The intersection point of the two lines (the “ground response point”) fulfils the conditions of equilibrium and compatibility, and shows the radial pressure *p(∞)* acting upon the lining far behind the face and the respective radial displacement *u(∞)* of the ground at the excavation boundary $r = a$. For determining the intersection point, an *a priori* assumption must be made concerning the ground displacement *u(e)* that occurs before the lining is installed (“pre-deformation”). Note that small variations in the assumed pre-deformation *u(e)* may lead to large variations in rock pressure, particularly in the case of a highly non-linear ground response. This sensitivity has prompted considerable research aimed at finding methods for estimating pre-deformation without needing to carry out costly spatial numerical analyses. Research efforts in the nineties were focused mainly to the axisymmetric problem of a cylindrical tunnel (Corbetta 1990, Bernaud 1991, Bernaud and Rousset 1996, Nguyen-Minh and Corbetta 1992, Nguyen-Minh and Guo 1993, 1996, Guo 1995, Panet 1995, AFTES 2002), while recent papers have examined the influence of the tunnel shape and of the anisotropy or heterogeneity of the initial stress field (Carranza-Torres and Fairhurst 2000, González-Nicieza *et al.* 2008).

The problem is, however, more fundamental than estimating the magnitude of pre-deformation: for geomaterials with path-dependent mechanical behaviour, the existence of a single “ground response curve” is in itself questionable, as the response of the ground depends on its stress history and, in the case of time-dependent processes such as creep (Kaiser 1980) or consolidation (Anagnostou 2007a), on the excavation advance rate as well. The method involving characteristic lines may nevertheless oversimplify reality even in the absence of time-dependency. So, for example, Amberg (1999) has remarked (on the basis of the results of design calculations for the Gotthard Base Tunnel) that three-dimensional simulations of tunnel excavation may lead both to higher ground pressures and to higher deformations than those predicted by plane strain calculations (i.e. to ground response points which are located above the ground response curve, e.g. point “3D” in Fig. 1b). Also Bliem (2001) recognized that for a given amount of pre-deformation the final lining pressure obtained by a spatial calculation may be higher than the value obtained by considering the ground response curve. Furthermore, the numerical results presented by Barla (2000, 2001) show a significant difference between the stresses predicted by two- and three-dimensional models, with a clear influence on the stress path experienced by the ground surrounding the tunnel.

The role of stress path has been examined in recent years also in the context of tunnelling or mining through hard brittle rocks (Pelli *et al.* 1995, Martin *et al.* 1999, Cai *et al.* 2002, Diederichs *et al.* 2004). So, for example, Eberhardt (2001) presented the results of a three-dimensional numerical study on the rotation of the principal stress axes in the vicinity of the tunnel face and on its effect on the direction of fracture propagation.

In the present paper, emphasis is placed on the influence of the stress path on the deformations and ground pressures developing in tunnels crossing weak rocks that are prone to squeezing and exhibit important plastic flow. More specifically, it is the purpose of this paper to show by comparative computations how greatly the ground response calculated using a more realistic spatial model may deviate from the response predicted through plane strain analyses (Section 3), to show the limitations and the nature of the simplifications involved even in the most sophisticated methods of pre-deformation estimation (Section 4) and to improve our understanding of the reasons for these deviations (Section 5).

The present investigation concerns only the effect of the computational domain (plane vs. spatial system). It should be noted, however, that the stress history of the ground and its response to tunnelling may be influenced also by time-effects. The latter are pronounced particularly when the ground becomes overstressed and are therefore important for squeezing behaviour. This aspect is not dealt-with by the present paper.

2 Problem layout and solution method

2.1 Problem layout

For the sake of simplicity and without compromising its general applicability, the comparative analyses of the present paper refer to a deep, cylindrical and uniformly supported tunnel that crosses a homogeneous and isotropic ground. The initial stress field is assumed to be uniform and hydrostatic. The mechanical behaviour of the ground is modelled as isotropic, linearly elastic and perfectly plastic according to the Mohr-Coulomb yield criterion with a non-associated flow rule.

The lining is modelled as an elastic radial support with stiffness $k = dp/du$, where p and u denote the radial loading and the radial displacement of the lining, respectively. The radial stiffness k of a ring-shaped lining is equal to $E_L d/a^2$, where a, d and E_L denote its radius, thickness and Young's modulus, respectively. The longitudinal bending stiffness of the lining will not be taken into account. (This effect is however of subordinate importance.) Lining installation occurs at a distance e behind the tunnel face (Fig. 1a).

Under the assumptions made above, the problem obeys rotational symmetry with respect to the tunnel axis y (Fig. 1a). The plane strain assumption leads to a one-dimensional problem for which a closed form solutions exist (Section 2.2), while the three-dimensional problem of the advancing tunnel heading reduces then to a two-dimensional axisymmetric problem that is solved numerically by the finite element method (Section 2.3).

2.2 Plane strain problem

According to the closed-form solutions presented by, e.g., Anagnostou and Kovári (1993), the displacements in the elastic range, i.e. if

$$\frac{\bar{p}}{\bar{\sigma}_0} \geq \frac{2}{m+1} \ , \tag{1}$$

are given by the following equation,

$$u(p) = \frac{a\bar{\sigma}_0}{E}(1+\nu)\left(1-\frac{\bar{p}}{\bar{\sigma}_0}\right), \tag{2}$$

while in the elasto-plastic range

$$u(p) = \frac{a\bar{\sigma}_0}{E}\left(\delta_1 + \delta_2\frac{\bar{p}}{\bar{\sigma}_0} + \delta_3\left(\frac{\bar{p}}{\bar{\sigma}_0}\right)^{-\delta_4}\right), \tag{3}$$

where

$$\begin{aligned} &\bar{p} = p + \frac{f_c}{m-1}, \quad \bar{\sigma}_0 = \sigma_0 + \frac{f_c}{m-1}, \quad m = \frac{1+\sin\phi}{1-\sin\phi}, \quad \kappa = \frac{1+\sin\psi}{1-\sin\psi}, \\ &\delta_1 = -(1-2\nu)(1+\nu), \quad \delta_2 = (1+\nu)\frac{(1-\nu)(1+m\kappa)-\nu(m+\kappa)}{m+\kappa}, \\ &\delta_3 = \frac{2(1-\nu^2)(m-1)}{m+k}\left(\frac{2}{m+1}\right)^{\delta_4}, \quad \delta_4 = \frac{\kappa+1}{m-1}. \end{aligned} \tag{4}$$

These equations assume that plastic flow takes place only in the plane of the tunnel cross section. According to the adopted Coulomb yield criterion, this is true only if the secondary axial stress is the strict intermediate principal stress. The effect of the axial stress on the deformation fields around a cylindrical cavity in a brittle Coulomb material has been investigated analytically by Nguyen-Minh and Berest (1979) and Reed (1988). Here attention is paid to the special case of a perfectly plastic material. The closed-form solution for the stress field and the ground response curve is given in the Appendix. According to this analysis, when the support pressure is low and the initial stress high, out-of-plane plastic strains develop as both the axial stress and the tangential stress fulfil the yield condition (so-called "edge flow"). The error introduced by neglecting the out-of-plane plastic strains may be considerable for materials exhibiting softening behaviour (Reed 1988) but, as shown below, is negligible for perfectly plastic materials.

Figure 2a shows ground response curves for an example with parameter values according to Table 1 (with c = 500 kPa). The dashed curve is based upon Eq. (3), which does not take into account the out-of-plane plastic flow, while the solid line has been calculated by the closed-form solution derived in the Appendix (Eq. A31). The marked points have been obtained numerically by the finite element method. (In the numerical calculations, edge flow is taken into account based upon the classical method of Koiter 1953.) The error caused by neglecting the out-of-plane strains is in this example negligible. In the theoretical case of ν = 0, the error is larger but still small (Figure 2b). The numerical solutions agree well with the analytical ones. Figure 3 provides a more complete picture. The diagram shows the error over the normalized support pressure for a friction angle ϕ = 15 or

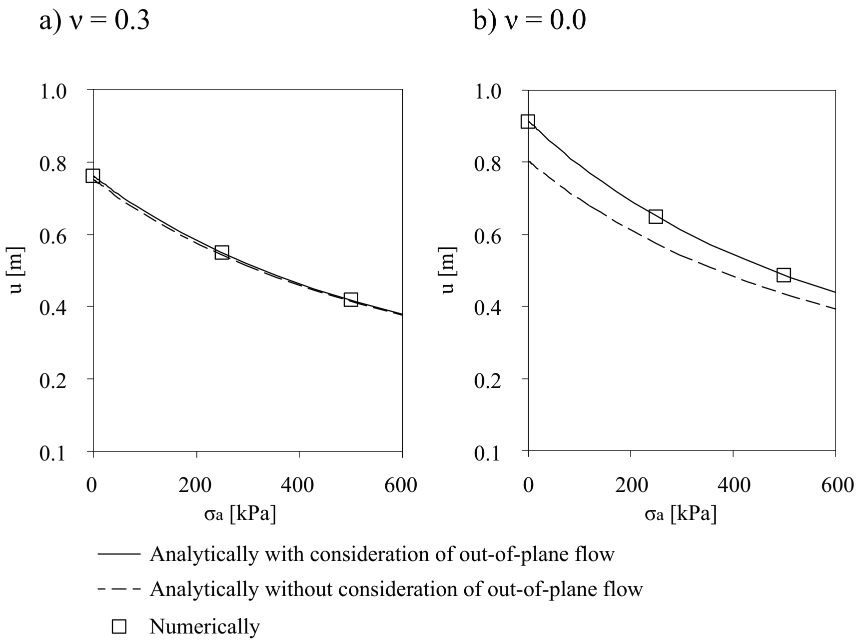

Fig. 2 Ground response curve with/without consideration of out-of-plane plastic flow (solid/dashed curve) as well as numerically obtained results (marked points): (a) Poisson's ratio ν = 0.30, (b) Poisson's ratio ν = 0.0 (c = 500 kPa, other parameters: see Table 1)

35°, the common range of Poisson's ratio (ν = 0.15 - 0.35) and the two borderline cases of the flow rule (ψ = 0° or ϕ). As can be seen from Figure 3, neglecting the plastic flow in the axial direction leads in general to an underestimation of the radial boundary displacement by a few per cent.

Table 1: Assumed model parameters

Parameter		Value
Initial stress	σ_0	12.5 MPa
Tunnel radius	a	4 m
Lining stiffness	k	variable
Unsupported span	e	variable
Young's Modulus (Ground)	E	1000 MPa
Poisson's ratio (Ground)	ν	0.3
Angle of internal friction (Ground)	φ	25°
Cohesion (Ground)	c	500 or 2000 kPa
Dilatancy angle (Ground)	ψ	5°

2.3 Axisymmetric problem

The numerical solution of the axisymmetric problem is usually based upon a simulation of the excavation and support installation that models the advancing tunnel heading step-by-step (cf., e.g., Franzius and Potts 2005). Since large stress- and deformation-gradients prevail in the vicinity of

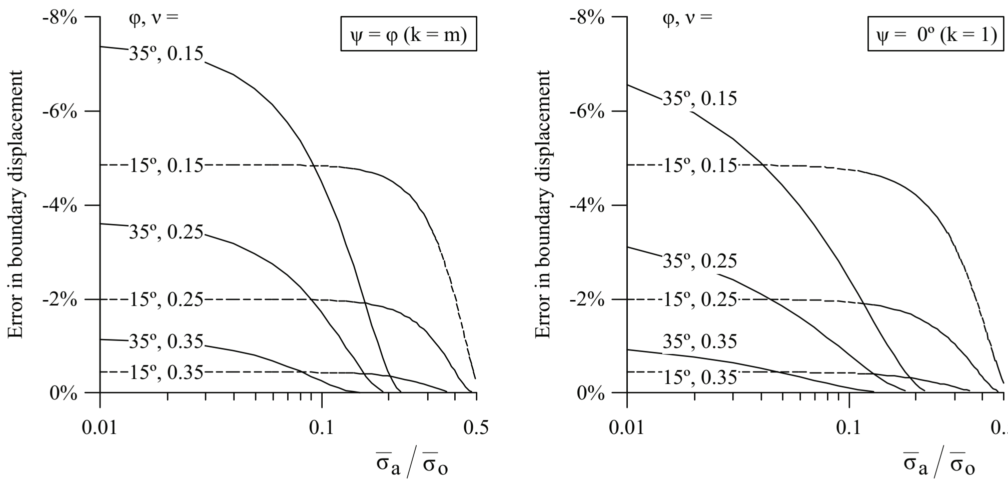

Fig. 3 Error caused by not considering the out-of-plane plastic flow

the tunnel face and the latter moves during the step-by-step simulation, either the finite element mesh has to be fine everywhere along the tunnel axis or adaptive re-meshing must be carried-out for each excavation step. Such an analysis is, therefore, very time-consuming even in the case of linear material behaviour.

The present problem, however, belongs to the large category of problems with constant conditions in the tunnelling direction (the stress- and deformation fields are steady with respect to the tunnel heading, i.e. they "advance" together with the face in the direction of excavation) and it is solved here by means of a single computational step. The basic principle behind this so-called "one-step solution method" can be traced back to the work of Nguyen-Quoc and Rahimian (1981) on steady crack propagation in elasto-plastic media, and it is that the time-coordinate can be eliminated from the equations governing the steady state by re-formulating the equations in a frame of reference that is fixed to the advancing heading. In such an approach, the co-ordinate *y* in the tunnelling direction (Fig. 1a) undertakes the role of the time-dimension in the integration of the elasto-plastic constitutive equations. Corbetta (1990) applied this method for the analysis of advancing tunnels in elasto-plastic and viscoplastic media (cf. also Corbetta and Nguyen-Minh 1992), while Anagnostou (2007a) proposed a generalization of the one-step solution method for coupled problems involving seepage flow and consolidation processes. Details concerning the calculation of the internal forces of the support elements (under consideration of the pre-deformations of the ground) can be found in Anagnostou (2007b).

Figures 4 and 5 compare numerical results obtained by the one-step solution method with the results of step-by-step computations. A sequential excavation and support installation procedure is determined by the following two geometrical parameters: the round length *s* and the minimum distance *e* between the leading edge of the support and the tunnel face (Fig. 4a). In the step-by-step method, the excavation and support cycles are simulated by activating support elements and deactivating ground elements stepwise over successive round lengths *s*. Each excavation round causes a stress re-distribution in the longitudinal direction and an additional load increment upon the installed support elements. The anterior parts of the support elements are more affected by the excavation of the core, because the effect of each excavation round decreases with the distance from the face. This leads to a saw-shaped distribution of the ground pressure and deformation

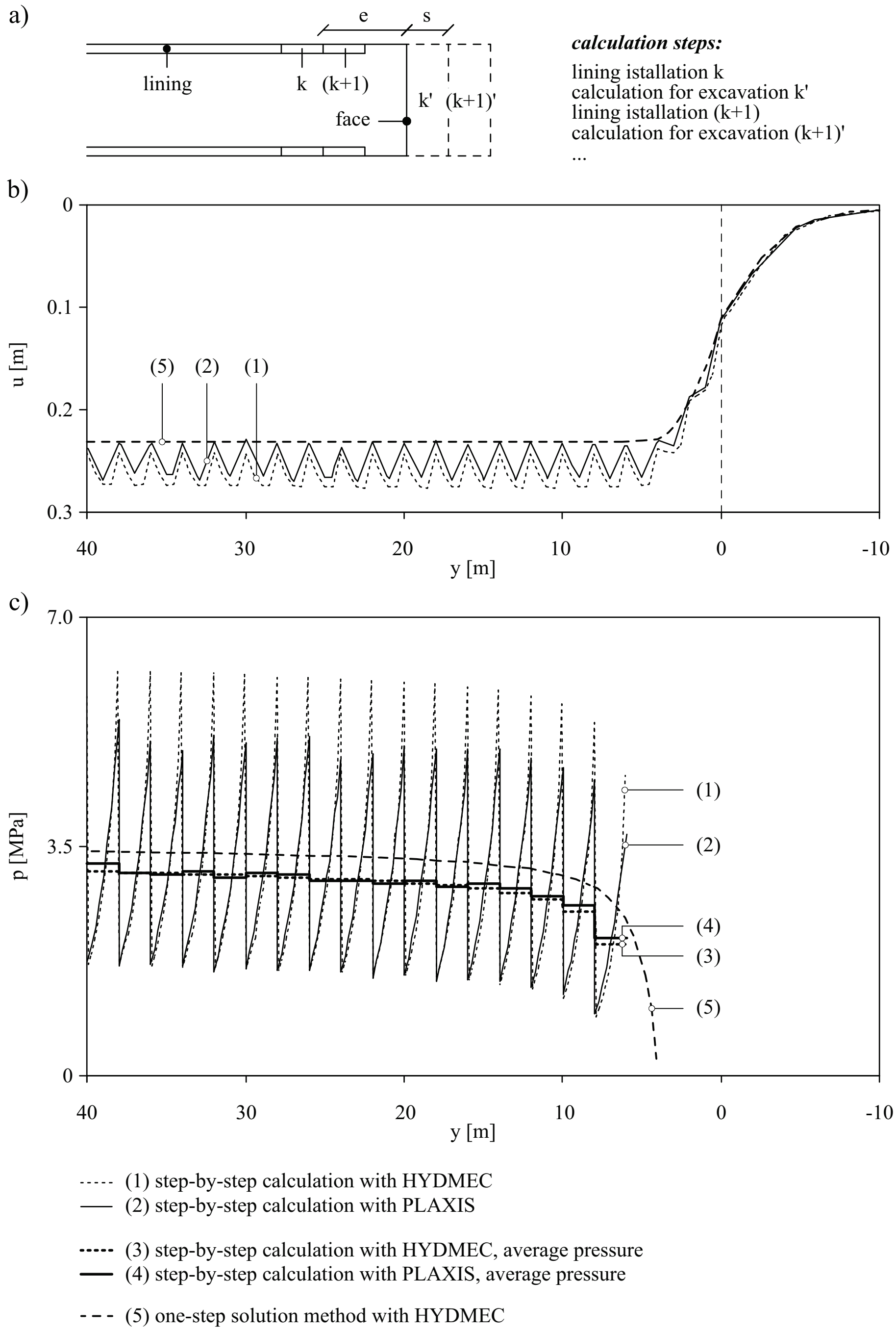

Fig. 4 (a) Calculation sequence in the step-by-step method; (b) radial displacement of the tunnel boundary; (c) distribution of the pressure acting upon the lining

along the tunnel wall. The lines 1 and 2 in Figure 4 have been obtained by means of step-by-step simulations performed by the finite element code HYDMEC of the ETH Zurich (Anagnostou 1992) and the commercial geotechnical finite element package PLAXIS (Brinkgreve 2002), respectively. The parameters of the numerical example are: round length s = 2 m, unsupported span e = 4 m, cohesion c = 500 kPa, lining thickness d = 50 cm, Young's modulus of the lining E_L = 30 GPa (see Table 1 for the other parameters). The lining was modelled as an elastic radial support with (PLAXIS simulation) or without (HYDMEC simulation) longitudinal bending stiffness. The saw-shaped distribution is typical for step-by-step simulations (cf., e.g., Bonnier *et al.* 2002 and Graziani *et al.* 2005) and, as can be seen from Figure 4, occurs even if taking into account the bending stiffness of the support. Furthermore, the comparison of Lines 1 and 2 in Figure 4 shows that the simplification introduced by neglecting the longitudinal bending stiffness of the lining is not decisive for the investigation of the final lining pressures and convergences.

The lines 5 in Figure 4 show the respective numerical results of the one-step solution method implemented in the finite element code HYDMEC. The distribution of the pressures and deformations along the tunnel is smooth because the round length does not represent a parameter in this method. In fact, the one-step solution method refers to the borderline case of a zero round length *s*. The length of the unsupported span is thus continuously equal to *e*, while in the step-by-step simulations it varies between *e* and *e+s* (Fig. 4a). Due to the shorter unsupported span, the one-step solution method leads to slightly lower ground deformations and slightly higher ground pressures. (For the comparison of the pressures, the numerical results of the step-by-step simulations have been averaged over each lining segment; see Lines 3 and 4 in Figure 4c.)

For the validation of the implementation of the one-step solution method into the finite element code HYDMEC, a series of step-by-step simulations has been carried-out with different values of the round length *s*. The lines marked by white symbols in Figure 5 show the influence of the round length *s* on the final lining pressure *p* and ground deformation *u* (average values and variation over the lining segment). One recognizes that the results of the step-by-step calculations approach the values obtained by the one-step solution method (black markers) with decreasing round length. The one-step solution method corresponds thus to the limiting case of a step-by-step model with zero round length.

3 Deviation from the plane strain response

In this section, the results of plane strain analyses will be compared to those of spatial analyses that take into account the advance of the tunnel heading. The analysis refers to a 500 m deep tunnel that has a radius a = 4 m. Table 1 summarizes the parameters of the model. The material constants (particularly, the low dilatancy angle) are typical for the weak kakiritic rocks from the Gotthard Base Tunnel (Vogelhuber *et al.* 2004). Concerning the shear strength of the ground, two cohesion values have been considered. The higher value (c = 2000 kPa) applies to a moderately squeezing ground, the lower (c = 500 kPa) to a heavily squeezing ground.

Typical linings have a stiffness k in the range 0.1 - 1 GPa/m. The calculations have been carried out for a wider range of stiffness values (0.01 - 100 GPa/m) in order to gain a complete picture of model behaviour. Furthermore, unsupported spans e of up to 16 m have been considered. The larger values for an unsupported span take into account in a simplified way the case of a yielding support that allows the occurrence of a free radial convergence ($u(0)$-$u(e)$ in Fig. 1a) and starts to exert a pressure at a distance $y = e$ behind the tunnel face.

Figure 6b shows the ground response curve (the solid line marked by "GRC") obtained by a closed-form, plane strain solution, as well as the results of the numerical calculations for the case

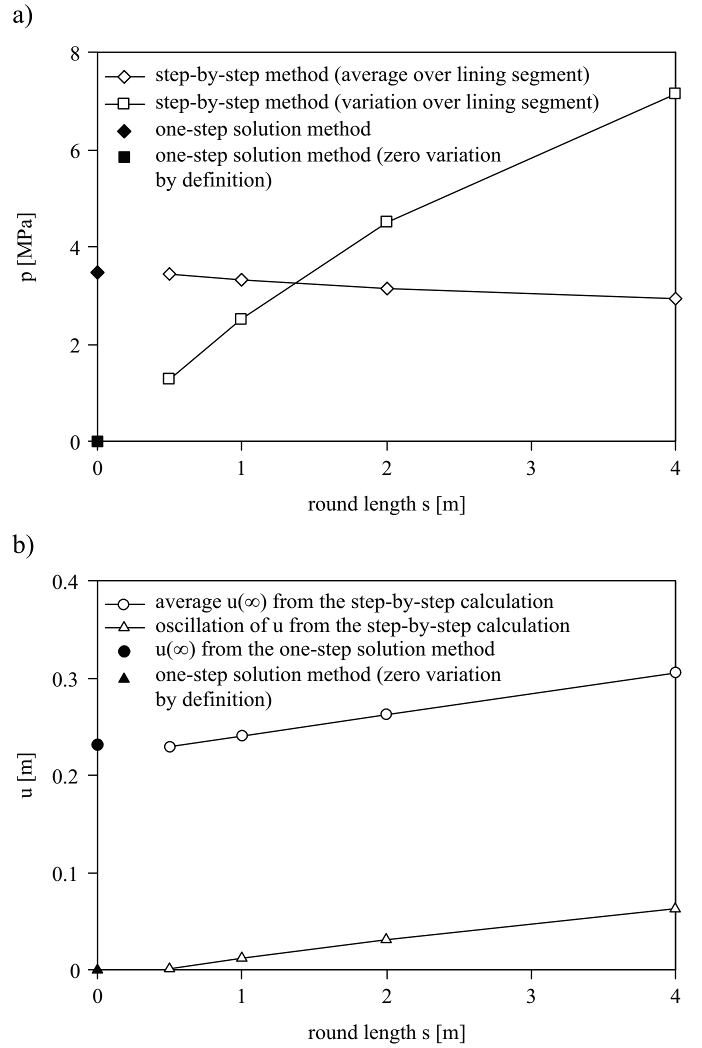

Fig. 5 Results of the step-by-step method as a function of round length *s* and results of the one-step solution method (plotted at *s* = 0)

of heavily squeezing ground (points marked by circles, e.g. $A_{1,2,3,...}$; see also Table 2). The numerical results show that the ground response deviates considerably from the plane strain curve (*GRC*). The stiffer the lining and the longer the unsupported span *e*, the more pronounced will be the difference. Plane strain analysis systematically underestimates ground pressures and deformations. The same observation, but to a lesser degree, can be made for the case of a moderately squeezing ground (Fig. 7b). The underestimation of ground pressures and deformations by the plane strain model is typical for elasto-plastic ground behaviour. For elastic behaviour of course there is no difference between the plane and the spatial model.

A plane strain analysis is adequate under the following conditions:

(i) It must lead to ground response points $(p(\infty), u(\infty))$ that are close to the ones obtained when taking into account the evolution of stress and deformation in the vicinity of the working face;

(ii) A practicable way exists to estimate the pre-deformations of the ground, i.e. the deformations that take place up to the installation of the support. As can be seen from Figures 6b and 7b, the

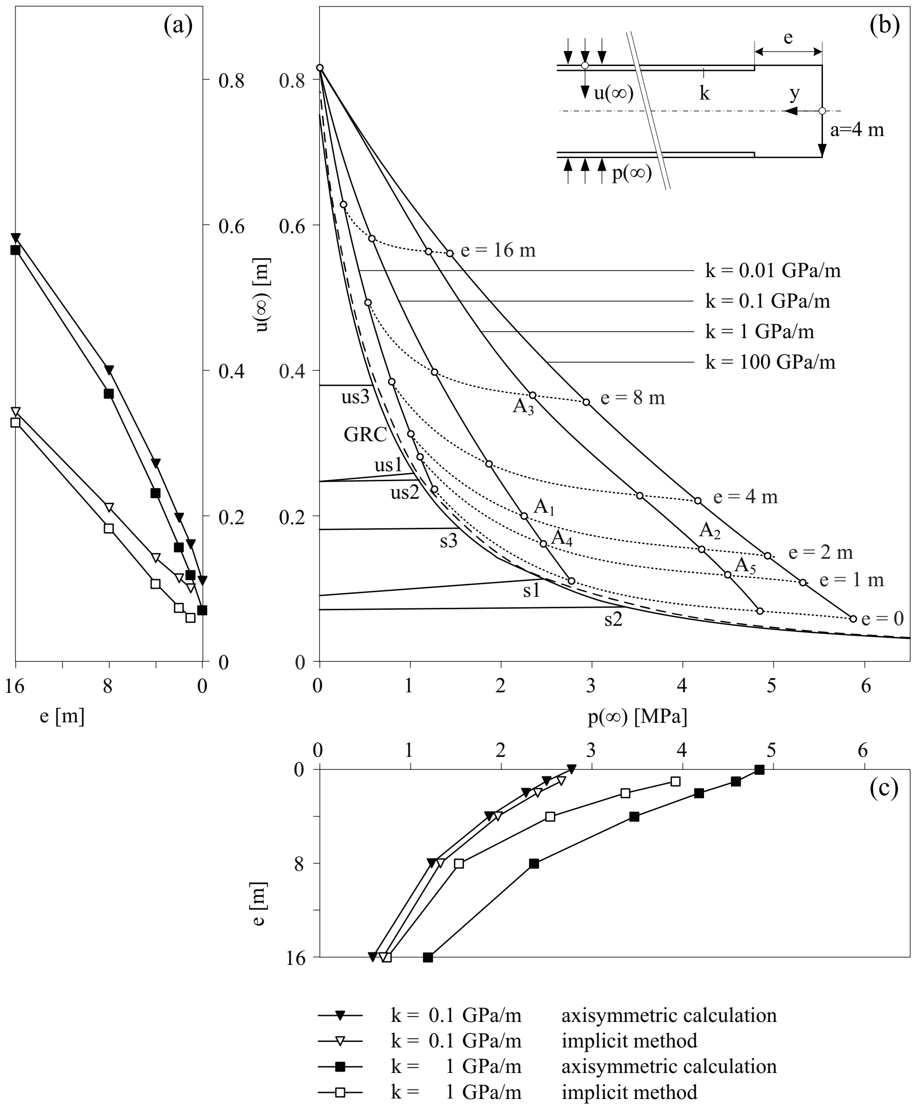

Fig. 6 Heavily squeezing ground. (a) Radial displacement *u(∞)* of the ground far behind the face as a function of the unsupported span *e*; (b) Ground response curve under plane strain conditions (GRC), ground response curve under axisymmetric conditions for the case of a uniform suppport pressure acting along the excavation boundary (dashed curve next to the GRC), ground response points ($A_{1,2,3,...}$; cf. Table 2) far behind the tunnel face (at *y/a = 75*) for different unsupported spans *e* and lining stiffnesses *k*, characteristic lines of support (*us1, us2, us3, s1, s2, s3*; cf. Table 2); (c) Radial pressure *p(∞)* acting upon the lining far behind the face as a function of the unsupported span *e*

first condition is fulfilled in the case of a lower stiffness lining (low *k*-values) or a lining installation close to the face (small *e*-values).

With respect to the second condition, the ground pressure and deformation values obtained by the convergence – confinement method will be examined next.

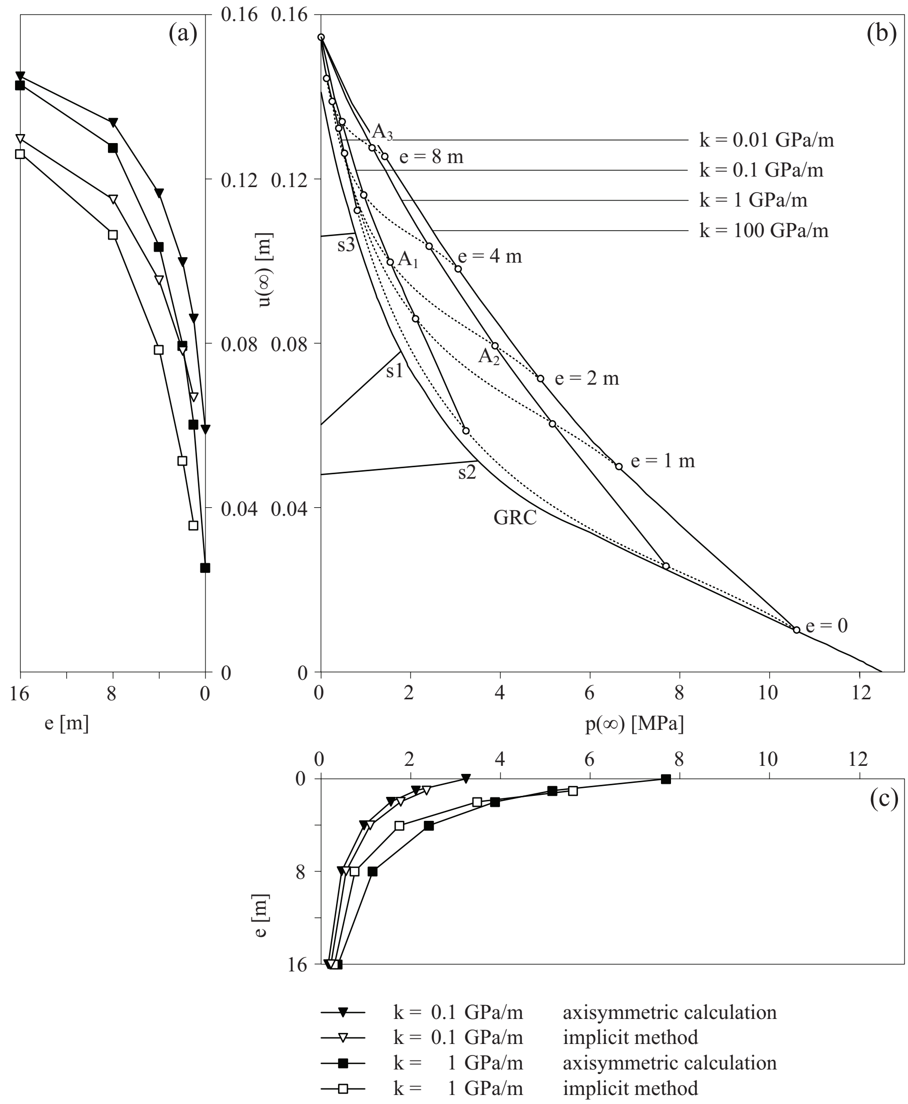

Fig. 7 Moderately squeezing ground. (a) Radial displacement $u(\infty)$ of the ground far behind the face as a function of the unsupported span e; (b) Ground response curve under plane strain conditions (GRC), ground response points ($A_{1,2,3,\ldots}$; cf. Table 2) far behind the tunnel face (at $y/a = 75$) for different unsupported spans e and lining stiffnesses k, characteristic lines of support ($s1$, $s2$, $s3$; cf. Table 2); (c) Radial pressure $p(\infty)$ acting upon the lining far behind the face as a function of the unsupported span e

Table 2 Parameters for support and ground response points in Figures 6 and 7

Line or point	*k* [GPa/m]	*e* [m]	Estimation of pre-deformation
us1	0.1	2	Based upon unsupported opening (Eq. 10)
us2	1	2	"
us3	1	8	"
s1	0.1	2	Implicit method (Eq. 13 and 14)
s2	1	2	"
s3	1	8	"
A_1	0.1	2	Not applicable (result of axisymmetric analysis)
A_2	1	2	"
A_3	1	8	"
A_4	0.1	1	"
A_5	1	1	"

4 Limitations of the convergence – confinement method

The estimation of pre-deformation, which is of paramount importance for any plane strain model, starts by considering the development of the radial displacement $\overline{u}_E(y)$ along the excavation boundary (*y > 0, r = a*) of an *unsupported* tunnel crossing a linearly *elastic* ground:

$$\overline{u}_E(y) = \overline{u}_E(\infty)\, F\left(\frac{y}{a}\right), \tag{5}$$

where $\overline{u}_E(\infty)$ denotes the final radial displacement far behind the face (given by Eq. 2 with *p* = 0), while the function *F* is defined as follows (AFTES 2002):

$$F(t) := 1 - 0.75\left(\frac{0.75}{0.75+t}\right)^2 \tag{6}$$

or, according to Corbetta (1990),

$$F(t) := 0.29 + 0.71\left(1 - \exp\left(-1.5t^{0.7}\right)\right). \tag{7}$$

As both expressions lead to similar results, Eq. (6) will be used in the comparative calculations of the present paper. Following Corbetta (1990) the development of convergence $\overline{u}(y)$ for the case of *elasto-plastic* ground can be obtained approximately by applying a so-called homothetic transformation to the elastic convergence $\overline{u}_E(y)$ (Fig. 8):

$$\frac{OP}{OE} = \frac{\overline{u}(\infty)}{\overline{u}_E(\infty)} = \text{constant}, \tag{8}$$

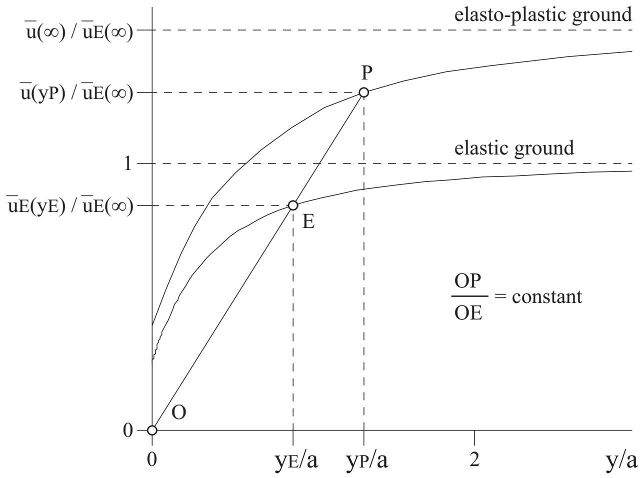

Fig. 8 Development of radial displacement along the excavation boundary of an unsupported tunnel crossing an elasto-plastic ground according to Nguyen-Minh and Guo (1996)

where $\overline{u}(\infty)$ denotes the final elasto-plastic convergence of an unsupported tunnel (given by Eq. 3 with p = 0). It follows from Eqs. (2), (3) and (8) that the so-called similitude ratio $\overline{u}(\infty)/\overline{u}_E(\infty)$ depends on the initial stress σ_0, on the Poisson's ratio ν and on the plasticity constants c, ϕ and ψ. From Figure 8 it follows that:

$$\overline{u}(y_P) = \frac{\overline{u}(\infty)}{\overline{u}_E(\infty)} \overline{u}_E(y_E) \ ; \quad y_E = \frac{\overline{u}_E(\infty)}{\overline{u}(\infty)} y_P \quad . \tag{9}$$

Eqs. (5) and (9) yield with $y_P = e$ the convergence at the point of support installation:

$$\overline{u}(e) = \overline{u}(\infty)\, F\left(\frac{\overline{u}_E(\infty)}{\overline{u}(\infty)} \frac{e}{a} \right) . \tag{10}$$

Eq. (10) offers the simplest way of estimating pre-deformation, but at the same time it leads, as pointed out by AFTES (2002), to a serious underestimation of ground pressure. This can be illustrated by comparing the numerical results of Figure 6b with the results obtained by the convergence – confinement method. The straight lines *us1, us2* and *us3* are the characteristic lines for three linings with different stiffnesses k and an unsupported span e (Table 2). Line *us1* applies to a rather soft lining (k = 0.1 GPa/m, i.e. a 15 cm thick ring with a Young's modulus of only 10 GPa) installed at e = 2 m behind the face. The intersection point of the line *us1* with the ground response curve gives the ground pressure and deformation according to the convergence-confinement method. It is lower - by a factor of 2 - than the pressure obtained by the axisymmetric analysis (point A_1). Lines *us2* and *us3* apply to a higher lining stiffness (k = 1 GPa/m, i.e. a 50 cm thick ring with a Young's modulus of 30 GPa) and an unsupported span e of 2 m or 8 m, respectively. Points A_2 and A_3 mark the respective results of the axisymmetric analysis. Here, the convergence-confinement method underestimates the pressure by a factor of about 4.

As Eq. (10) is based upon the development of convergence along an *unsupported* opening while a stiff lining reduces not only the final convergence but the pre-deformations as well, the underestimation of pressure by the convergence-confinement method has been attributed to the overestimation of pre-deformation (cf., e.g. AFTES 2002). We see, however, from Figure 6b that the deformations are actually only slightly overestimated. The fact that all of the ground response points

$A_{1,2,3,...}$ are located above the plane strain ground response curve shows that the problem is more fundamental: a plane strain analysis cannot reproduce both the deformations and the pressures. In order to determine the ground pressure through a plane strain analysis, the pre-deformations have to be underestimated.

A more advanced, so-called implicit method (Guo 1995, Nguyen-Minh and Guo 1996) attempts to resolve this problem basically by applying a reduction factor Φ to the "unsupported" pre-deformation $\bar{u}(e)$:

$$u(e) = \Phi\left(\frac{u(\infty)}{\bar{u}(\infty)}\right)\bar{u}(e) \ , \tag{11}$$

where $u(e)$ and $u(\infty)$ denote the pre-deformation and final convergence of the supported opening, respectively, while the function Φ is defined as follows:

$$\Phi(t) := 0.55 + 0.45t - 0.42(1-t)^3 \ . \tag{12}$$

Eqs. (10) and (12) lead to the following expression for the pre-deformation:

$$u(e) = \bar{u}(\infty)\, F\left(\frac{\bar{u}_E(\infty)}{\bar{u}(\infty)}\frac{e}{a}\right)\Phi\left(\frac{u(\infty)}{\bar{u}(\infty)}\right) \ . \tag{13}$$

According to Eq. (13), the pre-deformation $u(e)$ depends on the final displacement $u(\infty)$ and thus (cf. Eq. 2) on the unknown final support pressure $p(\infty)$ as well. The latter is, however, related to the deformation of the support:

$$p(\infty) = k\ (u(\infty) - u(e)) \ . \tag{14}$$

Eqs. (13) and (14) form a system for the support pressure $p(\infty)$ and the pre-deformation $u(e)$. By inserting $u(e)$ from Eq. (13) into Eq. (14) we obtain a non-linear equation for the support pressure $p(\infty)$, which can easily be solved using Newton's iteration method.

The pre-deformations underlying the characteristic lines of support *s1*, *s2* and *s3* in Figure 6b have been calculated in this way. Line *s1* applies to a soft lining (k = 0.1 GPa/m) installed at e = 2 m behind the face. The intersection point of the characteristic line *s1* with the ground response curve is located below the respective ground response point A_1, i.e. it shows a practically equal ground pressure but underestimates the radial displacement. At a higher lining stiffness (lines *s2* and *s3*), both the ground pressure and the pre-deformation are underestimated considerably (by 1 MPa and 15-20 cm, respectively, compare with points A_2 and A_3). In order to achieve a better agreement with the numerically obtained ground pressure value, an even smaller and unrealistic pre-deformation must be assumed. Note that, due to the large dp/du - gradient of the plane strain ground response curve in the relevant pressure range, small variations in the assumed pre-deformation lead to significant variations in the ground pressure.

Figures 6a and 6c provide a more complete picture of the differences between the results of the convergence-confinement method and the axisymmetric analyses. The diagrams show the ground pressure p and the ground displacement u, respectively, as a function of the length e of unsupported span for two values of lining stiffness: a soft lining (k = 0.1 GPa/m, e.g. a 15 cm thick ring with a Young's modulus of only 10 GPa) and a rather stiff lining (k = 1 GPa/m, e.g. a 50 cm thick ring with a Young's modulus of 30 GPa). According to Figure 6c, the ground pressures predicted by the implicit method for the soft lining agree well with the numerical results for all *e* – values, while the deformations are underestimated by a factor of 1.5 to 2, particularly for long unsupported spans (Fig. 6a). For the stiff lining, however, the pressures are underestimated considerably (up to 1 MPa). A similar trend can be observed also for the moderately squeezing ground (Fig. 7). It is, however, remarkable that the results of the convergence-confinement method agree here better with the ones of the axisymmetric analyses.

On the basis of these comparisons, it can be concluded that the convergence-confinement method, even in combination with advanced methods of pre-deformation estimation, underestimates the ground pressure and deformation particularly for stiff linings, long unsupported spans and heavily squeezing ground with highly non-linear material behaviour.

5 Stress and deformation history and its effect on ground response

Next, the numerical results obtained for the case of the heavily squeezing ground will be studied in detail in order to explain the reasons for the deviation of the ground response values from those that were predicted under plane strain conditions.

5.1 Stresses and deformations

Figure 9 shows the region with plastic deformations and the stress distribution along the excavation boundary ($r = a$) for an unsupported opening (Fig. 9a), as well as for three supported tunnels with a different lining stiffness k and unsupported spans e (Fig. 9b, 9c and 9d). The term "past-yield zone" will be explained later in this section. As can be seen from Figure 9, the axial stress σ_{yy} ahead of the face decreases with the approaching excavation from its initial value σ_0 (which prevails far ahead of the face) to zero (at the unsupported tunnel face). Due to the lowered axial stress, the core cannot sustain the radial pressure exerted by the surrounding ground: the core yields and, consequently, larger radial deformations u develop ahead of the face, while both the radial and tangential stresses (σ_{rr}, σ_{tt}) decrease (Fig. 11). This happens within the plastic zone, which extends, in this example, up to a distance of one - two radiuses ahead of the face (Fig. 9). As indicated by the peak in the tangential stress σ_{tt} (at the boundary of the plastic zone at $r = a$), a stress concentration occurs in the elastic region ahead of the plastic zone. Although this peak is slightly more pronounced if the tunnel is unsupported (Fig. 9a), Figure 9 shows that the stress field ahead of the face is largely independent of the support characteristics.

At the face, the radial stress becomes equal to zero, while both the tangential and axial stresses (σ_{tt}, σ_{yy}) become - in accordance with the assumed yield condition - equal to the uniaxial compressive strength f_c. The continuation of excavation does not alter the stresses at the wall ($r = a$) of an *unsupported* tunnel (Fig. 9a). In a supported tunnel, however, the radial stress at the tunnel wall remains equal to zero over the unsupported span $0 < y < e$ but afterwards increases due to the

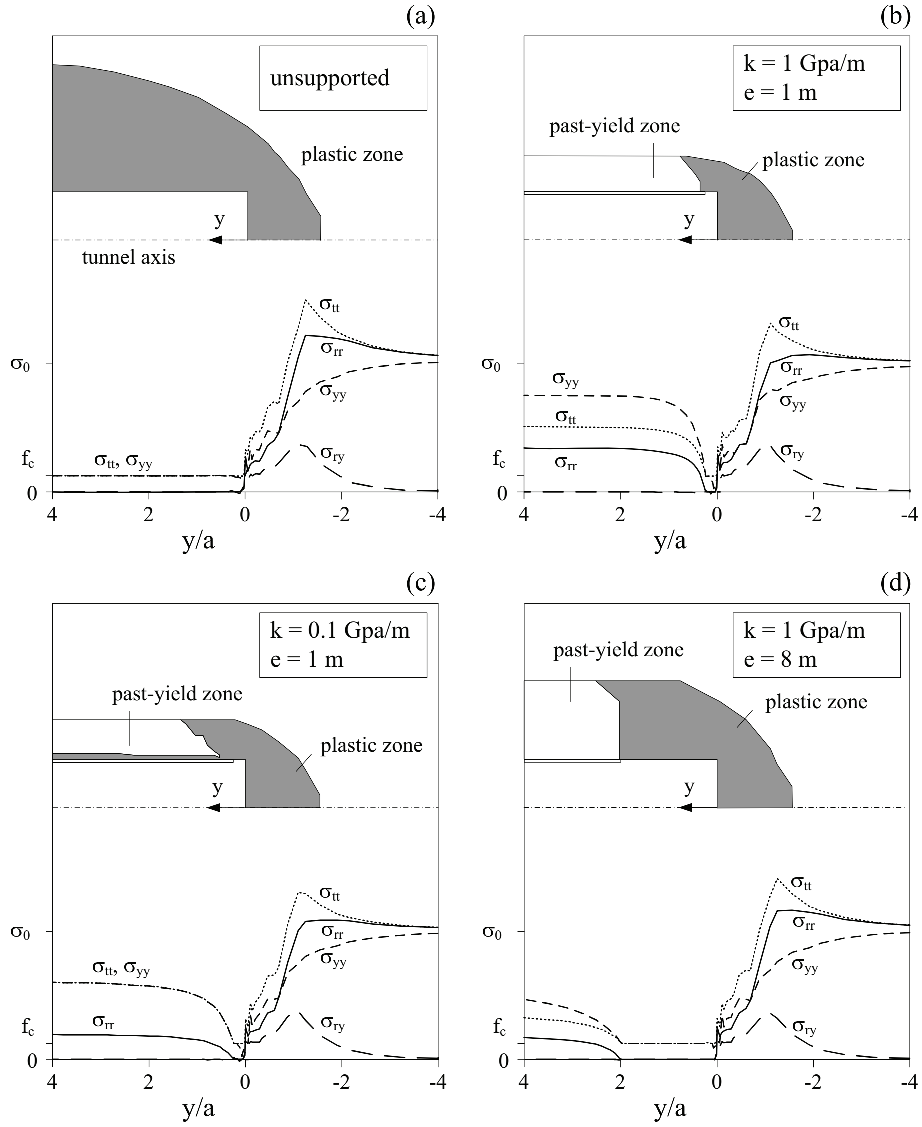

Fig. 9 Plastic zone and history of the radial (σ_{rr}), tangential (σ_{tt}), axial (σ_{yy}) and shear stress (σ_{ry}) along the tunnel boundary ($r = a$). Note that the cases (b), (c) and (d) correspond to the points A_5, A_4 and A_3 of Figure 6b, respectively

installation of the lining, as the latter offers a resistance to the deformations of the ground caused by the subsequent excavation (Fig. 9b, 9c and 9d). The axial and the tangential stress increase as well with the distance *y* from the face, because the ground - on account of Coulomb's yield condition - is able to sustain more pressure in the tangential and axial direction due to radial confinement. In the case of a *stiff* lining (Fig. 9b and 9d), the axial stress σ_{yy} increases more rapidly than the tangential stress σ_{tt} and becomes the highest principal stress. This is because a stiff lining facilitates arching in the longitudinal direction, particularly if installed close to the face (Fig. 9b). In the case of a *soft* lining (Fig. 9c), the ground at the excavation boundary also continues to yield after lining installation (both the axial and tangential stress increase with σ_{rr}, thus fulfilling the yield condition of Coulomb).

Figure 10a shows the stress path in the principal stress space (σ_3, σ_1) for an *unsupported* tunnel. The points *A* to *F* in the diagram refer to the location of the advancing face (see Fig. 11). The

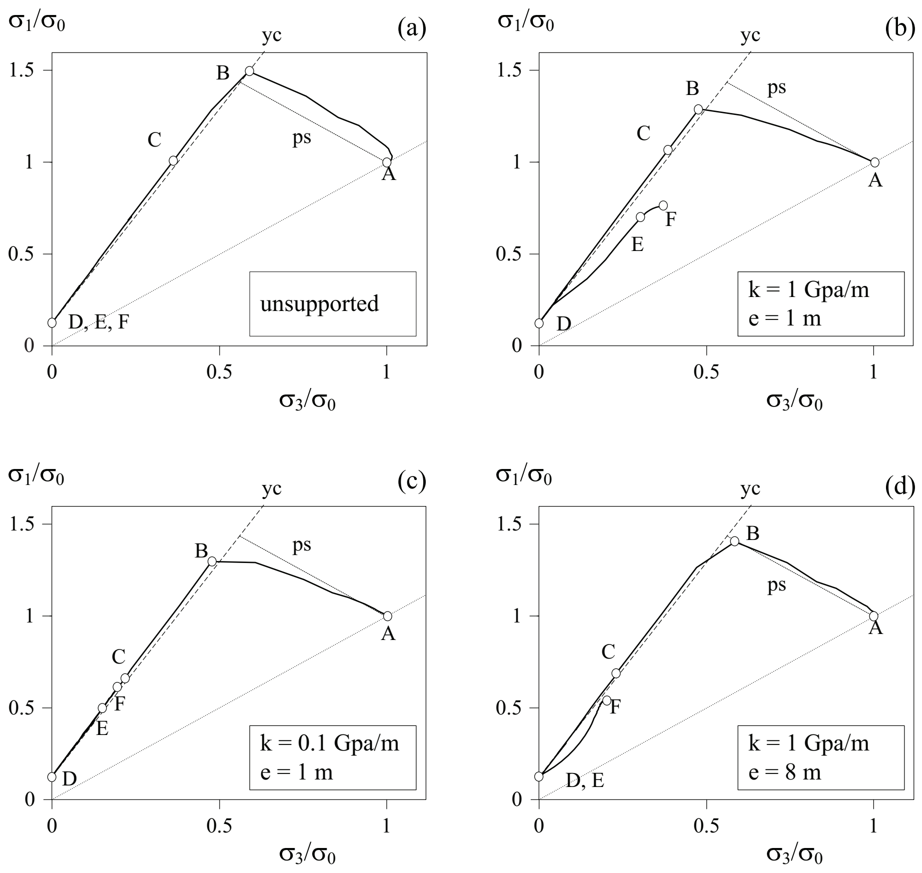

Fig. 10 Principal stress paths along the tunnel boundary (line *yc* = yield condition, line *ps* = elastic portion of the stress path under plane strain conditions, see Fig. 11 for the location of points A to F). Note that the cases (b), (c) and (d) correspond to the points A_5, A_4 and A_3 of Fig. 6b, respectively

stress state reaches the yield condition at Point *B* ahead of the face, follows the yield condition down to point *D* (which is located at the tunnel face) and remains afterwards constant. In the plastic zone developing around the opening (Fig. 9a), the deformations are partially irreversible and the stress field fulfils the yield condition.

In the presence of a *stiff lining* (Fig. 10b and 10d), the stress state reaches the yield condition slightly closer to the face, becomes bi-axial at the tunnel face (point *D*) and remains bi-axial over the unsupported span (stress state *D* applies for $e < y < 0$). With the development of radial pressure from the lining, however, the stress state again becomes elastic ("elastic re-compression", cf. Gärber, 2003). The deformations within the so-called "past-yield zone" (Fig. 9b and 9d) are partially irreversible, however, while the stress state is within the elastic domain (the ground in this region will have experienced yielding and irreversible deformations in the past). Figure 12 shows the results of a parametric study on the extent of the plastic zone. The marked points have been obtained by a series of axisymmetric calculations with different values of lining stiffness *k* and show the radiuses ρ_{pl} and ρ_{py} of the plastic zone and of the past-yield zone, respectively, as well as the respective ground pressure p_∞ developing upon the lining far behind the face. Note that the plane strain analysis (solid curve ρ_{2D}) underestimates the extent of the region experiencing irreversible deformations in the case of stiff linings ($\rho_{2D} < \rho_{py}$ at high *k* - values).

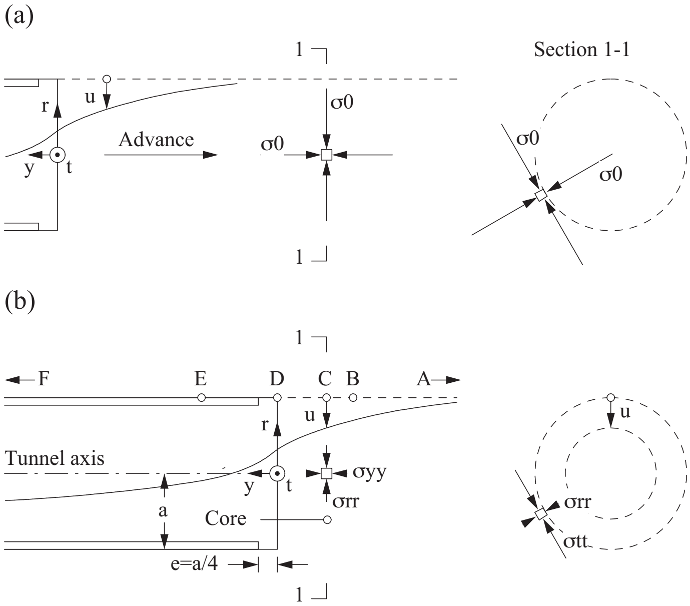

Fig. 11 (a) State prevailing in a cross-section far ahead of the face; (b) qualitative representation of the effect of the approaching excavation and location of the points *A* to *F* referred by Figure 10

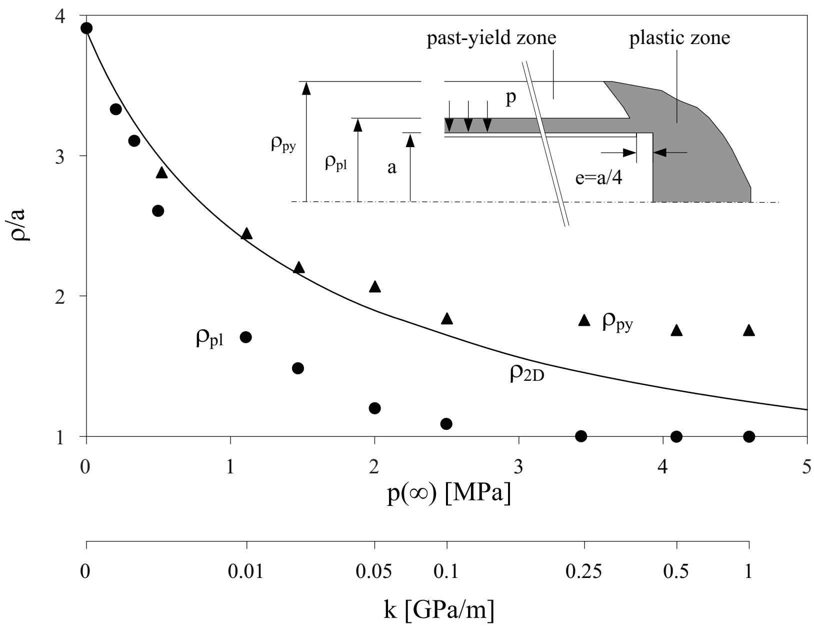

Fig. 12 Radius ρ_{2D} of the plastic zone developing under plane strain conditions as a function of support pressure *p* (solid curve), radius of the plastic zone (ρ_{pl}) and of the zone with past yielding (ρ_{py}) developing far behind the face under axisymmetric conditions for different values of the support stiffness *k*

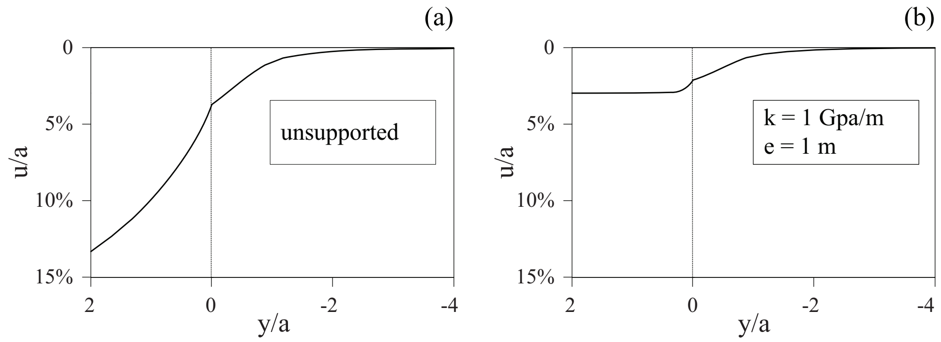

Fig. 13 Radial displacement *u/a* along the tunnel boundary (a) for an unsupported tunnel; (b) for a tunnel supported by a stiff lining installed close to the face (corresponds to point A_5 of Fig. 6b)

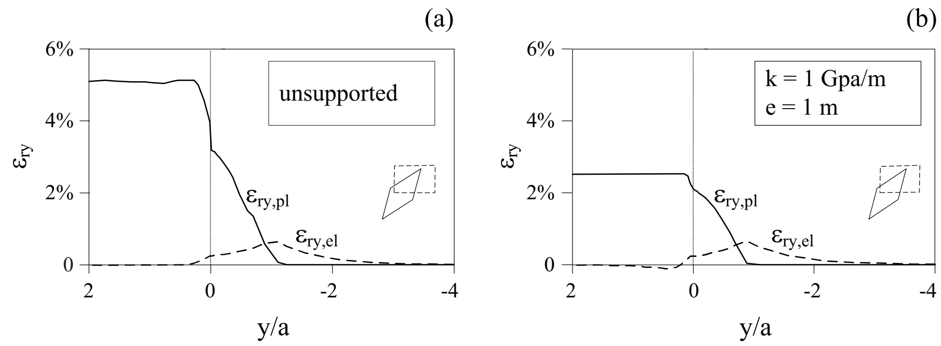

Fig. 14 Elastic and plastic shear strain components ($\varepsilon_{ry,el}$, $\varepsilon_{ry,pl}$) along the tunnel at *r/a* = 1.2 (a) for an unsupported tunnel; (b) for a tunnel supported by a stiff lining installed close to the face (corresponds to point A_5 of Fig. 6b)

In the vicinity of the face, the longitudinal gradient of the radial displacement is large, because the core partially hinders the deformations (Fig. 13). Consequently, the ground is subject to shearing and thus to a rotation of the principal stress axes in the *r-y* plane. The rotation of the principal stress axes is temporary as the shear stress σ_{ry} disappears (the principal stresses are oriented in the radial, tangential and axial directions) far ahead and far behind the face (Fig. 9). Note that the major part of the shear strain ε_{ry} is irreversible (Fig. 14) and, consequently, the ground remains in an intensively sheared state (in the *r-y*-plane) far behind the face although the shear stresses disappear (Fig. 9).

5.2 Reasons for the deviations in ground response

The behaviour of the axisymmetric model discussed in the last section has two particularly conspicuous features: (i) the development of irreversible shear strains in the *r-y*-plane associated with the rotation of the principal axes in the vicinity of the face; (ii) the complete radial unloading of the excavation boundary over the unsupported span and an increase in radial stress following the installation of the lining.

In a plane strain analysis it applies that: (i) the out-of-plane shear strains are by definition zero, while (ii) the radial stress at the excavation boundary decreases monotonously from its initial value σ_0 to the support resistance $p(\infty)$. For these reasons, the features described above cannot be reproduced by a plane strain analysis and this might, therefore, explain the ground response deviations discussed in Section 3.

The results obtained for the case of an *unsupported* tunnel show, however, that point (i) cannot be responsible for the error of the plane strain model: the axisymmetric analysis leads, in spite of the large irreversible shear strains ε_{ry} (Fig. 14a), to a final convergence, which is practically equal to the one obtained by the closed-form, plane-strain solution (Fig. 6). Note also that according to Figure 6b and 7b, the distance of the ground response points ($A_{1,2,3,...}$) from the plane strain ground response curve (*GRC*) increases systematically with increasing lining stiffness, although the longitudinal convergence gradients and, consequently, the shear strains ε_{ry} will decrease in the presence of a stiffer lining. Additional evidence of this is provided by axisymmetric analyses for the hypothetical case of a support that is installed *immediately after excavation at the tunnel face* and exerts *right from the start* a *constant uniform pressure* (i.e., $\sigma_{rr} = p(\infty)$ at $r = a$ for all $y > 0$). The results for this case are given by the dashed curve plotted next to the plane strain solution (solid curve *GRC*) in Figure 6b. The dashed curve practically coincides with the plane strain ground response curve, in spite of the plastic shear strains ε_{ry} developing in the vicinity of the face. The stress path followed by the ground in this case is similar to the plane strain model in that the support does not allow for a complete radial de-stressing of the excavation boundary.

So the deviation of the ground pressures developing upon a support must be due to the above-mentioned point (ii), i.e. to the inability of any plane strain model to map the radial stress reversal that follows the installation of the lining. If this suggestion is true, then we would expect that the error introduced by the plane strain assumption will increase with the amount of radial stress reversal, i.e. with the length of the stress path portion *DF* in Fig. 10 or, since stress state *D* is biaxial, with the final pressure $p(\infty)$ and thus with the lining stiffness *k* (the unsupported span *e* being fixed).

Figure 6b shows precisely this behaviour. For example, the ground response point A_4 that results from the axisymmetric calculation for a soft support (k = 0.1 GPa/m, installed at e = 1 m) is closer to the plane strain ground response curve (*GRC*) than the ground response point A_5 that applies to a stiff support (k = 1 GPa/m, installed also at e = 1 m). As can be seen from Figure 10, the elastic re-compression that follows support installation is less pronounced in the case of a soft support (the path portion *DF* is shorter in Fig. 10c than in Fig. 10b). In general, the stiffer the lining (the value of the unsupported span *e* being fixed), the larger will be the deviation from the ground response curve.

Let us consider now the effect of an unsupported span *e* for a fixed value of lining stiffness *k*. Cases (b) and (d) in Figure 9 involve a stiff lining (k = 1 GPa/m) installed at e = 1 or 8 m, respectively. The deviation from the ground response curve is larger in the case of the longer unsupported span (compare point A_3 with point A_5 in Fig. 6b). This is because the biaxial stress state (point *D* in Figure 10d), rather than the final stress state (point *F* in Figure 10d), governs the extent of the plastic zone (Fig. 9d) and the magnitude of deformation, since it prevails over the long unsupported portion of the tunnel. The deviation from the ground response curve therefore increases with the length *e* of unsupported span.

At the same time, however, the longer the unsupported span, the lower will be the final pressure $p(\infty)$, the smaller will be the difference between the final stress state and the temporary biaxial stress state, and the less pronounced will be the radial stress reversal. Consequently, the deviation from the ground response curve will also be smaller. The net effect of an unsupported span is therefore more complicated than that of lining stiffness. The error introduced by the plane strain assumption is small for linings installed close to the face, increases with the unsupported span e but decreases again at very large values of e (see, e.g., solid line for k = 1 GPa/m in Fig. 6b).

6 Conclusions

An axisymmetric model that takes into account the sequence of excavation and lining installation will always lead to ground response points above the plane strain ground response, i.e. the convergence corresponding to a certain ground pressure $p(\infty)$will always be larger than the one obtained by a plane strain analysis. This is due to the inability of the plane strain model to map the radial stress reversal that follows the installation of the lining. In general, the stiffer the lining and the longer the unsupported span e, the larger will be the deviation from the ground response curve.

The convergence-confinement method, even in combination with advanced methods of pre-deformation estimation, underestimates the ground pressure and deformation particularly for stiff linings, long unsupported spans and heavily squeezing ground with highly non-linear material behaviour. The inherent weakness of any plane strain analysis is that it cannot reproduce at one and the same time both the deformations and the pressures. This is relevant from the design standpoint particularly for heavily squeezing conditions that require a yielding support in combination with an over-excavation: in this case one needs reliable estimates of the deformations that must occur in order for the squeezing pressure to be reduced to a pre-defined, technically manageable level. In cases where the question of deformation is of secondary importance, however, a plane strain analysis in combination with an implicit method of pre-deformation estimation will suffice. For support completion close to the face, the differences in the results obtained by the different methods of analysis are not important from a practical point of view.

Appendix of Part I

Consideration of out-of-plane plastic flow in the ground response curve

Radial and tangential stress field

The radius ρ of the plastic zone as well as the distribution of the radial and tangential stresses (σ_{rr}, σ_{tt}) within the plastic zone ($a \leq r \leq \rho$) can be determined without taking into account the deformations because the equilibrium equation

$$\frac{d\sigma_{rr}}{dr} = \frac{\sigma_{tt} - \sigma_{rr}}{r} \tag{A1}$$

and the yield condition

$$\bar{\sigma}_{tt} = m\bar{\sigma}_{rr} \, , \tag{A2}$$

where the overscore denotes the stress transformation

$$\bar{\sigma} = \sigma + \frac{f_c}{m-1} \, , \tag{A3}$$

form a system for the determination of the two stress components. Eq. (A2) presupposes that σ_{rr} < σ_{yy} ≤ σ_{tt}. This condition is always satisfied (Reed, 1988). Taking into account the condition

$$\sigma_{rr}\big|_{r=a} = \sigma_a \tag{A4}$$

prevailing at the tunnel boundary as well as the requirement of stress continuity at the interface between the plastic and the elastic zone, i.e.

$$\bar{\sigma}_{rr}\big|_{r=\rho} = \frac{2\bar{\sigma}_0}{m+1} \, , \tag{A5}$$

the integration of Eqs. (A1) and (A2) leads to the well-known expressions

$$\bar{\sigma}_a \quad \le \quad \bar{\sigma}_{rr} = \bar{\sigma}_a \left(\frac{r}{a}\right)^{(m-1)} \quad \le \quad \frac{2\bar{\sigma}_0}{m+1} \quad (\text{for } a \le r \le \rho) \tag{A6}$$

and

$$\frac{\rho}{a} = \left(\frac{2}{m+1} \, \frac{\bar{\sigma}_o}{\bar{\sigma}_a}\right)^{\frac{1}{m-1}} \, . \tag{A7}$$

Axial stress field

Assuming that plastic flow does not occur in the axial direction, i.e.

$$\varepsilon_{yy,pl} = 0 \, , \tag{A8}$$

the out-of-plane elastic strain is also equal to zero,

$$\varepsilon_{yy,el} = \varepsilon_{yy} - \varepsilon_{yy,pl} = 0 \, , \tag{A9}$$

and on account of Hooke's law,

$$\varepsilon_{yy,el} = \frac{1}{E}\Big((\sigma_{yy} - \sigma_0) - \nu(\sigma_{rr} - \sigma_0) - \nu(\sigma_{tt} - \sigma_0)\Big) \, , \tag{A10}$$

the axial stress σ_{yy} reads as follows:

$$\sigma_{yy} = \nu(\sigma_{rr} + \sigma_{tt}) + (1-2\nu)\sigma_0 \, . \tag{A11}$$

The assumption made (Eq. A8) presupposes that the axial stress is the strict intermediate stress, i.e.

$$\sigma_{rr} < \sigma_{yy} < \sigma_{tt} \, , \tag{A12}$$

or, on account of Eqs. (A2) and (A11),

$$\left(1-\nu(1+m)\right)\bar{\sigma}_{rr} \;<\; (1-2\nu)\bar{\sigma}_0 \;<\; \left(m(1-\nu)-\nu\right)\bar{\sigma}_{rr} \,. \tag{A13}$$

One can readily verify that the first inequality is always satisfied: in a trivial manner if $\nu > (1\text{-}sin\phi)/2$; and due to Eq. (A5) if $\nu < (1\text{-}sin\phi)/2$. The second inequality will be satisfied if

$$\bar{\sigma}_{rr} \;>\eta_4\;\bar{\sigma}_0\;,\;\;\text{where}\;\eta_4=\frac{1-2\nu}{m(1-\nu)-\nu}\quad, \tag{A14}$$

i.e. if the radial stress is higher than a critical value. Taking into account that the lowest radial stress to be considered in the determination of the ground response curve is equal to zero,

$$\bar{\sigma}_{rr} \;\geq \bar{\sigma}_{rr}(a)=\bar{\sigma}_a \;\geq\frac{f_c}{m-1}\quad, \tag{A15}$$

the inequality (A14) will be satisfied for the entire ground response curve if

$$f_c > \sigma_0\frac{1-2\nu}{1-\nu}\;\;. \tag{A16}$$

Incompressible materials (ν = 0.5) fulfil this condition always. For ν < 0.5 and uniaxial compressive strength f_c lower than the value indicated by (A16), however, the out-of-plane stress (Eq. A11) obtained under the assumption of no plastic flow in the axial direction (Eq. A8) will be higher than the tangential stress thereby violating the yield criterion (Fig. 15). In order to satisfy the latter, i.e.

$$\bar{\sigma}_{yy} = m\bar{\sigma}_{rr}\;, \tag{A17}$$

plastic flow in the axial direction has to occur in the inner part of the plastic zone. The plastic flow does not influence the extend of the plastic zone ρ or the radial and tangential stress field, because these are determined by the equilibrium and the yield condition. Therefore, the radius ρ' of the inner part of the plastic zone can be calculated from Eq. (A6) and (A14), while the radial stress at $r = \rho'$ is given by the right hand side of inequality (A14):

$$\frac{\rho'}{a}=\left(\eta_4\,\frac{\bar{\sigma}_0}{\bar{\sigma}_a}\right)^{\frac{1}{m-1}},\qquad \bar{\sigma}_{\rho'}=\eta_4\;\bar{\sigma}_0\qquad. \tag{A18}$$

One can readily verify that $\rho' < \rho$, i.e. the plastic zone consists of an outer ring with $\sigma_{rr} < \sigma_{yy} < \sigma_{tt}$ and an inner ring with $\sigma_{rr} < \sigma_{yy} = \sigma_{tt}$ (Fig. 15).

Deformation field

The stress states within the inner ring satisfy both Eq. (A2) and Eq. (A17). The corresponding plastic potential functions are:

$$g_1(\sigma_{rr},\sigma_{tt},\sigma_{yy}) = \sigma_{tt} - \kappa\sigma_{rr}\;, \tag{A19}$$

$$g_2(\sigma_{rr},\sigma_{tt},\sigma_{yy}) = \sigma_{yy} - \kappa\sigma_{rr}\;, \tag{A20}$$

where κ depends on the dilatancy angle ψ (Eq. 4). As the stress states are located on the edges of the Coulomb plastic potential surface (which has a pyramidoidal form in the principal stress space)

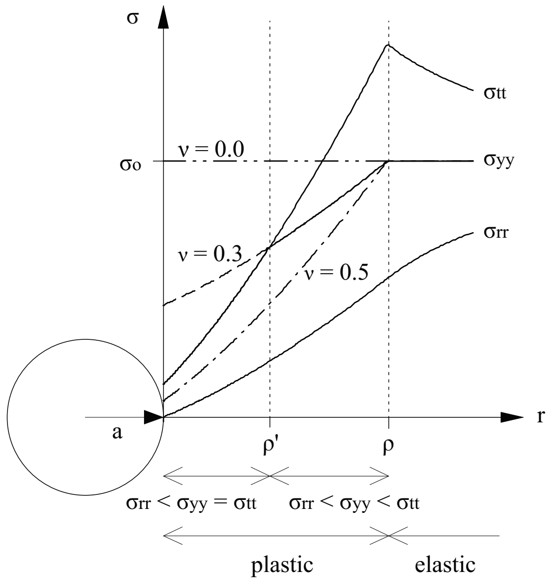

Fig. 15 Distribution of the radial stress σ_{rr}, of the tangential stress σ_{tt} and of the axial stress σ_{yy} for an unsupported tunnel (c = 500 kPa, other parameters: see Table 1)

and the latter is not continuously differentiable at the edges, the determination of the plastic strain increments proceeds according to Koiter (1953):

$$d\varepsilon_{tt,pl} = d\lambda_1 \frac{\partial g_1}{\partial \sigma_{tt}} + d\lambda_2 \frac{\partial g_2}{\partial \sigma_{tt}} = d\lambda_1 , \tag{A21}$$

$$d\varepsilon_{yy,pl} = d\lambda_1 \frac{\partial g_1}{\partial \sigma_{yy}} + d\lambda_2 \frac{\partial g_2}{\partial \sigma_{yy}} = d\lambda_2 , \tag{A22}$$

$$d\varepsilon_{rr,pl} = d\lambda_1 \frac{\partial g_1}{\partial \sigma_{rr}} + d\lambda_2 \frac{\partial g_2}{\partial \sigma_{rr}} = -\kappa\left(d\lambda_1 + d\lambda_2\right), \tag{A23}$$

where $d\lambda_1$ and $d\lambda_2$ denote the plastic multipliers. From these equations we obtain

$$\varepsilon_{rr,pl} + \kappa\left(\varepsilon_{tt,pl} + \varepsilon_{yy,pl}\right) = 0 . \tag{A24}$$

By taking into account the kinematical relations

$$\varepsilon_{rr} = \frac{du}{dr} \quad \text{and} \quad \varepsilon_{tt} = \frac{u}{r} \tag{A25}$$

as well as the strain decomposition

$$\varepsilon_{rr} = \varepsilon_{rr,el} + \varepsilon_{rr,pl} , \quad \varepsilon_{tt} = \varepsilon_{tt,el} + \varepsilon_{tt,pl} \quad \text{and} \quad \varepsilon_{yy} = \varepsilon_{yy,el} + \varepsilon_{yy,pl} = 0, \tag{A26}$$

the relationship between the plastic strains (Eq. A24) leads to

$$\frac{du}{dr} + \kappa \frac{u}{r} = \varepsilon_{rr,el} + \kappa\left(\varepsilon_{tt,el} + \varepsilon_{yy,el}\right). \tag{A27}$$

This is a differential equation for the radial displacement u because the right hand side is a known function of radius r (the elastic strains are interconnected with the stresses via Hooke's law and the stresses are given by Eqs. A2, A6 and A17). The solution reads as follows:

$$u(r)=u(\rho')\left(\frac{\rho'}{r}\right)^{\kappa}+\frac{a}{E}\left(-\eta_5\bar{\sigma}_a\left(\frac{r}{a}\right)^{m}\left(\left(\frac{\rho'}{r}\right)^{m+\kappa}-1\right)+\eta_6\bar{\sigma}_0\frac{r}{a}\left(\left(\frac{\rho'}{r}\right)^{\kappa+1}-1\right)\right), \tag{A28}$$

where

$$\eta_5=\frac{2\kappa(m(1-\nu)-\nu)+1-2m\nu}{m+\kappa}\ ,\quad \eta_6=\frac{(1+2\kappa)(1-2\nu)}{\kappa+1}, \tag{A29}$$

while the displacement $u(\rho')$ of the interface of the two plastic regions is obtained by applying Eq. (3) to the outer plastic ring:

$$u(\rho')=\frac{\rho'\bar{\sigma}_0}{E}\left(\delta_1+\delta_2\frac{\bar{\sigma}_{\rho'}}{\bar{\sigma}_0}+\delta_3\left(\frac{\bar{\sigma}_{\rho'}}{\bar{\sigma}_0}\right)^{-\delta_4}\right), \tag{A30}$$

where the radius ρ' and the contact pressure $\sigma_{\rho'}$ are given by Eq. (A18). The ground response curve is obtained from Eq. (A28) for $r = a$ and can be written in the following form:

$$u(a)=\frac{a\bar{\sigma}_0}{E}\left((\delta_1+\eta_1)+(\delta_2+\eta_2)\frac{\bar{\sigma}_a}{\bar{\sigma}_0}+(\delta_3+\eta_3)\left(\frac{\bar{\sigma}_a}{\bar{\sigma}_0}\right)^{-\delta_4}\right), \tag{A31}$$

where

$$\begin{aligned}\eta_1&=-\left(\kappa(1-\nu)-\nu\right)\frac{(1-2\nu)}{\kappa+1},\quad \eta_2=\left(\kappa(1-\nu)-\nu\right)\frac{(m(1-\nu)-\nu)}{m+\kappa},\\ \eta_3&=\left(\kappa(1-\nu)-\nu\right)\frac{(1-2\nu)(m-1)}{(m+\kappa)(\kappa+1)}\,\eta_4^{\delta_4}.\end{aligned} \tag{A32}$$

The coefficients η_1, η_2 and η_3 in Eq. (A31) are the contribution of the out-of-plane plastic flow. These terms shall be considered in the determination of the following portion of the ground response curve:

$$\bar{\sigma}_a<\eta_4\bar{\sigma}_0\ \ . \tag{A33}$$

The inequality (A33) has been obtained from Eq. (A18) for $\rho'/a > 1$.

One can readily verify by observing Eqs. (3) and (A31) that the error of the simplified Eq. (3), defined as

$$\text{Error}=\frac{u(a)\big|_{Eq.(3)}-u(a)\big|_{Eq.(A31)}}{u(a)\big|_{Eq.(A31)}}\quad , \tag{A34}$$

depends on the normalized support pressure $\bar{\sigma}_a / \bar{\sigma}_0$, on the Poisson's ratio ν, on the friction angle ϕ and on the plastic dilatancy angle ψ (or, equivalently, on the material constants m and κ).

References

AFTES 2002. Recommandations relatives a la methode convergence-confinement. Association Française des Travaux en Souterrain - Groupe de travail n°7 (animé par M. Panet avec la collaboration de A. Bouvard, B. Dardard, P. Dubois, O. Givet, A. Guilloux, J. Launay, Nguyen Minh Duc, J. Piraud, H. Tournery, H. Wong). *Tunnels et Ouvrages Souterrains*, 170, 79-89.

Amberg, W. 1999. Konzepte der Ausbruchsicherung für tiefliegende Tunnels. *Bauingenieur*, 74, 6, 278-283.

Anagnostou, G. 1992. Untersuchungen zur Statik des Tunnelbaus in quellfähigem Gebirge. *Mitteilung des Institutes für Geotechnik der ETH Zürich*, Vol. 201.

Anagnostou, G., Kovári, K. 1993. Significant parameters in elasto-plastic analysis of underground openings. *ASCE, Journal of Geotechnical Engineering*, 119 (3), 401-419.

Anagnostou, G. 2007a. The one-step solution of the advancing tunnel heading problem. In: Eberhardsteiner *et al*. (eds) *„ECCOMAS Thematic Conference on Computational Methods in Tunnelling"*.

Anagnostou, G. 2007b. Continuous tunnel excavation in a poro-elastoplastic medium. *Tenth international symposium on numerical models in geomechanics, NUMOG X, Rhodes*, 183-188.

Barla, G. 2001. Tunnelling under squeezing rock conditions. *Eurosummer-School in Tunnel Mechanics*, Innsbruck.

Barla, M. 2000. Stress paths around a circular tunnel. *Rivista Italiana di Geotecnica*, 34, 1, pp. 53-58.

Bernaud, D. 1991. *Tunnels profonds dans les milieux viscoplastiques: Approches expérimentale et numérique*. PhD thesis, Ecole Nationale des Ponts et Chaussées.

Bernaud, D., Rousset, G. 1996. The new implicit method for tunnel analysis. *Int. J. Numer. Anal. Meth. Geomech*. 20: 673-690.

Bliem, Ch. 2001. 3D finite element calculations in tunneling. *Advances in geotechnical engineering and tunneling*, Volume 4, Logos Verlag, Berlin.

Bonnier, P.G., Möller, S.C., Vermeer, P.A. 2002. Bending moments and normal forces in tunnel linings. *Paper presented at the 5th European Conference of Numerical Methods in Geotechnical Engineering*. Paris, France.

Brinkgreve, R.B.J. 2002. *PLAXIS, 2D - Version 8*. A.A. Balkema publishers, Lisse a.o.

Corbetta, F. 1990. *Nouvelles méthodes d' étude des tunnels profonds – Calculs analytiques et numériques*. PhD Thesis, Ecole des Mines de Paris.

Corbetta, F., Nguyen-Minh, D. 1992. Steady state method for analysis of advancing tunnels in elastoplastic and viscoplastic media. In: Pande & Pietruszczak (eds.), *Num. Methods in Geomech*., 747-757.

Cai, M., Kaiser, P.K., Uno, H., Taska, Y. 2002. Influence of stress-path on the stress-strain relations of jointed rocks. In: 2nd Int. Conf. on "New Development in Rock Mechanics and Rock Engineering", Shenyang, China, Rinton Press, Princeton, U.S.A., 60-65.

Carranza-Torres, C., Fairhurst, C. 2000. Application of the Convergence-Confinement Method of Tunnel Design to Rock Masses That Satisfy the Hoek-Brown Failure Criterion. *Tunnelling and Underground Space Technology*, vol. 15, No. 2, 187-213.

Diederichs, M.S., Villeneuve, M., Kaiser, P.K. 2004. Stress rotation and tunnel performance in brittle rock. *Tunnelling Association of Canada Symposium*. Edmonton. 8pgs.

Diederichs, M.S., Kaiser, P.K., Eberhardt E. 2004. Damage initiation and propagation in hard rock tunnelling and the influence of near-face stress rotation. *Int J Rock Mech & Min Sci.* Vol 41, 785-812.

Eberhardt, E. 2001. Numerical modelling of three-dimension stress rotation ahead of an advancing tunnel face. *Int. J. of Rock Mech. & & Min. Sci*., 38, 499-518.

Franzius, J.N., Potts, D.M. 2005. Influence of Mesh Geometry on Three-Dimensional Finite-Element Analysis of Tunnel Excavation. *Int. J. of Geomechanics*, Vol. 5, No. 3, 256-266.

Gärber, R. 2003. *Design of deep galleries in low permeable saturated porous media*. PhD Thesis, EPFL Lausanne.

González-Nicieza, C., Álvarez-Vigil, A.E., Menéndez-Diaz, A., González-Palacio, C. 2008. Influence of the depthe and shape of a tunnel in the application of the convergence-confinement method. *Tunnelling and Underground Space Technology*, 23, 25-37.

Graziani, A., Boldini, D., Ribacchi R. 2005. Practical estimate of deformations and stress relief factors for deep tunnels supported by shotcrete. *Rock Mech. & Rock Engng.*, 38, 345-372.

Guo, C. 1995. *Calcul des tunnels profonds soutenus – Méthode stationnaire et méthodes approchées*. PhD thesis, Ecole Nationale des Ponts et Chaussées.

Kaiser, P-K. 1980. Effect of stress-history on the deformation behaviour of underground openings. *13th Canadian Rock Mechanics Symposium*, Toronto, 133-140.

Koiter, W. T. 1953. Stress-strain relations, uniqueness and variational theorems for elasto-plastic materials with a singular yield surface. *Q. Appl. Mathem.* 11, 350-354.

Lombardi, G. 1971. Zur Bemessung der Tunnelauskleidung mit Berücksichtigung des Bauvorganges, *Schweiz. Bauzeitung*, Vol. 89, Heft Nr. 32.

Lombardi, G. 1981. Tunnel construction at great rock deformations, *Int. Tunnelling Congress "Tunnel 81"*, Düsseldorf, 353 - 384.

Martin, D., Kaiser, P.K., Tannant, D. 1999. Stress path and failure around mine openings. In: *9th ISRM Congress on Rock Mechanics*, Paris, FR: Balkema, 1:311-315.

Nguyen-Minh, D., Berest P. 1979. Etude de la stabilité des cavités souterraines avec un modèle de comportement élastoplastique radoucissant. *4eme Cong. de la Soc. Int. De Méc. Des Roches*, Montreux, vol. 1, 249-255.

Nguyen-Minh, D., Corbetta, F. 1992. New methods for rock-support analysis of tunnels in elastoplastic media. In: Kaiser & McCreath (eds), *Rock Support in Mining and Underground Construction*, 83-90.

Nguyen-Minh, D., Guo, C. 1993. Sur un principle d' interaction massif-soutenement des tunnels en avancement stationnaire. In: Ribeiro e Sousa & Grossmann (eds) *"Eurock' 93"*, 171-177.

Nguyen-Minh, D., Guo, C. 1996. Recent progress in convergence confinement method. In: Barla (ed.) *"Eurock' 96"*, 855-860.

Nguyen-Quoc, S., Rahimian, M. 1981. Mouvement permanent d' une fissure en milieu élastoplastique. *Journal de Mécanique appliquée*, Vol. 5, no 1, 95-120.

Panet, M., Guellec, P. 1974. Contribution à l' étude du soutènemant derrière le front de taille. *Proc. 3rd Congr. Int. Soc. Rock Mech.,* Vol. 2, Part B, Denver.

Panet, M. 1995. *Le calcul des tunnels par la méthode convergence-confinement*. Presses de l'Ecole Nationale des Ponts et Chaussées, Paris.

Pelli, F., Kaiser, P.K., Morgenstern, N.R. 1995. Effects of rock mass anisotropy and non-linearity on the near face stresses in deep tunnels. *Rock Mech. & Rock Engng.,* 28, 125-132.

Reed, M.B. 1988. The influence of out-of-plane stress on a plane strain problem in rock mechanics. *Int. J. Numer. Anal. Meth. Geomech.*, 12, 173-181.

Vogelhuber, M., Anagnostou, G., Kovári, K. 2004. The influence of pore water pressure on the mechanical behavior of squeezing rock. *Proc. 3rd Asian Rock Mechanics Symp.*, Kyoto.

Part II

The interaction between yielding supports and squeezing ground

Abstract: In this paper we investigate the interaction between yielding supports and squeezing ground by means of spatial numerical analyses that take into account the stress history of the ground. We also present design nomograms which enable the rapid assessment of yielding supports. The idea behind yielding supports is that squeezing pressure will decrease by allowing the ground to deform. When estimating the amount of deformation required, one normally considers the characteristic line of the ground, i.e. the relationship between the ground pressure and the radial displacement of the tunnel wall under plane strain conditions. The computation of the characteristic line assumes a monotonic decrease of radial stress at the excavation boundary, while the actual tunnel excavation and subsequent support installation involve a temporary complete radial unloading of the tunnel wall. This difference, in combination with the stress-path dependency of the ground behaviour, is responsible for the fact that the results obtained by spatial analysis are not only quantitatively, but also qualitatively different from those obtained by plane strain analysis. More specifically, the relationship between ground pressure and deformation at the final state prevailing far behind the face is not unique, but depends on the support characteristics, because these affect the stress history of the ground surrounding the tunnel. The yield pressure of the support, i.e. its resistance during the deformation phase, therefore proves to be an extremely important parameter. The higher the yield pressure of the support, the lower will be the final ground pressure. A targeted reduction in ground pressure can be achieved not only by installing a support that is able to accommodate a larger deformation (which is a well-known principle), but also by selecting a support that yields at a higher pressure.

Notation:

a	Tunnel radius
b	Spacing of steel sets (Fig. 1)
b'	Clear distance between the steel sets, length of the deformable elements (Fig. 1)
c	Ground cohesion
d	Lining thickness
d_{II}	Thickness of the deformable elements and of the lining during the deformation phase
d_{III}	Lining thickness after the deformation phase
e	Unsupported span
E_R	Young's modulus of the ground
E_L	Young's modulus of the lining
f_c	Uniaxial compressive strength of the ground
f_y	Yield strength of the highly deformable concrete elements
H	Depth of cover
k	Lining stiffness
k_I	Support stiffness before the deformation phase
k_{III}	Support stiffness after the deformation phase
n	Number of deformable elements and sliding connections in one cross-section
n_f	Number of friction loops per sliding connection
N	Lining hoop force
N_y	Lining hoop force during the deformation phase
N_f	Sliding resistance of one friction loop
p	Radial pressure acting upon the lining
$p(\infty)$	Final radial pressure acting upon the lining
p_y	Yield pressure of support
p_o	Initial stress
r	Radial co-ordinate (distance from tunnel axis)
s	Slot size in the circumferential direction (Fig. 1 and 2)
u	Radial displacement of the ground
u_{2D}	Radial displacement of the ground assuming plane strain conditions
$u(0)$	Radial displacement of the ground at the face
$u(\infty)$	Final radial displacement of the ground
u_y	Maximum radial displacement of support in the deformation phase
U_y	Normalized maximum radial displacement of support in the deformation phase
x	Axial co-ordinate (distance behind the tunnel face)
γ	Unit weight of the ground

ν Poisson's ratio of the ground

Δs Slot size reduction (Fig. 1)

ε Slot deformation $\Delta s/s$ (Fig. 2)

ε_y Slot deformation during the deformation phase

ρ_{2D} Radius of the plastic zone assuming plane strain conditions

σ_1 Maximum principal stress

σ_3 Minimum principal stress

σ_s Lining hoop stress

σ_{xx} Axial stress

σ_{rr} Radial stress

σ_{tt} Tangential stress

σ_{rx} Shear stress

ϕ Internal friction angle of the ground

ψ Dilatancy angle of the ground

1 Introduction

The term "squeezing" refers to the phenomenon of large deformations that develop when tunnelling through weak rocks. If an attempt is made to stop the deformations with the lining (so-called "resistance principle", Kovári 1998), a so-called "genuine rock pressure" builds up, which may reach values beyond the structurally manageable range. The only feasible solution in heavily squeezing ground is a tunnel support that is able to deform without becoming damaged, in combination with a certain amount of over-excavation in order to accommodate the deformations. Supports that are based on this so-called "yielding principle" can be structurally implemented in two main ways (Anagnostou and Cantieni, 2007): either by arranging a compressible layer between the excavation boundary and the extrados of a stiff lining (Fig. 1a) or through a suitable structural detailing of the lining that will allow a reduction in its circumference (Fig. 1b). In the first case the ground experiences convergences while the clearance profile remains practically constant. This solution has been proposed particularly for shield tunnelling with practically rigid segmental linings (Schneider *et al*. 2005, Billig *et al*. 2007). The second solution is the one usually applied today. It involves steel sets having sliding connections in combination with shotcrete (Fig. 1b, sections c-c and d-d, respectively).

Steel sets applied in squeezing ground usually have a top hat cross-section. The hoop force in the steel sets is controlled by the number and by the pre-tensioning of the friction loops connecting the steel segments. Up to 4 friction loops, each offering a sliding resistance of about 150 kN, may be used per connection. Shotcrete may be applied either after the occurrence of a pre-defined amount of convergence (as a recent example the lot Sedrun of the Gotthard Base Tunnel can be mentioned, see Kovári *et al.*, 2006) or, more commonly, right from the start. In order to avoid

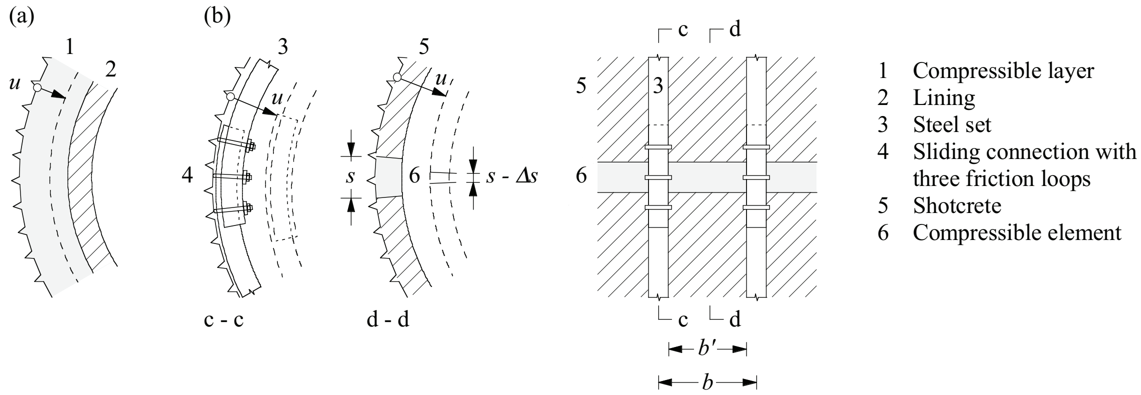

Fig. 1 Basic types of deformable supports: (a) compressible layer between lining and excavation boundary; (b) yielding supports with steel sets, shotcrete and compressible insets

overstressing of the shotcrete and, at the same time, to allow it to participate in the structural system, special elements are inserted into longitudinal slots in the shotcrete shell (Fig. 1b, section d-d). Figure 2 shows the typical load - deformation characteristics of such elements. As can be seen from the hoop force *N* vs. deformation ε relationships, the elements yield at a specific load level, thereby limiting the stress in the shotcrete shell. The so-called “lining stress controllers” (Schubert 1996, Schubert *et al.* 1999) consist of co-axial steel cylinders which are loaded in their axial direction, buckle in stages and shorten up to 200 mm at a load of 150 - 250 kN. Actual examples of this include the Galgenberg tunnel (Schubert, 1996), the Strenger tunnel (Budil *et al*., 2004) and the Semmering pilot tunnel (Schubert *et al*., 2000). Additionally, there are the recently-developed "highly-deformable concrete" elements (Kovári, 2005), which are composed of a mixture of cement, steel fibers and hollow glass particles. These collapse at a pre-defined compressive stress which is dependent on the composition of the concrete, thereby providing the desired deformability. These elements have been applied in the Lötschberg Base Tunnel and in the St. Martin La Porte site access tunnel of the Lyon Turin Ferroviaire (Thut *et al*., 2006a and 2006b).

The number *n*, the size *s* (in circumferential direction, Fig. 2) and the deformability of the compressible elements (or the sliding ways of the steel set connections) will determine the possible reduction of the circumference of the lining during the yielding phase, limiting the amount of radial displacement that can occur without damaging the lining. The elements selected must therefore be compatible with the planned amount of over-excavation. The latter represents an important design parameter. If it is too low, costly and time-consuming re-profiling works will be necessary. On the other hand, if it is too high, the over-profile will have to be filled by the cast-in-situ concrete of the final lining.

The idea behind all yielding support systems is that the ground pressure will decrease if the ground is allowed to deform. During construction, the support system and the amount of over-excavation can be adapted to changes in squeezing intensity through the use of advance probing, monitoring results and observations made in tunnel stretches excavated previously. In the planning phase, however, decision-making has to rely solely upon experience and geomechanical calculations. When estimating the required amount of over-excavation, the usual approach is to consider a tunnel cross-section far behind the tunnel face and to assume plane strain conditions. Where there is rotational symmetry, the plane strain problem is mathematically one-dimensional. The so-called characteristic line of the ground (also referred to as the "ground response curve", Panet & Guenot,

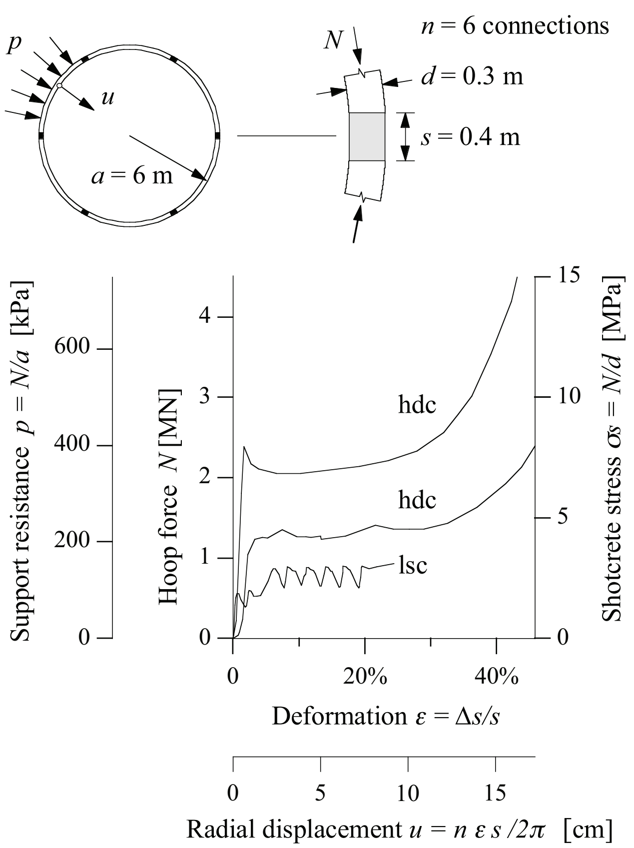

Fig. 2 Load - deformation characteristics (N, $\Delta s/s$) of compressible elements and respective convergence u vs. pressure p relationships for a circular lining with n = 6 insets. lsc: lining stress controllers (4 cylinders per linear meter) after Schubert *et al*. (1999); hdc: highly deformable concrete elements after Thut *et al*. (2006a, 2006b) having a yield stress of 4 - 7 MPa

1982) expresses the relationship between the radial stress p and the radial displacement u of the ground at the excavation boundary (Fig. 3a). Closed-form solutions exist for the ground response curve in a variety of constitutive models. The ground response curve can be employed for estimating the radial convergence $u(\infty)$ of the ground that must occur in order for the ground pressure to decrease to a chosen, structurally manageable value $p(\infty)$ (Fig. 3a).

The first problem with this approach is that the radial convergence $u(\infty)$ represents only an upper limit in terms of the amount of over-excavation required, because it includes the ground displacement $u(0)$ that has already occurred ahead of the tunnel face. The pre-deformation $u(0)$ introduces an element of uncertainty into the estimation of the required amount of over-excavation. This uncertainty is particularly serious in the case of heavily squeezing ground because its behaviour is highly non-linear and, consequently, small variations in the deformation will have a large effect on the pressure.

A second, more fundamental problem is that all plane strain solutions (whether closed-form solutions for the ground response curve or numerical simulations involving a partial stress release before lining installation) assume that the radial stress at the excavation boundary decreases monotonically from its initial value (far ahead of the face) to the support pressure (far behind the face), while the actual load history will include an intermediate stage with a complete unloading of the

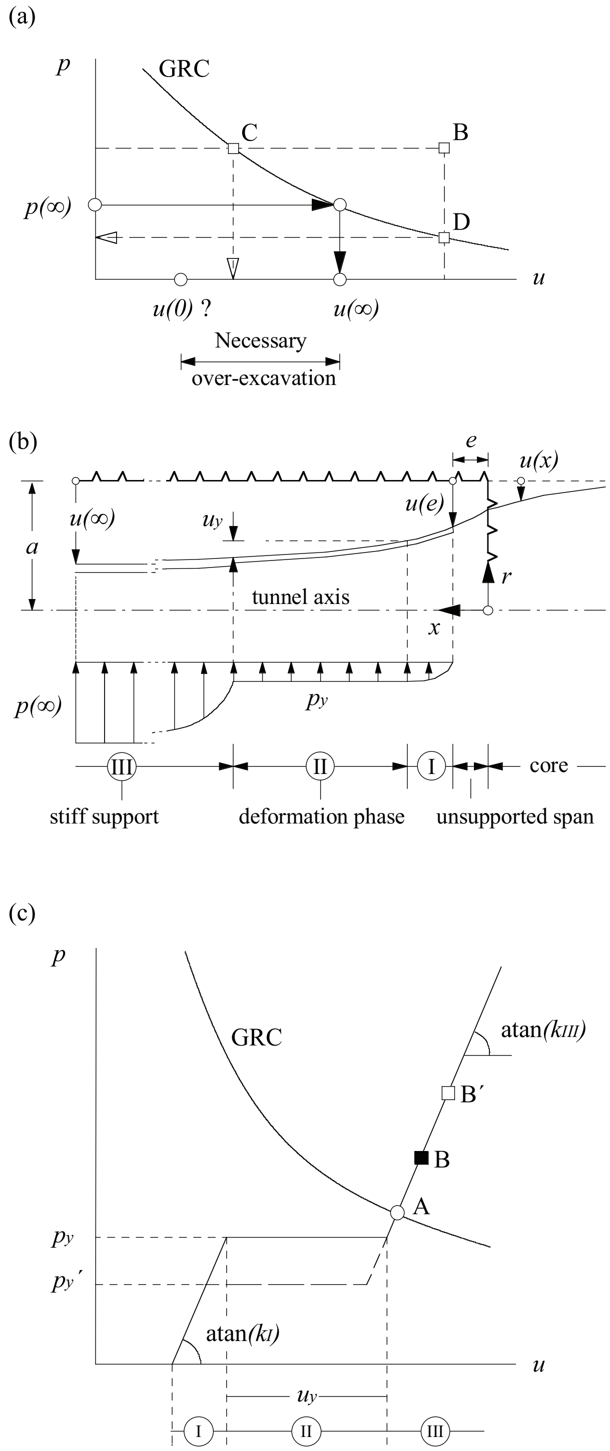

Fig. 3 (a) Determination of amount of over-excavation based upon ground response curve; (b) Development of ground pressure and deformation along the tunnel wall; (c) Ground - support interaction in the rotational symmetry model under plane strain conditions

excavation boundary in the radial direction: the radial boundary stress is equal to zero over the unsupported span $e > x > 0$ between the tunnel face and the installation point of the lining (Fig. 3b). Cantieni and Anagnostou (2007) have shown that the assumption of a monotonically decreasing radial stress may lead (particularly under heavily squeezing conditions) to a more or less serious underestimation of ground pressure and deformation. The actual ($u(\infty)$, $p(\infty)$) - points prevailing at the equilibrium far behind the face are consistently located above the ground response curve (Point B in Fig. 3a). This means that, a plane strain analysis cannot reproduce at one and the same time both the deformations and the pressures: in order to determine the ground pressure through a plane strain solution, the deformations have to be underestimated (point C in Fig. 3a) or, vice versa, in order to determine the deformations, the ground pressure has to be underestimated (point D in Fig. 3a). This is particularly relevant from the design standpoint for a yielding support, because in this case one needs reliable estimates both of the deformations (for determining the amount of over-excavation) and of the pressures (for dimensioning the lining).

Moving on from these results, the present paper investigates the interaction between yielding supports and squeezing ground by means of numerical analyses that take into account the evolution of the spatial stress field around the advancing tunnel heading.

In view of the well-known uncertainties of all computational models in tunnelling (in respect of the initial stress field, the constitutive behaviour and the material constants of the ground), it is reasonable to ask what is the value of such a refined model from the standpoint of practical design. In the present paper we see that an approach that takes account of the stress history leads to results, which are not only quantitatively but also qualitatively different from the ones obtained by plane strain analyses. The most significant and surprising result of our study is that the higher the yield pressure of the support, the lower will be the final pressure. In practical terms, the important conclusion here is that a yielding support should be designed so that it yields at the highest possible pressure. An ideal yielding support is one that starts to deform at a pressure just below the bearing capacity of the lining. As explained below, this result cannot be obtained through a plane strain model.

Figure 3c illustrates the ground - support interaction using the characteristic line method. In the case of rotational symmetry considered here, the radial displacement u vs. pressure p relationship for the yielding support can be obtained from the hoop force N vs. deformation ε curves of the compressible elements by means of simple algebraic operations (Fig. 2). The solid polygonal line in Figure 3c represents an idealized model of the characteristic line of a yielding support. Phase I is governed by the stiffness k_I of the system up to the onset of yielding. In Phase II the support system deforms under a constant pressure p_y. In the example of Figure 2, the yield pressure p_y amounts to 150 - 400 kPa depending on the type of the compressible elements. In the presence of steel sets (Fig. 1b), one should also take into account the resistance offered by the sliding connections (that is $n_f N_f / ba$, where n_f, N_f and b denote the number of friction loops per connection, the frictional resistance of one friction loop and the spacing of the steel sets, respectively). When the amount of over-excavation u_y is used-up, the system is made practically rigid (stiffness k_{III}), e.g. by applying shotcrete, with the consequence that an additional pressure builds up upon the lining (Phase III). Figure 3b shows schematically the development of radial pressure along the tunnel. The amount of over-excavation (u_y) and the yield pressure (p_y) are the main design parameters for a yielding support, while the stiffnesses k_I and k_{III} are of secondary importance for the cases that are relevant in practical terms.

The intersection point of the ground response curve with the characteristic line of the support (Fig. 3c, point A) fulfils the conditions of equilibrium and compatibility and shows the radial ground convergence and the final pressure acting upon the lining far behind the face. In the case of a support having a lower yield pressure p_y' and the same deformation capacity u_y (dashed polygonal line), one would obtain exactly the same intersection point, i.e. the same values of pressure and deformation. According to this approach, the yield pressure has no bearing on the final ground pressure developing upon the lining. We will see, however, that the actual equilibrium points (obtained by spatial, axisymmetric calculations) are located above the ground response curve (obtained under plane strain conditions) and that the final ground pressure is higher in the case of supports involving a lower yield pressure (the points B and B' in Figure 3c apply to yield pressures of p_y and p_y', respectively). Section 2 of this paper explains why this is so, providing thereby a new insight into the problem of ground - support interaction, while Section 3 investigates in detail the influence of the main design parameters (yield pressure p_y, deformation capacity u_y).

The influence of the yield pressure on the final rock pressure has never before been investigated. The literature contains only a few project-specific three-dimensional numerical studies (e.g., Amberg 1999, Fellner and Amann 2004). Furthermore, until now there has been no reliable simplified method for estimating the required amount of over-excavation. Since a plane strain analysis cannot reproduce at one and the same time both the deformation and the pressure, three-dimensional numerical computations are unavoidable at least for heavily squeezing conditions. We carried-out a comprehensive parametric analysis which involved more than 1,500 parameter combinations covering the relevant range of values and we developed dimensionless design nomograms that can be used for estimating the amount of over-excavation when applying yielding supports (Section 4).

All of the computations in the present paper apply to the case of rotational symmetry. The underlying assumptions are: a cylindrical tunnel; uniform support pressure over the circumferential direction (but of course variable in the longitudinal direction); a homogeneous and isotropic ground; a uniform and hydrostatic initial stress field. Figure 4 shows the computational domain and the boundary conditions. The assumption concerning the initial stress field does not allow determining bending moments, which would develop in the case of a non-hydrostatic initial stress field. However, yielding support design is mostly based upon the widely used method of characteristic lines, which assumes rotational symmetry as well and therefore agrees better with the chosen axisymmetric model.

Being aware of the great variety of the existing constitutive models, the mechanical behaviour of the ground was modelled here as linearly elastic and perfectly plastic according to the Mohr-Coulomb yield criterion, with a non-associated flow rule. This constitutive model is widely used in the engineering practice. The lining was modelled as a radial support having a deformation-dependent stiffness $k = dp/du$ (Fig. 3c). Tunnel face support has not been taken into account, and

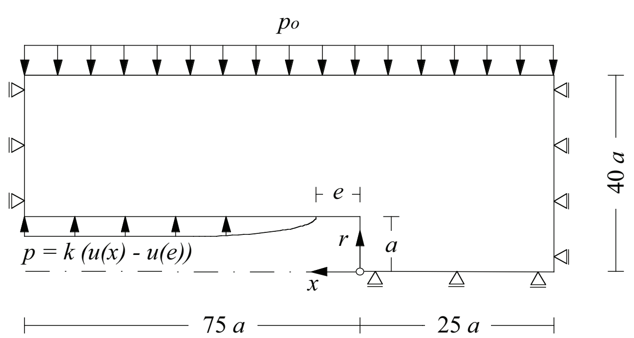

Fig. 4 Model dimensions (not to scale) and boundary conditions

nor have any time dependencies of the behaviour of the ground or of the shotcrete lining. The numerical solutions of the axisymmetric tunnel problem have been obtained by means of the Finite Element Method. The advancing tunnel heading was handled using the so-called "steady state method" (Corbetta 1990, Anagnostou 2007). As mentioned above, plane strain computations are inadequate for the analysis of yielding supports. However, results of such calculations will also be presented in the next Sections for the purpose of comparisons.

2 The influence of the stress path on ground - support interaction

This Section provides some useful insights into the effect of the stress path by a comparative analysis of two hypothetical support cases. Consider firstly a stiff, almost rigid lining (E_L = 30 GPa, d = 35 cm), which is installed at a distance of e = 24 m behind the tunnel face (the other parameters are given in Table 1). Figures 5a and 5b show on their left hand sides ("Support case 1") the support pressure development in the longitudinal direction and the radial displacement of the ground at the excavation boundary, respectively. The final ground pressure $p(\infty)$ prevailing far behind the lining installation point amounts to 700 kPa, while the radial convergence $u(\infty) - u(0)$ of the opening is about 52 cm. As it is assumed that the 24 m long span between the face and the lining has been left unsupported, this case is rather theoretical. It is equivalent, however, to a yielding support which is installed immediately at the tunnel face and which is able to accommodate a radial convergence of at least 52 cm while offering only negligible resistance to the ground in the deformation phase.

Consider now ("Support case 2") a yielding support that is installed directly at the face and offers a resistance of p_y = 700 kPa during the deformation phase (i.e., the yield pressure is assumed to be as high as the final ground pressure $p(\infty)$ in the first case). Let us, additionally, assume that the support is able to accommodate a sufficiently large deformation so that the ground – support system reaches equilibrium at the yield pressure p_y. The final ground pressure will therefore also

Table 1 Model parameters (numerical examples of Section 2 and 3)

Parameter		Value
Initial stress	p_0	12.5 MPa
Depth of cover	H	500 m
Unit weight of ground	γ	25 kN/m^3
Tunnel radius	a	4 m
Young's Modulus (Ground)	E_R	1000 MPa
Poisson's ratio (Ground)	ν	0.3
Angle of internal friction (Ground)	φ	25°
Cohesion (Ground)	c	500 kPa
Dilatancy angle (Ground)	ψ	5°

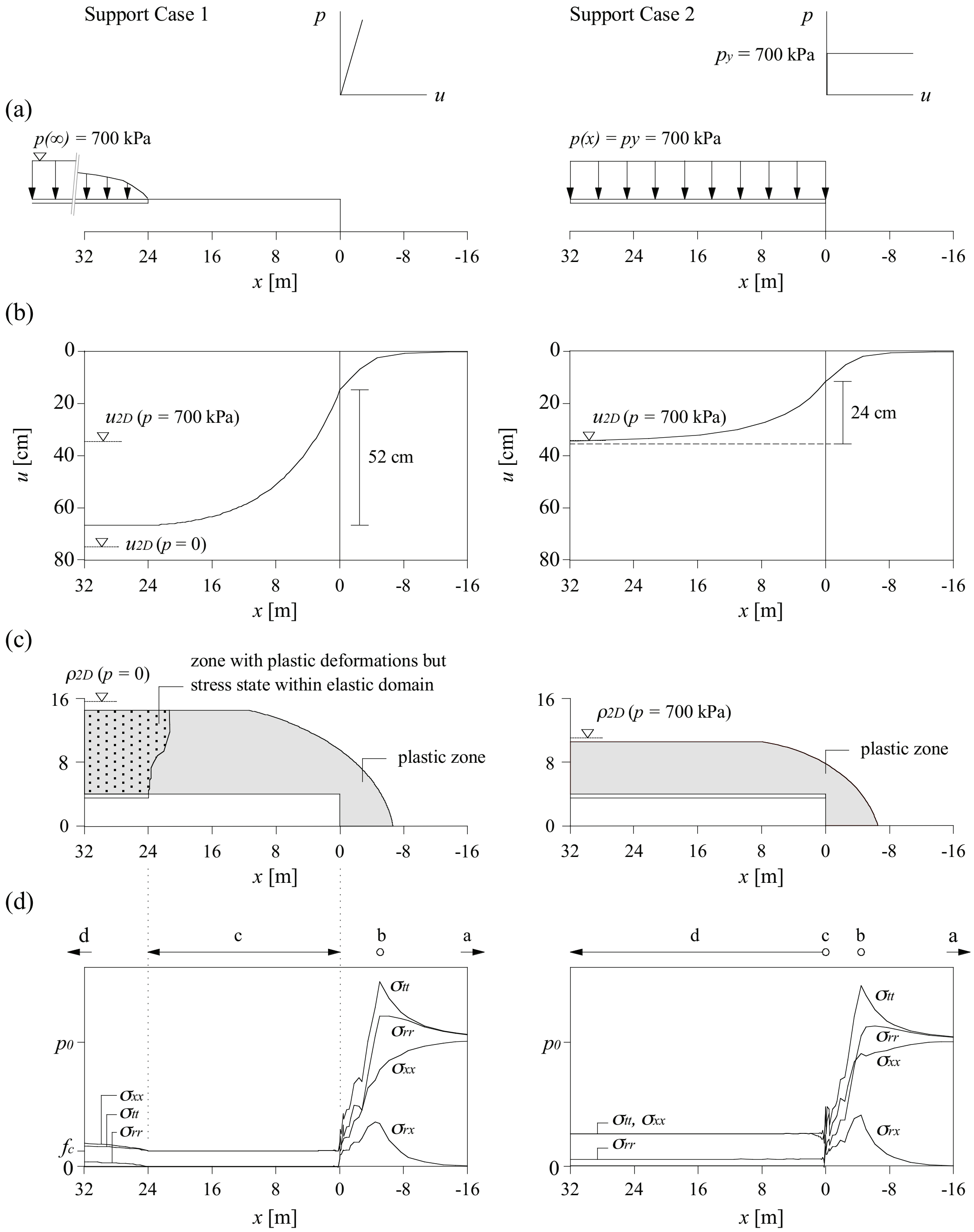

Fig. 5 Numerical results for a stiff support installed at e = 24 m behind the tunnel face (left hand side) and for a yielding support installed at the tunnel face (right hand side). (a) Ground pressure distribution along the tunnel wall (r = 4.01 m); (b) Radial displacement of the ground at the tunnel boundary; (c) Extend of the plastic zone; (d) Evolution of the stresses at the tunnel wall (r = 4.01 m)

amount to 700 kPa in this case. As the final radial convergence of the opening amounts in this case to about 24 cm (Fig. 5b, right hand side), the assumption made (that the system reaches equilibrium at the yield pressure) presupposes that the support is able to accommodate a convergence of at least 24 cm in the deformation phase.

The only difference between the two support cases mentioned above lies in the stress history: in the first case the pressure starts to develop at a distance e = 24 m from the face and reaches its final value of 700 kPa far behind the face, while in the second case the support pressure of 700 kPa acts right from the start (see Fig. 5a). This difference leads to a considerable variation in the longitudinal deformation profiles, particularly in the region behind the tunnel face (Fig. 5b): the final radial displacement of the ground at the excavation boundary is twice as high in support case 1 as it is in support case 2, while the displacements ahead of the tunnel face are approximately equal. In view of the support pressure distributions in Figure 5a, this result makes sense intuitively, while clearly differing from what one might expect under the characteristic line method.

According to the latter, the radial displacement should be the same in both support cases, because the relationship between ground pressure and deformation is unique (the ground response curve is one and the same for both cases as it does not depend on the support behaviour) and both cases have the same final ground pressure p of 700 kPa. For this pressure, a plane strain analysis would predict a radial displacement u_{2D} of approximately 35 cm. This value agrees well with the results of the axisymmetric analysis obtained for support case 2, but underestimates considerably the final displacement in support case 1 (Fig. 5b). For the latter, the axisymmetric analysis leads to a radial displacement, which is closer to the plane strain displacement for an unsupported opening (marked by $u_{2D}(p=0)$ in Fig. 5b).

Similar observations can be made regarding the extent of the plastic deformation zone (Fig. 5c): in support case 2 the final radius of the plastic zone amounts to 10.5 m, which is very close to the plane strain analysis result for a support pressure of 700 kPa (ρ_{2D} = 11.0 m). In support case 1 the plastic zone extends up to a radius of 14.5 m. This value is closer to the plane strain analysis prediction for an unsupported opening (15.6 m).

Figures 5d and 6 show the evolution of the stresses (σ_{xx}, σ_{rr}, σ_{tt}, σ_{rx}) at a point located at the tunnel boundary and the stress path in the principal stress diagram, respectively. The stress state at the

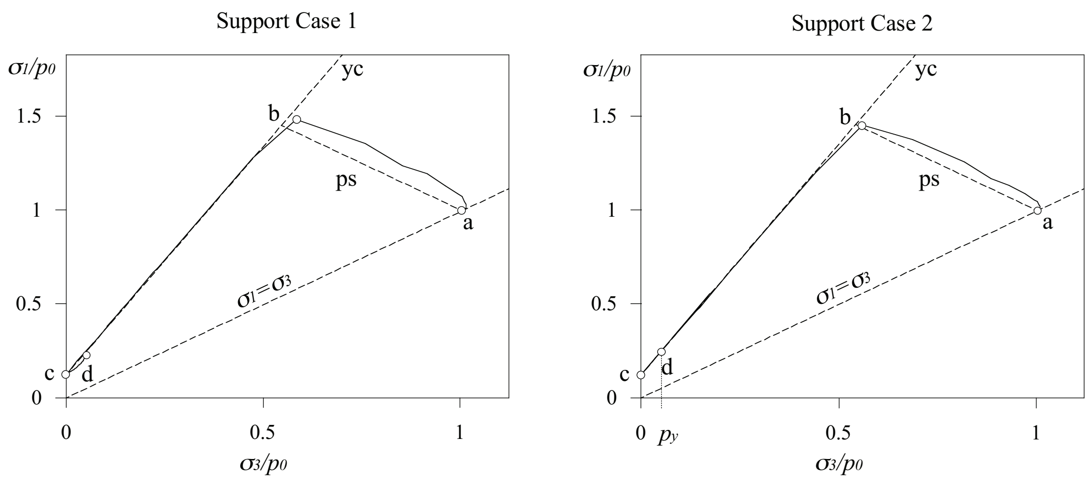

Fig. 6 Stress paths of the ground at the tunnel boundary in the principal stress diagram for a stiff support installed at e = 24 m behind the tunnel face (left hand side) and for a deformable support that reaches equilibrium at the yield pressure of 700 kPa (right hand side). Points "a", "b", "c", "d": stress state at the respective locations indicated in Figure 5d. Straight lines "yc" and "ps": yield condition and stress path under plane strain conditions, respectively

tunnel boundary locations marked by "a", "b", "c" and "d" in Figure 5d is given by the respective points in the principal stress diagram of Figure 6. According to Fig. 5d, the stress paths ahead of the tunnel face are very similar for the two support cases: with the approaching excavation, the axial stress σ_{xx} decreases from its initial value p_0 (in the field far ahead of the face) to zero (at the face). In the region far ahead of the tunnel face, a stress concentration can be observed (stress path portion "ab" in Fig. 6), while close to the face the axial confinement is lost to such a degree that the core yields and, as a consequence of Coulomb's yield criterion, the radial stress σ_{rr} and the tangential stress σ_{tt} decrease (stress path portion "bc" in Fig. 6). Immediately after excavation the radial stress becomes equal to zero, while both the tangential and the axial stresses become equal to the uniaxial compressive strength of the ground f_c (stress state "c" in Fig. 6). This stress state persists in support case 1 over the entire unsupported span. The radial stress increases to its final value of 700 kPa after the installation of the practically rigid lining, because the latter hinders further ground convergence (stress path portion "cd" in Fig. 6). In support case 2, the radial stress increases (due to the initial support stiffness k_l, see Fig. 3c) practically immediately after support installation to the yield pressure p_y and remains constant thereafter.

Plane strain analysis assumes a monotonic decrease in the radial pressure from its initial value (that prevails in the natural state far ahead the face) to the final value (that prevails after excavation far behind the face), while both support cases considered here involve an intermediate stage characterized by a complete unloading of the excavation boundary in the radial direction. The difference between the two support cases lies in the length of this intermediate stage: in support case 1, the biaxial stress state "c" persists over the entire, 24 m long unsupported span, while in support case 2, the stress state remains biaxial only very briefly, almost instantaneously at the face. This is why the intermediate biaxial stress state "c" (zero radial stress) governs both the extent of the plastic zone and the magnitude of ground deformations in support case 1 (the results are closer to the plane strain predictions for an unsupported opening), while the final triaxial stress state "d" (700 kPa radial stress) governs the support case 2 results (the final radius of the plastic zone and the radial displacement agree well with the plane strain results for an actual final support pressure of 700 kPa).

The results of a parametric study with different values for the unsupported span *e* provide additional evidence for the significance of the intermediate stage. Figure 7a shows the ground pressure $p(\infty)$ and the radial displacement of the ground $u(\infty)$ at the final equilibrium prevailing far behind the face for the two support cases discussed above as well as, for the purpose of comparison, the ground response curve obtained under plane strain conditions. Note that each point under support case 1 applies to another value of the unsupported length *e* (the *e* - values are reported besides the ordinate axis), while each point under support case 2 applies to another value of the yield pressure p_y (the p_y - values are equal to the final pressures $p(\infty)$ on the ordinate axis). The diagram illustrates quite plainly the non-uniqueness of the ground pressure vs. ground displacement relationship: the equilibrium points for support case 1 are consistently located above the ground response curve, while all of the support case 2 results agree well with the plane strain predictions.

Figure 7b is more useful from a practical point of view as it shows the radial convergence $u(\infty)$ - $u(0)$ of the opening instead of the radial displacement $u(\infty)$ of the ground. This diagram includes only the results of the axisymmetric computations because plane strain analysis yields the total radial displacement $u(\infty)$, but not the pre-deformation $u(0)$. Note that $u(\infty) - u(0)$ represents the minimum amount of over-excavation that is necessary in order to preserve the clearance profile. The

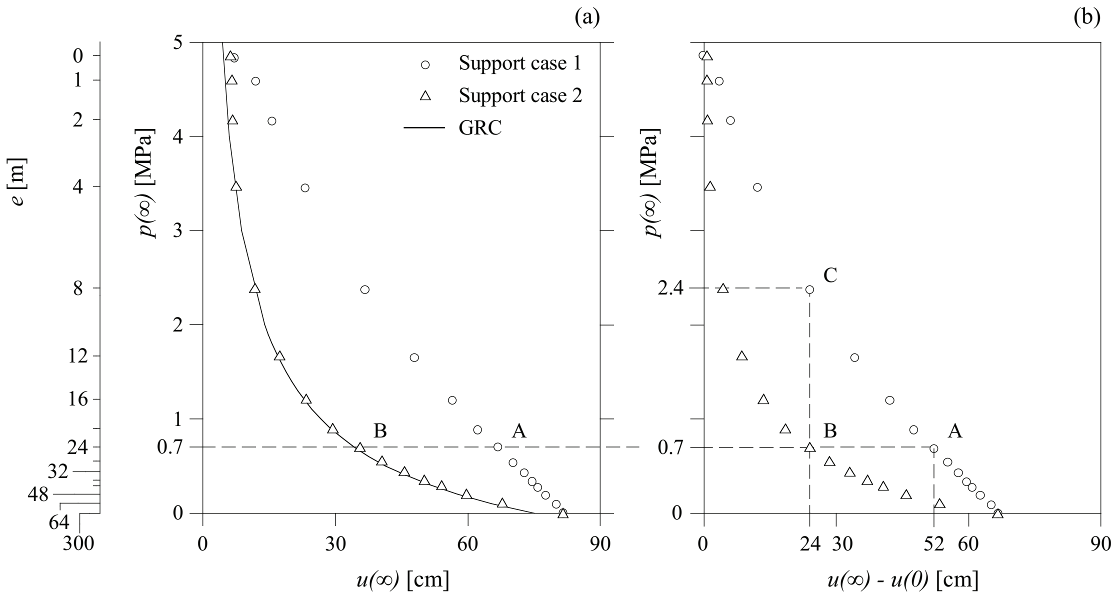

Fig. 7 (a) Ground response curve under plane strain conditions and final equilibrium points for a stiff support installed at a distance e behind the tunnel face ("support case 1") and for a deformable support that is installed at the tunnel face and has such a large deformation capacity that it reaches equilibrium at the yield pressure ("support case 2"); (b) Radial convergence of the tunnel wall and ground pressure at equilibrium for the two support cases

purpose of a yielding support is to reduce ground pressure to a pre-defined, structurally manageable level. Figure 7b points to the interesting conclusion that the amount of over-excavation - an essential design parameter - does not depend only on the ground quality and on the desired design load level, but also on the characteristics of the support. In order to reduce the ground pressure to 0.7 MPa, for example, the amount of over-excavation has to be 24 - 52 cm depending on the support system (see points A and B in Fig. 7b). On the other hand, for a given amount of over-excavation, the final ground load will depend on the support characteristics as well. For an over-excavation of, e.g., 24 cm, the final ground pressure in support case 1 will amount to 2.4 MPa, that is three to four times higher than the load in case 2 (see points B and C in Fig. 7b). This difference is considerable from a design standpoint.

Note that support case 1, which necessitates a larger amount of over-excavation for a given design load level (or attracts a higher ground load for a given amount of over-excavation), is equivalent to the case of a deformable support with negligible yield pressure. So Figure 7b actually indicates that a high yield pressure is favourable in terms of the final ground load and the amount of over-excavation. Moving on from this finding, we will examine in Section 3 the influence of yield pressure in more detail.

Before doing so, however, we will briefly examine the theoretical case of a ground with elastic behaviour. The response of an elastic material does not depend on stress history. Consequently, in both of the support cases discussed above, the final ground pressure and the ground displacement will fulfil Kirsch's solution, i.e. the final equilibrium points prevailing far behind the tunnel face will be located on the straight ground response line. The value of the final ground pressure fixes the value of the final ground displacement. The final ground displacement does not depend on how the radial stress at the excavation boundary evolves before reaching its final value. So, the ground displacement $u(\infty)$ will be the same for the two support cases in Figure 5. The pre-deformation $u(0)$, however, will be smaller in case 2, because the support exerts a pressure earlier than in case 1, which involves support installation at a greater distance behind the face. Consequently, the convergence of the opening $u(\infty) - u(0)$, i.e. the amount of over-excavation required, will be larger in case 2 for a given ground displacement $u(\infty)$ or for a given ground pressure $p(\infty)$. Also, for a given amount of over-excavation, the ground loading developing in case 2 will be higher than in case 1. This conclusion is diametrically opposite to the results obtained for elasto-plastic ground. The case of elastic ground behaviour is interesting only from the theoretical point of view, because large convergences that necessitate a yielding support are always associated with an overstressing of the ground and cannot be reproduced by assuming elastic material behaviour. Our examination of elastic behaviour shows, however, that the conclusions of the present paper are valid for heavily squeezing ground in particular.

3 The influence of yield pressure and yield deformation

In this Section we investigate numerically the effects of the main yielding support characteristics. All of the numerical analyses have been carried out for the parameters of Table 1 and an unsupported span of e = 1 m. For the sake of simplicity, the tunnel radius was kept fixed, i.e., it was not increased by the amount of over-excavation that is required in order to preserve the clearance profile when the support deforms. Figure 8a shows the characteristic lines of the tunnel supports, while Table 2 summarizes the numerical values of their parameters. The yielding supports are assumed to deform at a constant pressure p_y of 0 - 1.2 MPa up to a radial displacement of u_y = 0.15 m (cases O, A, B, C and D) or 0.30 m (cases O', A', B', C' and D') and to be practically rigid after the deformation phase. Yielding pressures like the ones assumed for cases A, A', B and B' are today realistic. Recently developed ductile concrete elements of particularly high yield strength (up to 20 MPa, Solexperts 2007) make higher yield pressures (such as in cases C and C') seem feasible at least in principle. Cases D and D' are only of theoretical interest (the assumed yield pressure is unrealistically high) and are considered here only in order to show complete model behaviour. The same is true for support S, whose yield pressure has been set so high that the ground - support system reaches equilibrium before the support yields.

The marked points in Figure 8a represent the loading $p(\infty)$ and the radial displacement $u(\infty) - u(e)$ of the support at the equilibrium state far behind the tunnel face. Figure 8b shows the corresponding equilibrium points $(u(\infty), p(\infty))$ of the ground and additionally, for the purposes of comparison, the ground response curve under plane strain conditions (solid line GRC) as well as the ground pressure and deformation for a practically rigid lining (point R).

As the effect of yield deformation u_y is well known, attention is paid here to the effect of yield pressure p_y. We examine how the equilibrium point changes in relation to the yield pressure p_y (cases A, B, C, …) starting with a support that can undergo a radial displacement of u_y = 15 cm without offering any resistance to the ground (case O). The support O starts to develop pressure only after the utilization of the deformation margin u_y. As can be seen from Figure 8c (curve O), this happens

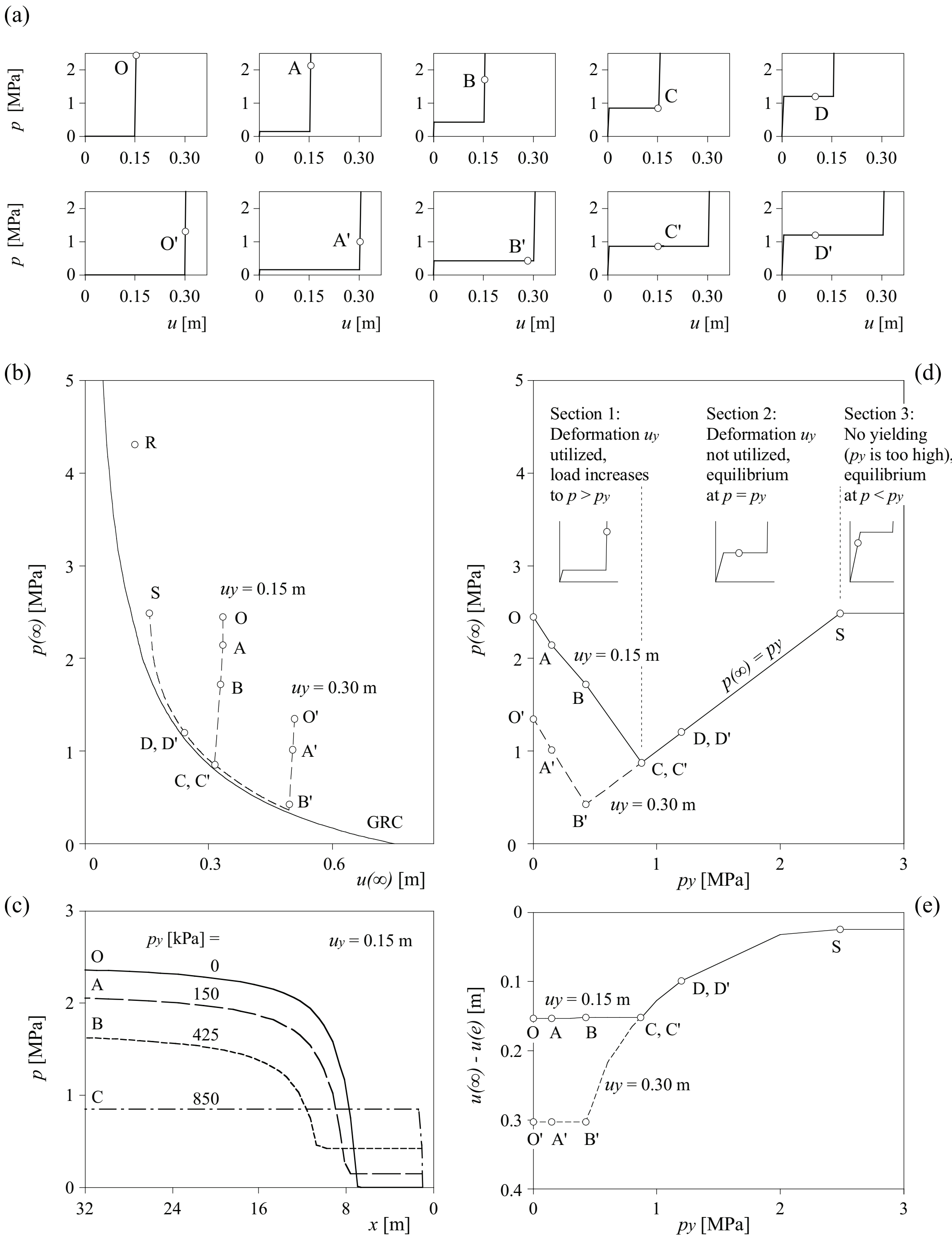

Fig. 8 (a) Characteristic lines of the analyzed yielding supports (cf. also Table 2) and final equilibrium points; (b) Ground response curve under plane strain conditions and final equilibrium points for the analyzed supports; (c) Ground pressure p vs. distance x behind the face for different values of the yield pressure p_y (support cases O, A, B and C); (d) Influence of the yield pressure p_y on the final ground pressure; (e) Influence of the yield pressure p_y on the radial displacement $u(\infty) - u(e)$ of the support

at a distance of about 7 m behind the tunnel face. So, support O is structurally equivalent to the case of a practically rigid lining with a 7 m long unsupported span (cf. Support Case 1 discussed in Section 2). Due to the stress path dependency of the ground behaviour (cf. Section 2), the equilibrium point for this case is located above the plane strain response curve. When the yield pressure

Table 2 Support parameters (see also Fig. 3c)

Case	k_I [(1)] [MPa/m]	p_y [kPa]	u_y [cm]	k_{III} [MPa/m]	Description	n [-]	s [cm]
R	n/a	n/a	0	656	35 cm thick lining according to resistance principle (E_L = 30 GPa).	n/a	n/a
O (O')	n/a	0	15 (30)	656	35 cm thick shotcrete lining with open longitudinal slots (E_L = 30 GPa[(2)]).	6 (6)	15 (30)
A (A')	100	150	15 (30)	656	Steel sets TH-44 spaced at 1 m with sliding connections by 4 friction loops each offering a resistance of 150 kN[(3)].	6 (6)	15 (30)
B (B')	100	425	15 (30)	656	Like A, but additionally 20 cm shotcrete with highly deformable concrete elements inserted into the slots (ε_y = 50%, f_y = 7 MPa, cf. Solexperts 2007).	6 (9)	30 (40)
C (C')	100	850	15 (30)	656	Like B, but with higher yield strength elements (f_y = 17 MPa, Solexperts 2007).	6 (9)	30 (40)
D (D')	100	1'200	15 (30)	656	Like C, but with a higher yield pressure.[(4)]	6 (9)	30 (40)
S	100	> 2'500	-[(5)]	-[(5)]	Like C, but with such a high yield pressure that yielding does not occur[(4)].	-[(5)]	-[(5)]

Notes:

(1) This parameter was kept constant in the numerical study as it is of subordinate importance. The actual k_I - values of the support systems described in the last columns of the table are 74 MPa/m (cases A and A'), 97 MPa/m (cases B' and C') and 114 MPa/m (cases B and C). A sensitivity analysis has shown that a variation of k_I in this range does not affect the numerical results.

(2) This value assumes that, by the time the longitudinal slots close, the shotcrete will have developed its final stiffness.

(3) After the yield phase, the support is set practically rigid (d_{III} = 35 cm, E_L = 30 GPa).

(4) The assumed yield pressure is only theoretically possible. This support has been simulated only in order to explain the model behaviour.

(5) The parameter is irrelevant for this case.

increases, the final ground pressure will decrease (Fig. 8c) and the equilibrium point will move towards the ground response curve (O→A→B, see Fig. 8b), i.e. the deviation from the ground response curve will become smaller at higher yield pressure values. Note that the ground deformation remains approximately constant as it is governed by the yield deformation u_y which is the same for the support cases O, A and B. At a sufficiently high yield pressure (850 kPa in this numerical example), the equilibrium point reaches the ground response curve (case C, Fig. 8b). In case C the ground - support system reaches equilibrium just before reaching the final rising branch of the characteristic line of the support, i.e. the deformation margin u_y = 0.15 m is just used up. At yield pressures higher than in case C, the amount of over-excavation is not utilized completely (Fig. 8a, case D) and the system reaches equilibrium at a ground pressure which is equal to the yield pressure. Consequently, the ground pressure, after reaching a minimum value (case C), increases with the yield pressure and, as discussed in Section 2, the equilibrium points approximately follow the ground response curve (Fig. 8b, C→D). Similar conclusions can be drawn from an examination of the numerical results for the larger deformation margin of u_y = 0.30 m (cases O', A', B', …). The deviation from the ground response curve is due to the increase in stress associated with the final rising branch of the characteristic line of the support after the deformation margin is used up (see Fig. 8a and 8b, cases O, A, B, O', A').

Figures 8d and 8e provide a complete picture of the effect of yield pressure p_y on the final ground loading $p(\infty)$ and on the lining convergence $u(\infty)$ - $u(e)$, respectively. There are three clear sections in the $p(\infty)$ vs. p_y and $(u(\infty)$ - $u(e))$ vs. p_y relationships: at low yield pressures (Fig. 8d, section 1), the amount of over-excavation is completely used up and an additional pressure builds up on the lining after the system is set rigid. The lining convergence remains practically constant and equal to the deformation margin u_y, while the ground load decreases with increasing yield pressure and reaches a minimum when the yield pressure is so high that the amount of over-excavation is just used up. At higher yield pressures (Fig. 8d, section 2), the squeezing deformations take only a fraction of the available deformation margin; the system comes to equilibrium under the yield pressure p_y and, therefore, the ground loading increases with p_y. With further increasing yield pressure, the deformation margin is utilized less and less, and at some point the system reaches equilibrium just before the onset of the yielding phase. From point S on (Fig. 8d, section 3), the yield pressure is no longer relevant (the loading and convergence of the support depend only on its initial stiffness).

It is remarkable that a similar reduction in the final ground pressure can be achieved not only by installing a support that is able to accommodate a larger deformation (which is a well-known principle), but also by selecting a support that yields at a higher pressure (see, e.g., cases A, C and C' in Fig. 8d).

4 Design nomograms

The relationship between the ground pressure $p(\infty)$ and deformation $u(\infty)$ at the final equilibrium far behind the face is not unique, but depends on the support characteristics, as these will affect the stress history of the ground surrounding the tunnel. In general, the ground - support equilibrium points are located above the ground response curve. The ground response curve defines the lower limits for possible ground - support equilibria and it therefore contains the most favourable equilibrium points, because it shows the minimum ground deformation that must take place in order for the ground pressure to decrease from its initial value to a given value. It also shows, vice versa, the minimum ground pressure at equilibrium for a given ground deformation.

Under which conditions do the equilibrium points fall on the ground response curve? According to the previous Section of this paper, deviations from the ground response curve are associated with the final rising branch of the characteristic line of the support and with the increase in radial stress, which follows the utilization of the deformation capacity u_y of the support. When the ground - support system reaches equilibrium at the yield pressure p_y, the history of the radial stress at the excavation boundary is similar to the stress history assumed by the plane strain model and this leads to equilibrium points which are located very close to the ground response curve. Since reaching equilibrium at the yield pressure p_y necessitates a sufficiently large deformation capacity u_y of the support, the yield pressure should be as high as possible in order to limit the amount of over-excavation. So, the ideal support system in squeezing ground is one that yields just before the ground pressure reaches the bearing capacity of the support.

Today's realistic yield pressures, however, are in general lower than the feasible long-term bearing capacities of tunnel supports. Consequently, if a support were able to accommodate such a large deformation u_y that it reached equilibrium at the yield pressure p_y, then its bearing capacity would be under-utilized. In order to bridge the difference between yield pressure and the bearing capacity of the support, the deformation margin u_y has to be used up completely and the ground pressure has to increase above the yield pressure. As explained above, plane strain computations are in this case inadequate as the actual equilibrium points are consistently located above the ground response curve. An analysis of ground - support interaction must take account of the stress history of the ground and this necessitates a spatial analysis. To facilitate the design of yielding supports for tunnels through squeezing ground, we carried-out a large number of such analyses and we worked

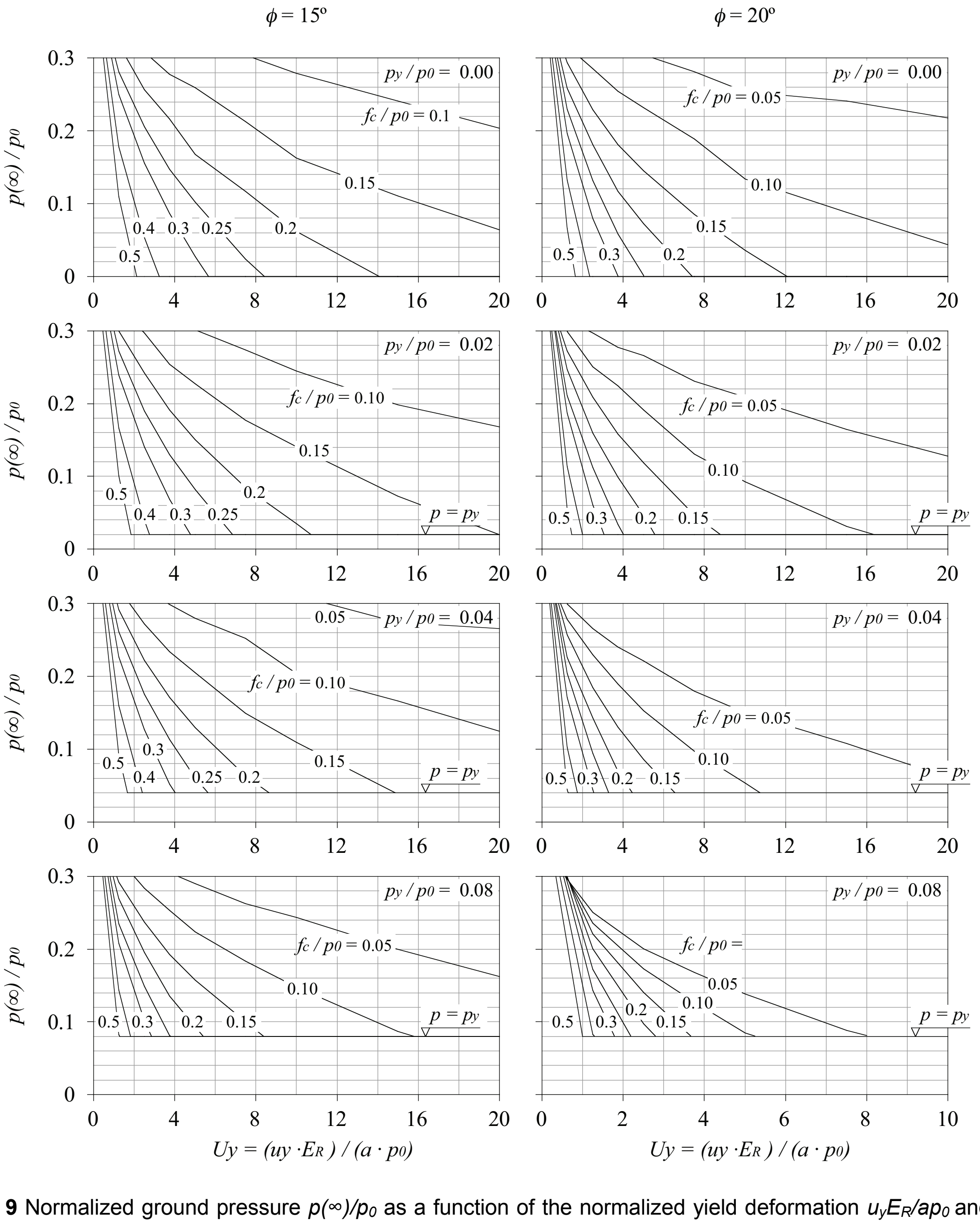

Fig. 9 Normalized ground pressure $p(\infty)/p_0$ as a function of the normalized yield deformation u_yE_R/ap_0 and of the normalized uniaxial strength of the ground f_c/p_0 for friction angles ϕ = 15 or 20° and for normalized yield pressures p_y/p_0 = 0 - 0.08 (other parameters: ν = 0.30, ψ = max (0, ϕ - 20°), e/a = 0.25, $ak_I/E_R = ak_{III}/E_R$ = 4)

out dimensionless nomograms that cover the relevant parameter range.

The final ground pressure $p(\infty)$ developing upon the support far behind the tunnel face depends in general on the material constants of the ground (E_R, ν, f_c, ϕ, ψ), on the initial stress p_0, on the problem geometry (tunnel radius a, unsupported span e) and on the support parameters taken from Figure 3c (u_y, p_y, k_I, k_{III}):

$$p(\infty) = f\left(E_R, \nu, f_c, \phi, \psi, p_0, a, e, u_y, p_y, k_I, k_{III}\right) \ . \tag{1}$$

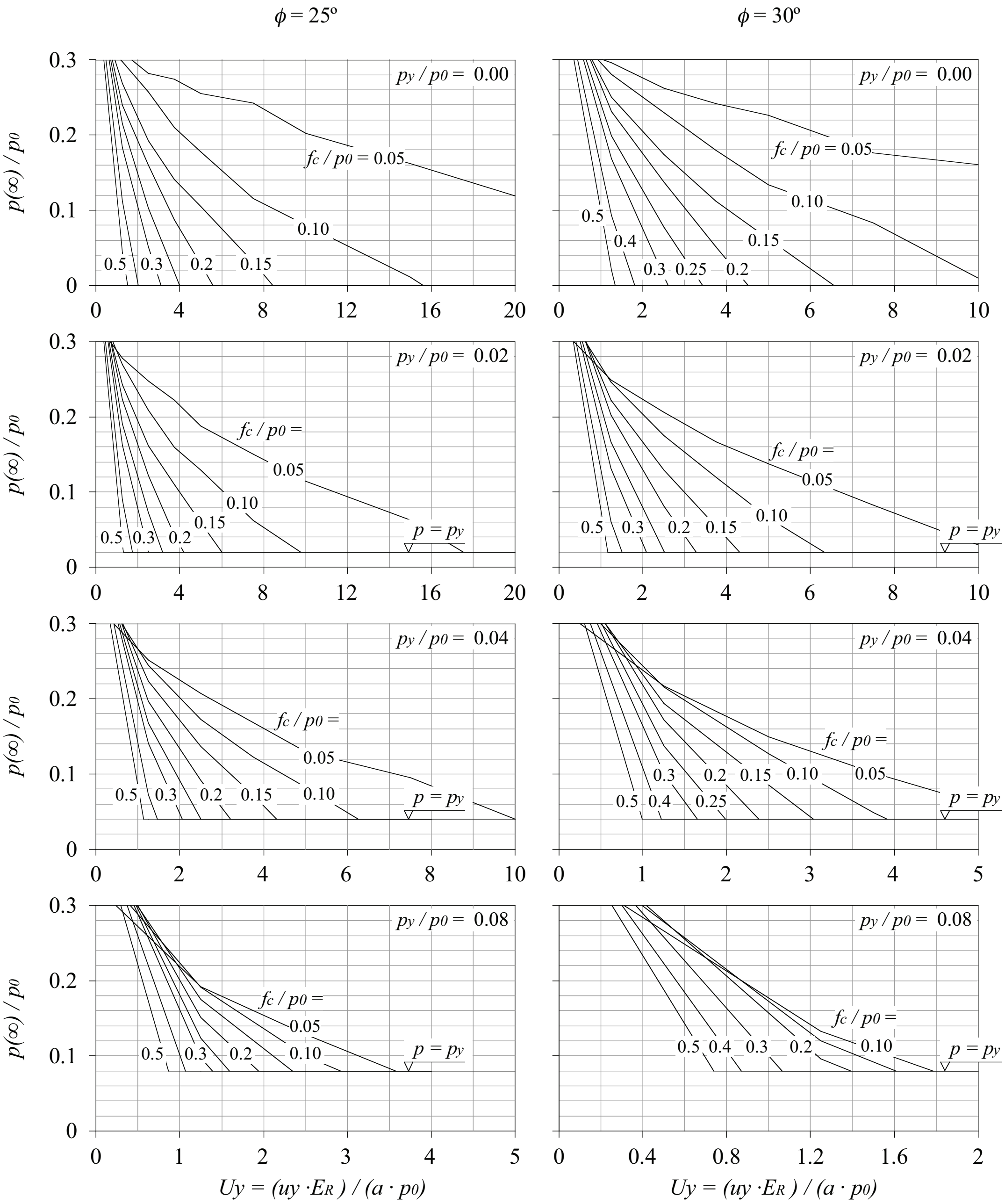

Fig. 10 Normalized ground pressure $p(\infty)/p_0$ as a function of the normalized yield deformation u_yE_R/ap_0 and of the normalized uniaxial strength of the ground f_c/p_0 for friction angles ϕ = 25 or 30° and for normalized yield pressures p_y/p_0 = 0 - 0.08 (other parameters: ν = 0.30, ψ = max (0, ϕ - 20°), e/a = 0.25, $ak_I/E_R = ak_{III}/E_R$ = 4)

The number of parameters can be reduced from twelve to nine by performing a dimensional analysis and by also taking account of the fact that the displacements of an elasto-plastic medium depend linearly on the reciprocal value of the Young's modulus E_R (Anagnostou and Kovári, 1993):

$$\frac{p(\infty)}{p_0} = f\left(\frac{u_y E_R}{a p_0}, \frac{f_c}{p_0}, \frac{p_y}{p_0}, \phi, \nu, \psi, \frac{e}{a}, \frac{a k_I}{E_R}, \frac{a k_{III}}{E_R}\right) . \tag{2}$$

In view of the still large number of variables, a trade-off has had to be made between the completeness of the parametric study and the cost of computation and data processing. In order to limit

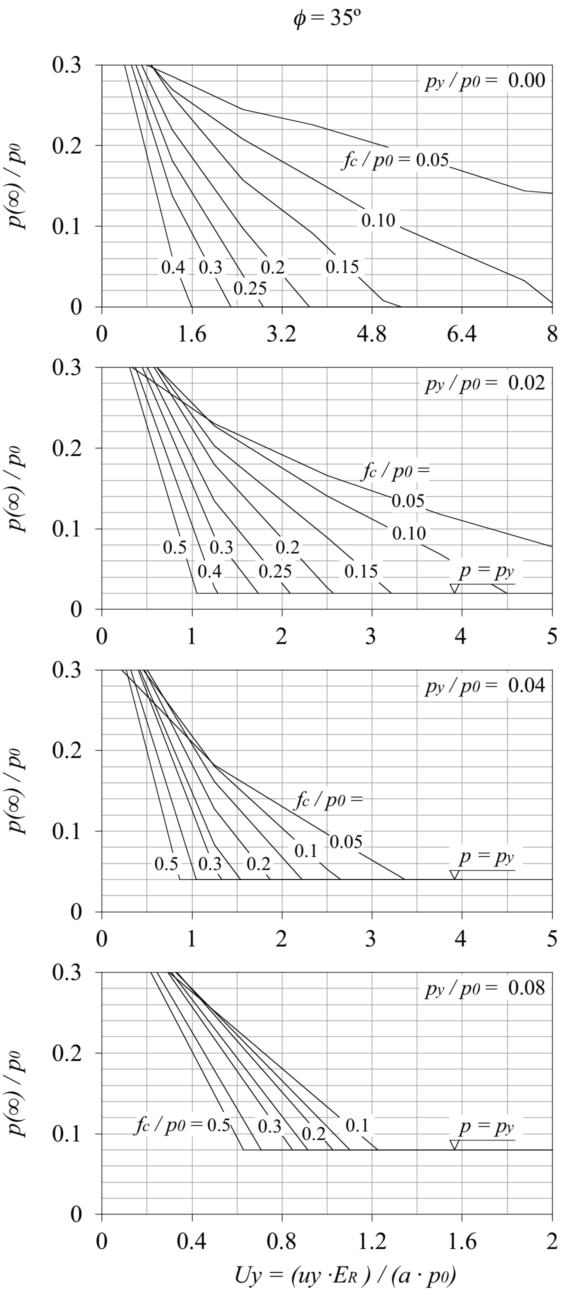

Fig. 11 Normalized ground pressure $p(\infty)/p_0$ as a function of the normalized yield deformation u_yE_R/ap_0 and of the normalized uniaxial strength of the ground f_c/p_0 for friction angle ϕ = 35° and for normalized yield pressures p_y/p_0 = 0 - 0.08 (other parameters: ν = 0.30, ψ = max (0, ϕ - 20°), e/a = 0.25, $ak_I/E_R = ak_{III}/E_R$ = 4)

the amount of numerical calculations and the number of nomograms, the Poisson's number of the ground was kept constant to $\nu = 0.3$, while the angle of dilatancy ψ was taken equal to ϕ - 20° for ϕ > 20° and to 0° for ϕ < 20° (Vermeer and Borst, 1984). Furthermore, the ratio e/a was kept constant to 0.25 in accordance with common round lengths of e = 1 - 1.5 m and typical cross section sizes of traffic tunnels (a = 4 - 6 m). Finally, the supports have been assumed to be practically rigid up to the onset of the yielding phase as well as after the utilization of the deformation capacity ($ak_I/E_R = ak_{III}/E_R = 4$). The initial support stiffness ak_I/E_R is of subordinate importance for the final ground pressure, but the assumption of practically rigid behaviour after the deformation phase may lead to a considerable overestimation of the ground pressure if the actual stiffness ak_{III}/E_R is much lower than the value assumed for the numerical calculations. Comparative numerical analyses have shown that the error involved in a rigid support assumption is small (an overestimation of ground pressure by up to 10-20%) if the normalized final support stiffness ak_{III}/E_R is higher than 1-2 or if the lining is thicker than $a(E_R/E_L)$, where a, E_R and E_L denote the tunnel radius and the Young's Modulus of the ground and of the lining, respectively. This condition is fulfilled in most cases of tunnelling through squeezing ground.

The nomograms in Figures 9 to 11 apply to different values of friction angle ϕ and yield pressure p_y. They show the normalized ground pressure $p(\infty)/p_0$ as a function of the normalized yield deformation $u_y E_R/ap_0$ and allow an estimation to be made of the amount of deformation that must take place in order for the ground pressure to decrease to a technically manageable level. Note that the nomograms are based on the assumptions mentioned at the end of Section 1. If the actual conditions deviate from these assumptions, the results should be considered with care. For example, a non-hydrostatic stress field or a non-circular cross-section may lead to considerable asymmetric convergences or the development of high bending moments in the lining. The nomograms represent, nevertheless, a valuable decision making aid at least in the preliminary design phase.

5 Application examples

Table 3 shows, by means of two practical examples, how to apply the nomograms step by step.

The first example (Columns 1 to 3) refers to a 250 m deep tunnel. Column 1 applies to a yielding support consisting of steel sets with sliding connections that deform at a ground pressure p_y of 60 kPa (Rows 15 to 22). For a lining thickness of 30 cm following the deformation phase and a design value of 15 MPa for the lining hoop stress σ_s, the final pressure $p(\infty)$ amounts to 0.9 MPa (Rows 11 to 13). In order to reduce the ground pressure to this value, the support should be able to accommodate a deformation u_y of 33 cm (Rows 23 to 25). This can be realized by arranging six 34 cm wide longitudinal slots in the shotcrete shell (Rows 26 and 27).

Assume now that, in addition to the over-excavation and to the support measures according to Column 1, deformable concrete elements of 10 MPa yield strength are applied, thereby increasing the yield pressure p_y to 380 kPa (Column 2, Rows 20 to 22). As the deformable concrete elements become practically rigid at a strain ε_y of about 50% (Fig. 2), the support will experience a convergence u_y of only 16 cm during the deformation phase (Row 25). For these values of yield pressure p_y and deformation u_y, the ground pressure will rise to $p(\infty)$ = 0.68 MPa after the deformation phase

Table 3 Application examples

			(a) 250 m deep tunnel crossing claystones			(b) 800 m deep tunnel crossing sheared rock	
			1	2 (16)	3	4	5
1	Tunnel radius	a [m]	5			5	
2	Depth of cover	H [m]	250			800	
	Ground						
3	Unit weight	γ [kN/m^3]	20			25	
4	Young's Modulus	E_R [MPa]	300			1500	
5	Poisson's ratio	ν [-]	0.3			0.3	
6	Uniaxial compr. strength	f_c [kPa]	500			2000	
7	Angle of internal friction	φ [º]	25			25	
8	Dilatancy angle	ψ [º]	5			5	
9	Initial stress (1)	p_0 [MPa]	5			20	
10	Normalized compr. strength	f_c / p_0 [-]	0.1			0.1	
	Support after deformation phase						
11	Lining thickness	d_{III} [cm]	30	30	30	50	50
12	Concrete compress. stress	σ_s [MPa]	15	11.3 (15)	15	15	15
13	Final ground pressure	$p(\infty)$ [MPa]	0.9 (2)	0.68 (14)	0.9 (2)	1.5 (2)	1.5 (2)
14	Normalized ground pressure	$p(\infty) / p_0$ [-]	0.180	0.135 (13)	0.180	0.075	0.075
	Support during deformation phase						
15	Steel set spacing	b [m]	1.0			1.0	
16	Steel set clear distance	b' [m]	0.8			0.8	
17	Friction loop resistance	N_f [kN]	150			150	
18	Lining thickness	d_{II} [cm]	20			20	
19	Number of friction loops	n_f [-]	2	2	2	2	4
20	Yield stress of deform. elem.	f_y [MPa]	0	10	10	0	10
21	Max. slot deformation	ε_y [-]	100%	50%	50%	100%	50%
22	Yield pressure of support (3)	p_y [kPa]	60	380	380	60	440
23	Normalized yield pressure	p_y / p_0 [-]	0.012	0.076	0.076	0.003	0.022
24	Normalized yield deformation	U_y [-]	3.9 (4)	2 (12)	1.4 (5)	10 (6)	7 (7)
25	Yield deformation	u_y [cm]	33 (8)	16 (11)	12 (8)	67 (8)	47 (8)
26	Number of slots	n [-]	6	6	6	6	8
27	Slot size	s [cm]	34 (9)	34 (10)	25 (9)	70 (9)	74 (9)

Notes:

(1) $p_0 = H \gamma$

(2) $p(\infty) = \sigma_s d_{III} / a$

(3) $p_y = N_y / a$, where $N_y = n_f N_f / b + d_{II} b' f_y$

(4) Based upon interpolation between nomograms for (ϕ, p_y / p_0) = (25°, 0) and (25°, 0.02) in Fig. 10 (curves for f_c / p_0 = 0.1, $p(\infty) / p_0$ according to Row 14)

(5) As Note (4) but from nomogram for p_y / p_0 = 0.08

(6) As Note (4) but from nomogram for p_y / p_0 = 0.00

(7) As Note (4) but from nomogram for p_y / p_0 = 0.02

(8) $u_y = U_y a p_0 / E_R$

(9) $s = 2 \pi u_y / (n \varepsilon_y)$

(10) Value taken as in column 1

(11) $u_y = n s \varepsilon_y / (2 \pi)$

(12) $U_y = u_y E_R / (a p_0)$

(13) From Fig. 10, nomogram for ϕ = 25° and p_y / p_0 = 0.08 (curves for f_c / p_0 = 0.1, U_y acc. to Row 24)

(14) $p(\infty) = p_0 \ (p(\infty) / p_0)$

(15) $\sigma_s = p(\infty) a / d_{III}$

(16) In this column, the calculation proceeds from bottom to top

(Rows 24, 23, 14 and 13). The final hoop stress σ_s in the shotcrete shell is by 33% lower than it would be without deformable concrete elements (cf. Columns 1 and 2, Row 12). So, for the same amount of over-excavation and for the same number *n* and size *s* of longitudinal slots, the application of the higher yield pressure support reduces the risk both of a violation of the clearance profile during the deformation phase (since only 50% of the deformation margin of 33 cm is used up) and of an overstressing of the shotcrete shell after the deformation phase (since the hoop stress σ_s is by 33% lower than the design value of 15 MPa).

Alternatively, for the same final hoop stress (σ_s = 15 MPa), the minimum over-excavation and the size of the longitudinal slots can be reduced to 12 cm and 25 cm respectively by applying the higher yield pressure support (Column 3, Rows 25 and 27). In addition, the higher yield pressure will increase protection against crown instabilities during the deformation phase: Depending on the strength and on the structure of the rock mass, structurally-controlled block detachment or stress-induced loosening of an extended zone around the opening may occur (particularly in the case of a yielding support, as it promotes loosening by allowing the occurrence of larger deformations). If the resistance of the flexible joints is not sufficiently high, the support will experience settlement under the weight of the detached rock mass, with the result that both the over-excavation space and the deformation capacity of the support will be used up and therefore the behaviour of the support during subsequent squeezing will resemble that of a support based on the resistance principle. In order to safeguard against crown instabilities and to preserve the deformation capacity of the support, there has to be either a sufficiently high yield pressure (so that the lining does not deform already under the loosening pressure) or additional support through sufficiently long bolts.

Example (a) of Table 3 suggests the possibility of a trade-off between, on the one hand, the greater structural effort associated with achieving a high yield pressure, and on the other hand a larger amount of over-excavation (possibly in combination with more bolting). It should be noted, however, that such a trade-off may often not be possible. In mechanized tunnelling, for example, the options for a trade-off are reduced dramatically as the boring diameter largely pre-determines the space that is available for support (d_{III}) and deformation (u_y). At the same time, achieving a yield pressure p_y that is higher than the loosening pressure may be difficult for traffic tunnels of large diameter, because the potential size and loading of the loosened zone increases with the size of the opening (Terzaghi 1946), while the feasible yield pressure p_y of the support decreases with the tunnel radius *a* for given lining hoop force N_y ($p_y = N_y/a$), and structural detailing and material technology impose limits on the hoop force N_y. For example, deformable concrete elements of high yield strength increase the hoop force N_y but may cause overstressing of the green shotcrete if the rock pressure develops quickly. This aspect may be important particularly for mechanized tunnelling, as the daily advance may reach several meters even under adverse conditions.

Finally, the intensity of squeezing may also constrain the decision space. Columns 4 and 5 of Table 3 refer to an example with the particularly heavy squeezing conditions that are associated with very high overburden and sheared rock of low strength. In the case of a support consisting of steel sets with six sliding connections in the deformation phase and a 50 cm thick concrete lining afterwards, the required amount of over-excavation u_y and the sliding way *s* of the connections amount to 67 and 70 cm, respectively (Column 4). By applying a support of higher yield pressure (Column 5, Rows 19 and 20), the amount of over-excavation u_y can be reduced to 47 cm (Row 25). This convergence would necessitate the application of deformable concrete elements in eight, 74 cm wide longitudinal slots (note that the concrete elements can shorten by a maximum of ε_y = 50%). Deformable concrete elements of such a size have not been used in practice. The application of several smaller elements side by side would reduce the handling difficulties associated with weight, but only at the expense of reducing the flexural stiffness of the lining. The latter is important in the case of asymmetric squeezing. A larger number of longitudinal slots would involve a very great structural effort and would also necessitate closely spaced bolts in order to control the risk of a snap-through in the case of non-uniform rock deformation.

6 Closing remarks

We have shown that an analysis of the ground – yielding support interaction that takes into account the stress history of the ground leads to conclusions which are qualitatively different from those obtained through plane strain analysis. The ground pressure developing far behind the tunnel face in a heavily squeezing ground depends considerably on the amount of support resistance during the yielding phase. The higher the yield pressure of the support, the lower will be the final load. A targeted reduction in ground pressure can be achieved not only by installing a support that is able to accommodate a larger deformation (which is a well-known principle), but also through selecting a support that yields at a higher pressure. Furthermore, a high yield pressure reduces the risk of a violation of the clearance profile and increases safety level against roof instabilities (loosening) during the deformation phase.

These results are important from the standpoint of conceptual design, even if the range of potential project conditions, design criteria and technological constraints does not allow us to make generalizations about structural solutions for dealing with squeezing ground. Some basic design considerations have been illustrated through the use of practical examples. Additionally, the nomograms presented in this paper contribute to the decision-making process, as they allow for a quick assessment of different supports and of their sensitivity with respect to variations in geology.

References

Amberg, W. 1999. Konzepte der Ausbruchsicherung für tiefliegende Tunnels. Bauingenieur, 74 (6).

Anagnostou, G. 2007. Continuous tunnel excavation in a poro-elastoplastic medium. Numerical Models in Geomechanics (NUMOG X), Rhodes, Greece, 183 - 188.

Anagnostou, G., Cantieni, L. 2007. Design and analysis of yielding support in squeezing ground. 11th Congress of the International Society for Rock Mechanics, Lisbon, 829 - 832.

Anagnostou, G., Kovári, K. 1993. Significant parameters in elastoplastic analysis of underground openings. Journal of Geotechnical Engineering, 119 (3), 401 - 418.

Billig, B., Gipperich, Ch., Wulff, M., Schaab, A. 2007. Ausbausysteme für den maschinellen Tunnelbau in druckhaftem Gebirge. Taschenbuch für den Tunnelbau 2008, 32, 223 - 262, VGE Verlag GmbH, Essen.

Budil, A., Höllrigl, M., Brötz, K. 2004. Strenger Tunnel – Gebirgsdruck und Ausbau. Felsbau, 22 (1), 39 - 43.

Cantieni, L., Anagnostou, G. 2007. On the adequacy of the plane strain assumption in tunnel analyses. 11th Congress of the International Society for Rock Mechanics, Lisbon, 975 - 978.

Corbetta, F. 1990. Nouvelles méthodes d’ étude des tunnels profonds – Calculs analytiques et numériques. PhD Thesis, Ecole des Mines de Paris.

Fellner, D., Amann, F. 2004. Modelling yielding support by programming FLAC-2D / FLAC-3D. Eurock, Salzburg.

Kovári, K. 1998. Tunneling in Squeezing Rock. Tunnel, 5, 12 - 31.

Kovári, K. 2005. Method and device for stabilizing a cavity excavated in underground construction. US Patent Appl. 20050191138.

Kovári, K., Ehrbar, H., Theiler, A. 2006. Druckhafte Strecken im TZM Nord: Projekt und bisherige Erfahrungen. Geologie und Geotechnik der Basistunnels, Zürich, 239 - 252.

Panet, M., Guenot, A. 1982. Analysis of Convergence Behind the Face of a Tunnel. Tunnelling ’82. The Institution of Mining and Metallurgy, London, 197 – 204.

Schneider, E., Rotter, K., Saxer, A., Röck, R. 2005. Compex Support System - Komprimierbarer Ringspaltmörtel zur Bewältigung druckhafter Gebirgsbereiche bei TBM-Vortrieben mit starrem Tübbingausbau. Felsbau, 23 (5), 95 - 101.

Schubert, W. 1996. Dealing with squeezing conditions in alpine tunnels. Rock Mechanics and Rock Engineering, 29 (3), 145 - 153.

Schubert, W., Moritz, B., Sellner, P. 2000. Tunnelling methods for squeezing ground. GeoEng2000, Melbourne.

Schubert, W., Moritz, B., Sellner, P., Blümel, M. 1999. Tunnelling in Squeezing Ground – Recent Improvements. Felsbau, 17 (1), 56 - 58.

Solexperts 2007. hiDCon - Elements for Tunneling. www.solexperts.com.

Terzaghi, K. 1946. Rock defects and loads on tunnel supports. Rock tunneling with steel supports, Proctor and White Ed., Commercial Shearing and Stamping Co., Youngstown, Ohio.

Thut, A., Nateropp, D., Steiner, P., Stolz, M. 2006a. Tunnelling in Squeezing Rock - Yielding Elements and Face Control. 8th Int. Conference on Tunnel Construction and Underground Structures, Ljubljana.

Thut, A., Piedevache, M., Prouvot, J. 2006b. Projet Alptransit: Instrumentation et essais in-situ pour deux tunnels de base en contexte alpin. Tunnels et ouvrages souterrains, 198, 331 - 336.

Vermeer, P. A., Borst, R. d. 1984. Non-associated Plasticity for Soils, Concrete and Rock. Heron. Vol. 29 (3), 1 - 64.

PART III

ON A PARADOX OF ELASTO-PLASTIC TUNNEL ANALYSIS

Abstract: Elasto-plastic tunnel analysis may produce a paradox in the calculation of ground pressure whereby ground pressures appear to increase in relation to higher ground quality. More specifically, for an overstressed ground in combination with a stiff support, analysis may indicate greater loading of the support with a ground of high strength than with a ground of low strength (all of the other parameters being equal). This counter-intuitive outcome appears in all of the common calculation models (analytical plane strain analysis, numerical plane strain analysis and numerical axisymmetric analysis), although it does not correspond either to the ground behaviour that is intuitively expected or to ground behaviour observed in the field, thus raising doubts over the predictive power of common tunnel design calculations. The present paper discusses the assumptions made in the models that are responsible for the paradox: the assumption that ground behaviour is time-independent (whereas in reality overstressed ground generally creeps) and the assumption that the support operates with full stiffness close to the face (which is not feasible in reality due to the nature of construction procedures). When proper account is taken of either or both of these assumptions in more advanced models, the paradox disappears. As the models which generate the paradox are very commonly used in engineering and scientific practice, the investigations of the present paper may be of value, helping the engineer to understand the uncertainties inherent in the models and to arrive at a better interpretation of the results they produce.

Notation:

a	Tunnel radius
d	Lining thickness
d_S	Thickness of the TBM shield
E	Young's modulus of the ground
E_L	Young's modulus of the lining
$E_{L,28}$	Young's modulus of the lining after 28 days (= E_L)
E_S	Young's modulus of the TBM shield
$E_L(t)$	Time-dependent Young's modulus of the lining
e	Unsupported span
f	Yield function
f_c	Uniaxial compressive strength of the ground
g	Plastic potential
i	Point / interval (defined in Fig. 22)
j	Point / interval (defined in Fig. 22)
k	Lining stiffness
k_I	Support stiffness before the deformation phase of the yielding support
k_j	Average stiffness over the integration interval j
$k^{(i)}$	Stiffness of the fictitious lining layer i
k_S	Stiffness of the TBM Shield
m	Point / interval (defined in Fig. 22)
M	Bending moment
N	Hoop force
p	Rock pressure acting upon the lining
p_F	Face support pressure
p_I	Fictitious internal pressure in the plane strain analysis
p_j	Rock pressure at the point j
$p_j^{(i)}$	Pressure exerted by layer i at point j
p_y	Yielding support pressure
p_∞	Final rock pressure acting upon the lining far behind the face
$p(y)$	Rock pressure acting upon the lining at the axial coordinate y
r	Radial co-ordinate (distance from tunnel axis)
s	Round length in the step-by-step calculations
t	Time
$t_{95\%}$	Time needed in order to reach 95% of the time-dependent deformations

u	Radial displacement of the ground
u_C	Radial convergence of the opening
u_C^e	Elastic part of the radial convergence of the opening
u_C^p	Plastic part of the radial convergence of the opening
u_j	Radial displacement of the ground at point j
u_{oe}	Amount of over-excavation in case of a yielding support
u_y	Axial displacement
u_∞	Final radial displacement of the ground occurring far behind the face
$u(y)$	Radial displacement of the ground at the axial coordinate y
$\overline{u}$	Radial displacement (unsupported opening)
v	Advance rate of the excavation
y	Axial co-ordinate (distance behind the tunnel face)
y_j	Axial co-ordinate of point j
ΔR	Overcut between excavation and shield
Δp_j	Increase of pressure over the integration interval j
$\dot{\varepsilon}_{ij}$	Strain rate tensor
$\dot{\varepsilon}_{ij}^e$	Elastic part of the strain rate tensor $\dot{\varepsilon}_{ij}$
$\dot{\varepsilon}_{ij}^p$	Inelastic part of the strain rate tensor $\dot{\varepsilon}_{ij}$
η	Viscosity
λ	Stress relief factor
ν	Poisson's ratio of the ground
σ_o	Initial stress
σ_{ij}	Stress tensor
σ_{rr}	Radial stress
ϕ	Angle of internal friction of the ground
ψ	Dilatancy angle of the ground

1 Introduction

Under certain conditions which are frequently encountered in tunnel design, the computational models in common use predict that a poor quality ground will be more favourable for tunnel construction than a high quality ground. More specifically, the models suggest that a ground of higher strength develops a greater load upon the lining than the load developed by a low strength ground (all of the other parameters being equal). This is clearly contrary to the behaviour that might be expected both intuitively and on the basis of tunnelling experience, which is that overstressing of the lining or severe convergences are associated with ground of poor quality (e.g. Kovári and Staus 1996). The model behaviour deserves to be called a paradox, i.e. *“a seemingly absurd or contradictory statement or proposition which when investigated may prove to be well founded or true”* (Oxford Dictionary).

The paradox has been mentioned in passing in a number of older works dealing with the elasto-plastic analysis of tunnels (Nguyen-Minh and Corbetta (1992), page 86, Nguyen-Minh and Guo (1993), page 176, and Guo, (1995), page 90). More recently, it has been noted by Boldini *et al.* (2000) and Graziani *et al.* (2005), who obtained *"unforeseen results"* from axisymmetric elasto-plastic numerical analyses of advancing tunnels, and explained them by means of the convergence-confinement method (“*The decrease in the loading in the plastic case is caused by the increased convergence u_0 before the installation of the lining, which overshadows the negative effect of the flattening of the convergence curve in the plastic range"*). Also, Mair (2008) drew basically the same conclusion when discussing the results of plane strain analyses (*"This is because the weaker ground leads to higher deformations occurring ahead of the face prior to installation of the lining; the consequence of more ground deformation before installation is a smaller pressure induced on the lining"*). Furthermore, Ramoni and Anagnostou (2010) and Lavdas (2010) observed the counter-intuitive behaviour of the models with respect to the loading of TBM shields and of segmental linings, respectively.

Although the paradox has been noted by a number of authors, it is, interestingly, neither widely appreciated nor well understood in the broader engineering and scientific community. It may therefore perplex the tunnel engineer and raise doubts as to the predictive power of standard tunnel design calculations, which makes it deserving of closer investigation. This shall be attempted in the present paper.

Section 2 illustrates the paradox by means of results obtained from the application of commonly-used computational methods, investigating the conditions under which the paradox occurs and explaining why the paradox occurs. The computational methods in question are: the convergence-confinement method (CCM) for the classic, rotationally symmetric, plane-strain tunnelling problem; the plane strain numerical analysis for tunnels with an arbitrary cross-section; and the axisymmetric analysis for deep cylindrical tunnels. All of these methods exhibit the paradox with respect to the rock loading developing upon a stiff lining that is installed close to the face (the higher the rock strength, the higher the load), but predict the expected behaviour with respect to convergences (the higher the rock strength, the smaller the convergence).

Even if the reason for the low load predicted in the case of low strength ground is understood (as mentioned above, it is the stress relief associated with the yielding of the core ahead of the tunnel face), a question remains as to why such behaviour is not exhibited in nature or, in other words: what are the specific modelling assumptions that lead to the paradoxical model behaviour. The main part of the paper deals with these issues. Section 3 outlines possible reasons for the discrepancy between model behaviour and actual behaviour on the basis of qualitative factors, while Sections 4 to 8 investigate some of these possible reasons quantitatively and in-depth. Putting it in a nutshell, the paradoxical behaviour seen in the model is associated with the commonly-made simplifying design assumptions that ground behaviour is time-independent (while in reality the ground generally creeps, particularly in the case of squeezing) and that the support operates with full stiffness close to the face (while in reality the sequence of excavation and support installation is such that deformations inevitably occur).

2 Unexpected model behaviour

2.1 Convergence-confinement method

The convergence-confinement method (CCM) allows the ground pressure to be assessed by means of closed-form solutions, and is widely used in engineering practice for preliminary dimensioning of the lining (Panet 1995). The method applies to the rotationally symmetric problem of a deep, uniformly supported, circular tunnel crossing a homogeneous and isotropic ground which is subject to uniform and hydrostatic initial stress. Under the additional simplifying assumption of plane strain conditions, the problem becomes one-dimensional (i.e. all field variables depend solely on the distance *r* from the tunnel axis) and can be solved analytically. The solution can be presented in the form of a so-called “ground response curve”, which shows the relationship between the support pressure and the radial displacement of the tunnel boundary. The equations for the case of linearly elastic and perfectly plastic ground behaviour according to the Mohr-Coulomb yield criterion with a non-associated flow rule (which is the material model assumed throughout the present Paper) can be found, inter alia, in Anagnostou and Kovári (1993). Figure 1a shows the ground response curves for an example with the parameters of Table 1 and an uniaxial compressive strength f_c of 1 or 3 MPa.

The CCM investigates the interaction between ground and tunnel support graphically by plotting the ground response curve and the characteristic line of the lining in one and the same diagram. The latter shows the dependency of the radial displacement of the lining on the ground pressure acting upon the lining. The inclination of the characteristic line of the support depends on its stiffness *k*, while the origin of the characteristic line on the displacement axis (e.g., Point A in Fig. 1a) accounts for the pre-deformation of the ground, i.e. for the radial displacement that takes place before lining installation at a distance *e* behind the face. The pre-deformation occurs partially ahead of the tunnel face and partially over the unsupported span. In the computational example of Figure 1a the simplifying assumption was made that the pre-deformation *u(e)* follows the longitudinal displacement profile proposed by Chern *et al*. (1998):

$$u(e) = \bar{u}\left(1 + \exp\left(-0.91\frac{e}{a}\right)\right)^{-1.7}, \qquad (1)$$

where $\bar{u}$ and *a* denote the final unsupported convergence (i.e. the convergence that would occur in an unsupported tunnel far behind the face) and the tunnel radius, respectively. Figure 1a shows the characteristic lines of the lining for support installed directly at the tunnel face ($e = 0$, $u(e)/\bar{u}$ = 30%, dashed lines) or at a distance of e = 3 m behind the face ($u(e)/\bar{u}$ = 50%, solid lines).

The intersection point of the ground response curve and of the characteristic line (e.g. Point B in Fig. 1a) satisfies the conditions of equilibrium and compatibility and shows the ground pressure and deformation. It can be seen immediately from Figure 1a that, as a consequence of the smaller pre-deformations, the predicted ground pressure is higher in the case of a higher strength ground. This is clearly contrary to what one might expect intuitively. Figure 1b provides a more complete picture of the effect of ground strength f_c on final lining pressure.

In view of the paramount effect of pre-deformation on the final lining pressure, the question arises as to whether this unexpected model behaviour might be due to the simplifying assumption of Eq. (1), according to which the pre-deformation amounts to a constant fraction of the final unsupported convergences (i.e. a fraction which is the same for an elastic and for a highly-stressed ground). A similar behaviour can be observed when applying the improved longitudinal displacement profiles proposed Vlachopoulos and Diederichs (2009), which in contrast to Chern *et al*. (1998) consider the maximum plastic radius. The paradox persists even when applying the most advanced method of pre-deformation estimation, which is the so-called implicit method introduced by Nguyen-Minh and Guo (1996) and proposed, inter alia, by AFTES (2002). This method takes into account the lining stiffness and installation point in addition to the properties of the ground and to the extent of the plastic zone. A synopsis of the equations can be found in Cantieni and Anagnostou (2009a). As can be seen from the ground – support interaction diagram of Figure 1c, even this more sophisticated analysis method predicts that the load developing in the case of a ground having an uniaxial compressive strength of f_c = 1 MPa is lower than in the case of f_c = 3 MPa.

Figure 1d shows the results of a parametric study (performed with the CCM in combination with the implicit method) on the effect of ground strength f_c on final loading at different values of the unsupported span *e* and of the lining stiffness *k*. It is interesting to note that the softer the lining and the bigger the unsupported span, the less pronounced is the paradox. In conclusion, the reasons for this will be discussed later in Section 2.3.

Table 1 Model parameters

Parameter		Value	
Initial stress	σ_0	10 MPa	
Tunnel radius	a	4 m	
Unsupported span	e	variable	
Ground			
Young's Modulus	E	1 GPa	
Poisson's ratio	ν	0.3	
Angle of internal friction	φ	25°	
Dilatancy angle	ψ	5°	
Uniaxial compressive strength	f_c	variable	
Lining			
Radial stiffness	k	1 GPa/m	0.1 GPa/m
Young's modulus	E_L	30 GPa	10 GPa
Thickness	d	0.53 m	0.16 m

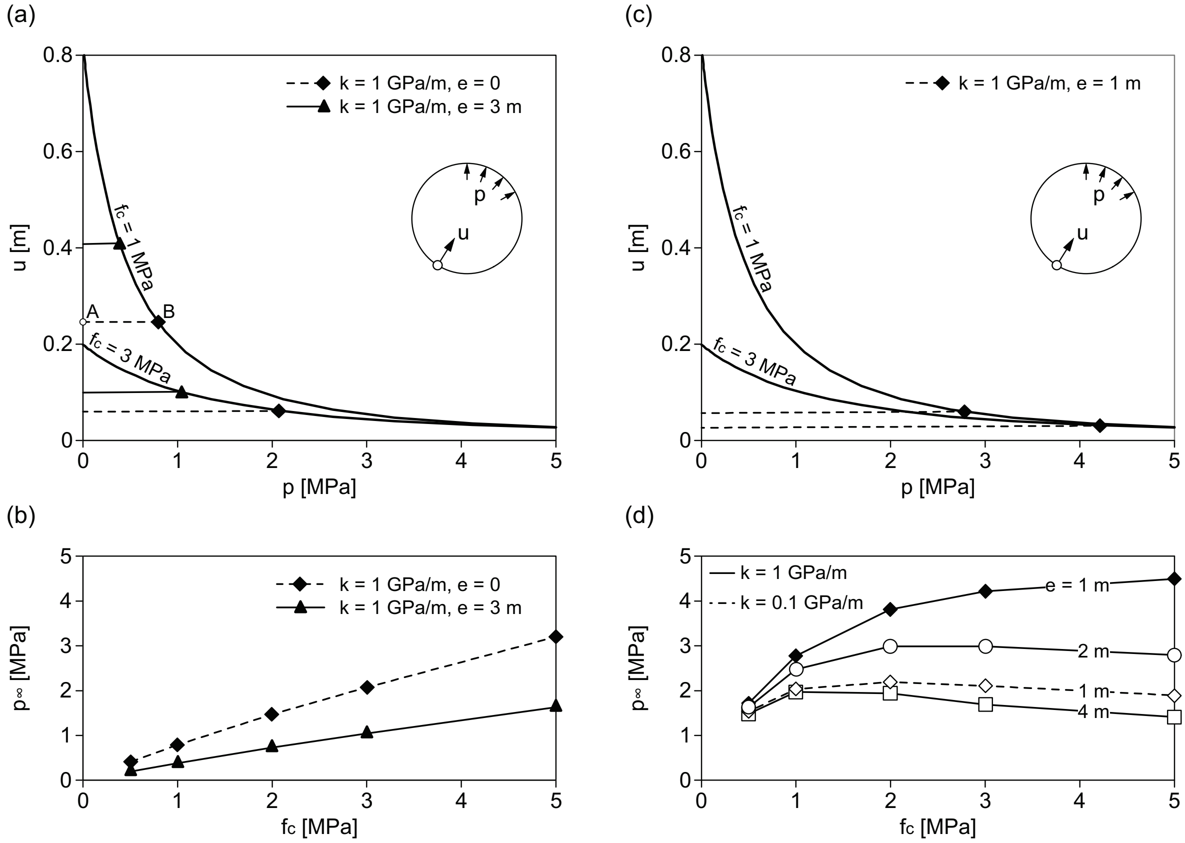

Fig. 1 Determination of the final lining pressure by the CCM for different values of the uniaxial compressive strength of the ground f_c, of the unsupported span *e* and of the radial stiffness of the lining *k*. (a) Ground-support interaction (pre-deformations according to Chern *et al*. 1998); (b) Final lining pressure as a function of the uniaxial compressive strength (pre-deformations according to Chern *et al*. 1998); (c) Ground-support interaction (pre-deformations according to the implicit method); (d) Final lining pressure as a function of the uniaxial compressive strength (pre-deformations according to the implicit method)

2.2 Numerical plane strain analysis

One might argue that the paradox described above may be interesting from a theoretical point of view, but is of minor importance in practical terms because the CCM is anyway an oversimplified analytical tool. The purpose of this Section is to emphasize that the fundamental principles of the CCM and the conclusions of the last Section apply also to the numerical plane strain analyses that are widely used for design purposes in engineering practice.

For the sake of simplicity and without loss of generality, let us consider again a deep-seated tunnel excavated full face under the same conditions as in the last Section (including Table 1, with the lining characteristics according to the last column). The only difference is that the tunnel cross-section is no longer circular, with the consequence that rotational symmetry is lost and the problem has to be solved numerically by the finite element method. In order to explain why the paradox persists, let us consider how a numerical plane strain analysis proceeds in such a case. In a plane strain analysis, the three-dimensional tunnel problem is simulated by considering a series of sections normal to the tunnel axis (e.g. Panet 1995). In the case of full face excavation, the computation consists of three steps.

The first step concerns the initial state ("State 0"), which prevails far ahead of the face. Depending on the available computer code, the initial stress field may be either defined or calculated.

The second step simulates the development of pre-deformations during the transition from the initial state to the state prevailing immediately before lining installation ("State 1") by reducing the radial stresses (as well as the shear stresses in the case of a non-hydrostatic initial stress field) acting on the tunnel boundary from their initial value σ_0 to the fictitious internal pressure p_l which simulates the supporting effect of the core. The amount of stress relief is usually expressed by the stress relief factor λ ($0 \le \lambda \le 1$):

$$p_l = (1 - \lambda)\, \sigma_0 \,. \tag{2}$$

A value of $\lambda = 1$ (complete stress relief) applies to the case of an unsupported tunnel, while $\lambda = 0$ (no stress relief) applies to the theoretical case where support is installed *before* excavation. The stress relief factor governs the amount of pre-deformation, accounts for the stiffness and for the installation point of the support and is estimated by one of the methods mentioned in the last Section. Figure 2 shows the stress relief factor λ (calculated according to the implicit method for the parameter values of Table 1) as a function of the uniaxial compressive strength f_c. The lower the ground strength, the more pronounced will be the yield of the core ahead of the face, the higher will be the stress relief factor λ and, consequently (cf. Eq. 2), the lower will be the fictitious internal pressure p_l.

The third step simulates the transition from State 1 to the final state prevailing far behind the face ("State 2") by activating the finite elements that simulate the support and by setting the tractions at the tunnel boundary equal to zero. The resulting values include the final displacement and rock load as well as the lining forces (bending moments, hoop forces). A stiff lining that is installed close to the face prevents the development of further convergences and thus further stress relief. As a consequence, the final lining loading practically corresponds to the radial stress prevailing at the tunnel boundary at State 1, i.e. to the internal pressure p_l, which, as mentioned above, decreases with the strength of the ground. The consequence is that a weak ground develops a lower loading.

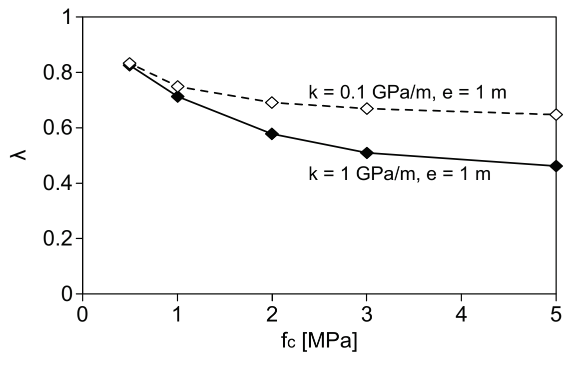

Fig. 2 Stress relief factor λ as a function of the normalized uniaxial compressive strength f_C/σ_0 for the radial stiffness of the lining k of 0.1 and 1 GPa/m (other parameters according to Table 1)

Figure 3 shows, as an example, the numerical results obtained by the FEM code PLAXIS (Brinkgreve 2002) for a non-circular tunnel with the model parameters of Table 1 (lining data according to the last column). The stress relief factors were taken from Figure 2 with a stiffness k = 1 GPa/m. The calculated bending moments and axial forces (although not manageable structurally) also illustrate the existence of the paradox. The paradox thus applies not only to analytical solutions that incorporate many simplifications, but also to the widely-used numerical plane strain computational method.

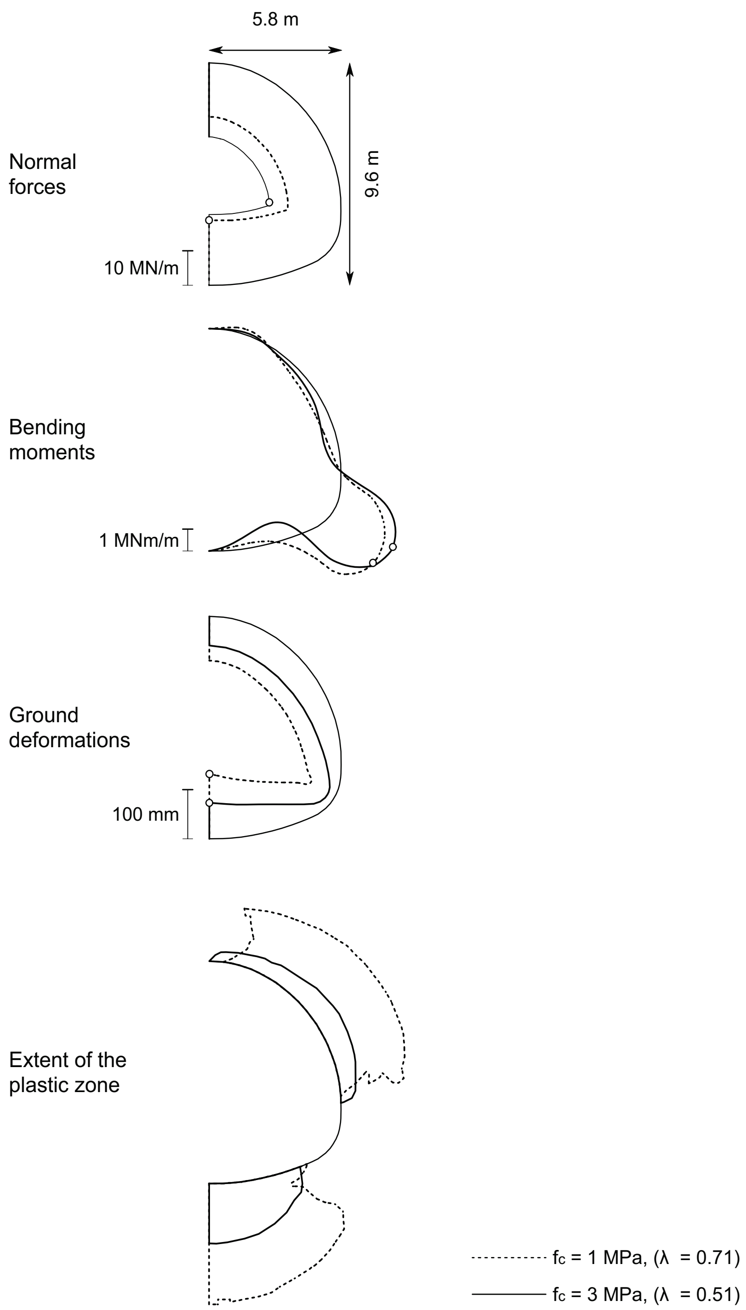

Fig. 3 Numerically determined distribution, (a), of the hoop force N, (b), of the bending moment M and, (c), of the deformation of the tunnel boundary u and, (d), extent of the plastic zone for two values of the uniaxial compressive strength f_c

2.3 Numerical axially symmetric analysis

On account of the uncertainties introduced by the simplifying assumptions of plane strain analyses with respect to pre-deformation (which, as discussed above, is a very important parameter), it is reasonable to ask whether the paradox is a problem specifically of the plane strain model or if it also occurs in spatial (i.e., three-dimensional or axisymmetric) analyses which do not involve assumptions about convergences ahead of the face. An additional reason for raising this question is that plane strain analyses, in contrast to spatial calculations, do not correctly reproduce the actual stress history of the ground, and this may influence the results not only quantitatively but also qualitatively (Cantieni and Anagnostou 2009a and 2009b).

Let us therefore investigate the behaviour of the axially symmetric model of a deep cylindrical tunnel. The problem setup is exactly the same as in Section 2.1, the only difference being that we no longer make the plane strain assumption. The problem is solved numerically by the so-called "steady state method", a method introduced by Nguyen-Minh and Corbetta (1991) for efficiently solving problems with constant conditions in the tunnelling direction by considering a reference frame, which is fixed to the advancing tunnel face. A comparison of the steady state method with the more widely used "step-by-step method", which handles the advancing face by deactivating and activating the ground and support elements, respectively, was presented recently in this Journal by Cantieni and Anagnostou (2009a). As discussed by the Authors, the steady state method applies to the borderline case of continuous tunnel advance (round length $s = 0$).

Figure 4a shows the model. The lining is modelled as an elastic radial support with stiffness $k = dp/du$, where p and u denote its radial loading and radial displacement, respectively. The radial stiffness k of a ring-shaped lining is equal to $E_L d/a^2$, where a, d, and E_L denote its radius, thickness, and Young's modulus, respectively. The longitudinal bending stiffness of the lining will not be taken into account. The lining is installed at a distance e behind the tunnel face.

Figure 4d shows the development of radial stress at $r = a$ (which for $y > e$ is identical with the lining loading) along the tunnel for two values of the uniaxial compressive strength of the ground f_c. It can be easily seen that – analogously to the results of the CCM - both the radial stress ahead of the face and the pressure developing upon the lining are lower in the case of the lower strength ground, while the deformations (particularly the ones occurring ahead of the face) and the extent of the plastic zone are larger (Fig. 4c and 4b, respectively).

In order to gain more information about the behaviour of the model, a parametric study was performed on the effects of ground strength f_c, unsupported length e and lining stiffness k. Figures 5a and 5b show the final lining pressure p_∞ as a function of the uniaxial compressive strength f_c (both normalized by the initial stress σ_0) for a stiff and a soft lining (k = 1 and 0.1 GPa/m, respectively). Both diagrams clearly show the counter-intuitive behaviour (the load increasing with the ground quality) at unsupported lengths e up to 2 m. Similarly to the CCM (Section 2.1), the stiffer the lining and the shorter the unsupported span, the more pronounced is the paradox.

The lower the strength of the ground, the more will the radial stress in the core ahead of the face decrease and, as the lining actually undertakes the role of the core after excavation, the lower will be the lining load. If the strength of the ground is high, however, the core ahead of the face will be able to sustain a high radial stress and, as a stiff lining that is installed close to the face does not allow for additional deformations and stress relief, a high load will develop upon the lining. On the other hand, a low stiffness lining or a long unsupported span allow deformations and stress relief to develop behind the face (whatever the strength of the ground) with the consequence that the paradox becomes less pronounced.

As the convergence of the excavated profile is a directly observable phenomenon in tunnelling, un-

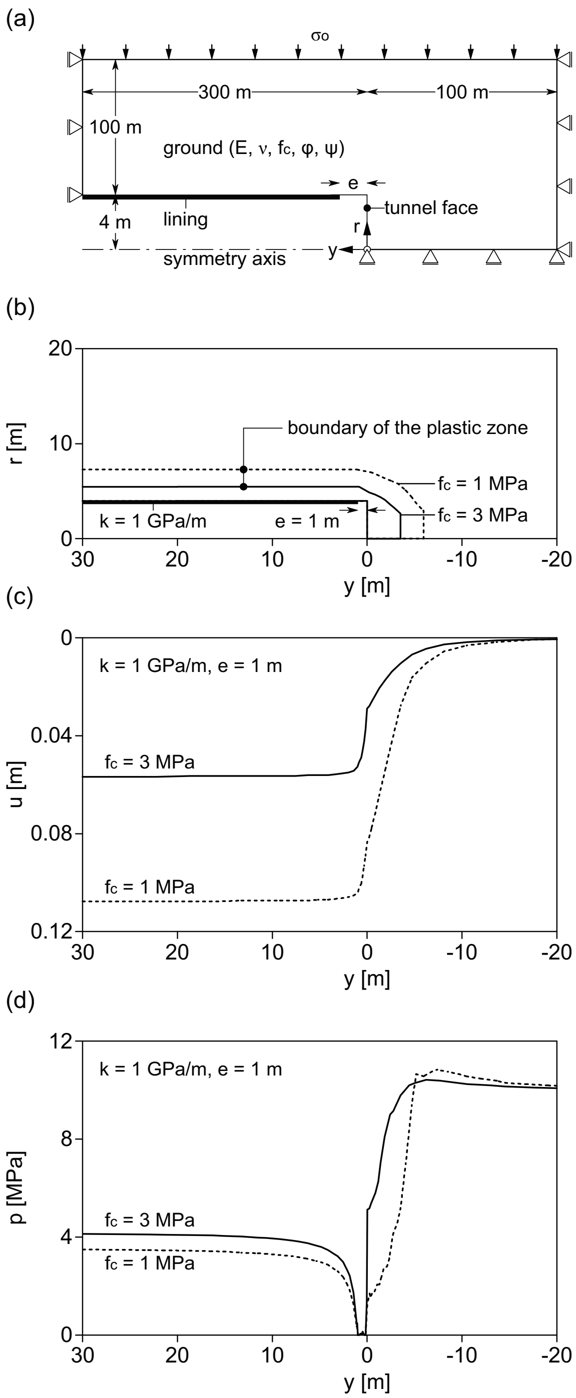

Fig. 4 (a) Axially symmetric model and boundary conditions; (b) extent of the plastic zone; (c) radial displacement *u* of the ground at the tunnel boundary; (d) radial stress at the tunnel boundary (for $y > e = 1$ m, the radial stress corresponds to the ground pressure on the lining)

like rock pressure (and in fact large convergences are what tunnel engineers associate with poor quality ground), it is interesting to check the model behaviour also with respect to deformations. Figures 5c and 5d show the convergence u_c of the excavated section ($u_c = u_\infty - u(0)$) as a function of the ground strength f_c and of the unsupported span e. It can be seen that the model predictions correspond to expectations: the lower the strength, the larger the convergence. This is true also concerning the convergence of an unsupported tunnel (Fig. 6). The model behaviour is counter-intuitive only with respect to the load developing upon the lining.

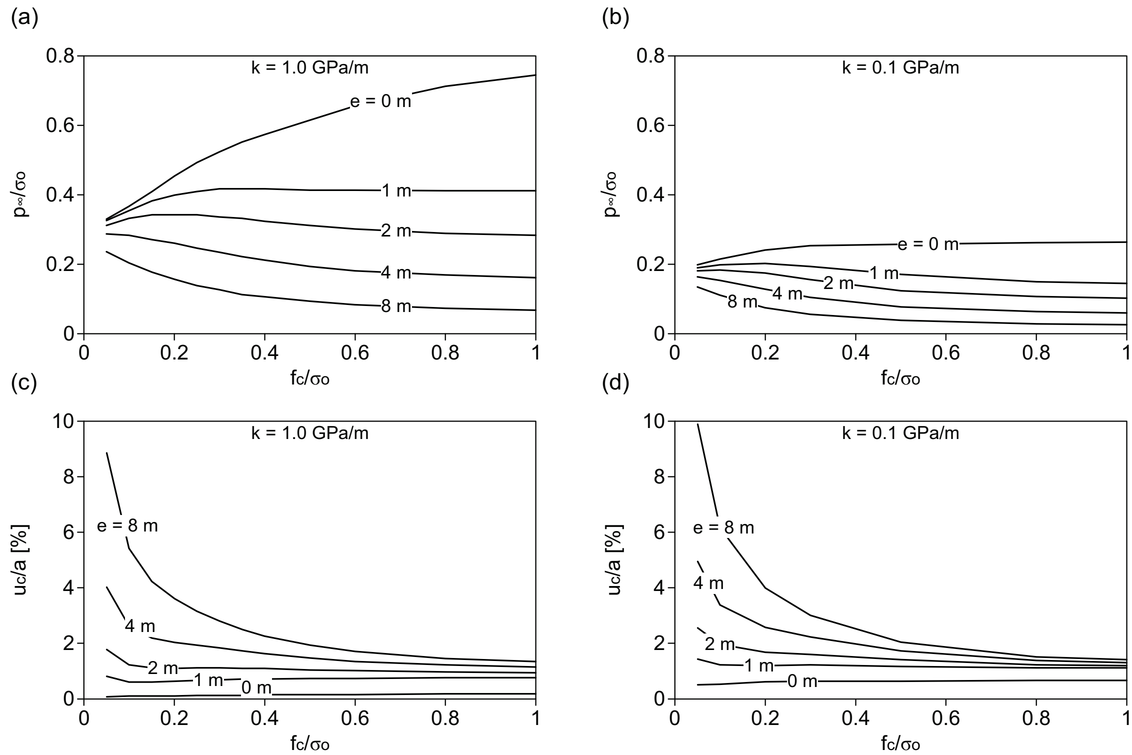

Fig. 5 Effect of the normalized uniaxial compressive strength f_C/σ_0, (a), on the normalized final lining pressure p_∞/σ_0 for a radial lining stiffness k of 1 GPa/m; (b), on the normalized final lining pressure p_∞/σ_0 for a radial lining stiffness k of 0.1 GPa/m; (c), on the normalized convergence u_C/a for a radial lining stiffness k of 1 GPa/m; and, (d), on the normalized convergence u_C/a for a radial lining stiffness k of 0.1 GPa/m

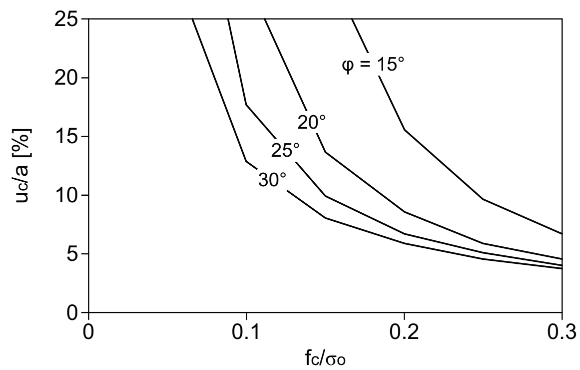

Fig. 6 Normalized radial convergence of an unsupported tunnel u_C/a as a function of the normalized uniaxial compressive strength f_C/σ_0 and of the angle of internal friction φ

3 Reasons for the discrepancy between model and reality

Although the reason for the unexpected model behaviour is understood, it is still puzzling, why such behaviour is not observed in reality. Obviously there must be one or more modelling assumptions which contradict what happens in reality and which are responsible for the observed difference between model behaviour and actual behaviour. The results of the last Section provide useful indications as to the relevant modelling assumptions.

The finding that the paradox is due to deformations and to the stress relief associated with the plastic yield of the ground *ahead* of the face indicates that the modelling assumptions which provide for this stress relief may be responsible for the paradox. As explained below under points (i) and (ii) there are at least two reasons why the actual deformations of the ground and the stress relief *ahead* of the face may be smaller than in the computational models of Section 2 which show the paradoxical behaviour.

The finding that the paradox occurs particularly under the modelling assumption that a stiff lining is installed near the face (and becomes less and less pronounced or disappears when the ground is allowed to converge *behind* the face) indicates that this modelling assumption may be an oversimplification. In fact, there are several sources of deviation between the model and reality which are associated with the development of deformations *behind* the face. These deviations may also explain the difference between the behaviour of the model and actual behaviour, i.e. the absence of the paradox in reality. The deformations *behind* the face may occur intentionally (as in the case of yielding supports, see point (iii) below) or unintentionally, for example due to support destruction (iv), due to the excavation and support installation sequence (v-vii) or due to the early stiffness of the support components (viii). Deformations even occur in cases with a presumably stiff support as in the case of a segmental lining in shield tunnelling (ix).

(i) Time-dependency of the ground behaviour

The first reason is of a fundamental nature, as it is associated with the rheological properties of the ground. Creep is particularly important in the case of overstressed ground (i.e., when the stresses reach its bearing capacity) and is therefore also important for the question under consideration. In general, plastic yielding develops with a certain delay which is dependent on its rheological properties. The latter, together with the advance rate, are decisive in terms of the extent of plastic yield and the amount of stress relief ahead of the advancing face. The higher the viscosity of the ground and the higher the advance rate, the smaller will be the plastic deformations and the stress relief and the less pronounced will be the paradox (the effect of the ground strength appears with a delay - behind the face). Section 4 confirms this hypothesis by means of numerical computations.

(ii) Face support or reinforcement

The second effect is associated with specific measures that are often applied in weak ground in order to stabilize the face or to limit its extrusion. Face bolting increases the bearing capacity of the core ahead of the face and, as the reinforced core is able to sustain a higher radial stress, limits stress relief. Consequently, the paradox should become less pronounced. Section 5 investigates this hypothesis and shows that the paradox disappears only at very high face support pressures that are barely feasible from a technical perspective.

(iii) Yielding support

Yielding supports are installed close to the face and allow the ground to converge under an approximately constant pressure. Figure 7 shows the support measures applied in the case of the yielding support developed for the Sedrun Lot of the Gotthard Base Tunnel. As the paradox becomes less pronounced or disappears when the ground is allowed to converge behind the face, it is reasonable to expect that it will not occur in the case of yielding supports. Section 6 confirms this hypothesis quantitatively. The model exhibits the expected behaviour: the higher the strength of the ground, the lower the rock pressure and the smaller the convergence.

(iv) Damage to the support

Decreasing ground quality in tunnelling is recognized through increasing convergences. In the case of a stiff support, large deformations can only occur if the ground pressure overstresses and damages the lining (Fig. 8). Damaged support offers only a low or zero resistance to deformations. As already discussed (Fig. 6), the model of an unsupported tunnel exhibits the expected behaviour: the convergences increase with decreasing ground strength.

(v) Partial face excavation

In the case of partial face excavation (e.g. the top heading, bench- and invert-excavation method), the stiffness of the support system is low before completing the excavation of the cross-section and closing the lining at the invert (A in Fig. 9). The initially low stiffness allows for convergences behind the face, which should reduce or even eliminate the paradoxical behaviour (according to the findings of Section 2).

(vi) Staggered support application

The construction process is usually such that the application of support measures (steel sets, shotcrete, bolts) is staggered along the tunnel alignment (Fig. 7, B in Fig. 9). The stiffness of the sup-

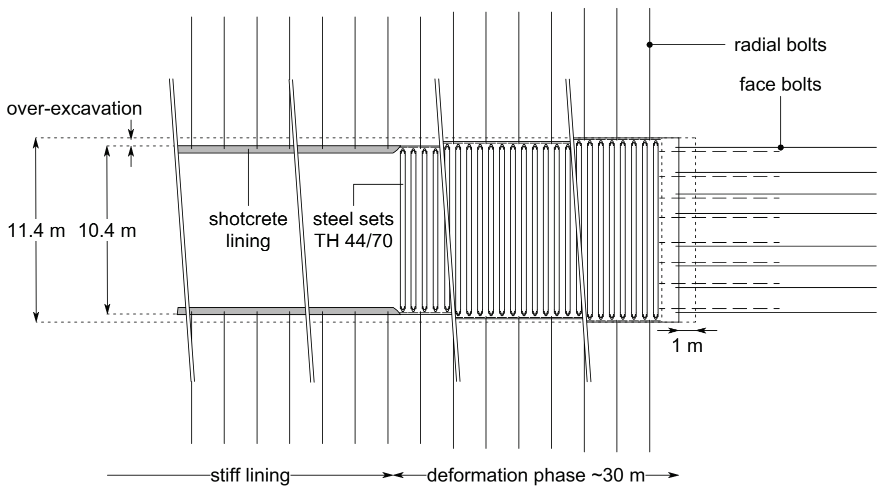

Fig. 7 Scheme of the yielding support system realized in the Sedrun Lot of the Gotthard Base Tunnel (after Ehrbar and Pfenninger 1999)

port system is initially low and increases with the distance from the face. The ground can thus converge in the regions close to the face, thereby reducing or eliminating the paradoxical behaviour.

(vii) Unsupported span

According to Figure 5, the cases with an unsupported span of e = 0 yield the most pronounced paradox. In conventional tunnelling, an unsupported span of e = 0 is not feasible. Even if all support components are installed immediately after each excavation round right at the face, the next excavation step (s > 0) would temporarily create an unsupported span (C in Fig. 9). Therefore, the modelling assumption of e = s = 0 (underlying the curves denoted by e = 0 of Fig. 5), which almost entirely prevents the development of convergence behind the face, represents only a theoretical limiting case.

(viii) Stiffness of green shotcrete

Another possible source of deformations behind the face is the low stiffness of green shotcrete. The final Young's modulus of shotcrete is normally reached only after several days. For high advance rates, the stiffness of the lining is therefore low near the face (D in Fig. 9). Section 7 investigates by means of numerical computations whether the paradox persists when taking this effect into account, and shows that it is a rather minor effect. The counter-intuitive model behaviour disappears only at very high advance rates (> 20 m/day).

(ix) TBM tunnelling

With respect to TBM tunnelling, the assumptions of e = 0 (no unsupported span) and s = 0 (zero round length), which lead to the most paradoxical model behaviour (Fig. 5), seem at a first glance to be realistic because of the continuous advance of the shield. However, the design of the machines always provides a certain “overcut” ΔR between bored profile and shield extrados, which is needed for steering the machine (and sometimes also for avoiding jamming of the shield). The

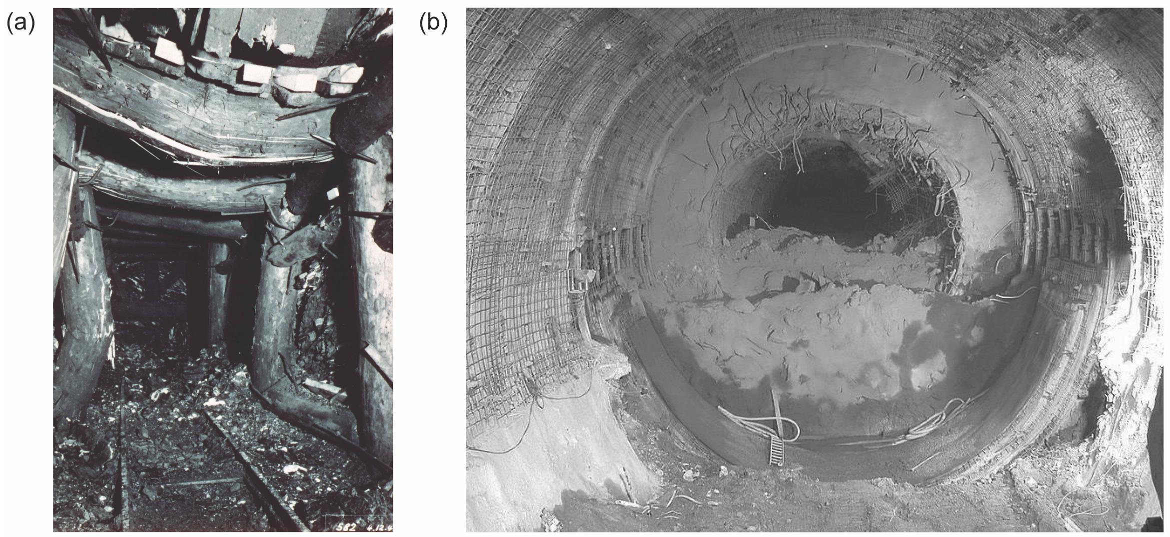

Fig. 8 (a) Historical picture of a tunnel with damaged wooden support; (b) reshaped cross-section (in the front of the picture) after the support was damaged (in the background of the picture) in the Faido Lot of the Gotthard Base Tunnel (courtesy of AlpTransit Gotthard AG, Switzerland)

overcut allows the ground to converge behind the face (E in Fig. 9). Additional deformations may occur behind the shield even in the presence of a stiff segmental lining, depending on the type and on the point of application of the backfill (F in Fig. 9). Section 8 investigates the effects of the overcut in more detail and shows that the overcut reduces or even eliminates the paradoxical behaviour.

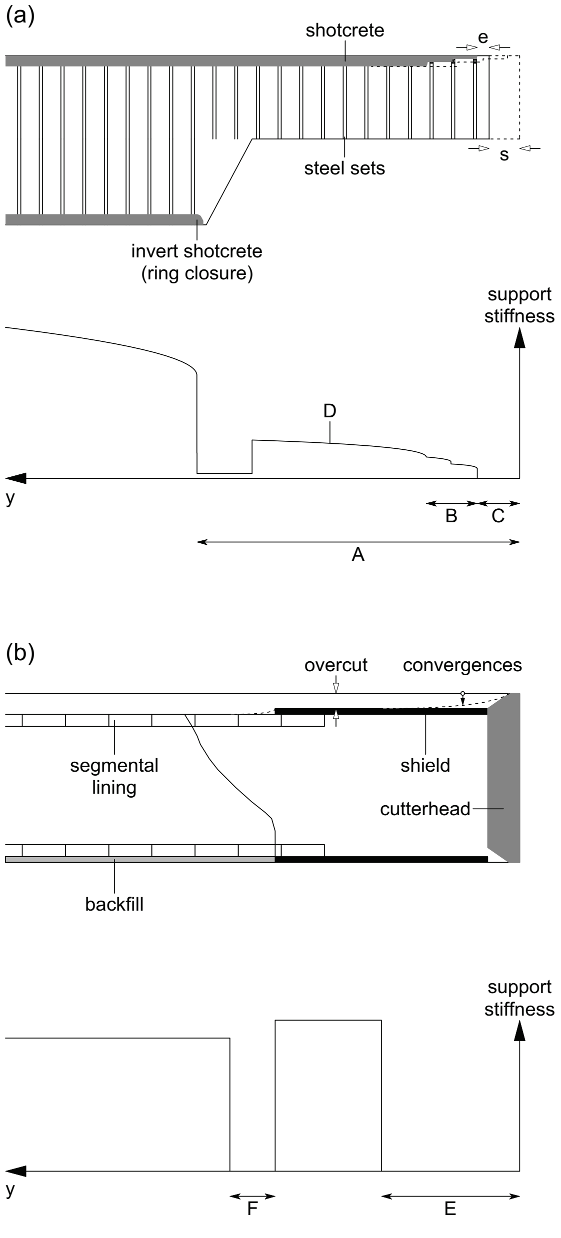

A: partial face excavation
B: staggered application of support measures
C: unsupported span after excavation step (e + s)
D: ageing of the shotcrete
E: overcut (no contact between ground and shield)
F: non-perfect backfill (no close-fitting between ground and lining)

Fig. 9 Sources of unavoidable deformations during (a) conventional tunnelling and (b) TBM tunnelling

4 Effect of creep

4.1 Computational model

Time-dependency is taken into account by applying the elasto-viscoplastic creep model after Madejski (1960). The inset in Figure 10 shows the micro-mechanical model, which consists of an elastic spring in series with a Bingham model. The strain rate $\dot{\varepsilon}_{ij}$ is resolved into an elastic and an inelastic part:

$$\dot{\varepsilon}_{ij} = \dot{\varepsilon}_{ij}^{e} + \dot{\varepsilon}_{ij}^{p} \quad . \tag{3}$$

The elastic part depends linearly on the stress rate (Hooke's law), while the inelastic part $\dot{\boldsymbol{\varepsilon}}_{ij}^{p}$, which represents combined viscous and plastic effects, reads according to the classic formulation of Perzyna (1966) as follows:

$$\frac{d\varepsilon_{ij}^{p}}{dt} = \frac{f}{\eta}\frac{\partial g}{\partial \sigma_{ij}} , \tag{4}$$

where f, g and η denote the yield function, the plastic potential and the viscosity, respectively. According to this equation, both the deviatoric and the volumetric strains are time-dependent. In contrast to more sophisticated time-dependent constitutive models (e.g. the SHELVIP model, Debernardi and Barla 2009, and the CVISC model, Itasca 2006), the instantaneous response of the assumed material model is purely elastic.

As the development of plastic deformations takes time, the extent of the plastic zone ahead of the

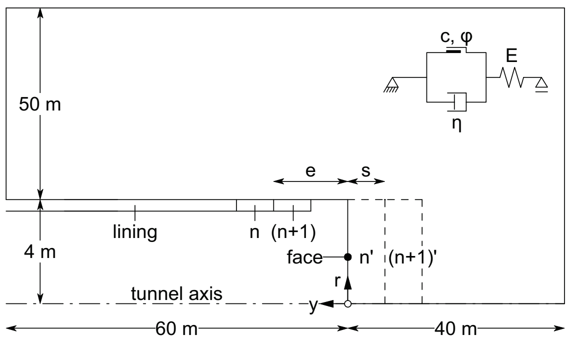

calculation steps:
lining istallation **n**
calculation for excavation **n'** in Δt = 0
transient calculation with Δt = 1 day
lining istallation (**n+1**)
calculation for excavation (**n+1)'** in Δt = 0
transient calculation with Δt = 1 day
...

Fig. 10 Problem layout and boundary conditions of the step-by-step numerical model including the sequence of the calculation steps and the micro-mechanical material model

Table 2 Response times of a circular unsupported tunnel under plane strain conditions

Viscosity η [kPa * day]	$t_{95\%}$
10^3	a few hours to a few days
10^4	a few days to a few weeks
10^5	a few weeks to a few months
10^6	a few months to a few years
10^7	several years

tunnel face and the magnitude of the pre-deformations also depend on the advance rate. It is easy to show (by means of a dimensional analysis) that the response of the model depends on the product of the advance rate v and the viscosity η (c.f. Bernaud 1991). The effect of a high advance rate is equivalent to that of a high viscosity. In the borderline case of an "infinitely" rapid excavation, only elastic deformations will occur around the advancing face. In general, the lower the advance rate, the larger will be the plastic deformations.

The ground pressure developing upon the lining is determined by means of a transient stress analysis based on an axially symmetric model (Fig. 10). The tunnel advance is simulated with 60 excavation steps, each containing an instantaneous advance of s = 1 m, followed by a transient calculation covering a period of 1 day (overall advance rate v = 1 m/day). Figure 10 shows the sequence of excavation and support installation. After 60 steps, tunnel advance is halted and a transient analysis is performed in order to study the development of deformations and rock pressures during the standstill. The analysis stops when a steady state is reached, i.e. when the extrusion rate of the face becomes very small.

For the purpose of comparison, we also carried out time-independent elasto-plastic computations (η = 0). In contrast to Section 2.3, the time-independent problem of the present Section was also solved by the step-by-step method, in order to eliminate the effect of the round length s, which is equal to zero in the steady state method.

The calculations have been carried out with the parameters of Table 1, an unsupported span of e = 1 m and various viscosity values. Table 2 gives a sense of the numerical values of viscosity η (a less familiar material constant) by making reference to the response of the relatively simple model of a circular unsupported tunnel under plane strain conditions. The time $t_{95\%}$ denotes the period that must elapse in order that the time-dependent convergence reaches 95% of its final value. Details can be found in the Appendix A.

4.2 Model behaviour

Figures 11a and 11b show the pressure distribution upon the lining for elasto-plastic (η = 0) and elasto-viscoplastic (η = 10^6 kPa*day) ground behaviour, respectively, and for two values of the uniaxial compressive strength f_c. In contrast to elasto-plastic ground, elasto-viscoplastic ground responds as expected (the load increases with decreasing ground strength). The reason for the model behaviour becomes evident if we consider the radial deformations in the ground ahead of

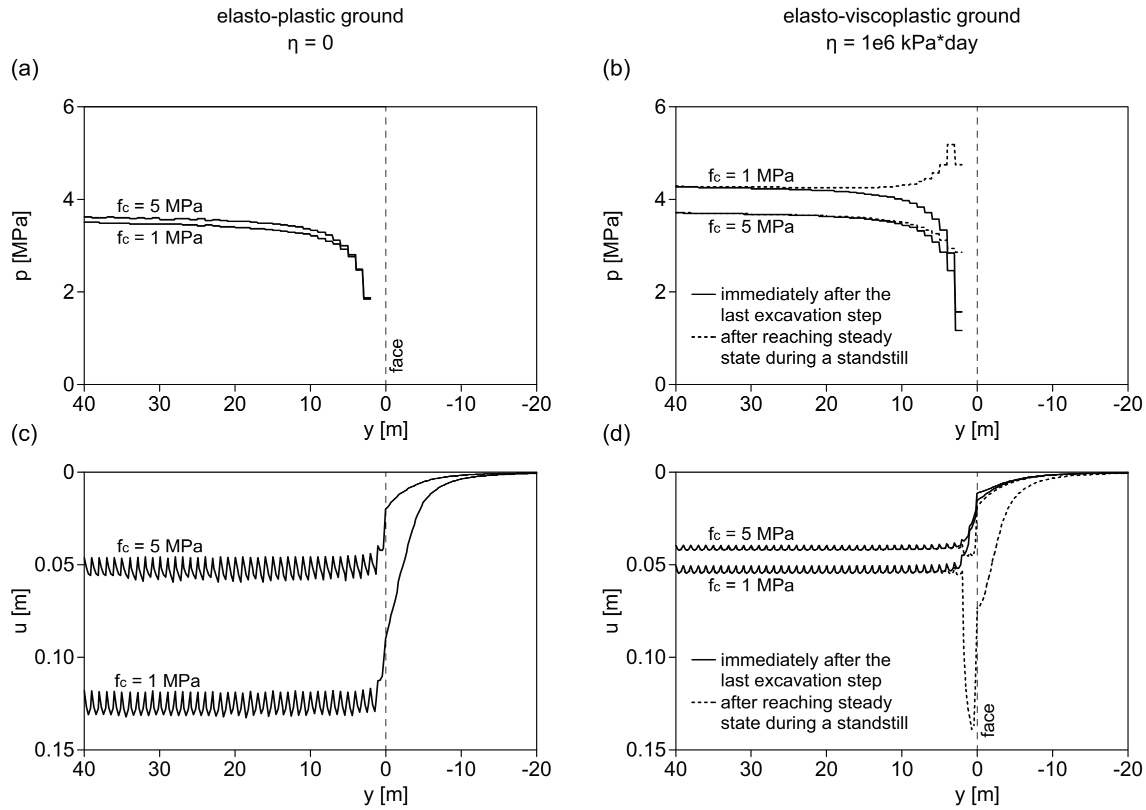

Fig. 11 Development of ground pressure along the tunnel (a) for elasto-plastic ground with time-independent response, (b) for an elasto-viscoplastic ground. Radial convergences along the tunnel (c) for elasto-plastic ground with time-independent response, (d) for an elasto-viscoplastic ground (c.f. Gioda and Cividini 1996)

the face (Fig. 11c and 11d). In contrast to elasto-plastic ground, the radial deformations ahead of the face and thus also the stress relief in elasto-viscoplastic ground depend only slightly on the ground strength f_c, because the short-term response is mainly elastic for the assumed advance rate and viscosity.

Figure 12 shows the results of a parametric study into the effects of viscosity η and ground strength f_c on the lining pressure developing at a distance of five tunnel diameters behind the face. It can be seen that the paradox ceases to exist at viscosities $\eta \geq 10^5$ kPa*day, i.e. when the response of the

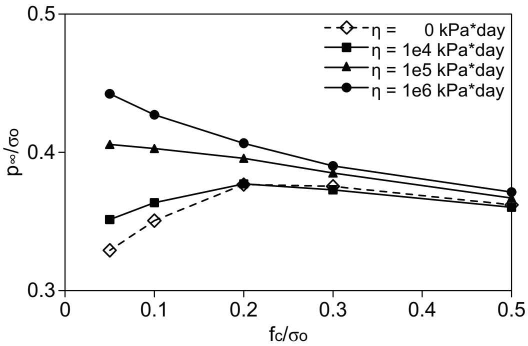

Fig. 12 Normalized final pressure on the lining p_∞/σ_0 as a function of the normalized uniaxial compressive strength f_C/σ_0 and of the viscosity η

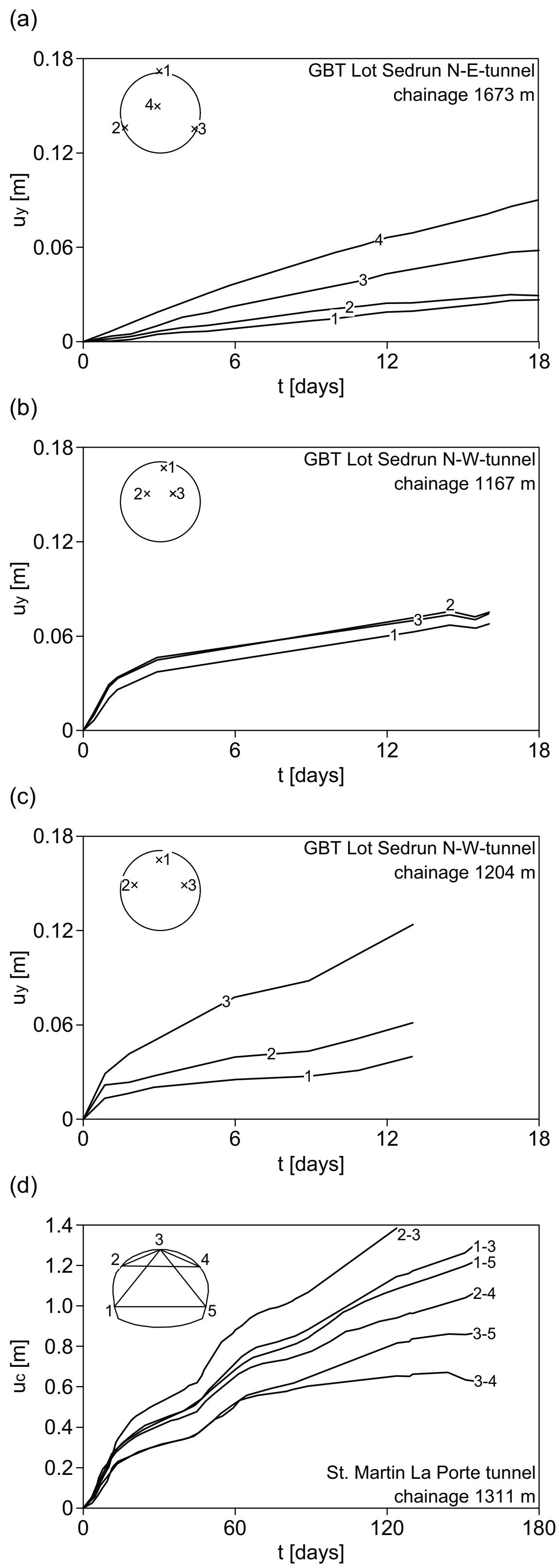

Fig. 13 Time-development, (a-c), of the face extrusion u_y in the Sedrun Lot of the Gotthard Base Tunnel (courtesy of AlpTransit Gotthard AG, Switzerland) and, (d), of the convergence u_c in the Saint Martin La Porte tunnel (Barla *et al.* 2008)

ground to tunnelling takes at least a few weeks (Table 2). Such a slow response is nothing unusual. For example, Figures 13a to 13c show the time-development of the face extrusion measured during excavation standstills at some cross-sections in the northern stretch of the Sedrun Lot, which is part of the new Gotthard Base Tunnel. The deformations develop within a period of 1 week to 1 month. The convergences recorded in the Saint Martin La Porte tunnel show that the transient process may even continue for several months (Fig. 13d).

In conclusion, as a consequence of the time-dependency of the ground response, the stress relief ahead of the face may be much less pronounced than predicted by the simplified time-independent computational models. This is sufficient to make the paradox disappear.

5 Effect of face reinforcement

5.1 Computational model

The effect of face reinforcement on the extrusion of the core has been studied intensively for shallow (e.g. Wong *et al.* 2004; Peila 1994) and also for deep tunnels (e.g. Oreste *et al.* 2004). The reinforcement provides an additional confinement for the ground in an axial direction, which increases the bearing capacity of the core, i.e. its ability to sustain a radial pressure, and therefore reduces the stress relief, which, as discussed in Section 2, is the main cause of the counter-intuitive behaviour.

The quantitative investigation of these effects is based upon the axially symmetric model of Figure 4a. The face reinforcement is taken into account in a simplified manner by prescribing a uniform pressure p_F to the face (cf. inset of Fig. 14).

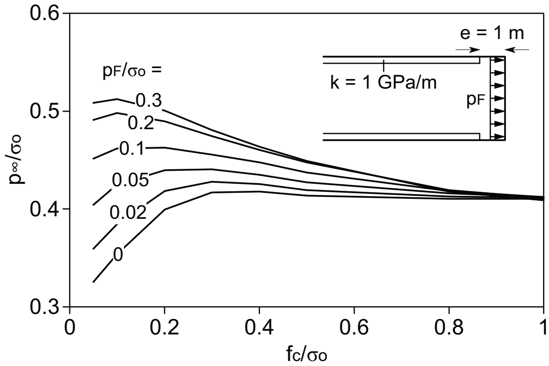

Fig. 14 Final lining load p_∞ as a function of the uniaxial compressive strength f_c and of the face support pressure p_F (all values normalized by the initial stress σ_0)

5.2 Model behaviour

Figure 14 shows the ground pressure developing upon the lining in the final state far behind the tunnel face as a function of the normalized ground strength f_c and of the normalized face support pressure p_F. The higher the face support pressure, the higher will be the final load. The model behaviour agrees with the results of Boldini *et al.* (2000) and Kasper and Meschke (2006), but does not seem to support the hypothesis formulated by Lunardi (2000), which postulates that the stresses on the lining are lower when the advance core is reinforced.

As expected on the basis of qualitative factors, the paradox becomes less and less pronounced with increasing face pressure and disappears at pressures p_F higher than 0.1 – 0.2 σ_0. This threshold value is not feasible in the case of deep tunnelling under a high initial stress σ_0. Consider, for example, a heavy face support consisting of one 300 kN bolt per sqm, thus providing a face pressure p_F of 0.3 MPa. In order that the normalized face support pressure p_F/σ_0 is higher than the threshold value of 0.1 - 0.2, the depth of cover should be smaller than about 100 m. Face reinforcement is of secondary importance as far as the topic of the present Paper is concerned.

6 Effect of yielding support

6.1 Computational model

The present Section investigates whether the deformations behind the face, which occur intentionally by means of a yielding support, eliminate the paradox. For the purpose of the present investigation, the mixed boundary condition presented in the recent paper of Cantieni and Anagnostou (2009b) will be applied in order to map the complete behaviour of the yielding support system. The response of the yielding support to loading can be approximated by a tri-linear characteristic line (Fig. 15a). The first part of the characteristic line is governed by the stiffness k_l of the system up to the onset of yielding. The second part of the line corresponds to the phase, where the support system deforms under a constant pressure p_y. When the amount of over-excavation u_{oe} is used up, the third phase is initialised. The system is made practically rigid (stiffness k), e.g. by applying shotcrete, with the consequence that an additional pressure accumulates upon the lining. A yielding support which consists of sliding steel sets placed every 0.5 m, each offering a sliding hoop resistance of 800 kN (four friction loops offering a sliding resistance of 200 KN each), will provide a yielding support pressure p_y equal to 400 kPa. After the over-excavation gap is used up, a shotcrete lining is placed, which offers a stiffness k of 1 GPa/m. The stiffness k_l is of subordinate importance for the final ground pressure and is taken as 1 GPa/m. With the exception of this boundary condition, the numerical model is the same as previously (Fig. 4a).

6.2 Model behaviour

Figure 15b shows the ground pressure developing upon the lining in the final state far behind the tunnel face as a function of the normalized ground strength f_c and of the amount of over-excavation u_{oe}. The upper line (u_{oe} = 0) denotes a rigid support installed 1 m behind the face (c.f. line e = 1 m in Fig. 5a) and shows the paradox. If a very small theoretical over-excavation u_{oe} of 0.05 m is applied, the paradox disappears. In the present example, the over-excavation will not be used up completely in the case of high amounts of over-excavation. Consider, for instance, an over-excavation of 0.4 m. The final rock pressure acting upon the lining is equal to the yielding support pressure p_y for all ground strengths, because the over-excavation is not used completely and thus the third phase of the system is not reached. (For a detailed analysis of the interaction between yielding supports and ground see Cantieni and Anagnostou, 2009b). Figure 15c shows the conver-

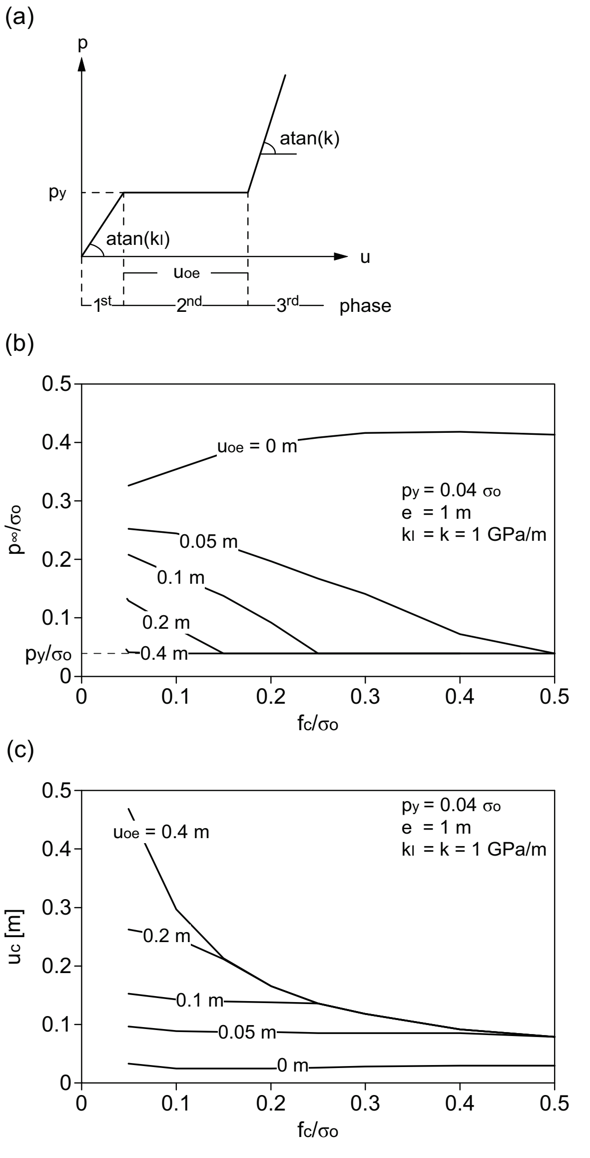

Fig. 15 Normalized convergence u_C/a as a function of the normalized uniaxial compressive strength f_C/σ_0 and of the normalized yield pressure p_y/σ_0 of the support

gences of the opening u_C (sum of the convergences of the support and the convergences over the unsupported span) as a function of the normalized ground strength f_c. The deformations also show an intuitive behaviour: lower convergences for increasing ground quality, particularly for cases where the over-excavation is not used up.

In summary, the model of a tunnel with yielding support shows an intuitive behaviour for both the rock pressure on the lining and the ground convergences.

7 Effect of the low stiffness of green shotcrete

7.1 Computational model

In general, a shotcrete lining develops its stiffness over time and reaches its long-term stiffness a certain distance behind the face. The assumption of a stiff shotcrete lining right from the start is valid only for low advance rates. The higher the advance rate, the newer will be the shotcrete and the lower its resistance to ground deformations in the vicinity of the face. The time-dependent interaction between shotcrete and the ground has been investigated, e.g. by Graziani *et al.* (2005), Oreste (2003), Boldini *et al.* (2005) and Pöttler (1990). In the present Section we focus on the question of whether the paradox (which, as stated in Section 2, is particularly pronounced in the case of stiff linings) persists when taking into account the initially low stiffness of green shotcrete.

In our computations, the time-dependency of the Young's modulus of shotcrete $E_L(t)$ is taken into account by adopting the empirical relationship of Chang (1994):

$$E_L(t)\,/\,E_{L,28} = 1.062\ \exp\left(-\frac{0.446}{t^{0.6}}\right), \tag{5}$$

where $E_{L,28}$ denotes the Young's modulus of shotcrete at 28 days (taken to 30 GPa in the present case) and t is the shotcrete age in days. Figure 16a shows the evolution of the normalized Young's

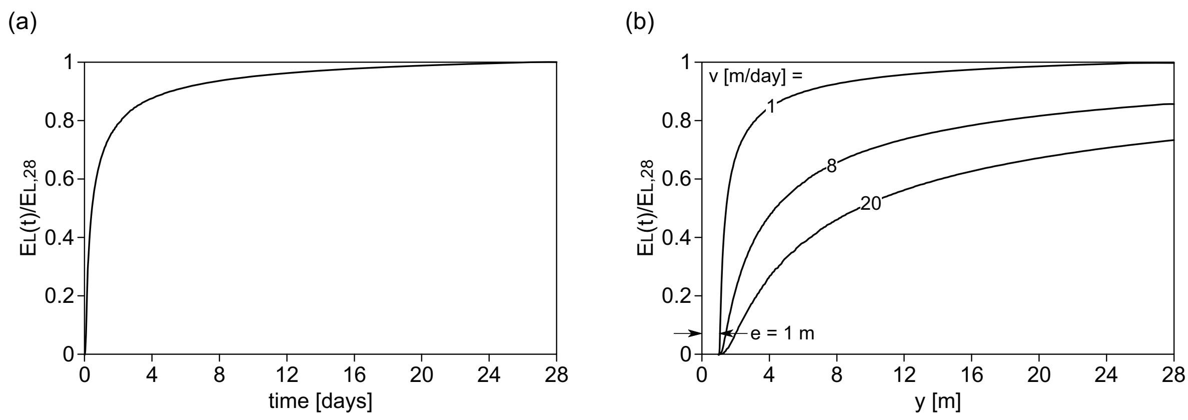

Fig. 16 (a) Time-development of the Young's modulus of the shotcrete after Chang (1994); (b) Normalized Young's modulus of the shotcrete as a function of the distance from the face and of the advance rate v

modulus of the shotcrete over the time, while Figure 16b, which is nothing more than a simple transformation of Figure 16a, shows the distribution of the Young's modulus along the tunnel for advance rates of 1, 8 and 20 m/day.

Again, the axially symmetric numerical model of Figure 4a is used and the problem is solved by the steady state method. The time-dependency of the shotcrete stiffness (Fig. 16a) or the spatial variation of the stiffness along the tunnel (Fig. 16b) is taken into account numerically by considering a series of superimposed lining layers (see Appendix B for details).

7.2 Model behaviour

Figure 17 illustrates the effect of the advance rate v on the distribution of ground pressure along the tunnel for a lower and for a higher uniaxial compressive strength f_c of the ground, while Figure 18 provides a more complete picture of these effects on the final lining load. The results agree with those of Graziani *et al.* (2005) concerning the effect of the advance rate on the final lining pressure.

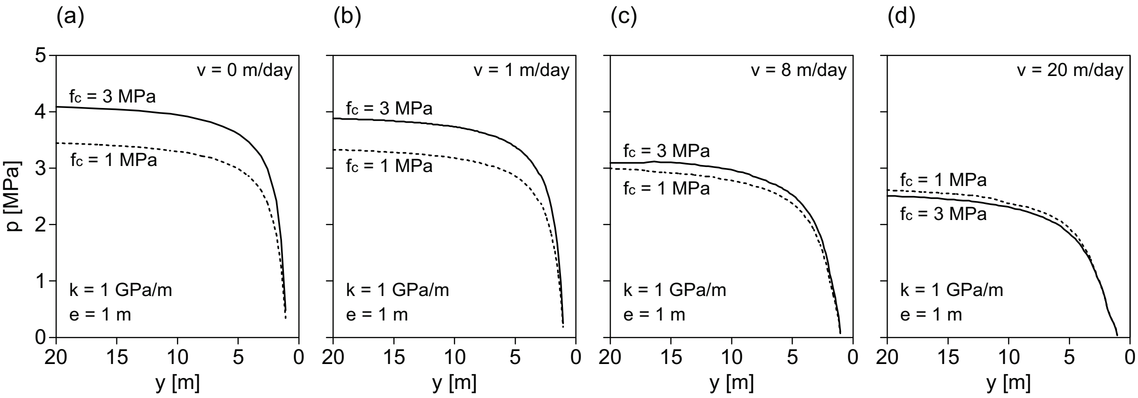

Fig. 17 Development of the ground pressure acting upon the lining for advance rates v of 0 – 20 m/day

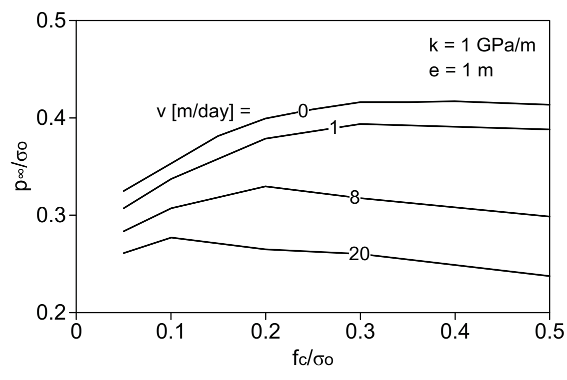

Fig. 18 Normalized final lining load p_∞/σ_0 as a function of the normalized uniaxial compressive strength f_C/σ_0 and of the advance rate v

As a consequence of the reduced stiffness of the shotcrete near the face, the counter-intuitive behaviour becomes less and less pronounced as the advance rate increase, but nevertheless does not disappear even at very high advance rates (20 m/day). Advance rates such as this cannot be realized in combination with shotcrete.

In conclusion, the counter-intuitive model behaviour persists even when taking into account the changes to the shotcrete over time.

8 Effect of the overcut in shield tunnelling

8.1 Computational model

We shall next investigate whether the deformations that inevitably occur in shield tunnelling are such that the paradox disappears. The computations concern the same axially symmetric computational model as in Figure 4a. The only difference is the boundary condition at the tunnel wall, which in the present case accounts, (i), for the gap existing around the shield due to the overcut ΔR (Fig. 9b) and, (ii), for the complete radial unloading of the excavation boundary at the installation point of the segmental lining immediately behind the shield tail (at y = 8 m). Details concerning the modelling of the ground-support interface can be found in Ramoni and Anagnostou (2011). Taking into account the modulus of elasticity of the steel (E_S = 210 GPa) and assuming a shield thickness of d_S = 8 cm, the radial stiffness of the shield is taken as k_S = 1 GPa/m.

8.2 Model behaviour

Figures 19a, b and c show the distribution of the ground pressure along the tunnel (shield up to y = 8 m, segmental lining for y > 8 m) for an overcut ΔR of 0, 0.15 m and 0.30 m, respectively, and for

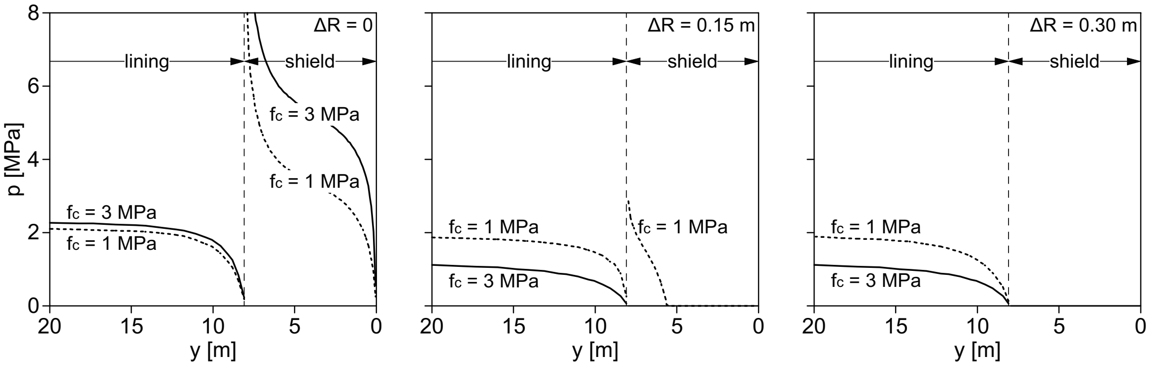

Fig. 19 Development of the ground pressure p along the tunnel (shield and lining) for two values of the uniaxial compressive strength f_c and for an overcut ΔR of 0 - 0.30 m

two values of the uniaxial compressive strength f_c. Let us consider first the case of zero overcut. (As an overcut is always foreseen for the purpose of steering the machine, this case is rather theoretical but may occur also in practice in exceptional cases, e.g. due to packing of the gap around the shield with fines.) The model behaviour is counter-intuitive in this case (Fig. 19a), in that the higher strength ground develops a higher load than the lower strength ground. The paradox is particularly pronounced in relation to the shield loading and also applies to the lining.

In the case of an overcut ΔR of 0.15 m or higher, however, the system allows for deformations to occur behind the face and thus the paradox disappears. According to Figure 19b, the ground closes the gap and starts to exert a load upon the shield only in the case of the lower strength value (f_c = 1 MPa). In the case of an even larger overcut (ΔR = 0.30 m, Fig. 19c), the gap around the shield remains open even for the lower strength value.

9 Conclusions

The computational models commonly used for tunnel design predict under certain conditions (i.e. support from a stiff lining near to the tunnel face, weak ground, high initial stress) that the load developing upon the lining increases with the strength of the ground. Such behaviour deserves to be called a paradox because it is clearly contrary to what one would expect on the basis of intuition and tunnelling experience. The reason for this counter-intuitive behaviour is the stress relief which takes place in the ground ahead of the face and which is more pronounced in the case of a low strength ground. The decisive simplifying modelling assumptions, i.e. the assumptions which cause the difference between model behaviour and actual behaviour, are related: (i), to the rheological behaviour of the ground (which is usually neglected in design computations, but is particularly important in the case of overstressed ground, limiting the extent of stress relief ahead of the face); and, (ii), to the stiffness of the support system, which may - due to the nature of construction procedures - be considerably lower than it is assumed to be in the design calculations. The effects of face reinforcement or of the time-dependency of the shotcrete stiffness are of secondary importance with respect to the investigated aspect of the model behaviour.

The findings of the present Paper illustrate the uncertainties (both quantitative and qualitative) that exist in all computational models – even in the very familiar and well-established ones - and emphasize the importance of a careful interpretation of the computational results and of a critical review of the underlying modelling assumptions. Taking into account the two main effects mentioned above in the design computations eliminates the paradoxical model behaviour.

Appendix A of Part III

Demonstration of the meaning of the viscosity η

In order to demonstrate the meaning of the viscosity values we examine the classic rotationally symmetric tunnel problem under plane strain conditions. The constitutive model was presented in Section 4, while the model parameters are given in Table 1.

Starting from the initial state, we first simulate tunnel excavation on the assumption that it occurs instantaneously. We then carry out a transient analysis until a steady state is reached. Figure 20 shows the typical time-development of the convergence. One can see the instantaneous, excavation-induced convergence, which, as explained in Section 4, is purely elastic. As a measure of how rapidly the ground responds to tunnel excavation, an arbitrary characteristic time period may be adopted – for example, the time $t_{95\%}$ that must elapse in order that the time-dependent convergence reaches 95% of its final value. In the example of Figure 20 (viscosity $\eta = 10^5$ kPa * day), this time period will be about 15 days long. For dimensional reasons, the characteristic time is proportional to the viscosity η (a viscosity ten times higher will mean that the time taken to reach a given deformation will increase by a factor of ten).

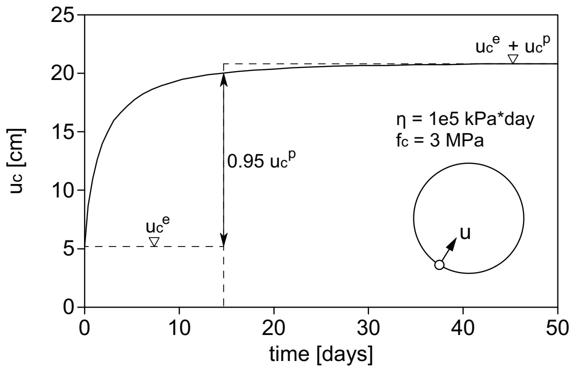

Fig. 20 Time-development of the convergence of an unsupported circular tunnel under plane strain conditions

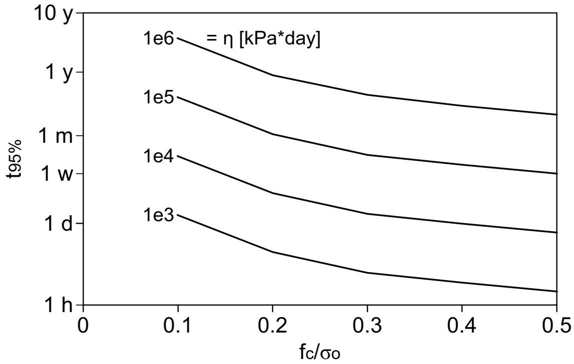

Fig. 21 Characteristic time $t_{95\%}$ as a function of the normalized uniaxial compressive strength f_C/σ_0 and of the viscosity η (the time axis labels y, m, w, d and h denote year, month, week, day and hour, respectively)

Table 2 is based upon the results of a parametric study into the effects of the uniaxial compressive strength f_c and the viscosity η on the characteristic time $t_{95\%}$ (Figure 21).

Appendix B of Part III

Numerical modelling of time-dependent support stiffness

Boundary condition for a lining of constant stiffness

The resistance of a lining with constant stiffness *k* is taken into account in the steady state numerical solution method by imposing (as a boundary condition) a radial pressure *p(y)* which is proportional to the deformation *of the lining* at location *y* and depends therefore not only on the convergence *u(y)* of the ground but also on its deformation *u(e)* at the installation point *(y = e)* of the lining (Anagnostou 2007):

$$p(y) = k\,(u(y) - u(e))\,. \tag{B-1}$$

Boundary condition for a lining of time-dependent stiffness

In the case of a lining with time-dependent properties, however, the calculation of the pressure along the lining has to be carried out by numerical integration in the opposite direction to that of the tunnel advance (Anagnostou 2007). Figure 22a shows schematically the integration points and intervals. The pressure p_{j+1} at point *j*+1 can be expressed by following equation:

$$p_{j+1} = p_j + \Delta p_{j+1}\,, \tag{B-2}$$

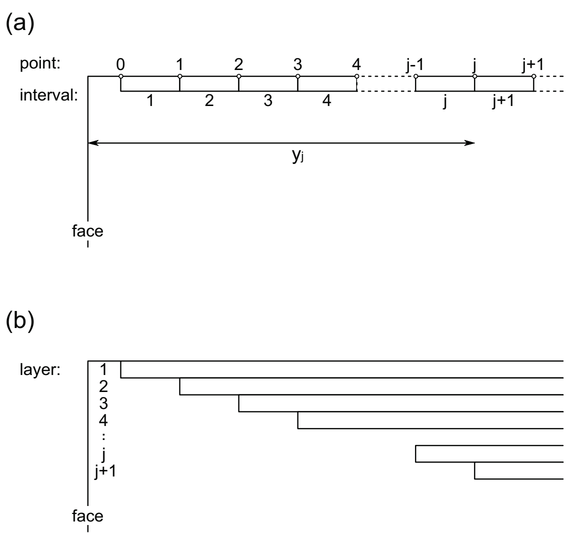

Fig. 22 (a) Definition of the lining segments and nodes, (b) Definition of the lining layers

where Δp_{j+1} denotes the increase in pressure over the integration interval j+1, which extends from point j to point j+1:

$$\Delta p_{j+1} = k_{j+1}\,(u_{j+1} - u_j)\,, \tag{B-3}$$

where u_{j+1}-u_j is the increase in ground deformation from point j to point j+1, while k_{j+1} denotes the average stiffness over the integration interval j+1:

$$k_{j+1} = \frac{E_L(t)d}{a^2}\,, \tag{B-4}$$

where d is the thickness of the lining, a is the tunnel radius, $E_L(t)$ is the Young's modulus of the lining (according to Eq. 5) and t is the age of the shotcrete. The latter depends on the distance from the face and on the advance rate:

$$t = \frac{(y_j + y_{j+1})/2}{v}\,. \tag{B-5}$$

Implementation of the boundary condition in the numerical model

The boundary condition described by the Eqs. (B-2) to (B-5) is implemented in the numerical model by a series of superimposed fictitious lining layers, each having a different stiffness $k^{(i)}$ and starting at a different distance behind the face (Fig. 22b): The fictitious lining layer i starts at integration point i-1 (and, therefore, the radial displacement u_{i-1} represents the pre-deformation to be considered for this layer), contains all integration intervals ≥ i and has a stiffness which is equal to the increase in stiffness from the integration interval i-1 (i.e. the integration interval just before the starting point of the fictitious layer i) to integration interval i (i.e. the first integration interval belonging to fictitious layer i):

$$k^{(i)} = k_i - k_{i-1} \quad \text{(with } k_0 = 0\text{)}. \tag{B-6}$$

It will subsequently be demonstrated that the superimposed fictitious lining layers defined in this way are equivalent to a lining with a time-dependent stiffness, i.e. they provide a total support pressure which is equal to that of Eqs. (B-2) and (B-3).

Proof

First of all, one can readily verify that Eq. (B-6) ensures that the total stiffness offered by the superimposed fictitious lining layers in an arbitrary interval m is equal to the stiffness k_m of the shotcrete lining over this interval. The total stiffness offered by the superimposed fictitious layers is equal to the sum of the stiffnesses of the layers containing the interval m, i.e. of the layers 1 to m. Consequently, the total stiffness is equal to

$$\sum_{i=1}^{m} k^{(i)} = \sum_{i=1}^{m} \left(k_i - k_{i-1}\right) = k_m\,. \tag{B-7}$$

As each fictitious lining layer has a constant stiffness, its resistance to deformation can be calculated on the basis of Eq. (B-1). Taking into account the layer stiffness according to Eq. (B-6), as well as the relevant pre-deformation of each layer (which as said above is equal to u_{i-1} for layer i), the pressure exerted by an arbitrary layer i at an arbitrary point j reads as follows:

$$p_j^{(i)} = k^{(i)} \left(u_j - u_{i-1}\right) = \left(k_i - k_{i-1}\right)\left(u_j - u_{i-1}\right). \tag{B-8}$$

The total pressure at point *m* is obtained by a summation of the pressures of the layers that contain point *m*, i.e. of the layers 1 to *m*:

$$p_m = \sum_{i=1}^{m} p_m^{(i)} = \sum_{i=1}^{m}\left(k_i - k_{i-1}\right)\left(u_m - u_{i-1}\right). \tag{B-9}$$

Analogously, for point *m*+1,

$$\begin{aligned} p_{m+1} &= \sum_{i=1}^{m+1}\left(k_i - k_{i-1}\right)\left(u_{m+1} - u_{i-1}\right) = \\ &= \sum_{i=1}^{m}\left(k_i - k_{i-1}\right)\left(u_m - u_{i-1}\right) + \sum_{i=1}^{m}\left(k_i - k_{i-1}\right)\left(u_{m+1} - u_m\right) + \left(k_{m+1} - k_m\right)\left(u_{m+1} - u_m\right) = \\ &= p_m + \sum_{i=1}^{m+1}\left(k_i - k_{i-1}\right)\left(u_{m+1} - u_m\right) = p_m + k_{m+1}(u_{m+1} - u_m)\,, \end{aligned} \tag{B-10}$$

which agrees with Eqs. (B-2) and (B-3).

References

AFTES 2002. Recommandations relatives à la methode convergence-confinement. Association Française des Travaux en Souterrain, Groupe de travail n°7 (animé par M. Panet avec la collaboration de A. Bouvard, Dardard B, Dubois P, Givet O, Guilloux A, Launay J, Nguyen Minh Duc, Piraud J, Tournery H, Wong H). Tunnels et Ouvrages Souterrains 170:79-89

Anagnostou, G. 2007. Continuous tunnel excavation in a poro-elastoplastic medium. In: Pande, Pietruszczak (eds) Numerical Models in Geomechanics (NUMOG X), Rhodes, Greece. Taylor & Francis, pp 183-188

Anagnostou, G., Kovári, K. 1993. Significant parameters in elastoplastic analysis of underground openings. Journal of Geotechnical Engineering 119 (3):401-418

Barla, G., Bonini, M., Debernardi, D. 2008. Time Dependent Deformations in Squeezing Tunnels. In: The 12th International Conference of International Association for Computer Methods and Advances in Geomechanics (IACMAG), Goa, India, pp 4265-4275

Bernaud, D. 1991. Tunnels profonds dans les milieux viscoplastiques: approches expérimentale et numérique. PhD Thesis, Ecole Nationale des Ponts et Chaussées, Paris, France

Boldini, D., Graziani, A., Ribacchi, R. 2000. L’analisi tensio-deformativa al fronte di scavo e nella zona del retrofronte. In: Lo scavo meccanizzato delle gallerie, mir2000 - VIII ciclo di conferenze di meccanica e ingegneria delle rocce, Torino, Pàtron Editore Bologna, pp 159-216

Boldini, D., Lackner, R., Mang, H.A. 2005. Ground-Shotcrete Interaction of NATM Tunnels with High Overburden. Journal of Geotechnical and Geoenvironmental Engineering July:886-897

Brinkgreve, R.B.J. 2002. PLAXIS 2D, Version 8. Lisse, Netherlands

Cantieni, L., Anagnostou, G. 2009a. The effect of the stress path on squeezing behaviour in tunnelling. Rock Mechanics and Rock Engineering 42 (2):289–318. doi:10.1007/s00603-008-0018-9

Cantieni, L., Anagnostou, G. 2009b. The interaction between yielding supports and squeezing ground. Tunneling and Underground Space Technology 24 (3):309-322. doi:10.1016/j.tust.2008.10.001

Chang, Y. 1994. Tunnel support with shotcrete in weak rock – A rock mechanics study. Ph.D., Royal Institute of Technology, Stockholm, Sweden

Chern, J.C., Shiao, F.Y., Yu, C.W. 1998. An empirical safety criterion for tunnel construction. In: Regional Symp. on Sedimentary Rock Engineering, Taipei, Taiwan, pp 222-227

Debernardi, D., Barla, G. 2009. New Viscoplastic Model for Design Analysis of Tunnels in Squeezing Conditions. Rock Mechanics and Rock Engineering (42):259-288. doi:10.1007/s00603-009-0174-6

Ehrbar, H., Pfenninger, I. 1999. Umsetzung der Geologie in technische Massnahmen im Tavetscher Zwischenmassiv Nord. In: Vorerkundung und Prognose der Basistunnels am Gotthard und am Lötschberg, Symposium Geologie Alptransit, Zurich, Switzerland. A.A.Balkema Rotterdam Brookfield, pp 381-394

Gioda, G., Cividini, A. 1996. Numerical methods for the analysis of tunnel performance in squeezing rocks. Rock Mechanics and Rock Engineering 29 (4):171-193

Graziani, A., Boldini, D., Ribacchi, R. 2005. Practical estimate of deformations and stress relief factors for deep tunnels supported by shotcrete. Rock Mechanics and Rock Engineering 38 (5):345-372

Guo, C. 1995. Calcul des tunnels profonds soutenus - méthode stationnaire et méthodes approchées. PhD Thesis, Ecole Nationale des Ponts et Chaussées, Paris, France

Itasca 2006. Flac2D 5.0, User's Manual. Itasca Inc., Minneapolis, USA

Kasper, T., Meschke, G. 2006. On the influence of face pressure, grouting pressure and TBM design in soft ground tunnelling. Tunnelling and Underground Space Technology 21 (2):160-171

Kovári, K., Staus, J. 1996. Tunnelbau in druckhaftem Gebirge, Falldarstellungen. ETH Zurich, Institut für Geotechnik, August 1996

Lavdas, N. 2010. Einsatzgrenzen von Tübbingausbau beim TBM - Vortrieb in druckhaftem Gebirge. Master Thesis, ETH Zurich, Zurich, Switzerland

Lunardi, P. 2000. The design and construction of tunnels using the approach based on the analysis of controlled deformation in rocks and solis. Tunnels & Tunnelling International *special supplement, ADECO-RS approach* (May)

Madejski, J. 1960. Theory of non-stationary plasticity explained on the example of thick-walled spherical reservoir loaded with internal pressure. Archiwum Mechaniki Stosowanej 5/6 (12):775-787

Mair, R.J. 2008. Tunnelling and geotechnics: new horizons. Géotechnique 58 (9):695-736. doi: 10.1680/geot.2008.58.9.695

Nguyen-Minh, D., Corbetta, F. 1991. New calculation methods for lined tunnels including the effect of the front face. In: 7th Congress of the ISRM, Achen, pp 1334-1338

Nguyen-Minh, D., Corbetta, F. 1992. New methods for rock-support analysis of tunnels in elastoplastic media. In: McCreath K (ed) Rock Support in Mining and Underground Construction, Sudbury, Canada, Balkema, Rotterdam, pp 83-90

Nguyen-Minh, D., Guo, C. 1993. Sur un principle d' interaction massif-soutenement des tunnels en avancement stationnaire. In: Ribeiro, Sousa, Grossmann (eds) Eurock' 93, Lisboa, Portugal, Balkema, Rotterdam, pp 171-177

Nguyen-Minh, D., Guo, C. 1996. Recent progress in convergence confinement method. In: Barla G (ed) Eurock'96, Torino, Italy, Balkema Rotterdam, pp 855-860

Oreste, P., Peila, D., Pelizza, S. 2004. Face Reinforcement in Deep Tunnels. Felsbau 22 (4):20-25

Oreste, P. 2003. A procedure for determining the reaction curve of shotcrete lining considering transient conditions. Rock Mechanics and Rock Engineering 36 (3):209-236

Panet, M. 1995. Le calcul des tunnels par la méthode convergence-confinement. Presses de l'école nationale des ponts et chaussées, Paris, France

Peila, D. 1994. A theoretical study of reinforcement influence on the stability of a tunnel face. Geotechnical and Geological Engineering 12:145-168

Perzyna, P. 1966. Fundamental Problems in Viscoplasticity. *Advances in Applied Mechanics* 9:243-377

Pöttler, R. 1990. Time-dependent rock - shotcrete interaction. A numerical shortcut. Computers and Geotechnics 9:149-169

Ramoni, M., Anagnostou, G. 2010. Thrust force requirements for TBMs in squeezing ground. Tunnelling and Underground Space Technology 25 (4):433-455

Ramoni, M., Anagnostou, G. 2011. The Interaction Between Shield, Ground and Tunnel Support in TBM Tunnelling Through Squeezing Ground. Rock Mech Rock Engng 44 (1):37-61. doi:101007/s00603-010-0103-8

Vlachopoulos, N., Diederichs, M.S. 2009. Improved Longitudinal Displacement Profiles for Convergence Confinement Analysis of Deep Tunnels. Rock Mech Rock Engng 42:131-146

Wong, H., Trompille, V., Dias, D. 2004. Extrusion analysis of a bolt-reinforced tunnel face with finite ground-bold bond strength. Can Geotech J 41:326-341. doi:10.1139/T03-084

PART IV

ON THE VARIABILITY OF SQUEEZING IN TUNNELLING

The intensity of rock deformations and rock pressures in a tunnel section where there are squeezing conditions may vary over short distances. The variability of squeezing can be traced back to heterogeneities of the ground at different scales and with respect both to its mechanical and to its hydraulic characteristics. Often the cause of this phenomenon is an advance through a sequence of rock zones with different degrees of crushing or shearing. The results of numerical calculations indicate that even relatively thin competent rock interlayers may have a pronounced stabilizing effect. However, even in a macroscopically homogeneous rock mass, a large variation of deformations may be observed. This can be explained theoretically by the fact that the results of ground response analyses are highly sensitive to minor changes in rock properties.

1 Introduction

Tunnel excavation in weak rocks may trigger large time-dependent deformations. Often the intensity of squeezing varies over short distances for one and the same excavation method, temporary support, depth of cover and lithology (Kovári 1998). The variability of squeezing makes tunnel construction very demanding as it decreases the predictability of the conditions ahead of the tunnel face even after experience has been built up with a specific geological formation during excavation. The present paper aims at a better understanding of the observed variability, which can be traced back basically to two different causes. On the one hand, relatively small fluctuations in the mechanical and hydraulic properties of a macroscopically homogeneous rock mass may have a major effect on the developing deformations and pressures. On the other hand, rock structure heterogeneity (even on the scale of few meters) may lead to significant variations in the ground response. Section 2 discusses the sensitivity of ground response to small variations in rock mass properties by means of computational results and with reference to tunnelling experience, while Section 3 deals with the case of a heterogeneous rock mass consisting of alternating weak and hard rock zones.

2 The sensitivity of ground response

2.1 Tunnelling experience – Case 1

As an example of squeezing variability, the northern Tavetsch massif crossed by the new Gotthard Base Tunnel at a depth of 800 m is worthy of mention. During mountain formation this zone was subjected to intensive tectonic action, resulting in alternating layers of thickness in the range of decimetres to decametres, which consist of intact to more or less strongly kakiritic gneisses, slates, and phyllites (the term “kakirite” denotes a broken or intensively sheared rock, which has lost a large part of its original strength, cf. Schneider 1997). The critical zone was about 1150 m long. Squeezing was tackled through a yielding support system (Kovári *et al.* 2006). In the first half of this zone, excavation proceeded through alternating layers of more or less kakiritized rock. The layers are oriented perpendicularly to the tunnel axis. Figure 1 shows the horizontal displacements of the walls of the two tubes as well as the degree of rock kakiritization. The latter was determined based upon a project-specific classification scheme and according to inspections of the exposed rock. According to Figure 1, the convergences observed within apparently homogeneous zones vary considerably (see, e.g., western tube, ch. 1240 to 1300). On the other hand, a rough correlation exists between the degree of kakiritization, the thickness of the weak zones and the observed displacements. It is, for example, remarkable that in a short zone with extreme kakiritization smaller convergences occurred than in a similar longer zone (eastern tube ch. 1183 to 1190 and 1255 to 1285). Furthermore, the deformations occurring in the weakest zones seem to depend also on the

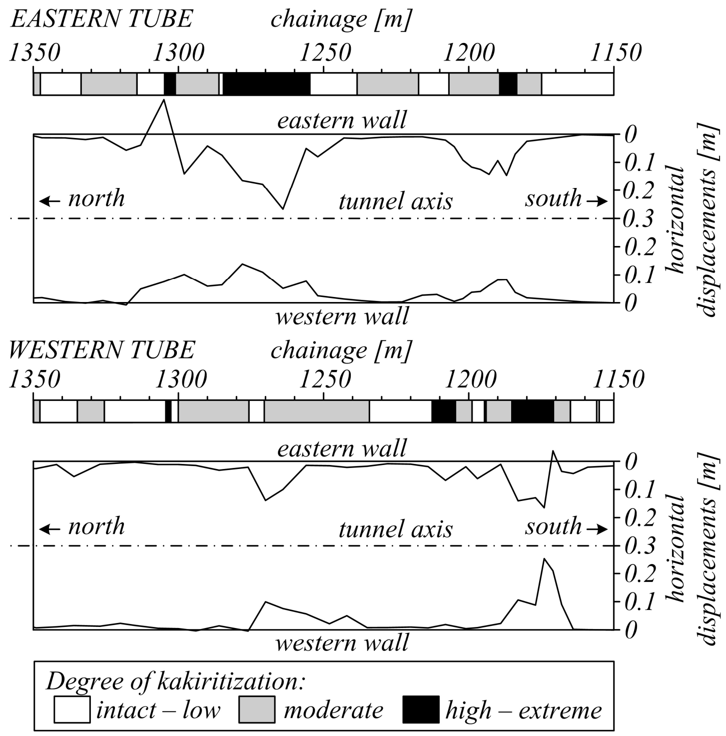

Fig. 1 Gotthard Base Tunnel, northern Tavetsch massif: Horizontal displacements of the tunnel walls occurring in the part of the tunnel between 5 and 30 m behind the face (by choosing an advance-dependent illustration the influence of standstills and different advance rates can be reduced as the deformations are, in the present case, mainly due to the stress re-distribution associated with the advance of the face)

quality of the adjacent, more competent rock. So, heterogeneities at different scales are responsible for the observed variability.

The variability of the squeezing can be explained quantitatively by means of computational results obtained on the basis of a simple rotational symmetric model of a circular opening. The mechanical characteristics of the kakiritic rocks have been established by means of a comprehensive laboratory testing program that was carried out in the design stage of the Gotthard Base Tunnel. Particular attention was paid to the control of pore water pressure during testing.

Both consolidated drained and consolidated undrained triaxial compression tests have been carried out. Despite the complex and changeable structure of kakiritic rocks, the test results have been remarkably uniform and can be approximated satisfactorily by an elastic, perfectly plastic constitutive model using the Mohr- Coulomb yield criterion (Vogelhuber 2007). From the evaluation of 63 tests, it was possible to derive average strength constants of c = 0.6 MPa and ϕ = 26.7°. The variation of the friction angle was particularly large (Fig. 2a). Figure 2b illustrates how sensitively the model behaviour depends on this parameter. The solid lines apply to the average friction angle and show the convergence as a function of the overburden for an unsupported tunnel (p = 0) as well as for a high support resistance (p = 2 MPa), while the hatched area shows the effect of a variation of the friction angle by ±15% (see Fig. 2a). Accordingly, the variation in the friction angle can have a far greater effect on the intensity of squeezing than the depth of cover. The sensitivity of the results with respect to the friction angle is particularly noticeable at low support resistances and high depths of cover. The next example shows, however, that an extreme squeezing variability is in no way limited to deep tunnels.

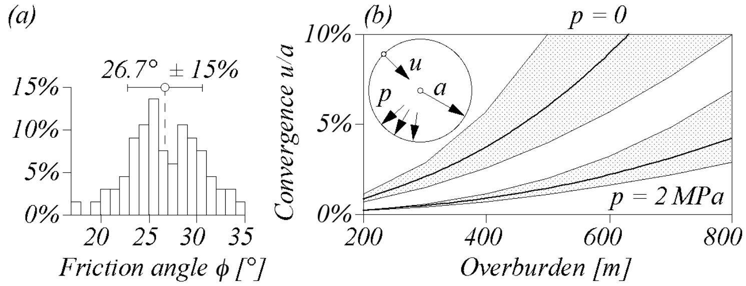

Fig. 2 (a) Distribution of friction angle (data from Vogelhuber 2007). (b) Convergence *u/a* as a function of the overburden (material constants: Young's modulus E = 2000 MPa, Poisson's ratio ν = 0.30, friction angle ϕ = 26.7° ± 15%, cohesion c = 0.6 MPa, dilatancy angle ψ = 5°)

2.2 Tunnelling experience – Case 2

Case 2 refers to a shallow tunnel constructed in the 1990s in South America. This tunnel had a horseshoe cross-section (Fig. 3b) and was excavated full face. In spite of the small overburden (50 m), convergences of up to 1 m occurred in a 200 m long critical zone consisting of intensively sheared graphitic phyllites. (Fig. 3a).

The very low resistance of the support (open shell without an invert lining, Fig. 3b) applied in combination with the sensitivity of ground behaviour to small variations in the friction angle (which is large at low support pressures, Fig. 3c) provides an explanation for the observed large variability of squeezing (0 - 10% convergence in a macroscopically homogeneous rock mass).

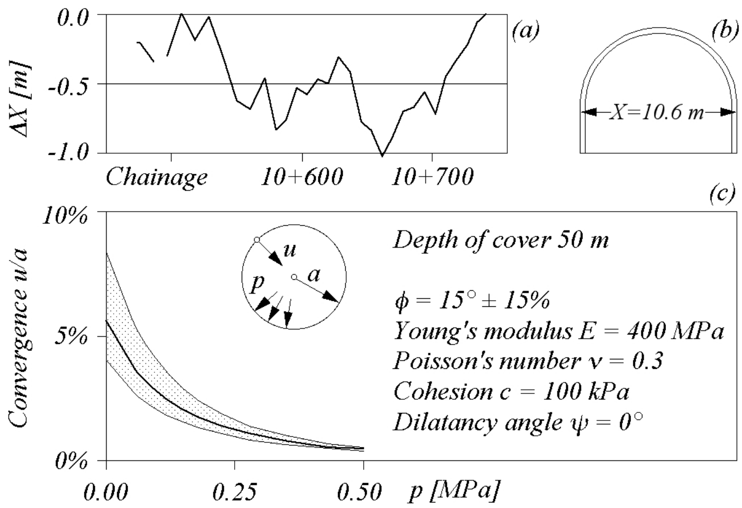

Fig. 3 Tunnel crossing graphitic phyllites: (a) Horizontal convergence ΔX in the critical zone; (b) Tunnel cross section; (c) Sensitivity of the ground response to a variation of the friction angle by 15%

2.3 The effects of hydraulic properties

Laboratory tests, field observations and theoretical considerations show that consolidation processes are, in addition to creep, highly important for the time-dependency of squeezing (Vogelhuber *et al.* 2004). The permeability of the ground governs the rate of the deformations associated with the dissipation of excess pore pressures. Squeezing rocks, such as shales, mudstones or altered metamorphic rocks, exhibit very low permeabilities. Thin permeable interlayers may cause, however, a substantial acceleration of the deformations as they lead to a shortening of the drainage paths. The same applies to the case of alternating layers of weak and hard rock, as the latter are often fractured and therefore increase the overall permeability. Consequently, permeability variations occurring within a macroscopically homogeneous rock mass may also lead to significantly different squeezing intensities. In the numerical example of Figure 4, the convergence occurring at a distance of two diameters behind the tunnel face varies between 1% and 5%, depending on the overall permeability.

3 Heterogeneous rock structures

As mentioned in Section 2.1, the rock structure that was encountered during excavation of the Gotthard Base Tunnel in about the first half of the northern Tavetsch massif was characterized by a sequence of weak and competent rock zones striking perpendicularly to the tunnel axis. When crossing alternating weak and hard rock zones, shear stresses are mobilized at their interfaces because the competent rock zones deform less than the weak zones. This so-called “wall-effect” was analysed by Kovári & Anagnostou (1995) for the borderline case of rigid competent rock. The interface shear stresses reduce the deformations of a weak zone considerably but, on the other hand, the weak ground imposes, via the shear stresses, an additional load on the competent rock. This

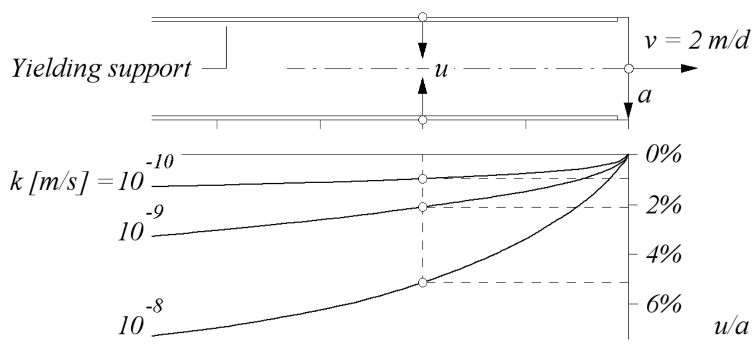

Fig. 4 Convergence along a tunnel with yielding support (250 kPa pressure) during continuous excavation (advance rate v = 2 m/d, permeability k = 10^{-10} – 10^{-8} m/s, Young’s modulus E = 1 GPa, Poisson’s number ν = 0.30, UCS = 0.75 MPa, friction angle ϕ = 25°, dilatancy angle ψ = 5°, initial stress σ_0 = 7.5 MPa, initial pore pressure p_0 = 1 MPa; computational model after Anagnostou 2007)

may lead to overstressing of the competent rock and thus reduce or eliminate its stabilizing effect. It is obvious, that the thinner the competent rock interlayers, the less they will stabilize the weak zones; and, vice versa, the thinner the weak zones are, the less will be the loading imposed by them on the competent rock. So, the wall-effect depends, in general, on the thicknesses of the alternating layers as well as on the strength and deformability both of the hard and the weak zones.

These interactions have been studied through axisymmetric numerical analyses looking at an unsupported cylindrical tunnel of radius a = 4 m that crosses alternating hard and weak layers of thickness h and w, respectively (Figure 5). The numerical model is delimited by the tunnel boundary (at $r = a$), the symmetry planes of two adjacent layers (at $y = h/2$ and $-w/2$, respectively) and the far field boundary (at r = 25 a). The hydrostatic and uniform initial stress σ_0 was taken to be equal to 10 MPa. The excavation was simulated thought a stepwise reduction of the tunnel boundary tractions from σ_0 to zero. The ground was modelled as an isotropic, linearly elastic, perfectly plastic material obeying the Mohr-Coulomb yield criterion. The material constants (see caption for Figure 5) have been chosen on the basis of the results of the investigation programme for the Tavetsch massif (Vogelhuber 2000).

According to Figure 5b, the interface shear stress τ_{ry} increases from zero (at the free excavation boundary) to its maximum value at the boundary of the plastic zone of the weak layer.

The orientation of the principal stresses of the weak zone indicates an arching effect in the longitudinal direction, which is favourable for the weak layer but leads to the above-mentioned additional

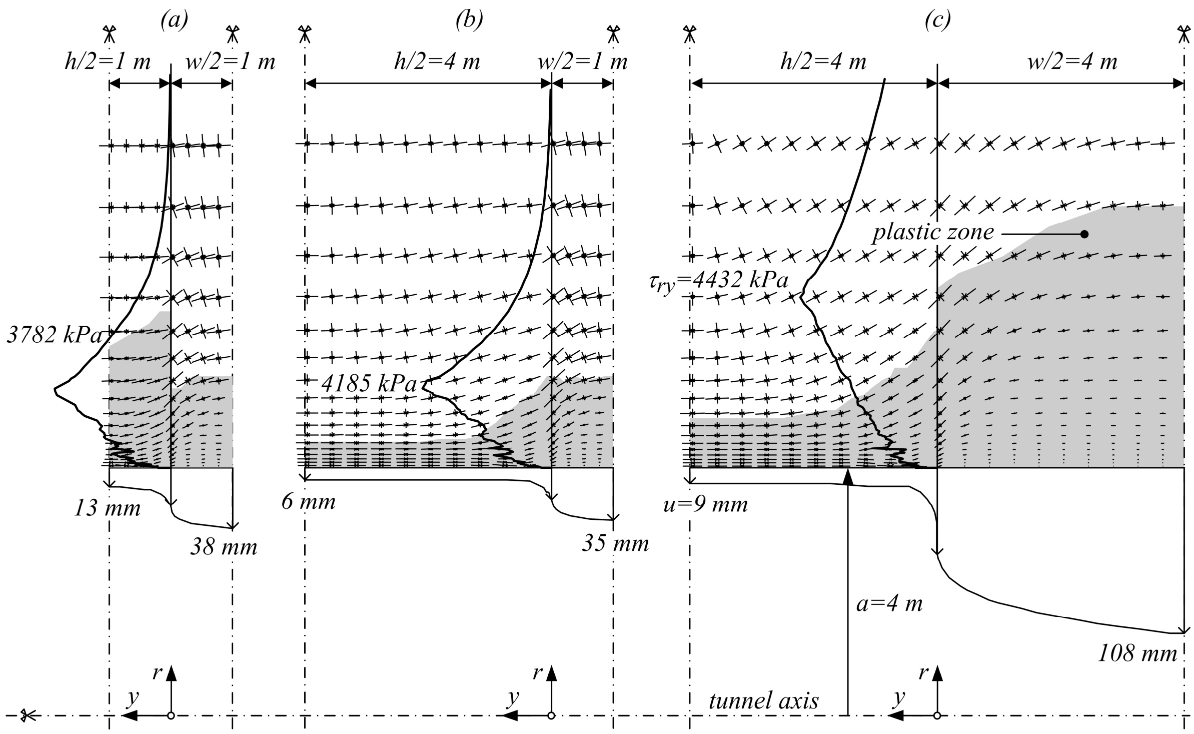

Fig. 5 Convergence u, plastic zone (hatched area), shear stress τ_{ry} along the interface of the two zones (y = 0) and principal stress orientation for (a) w/h = 1, w/a = 0.5; (b) w/h = 0.25, w/a = 0.5; and (c) w/h = 1, w/a = 2 (material constants: Young's Modulus E_{hard} = 10 GPa, E_{weak} = 1 GPa, Poisson's ratio ν = 0.3, friction angle φ = 25°, cohesion c_{hard} = 5 MPa, c_{weak} = 0.5 MPa, dilatancy angle ψ = 5°)

loading of the hard rock layer. This can been seen also by comparing the extend of the plastic zone developing in the present case (up to r = 1.35 a) with the plastic zones developing in a homogeneous ground (for w/a and $h/a \to \infty$, the plastic zone would reach up to r = 3.38 a and r = 1.08 a in the weak rock and in the hard rock, respectively).

A continuous reduction of the hard rock interlayer thickness from case (b) to case (a) has the consequence that the hard rock is getting more and more loaded (larger plastic zone and deformations). The interface shear stresses, the convergences, the stresses and the radius of the plastic zone in the weak layer do not change significantly. On the other hand, an increase of the weak zone thickness from case (b) to case (c) leads to considerably larger plastification and convergences of the weak rock. The interface shear stresses are also mobilized over a larger area and as a consequence the hard rock zone becomes more stressed. It is noticeable that the maximum convergences (at the symmetry plane of the weak zone) depend mainly on the weak zone length.

Figure 6 shows the results of a parametric study concerning the effects of the layer thicknesses w and h. The diagram shows the maximum convergence u_{max} (normalized by the convergence $u_{w,2D}$ that would develop in a very long weak zone) as a function of the thickness of the weak zone w/a. The values on the ordinate axis can be seen as a convergence reduction factor associated with the wall-effect. The latter is considerable for weak zones even as thick as about four diameters (w/a < 8 or w = 40 m for a normal traffic tunnel cross-section). With decreasing thickness of the hard zones, the wall-effect becomes less pronounced but it is still considerable at h/w = 1/16.

We examined, furthermore, how thin the alternating hard and weak zones must be in order that the convergence along the tunnel becomes approximately uniform. Figure 7 applies to alternating layers of equal thickness (h = w) and shows the ratio of minimum to maximum convergence (a measure for the convergence uniformity) as a function of the normalized layer thickness. At w/a = h/a = 1/2 (point A) the variation in convergence is still considerable (u_{min} / $u_{max} \approx$ 1/3): In a tunnel with a diameter of 10 m, the convergences would vary by a factor of three within 2 to 3 m (an interesting result particularly when taking into account the fact that monitoring stations are usually 5 – 10 m apart).

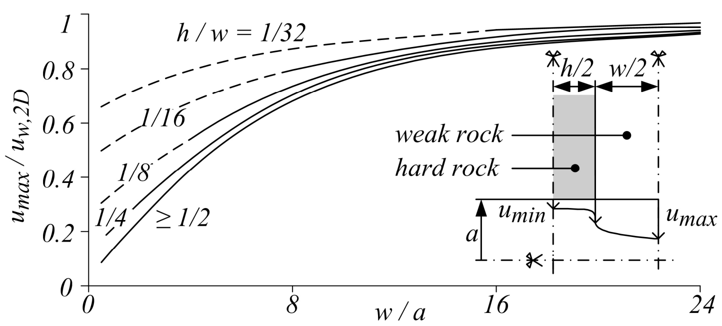

Fig. 6 Maximum convergence u_{max} normalized by the plane strain convergences $u_{w,2D}$ developing in a long weak zone ($u_{w,2D}$ = *447 mm*) for different layer thicknesses

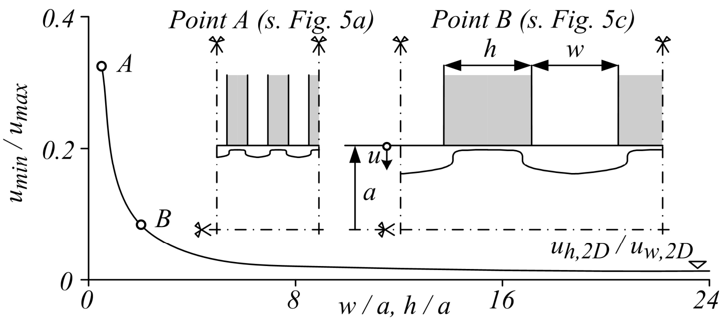

Fig. 7 Degree of convergence uniformity for *h/w = 1*

It should be noted that the computational model assumes perfectly plastic behaviour for competent rock as well. Brittle failure and strength loss of the competent rock due to overstressing (Fig. 5) would reduce the wall-effect, thereby leading to more uniform and also larger convergences. The presence of a lining would probably also increase the uniformity.

4 Conclusions

The frequently observed phenomenon of squeezing variability can be traced back to heterogeneities of the ground on different scales and with respect both to its mechanical and to its hydraulic characteristics. The results of numerical calculations indicate that even relatively thin competent rock interlayers may have a pronounced stabilizing effect.

Acknowledgements

The authors acknowledge the AlpTransit Gotthard AG for the permission to publish data from the Gotthard Base Tunnel.

References

Anagnostou, G. 2007. Continuous tunnel excavation in a poro-elastoplastic medium. Proceedings of NUMOG X Tenth International Symposium on Numerical Models in Geomechanics, Rhodes.

Kovári, K., Anagnostou G. 1995. The ground response curve in tunnelling through short fault zones. 8th Congress of the Int. Soc. for Rock Mech., Tokyo, Japan.

Kovári, K. 1998. Tunnelling in squeezing rock. Tunnel, 5, 12-31.

Kovári, K., Ehrbar, H., Theiler, A. 2006. Druckhafte Strecken im TZM Nord: Projekt und bisherige Erfahrungen. In Löw (ed), Geologie und Geotechnik der Basistunnels, pp. 239-252, Zürich: Vdf Hochschulverlag.

Schneider, T.R. 1997. Behandlung der Störzonen beim Projekt des Gotthard Basistunnels, Felsbau, 6/97.

Vogelhuber, M. 2000. Triaxialversuche im Labor, Sondierbohrung SB 3.2, AlpTransit - Gotthard Basistunnel, Institut für Geotechnik, ETH Zürich.

Vogelhuber, M., Anagnostou, G., Kovári, K. 2004. Pore Water Pressure and Seepage Flow Effects in Squeezing Ground. Proc. X MIR Conference "Caratterizzazione degli ammassi rocciosi nella progettazione geotecnica", Torino.

Vogelhuber, M. 2007. Der Einfluss des Porenwasserdrucks auf das mechanische Verhalten kakiritisierter Gesteine. PhD Thesis. ETH Zurich.

PART V

INTERPRETATION OF CORE EXTRUSION MEASUREMENTS IN TUNNELLING THROUGH SQUEEZING GROUND

Abstract: Squeezing intensity in tunnelling often varies over short distances, even where there is no change in the excavation method or lithology. Reliable predictions of the ground conditions ahead of the face are thus essential in order to avoid project setbacks. Such predictions would enable adaptations to be made during construction to the temporary support, to the excavation diameter and also to the final lining. The assessment of the behaviour of the core ahead of the face, as observed by means of extrusion measurements, provides some indications as to the mechanical characteristics of the ground. If the ground exhibits a moderate time-dependent behaviour, a prediction of the convergences is feasible, provided that the interpretation of the core extrusion takes into account the effects of the support measures. If the ground behaviour is pronouncedly time-dependent, however, convergence predictions become very difficult, because the extrusion of the core depends on the short-term characteristics of the ground, which may be different from the long-term properties that govern the final convergences. The case histories of the Gotthard Base Tunnel and of the Vasto tunnel show that there is a weak correlation between the axial extrusions and the convergences of the tunnel. In order to identify potentially weak zones on the basis of extrusion measurements, careful processing of the monitoring data is essential, in order to take account of the effects of tunnel support and time, and to eliminate errors caused by the monitoring process.

Notation:

a	Tunnel radius
A_F	Area of the tunnel face
d	Distance between tunnel face and measuring point on the tunnel axis
d_c	Distance between tunnel face and measuring point on the tunnel boundary
E	Young's modulus of the ground
e	Unsupported span
$f_i()$	Function (i = 1, 2, 3, …)
f	Yield function
f_c	Uniaxial compressive strength of the ground
g	Plastic potential
H	Overburden
k	Radial stiffness of a ring-shaped lining
$L_{i,t}$	Distance between the reference point R and point i (i = A, B) at time t
$L_{i,0}$	Initial distance between the reference point R and point i (i = A, B)
$p(y)$	Radial pressure at the tunnel boundary
p_o	Initial stress
p_y	Yield pressure of the tunnel support
r	Radial co-ordinate (distance from tunnel axis)
s	Round length in the step-by-step calculations
S	Face advance (multiple of s)
t	Time
u	Displacement of the ground
u_r	Radial displacement of the ground at the tunnel boundary
u_c	Radial ground displacement developing behind the face (convergence)
u_y	Axial displacement of the ground at the tunnel axis
$u_{y,i}$	Axial displacement of the point i at the tunnel axis (i = A, B, O, R)
v	Advance rate of the excavation
y	Axial co-ordinate
y_i	Axial co-ordinate of Point i (i = A, B)
y_F	Axial co-ordinate of the tunnel face
$\Delta u_{y,A}(d,S)$	Change in axial displacement of point A caused by a face advance of S (d denotes the distance of point A from the face after the face advance)
ε_y	Axial strain of the ground at the tunnel axis

$\varepsilon_{y,AB}(d)$	Average axial strain of the ground between the points A and B, whereby Point A is located at distance *d* ahead of the face.
$\varepsilon_{t,c}$	Tangential ground strain at the tunnel boundary developing behind the face (convergence normalized by the tunnel radius)
$\Delta\varepsilon_{t,c}$	Change in tangential ground strain at the tunnel boundary for a specific face advance
$\Delta L_{A,t}$	Change in the distance of point A from reference point R at time *t*
$\Delta L_{B,t}$	Change in the distance of point B from reference point R at time *t*
$\dot{\varepsilon}_{ij}$	Strain rate tensor
$\dot{\varepsilon}_{ij}^{e}$	Elastic part of the strain rate tensor $\dot{\varepsilon}_{ij}$
$\dot{\varepsilon}_{ij}^{p}$	Inelastic part of the strain rate tensor $\dot{\varepsilon}_{ij}$
η	Viscosity
ν	Poisson's ratio of the ground
σ_r	Radial stress
ϕ	Angle of internal friction of the ground
ψ	Dilatancy angle of the ground

1 Introduction

Squeezing intensity can vary greatly over short distances even where there is no change in the excavation method, temporary support, depth of cover or lithology (Kovári 1998). This variability makes tunnelling in squeezing ground very demanding, as it decreases the predictability of the conditions ahead of the face even after some experience has been gained with a specific geological formation during excavation. The variability can be traced back to two different reasons (Cantieni and Anagnostou 2007): (i) rock structure heterogeneity (even on the scale of few meters) may lead to significant variations in the ground response; and, (ii), small fluctuations in the mechanical and hydraulic properties of a macroscopically homogeneous rock mass may have a major effect on the development of deformations and pressures.

Uncertainties concerning rock structure heterogeneity can be reduced by advance probing. However, the uncertainties concerning ground response will remain. Therefore, the prediction of squeezing intensity represents one of the most difficult challenges when tunnelling through squeezing ground. A timely prediction of the conditions ahead of the face would enable adaptations to be made during construction to the temporary support, excavation diameter and final lining. A number of authors have therefore attempted to identify early indicators of ground quality on the basis of field measurements. Steindorfer (1998) proposed a method of predicting changes in rock mass quality ahead of the face based on the displacement vector orientations obtained by geodetic measurements in the tunnel. Jeon *et al.* (2005) underpinned the method theoretically by means of

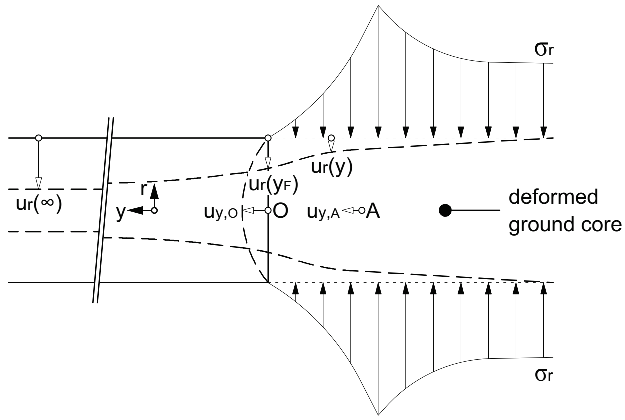

Fig. 1 Schematic mechanism of core extrusion

numerical computations, but pointed out that it is very difficult to make a prediction under complex geological conditions. Sellner (2000) proposed a method of predicting the displacement of the tunnel boundary based on Sulem *et al.* (1987). This method requires an estimation to be made of the ground convergences ahead of the face, however, and this can be done only by estimating the parameters of the function defined by Sulem *et al.* (1987) on the basis of experiences.

Despite improvements in the theoretical assessment of the squeezing phenomenon, and despite the experiences gained with different construction methods, there are still no reliable methods of prediction available.

The analysis of deformation measurements in the ground ahead of the face seems to be promising with regard to ground response predictions, as the radial loading and axial extension of the core ahead of the face can be seen as a large scale in-situ test.

Figure 1 shows the mechanism leading to face extrusion schematically. The ground core ahead of the face loses its axial confinement as the tunnel face approaches. The loss of confinement reduces the radial resistance of the ground core, and the core thus deforms due to the radial load σ_r exerted by the surrounding ground. In squeezing ground, the core yields under the radial loading and extrudes into the opening. The magnitude of the extrusion depends on the mechanical properties of the ground, the depth of cover and the support measures applied at the tunnel circumference and at the tunnel face. If the ground exhibits a time-dependent behaviour (either due to creep or to consolidation) the extrusion will depend also on the rate of advance and on the duration of any standstills.

In the past, extrusion measurements have been used mostly to control face stability. Lunardi (1995) first used such measurements in squeezing ground for the assessment of both face stability and the expected convergences. A recent case history showing a correlation between the extrusions, the convergences and the overburden is the Pianoro tunnel (Lunardi and Gatti 2010).

The extrusion of the face during a standstill in squeezing ground can be from several centimetres to decimetres (cf. Cantieni and Anagnostou 2011), but it is not problematic in conventional tunnelling as long the face remains stable (Kovári 1998). In TBM tunnelling, the excavation speed is normally high enough to avoid jamming of the cutter head during regular TBM operation, as the extruding ground is excavated as part of the boring process. Immobilization may, however, occur during a standstill (Ramoni and Anagnostou 2010). Extreme extrusions have been observed, for example, during the construction of the Gilgel Gibe II Tunnel in Ethiopia. After encountering a fault zone, the face extruded very quickly (40 to 60 mm/hour), and pushed back the TBM for about 60 cm (De Biase *et al.* 2009).

The present paper investigates whether it is possible to predict the ground response to tunnelling by assessing the axial extrusion of the core ahead of the face. The paper starts with a review of the analytical, empirical and numerical approaches proposed in the literature for the quantitative assessment of core extrusion (Section 2). Section 3 briefly sets out the methods for monitoring extrusion, discusses some aspects of data processing and reviews monitoring results from case histories found in the literature. Section 4 investigates theoretically, by means of numerical analyses, the possibility of using extrusion data as an early indicator of tunnel convergence. Finally, extrusion and convergence measurements from the Gotthard Base Tunnel are presented and discussed in detail with regard to the predictability of ground response (Section 5).

2 Computational methods for estimating extrusion

Based on a spherical model of the tunnel face (Egger 1980) and on undrained ground behaviour, Mair (2008) introduced so-called “influence lines”, which show the increase in axial displacement of a point ahead of the face due to the advancing face. Wong *et al.* (2000a) proposed spherical models for the determination of face extrusions, incorporating the effect of face reinforcement using bolts. However, the extrusions determined through laboratory experiments could not be reproduced by the analytical solution (Trompille 2003). Analytical approaches may allow a fast assessment to be made of extrusions, but the numerous simplifications (e.g. spherical face, disregard of the actual stress state) limit their predictive power.

Lunardi (2000) proposed a relation between extrusion and the radial displacements that occur ahead of the face (so-called pre-convergences), based on a volume balance of the ground ahead of the face (neglecting the dilatancy that often accompanies plastic yielding). The determination of the pre-convergences allowed him to calibrate the ground response curve and thus estimate the final lining loading by means of the convergence confinement method.

Hoek (2001) presented an approach obtained by curve-fitting of the numerical results for the axial and tangential strains in function of the internal support pressure. In case of an unsupported tunnel, the equations lead to a constant ratio of 1.5 between the tangential and the axial strains. Lee and Rowe (1990) presented, also based on numerical computations, a relationship between the extrusion of the face and the face support pressure for a tunnel with a rigid lining up to the face.

Kovári and Lunardi (2000) and Bernaud *et al.* (2009) investigated the influence of face bolting on the extrusion of the face by means of axisymmetric numerical computations. Peila (1994) and Oreste *et al.* (2004) investigated the deformation behaviour and face stability of shallow and deep tunnels, respectively, by means of three-dimensional numerical models. The face reinforcement was modelled with horizontal pipes embedded in the ground ahead of the face.

The ground may respond faster or slower to tunnel excavation, depending on its rheological properties. Slow ground response may reduce the extrusion of the core significantly, thus making it difficult to predict squeezing intensity (Barla 2009). The time-dependency of ground behaviour in squeezing ground can be traced back to two mechanisms: consolidation and creep (cf. Anagnostou and Kovári 2005). Ghaboussi and Gioda (1977) showed by means of numerical computations for a visco-elastic ground behaviour that the radial displacements of the ground ahead of the face depend (among other parameters) both on the advance rate and on the viscosity of the ground. Myer *et al.* (1981) illustrated the effect of the advance rate on the axial strain ahead of the face by means of physical models. According to their experimental results, the faster the advance, the smaller the extrusion of one and the same material will be. A comprehensive spatial numerical investigation for a tunnel advance in visco-plastic ground was carried-out by Bernaud (1991). Pellet *et al.* (2009) noticed substantial face extrusion when using Lemaitre's visco-plastic damage model. Anagnostou (2007b) showed for the case of a water bearing, low permeability ground that the extrusion of the tunnel face depends on the permeability and on the advance rate (all other parameters remaining constant).

3 Extrusion measurements

3.1 Measurement methods

The axial deformations of the ground ahead of the face are monitored usually by means of sliding micrometers (Kovári *et al.* 1979). The sliding micrometer allows high precision measurements of the strain distribution along a line ahead of the face with a resolution of 1 m intervals. The main disadvantage of the sliding micrometer is the time consuming measuring procedure, which interferes with excavation work at the face (Steiner and Yeatman 2009). The sliding micrometer has been applied successfully under both non-squeezing and squeezing conditions (e.g. Lunardi and Focaracci 1999). As experienced in the Gotthard Base Tunnel (Tavetsch intermediate massif section), however, its application may be problematic under heavily squeezing conditions (damaged due high water or rock pressure; Thut *et al.* 2006).

A recent development that resolves the above-mentioned problems is the so-called Reverse-Head-extensometer (RH-extensometer) (Thut *et al.* 2006; Steiner 2007). In contrast to the normal extensometers (which are used for measuring the radial displacements of the ground in tunnelling), the measuring head of the RH-extensometer, which includes the data logger, is installed at the end of a borehole far ahead of the face, thus allowing a continuous monitoring of deformations with little obstruction to the excavation work (Figure 2a). The communication cable which is used for data readout is located in a central tube and can be accessed at the face (Steiner and Yeatman 2009).

The data recorded by means of sliding micrometers or extensometers ahead of the face requires careful processing in order to avoid erroneous results. Two sources of error will be discussed in the next section.

3.2 Data processing

The interpretation of the monitoring data should account for the effects (i) of the reference point displacement and, (ii), of the zero reading (Figure 2b and 2c, respectively).

Sliding micrometers measure the length changes of the intervals defined by the successive measuring points. As discussed by Kovári (1998), Wong *et al.* (2000b) and Trompille (2003), the total displacements of the measuring points (e.g., the displacement $u_{y,A}$ of point A) can be determined by summing the length changes of the successive intervals, provided that the displacement $u_{y,R}$ of the reference point (which is located at the deepest point of the borehole) is known (e.g. by measuring it independently with an overlapping measuring device) or it can be assumed to be practically zero (which is true only if it is located outside the influence zone of the advancing tunnel face):

$$u_{y,A} = \Delta L_{A,t} + u_{y,R} \,, \qquad (1)$$

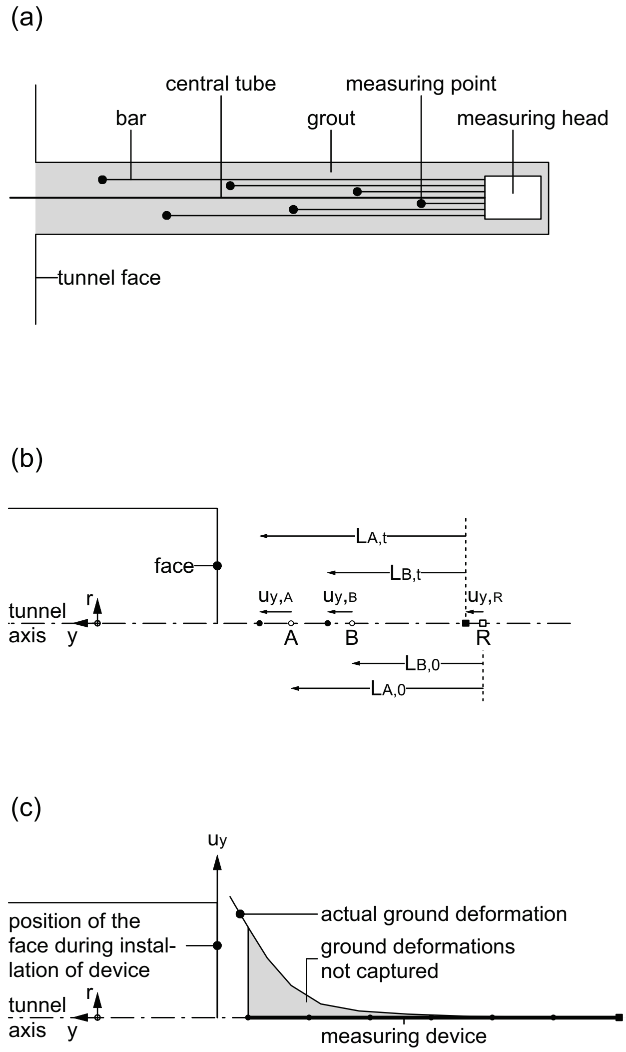

Fig. 2 a) Scheme of the RH-extensometer (after Thut *et al.* 2006); b) "Non-fixed reference point" limitation; c) Limitation concerning the "zero reading"

where $\Delta L_{A,t}$ denotes the sum of the length changes of the intervals between the point A and the reference point R. Similar remarks apply to RH-extensometers, the only difference being that these instruments measure directly the length change of the intervals defined by the measuring points (e.g. point A) and the reference point R.

The uncertainties associated with a non-fixed reference point are irrelevant for the distribution of the axial strain ε_y. An interpretation of the observed behaviour in terms of strain ε_y (rather than in terms of displacement) is therefore advantageous, and provides a better picture of the ground. The sliding micrometers measure the length changes of successive 1 m long intervals, thus leading directly to the strain distribution along the measuring line. In the case of RH-extensometers, the strain profile can easily be calculated from the measured length changes. The average strain $\varepsilon_{y,AB}$ over the interval defined by measuring points A and B reads as follows (Figure 3a):

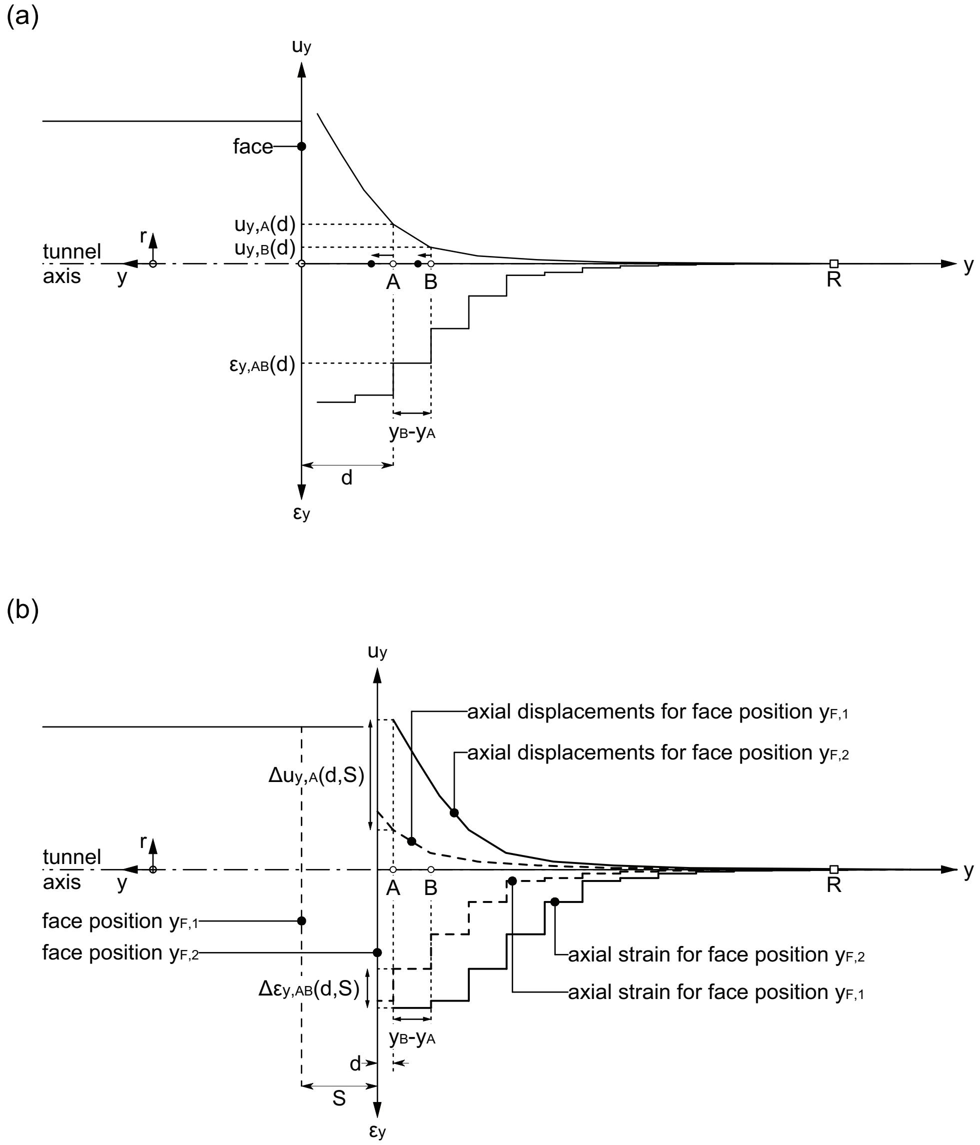

Fig. 3 a) Definition of the axial displacement u_y and strain ε_y; b) Definition of the increase in axial displacement Δu_y and in strain $\Delta\varepsilon_y$ due to a face advance by S

$$\varepsilon_{y,AB} = \frac{\Delta L_{A,t} - \Delta L_{B,t}}{y_A - y_B} \,. \tag{2}$$

A further limitation is imposed by the time and location of the zero reading (Figure 2c). If the measuring device is installed too close to the face (i.e. within its influence zone) the measured data will apply only to the changes in extrusion taking place after the installation of the measuring device (Lunardi and Focaracci 1999).

The effects mentioned reduce the length of the measuring line that can be used for the assessment of ground displacements considerably. As discussed by Wong *et al.* (2000b), in the case of one single measuring device installed right at the face, the affected length of the measuring line amounts to two times the influence length of the tunnel face. The ”non-fixed reference point”- and the “zero reading”-effects can be avoided by an appropriate arrangement of the measuring lines or by a specific way of analysing the data.

The problem concerning the displacement of the reference point can be by-passed either by installing a series of extensometers with sufficient overlapping lengths (Steiner and Yeatman 2009) or by analysing the axial strains ε_y rather than the axial displacements u_y.

The “zero reading”-effect can be avoided by installing the extensometer a sufficient distance from the face in undisturbed ground, or by installing a series of overlapping extensometers (the new extensometer must be installed before the influence zone of the advancing tunnel face reaches the reference point of the preceding extensometer). When analysing, the error associated with a “zero reading” can also be avoided by considering the increase in axial strains $\Delta\varepsilon_y$ or the increase in displacement Δu_y (Figure 3b) caused by a face advance of S (rather than considering the total response of the ground to tunnelling).

3.3 Case histories

Extrusion measurements have been performed in a number of tunnel projects in the recent years (Table 1). Some selected cases will be discussed below.

Tartaiguille tunnel

The Tartaiguille tunnel will be looked at as a first example. It forms part of the French high-speed railway line between Lyon and Marseilles (Paulus 1998). The tunnel was constructed between 1995 and 1998. Its length is 2338 m and the maximum overburden amounts to 137 m. The tunnel crosses several Cretaceous formations. The section of the tunnel, which is investigated in the present paper, is located in marly clays of the so-called “lower Stampien”. Figure 4a shows the geological longitudinal profile of the tunnel. The tunnel was excavated full face (A_F = 180 m^2) with 90 fibreglass bolts for face reinforcement (between chainage 495 m and 1370 m). More detailed descriptions of the project can be found elsewhere (e.g. Lunardi 2008; Wong *et al.* 2000b). The extrusion of the face was monitored by sliding micrometers. The present case study discusses the extrusions between chainage 1251 m and 1215 m (rectangle in Figure 4a). The excavation advances in the direction of the decreasing chainage.

Figure 4b shows the axial displacement assuming a fixed reference point and the longitudinal section of the tunnel at the position of the installation of the sliding micrometer. Additionally, the figure also shows the cross section of the tunnel. The maximum extrusion u_y at the face increases for the first six readings and remains constant afterwards. Figure 4c shows the so-called influence lines of the axial displacements u_y (assuming a fixed reference point). They show, analogously to the influence lines known from structural engineering, the axial deformation u_y (or strain ε_y) of a point in the function of its distance d to the approaching face. According to Wong *et al.* (2000b) the first 15 measuring points (the upper diagram of Figure 4c) and the last 15 (the lower diagram of Figure 4c) measuring points do not show the correct displacements u_y profile of the ground, due to the "zero reading"-effect and to the "fixed reference point"-effect, respectively (cf. Section 3.2), and therefore cannot be used for data interpretation.

Table 1 Tunnel projects with extrusion monitoring documented in the literature

Tunnel	References
Tartaiguille	Wong *et al.* 2000b; Wong *et al.* 2004 Wong and Trompille 2000 Lunardi 1999, 2008
Raticosa	Boldini *et al.* 2004 Bonini *et al.* 2009 Lunardi and Focaracci 1999 Barla *et al.* 2004 Lunardi *et al.* 2009 Barla 2005
Vasto	Lunardi and Focaracci 1997 Lunardi 1998
Saint Martin La Porte access gallery (Lyon-Turin Base Tunnel)	Russo *et al.* 2009
Marinasco	Barla and Barla 2004
San Vitale	Cosciotti *et al.* 2001 Rossi 1995 Lunardi and Bindi 2004
Osteria	Barla 2005 Barla *et al.* 2004
Bois de Peu (France)	Eclaircy-Caudron *et al.* 2009
Sedrun Lot of the Gotthard Base Tunnel	Steiner and Yeatman 2009 Steiner 2007

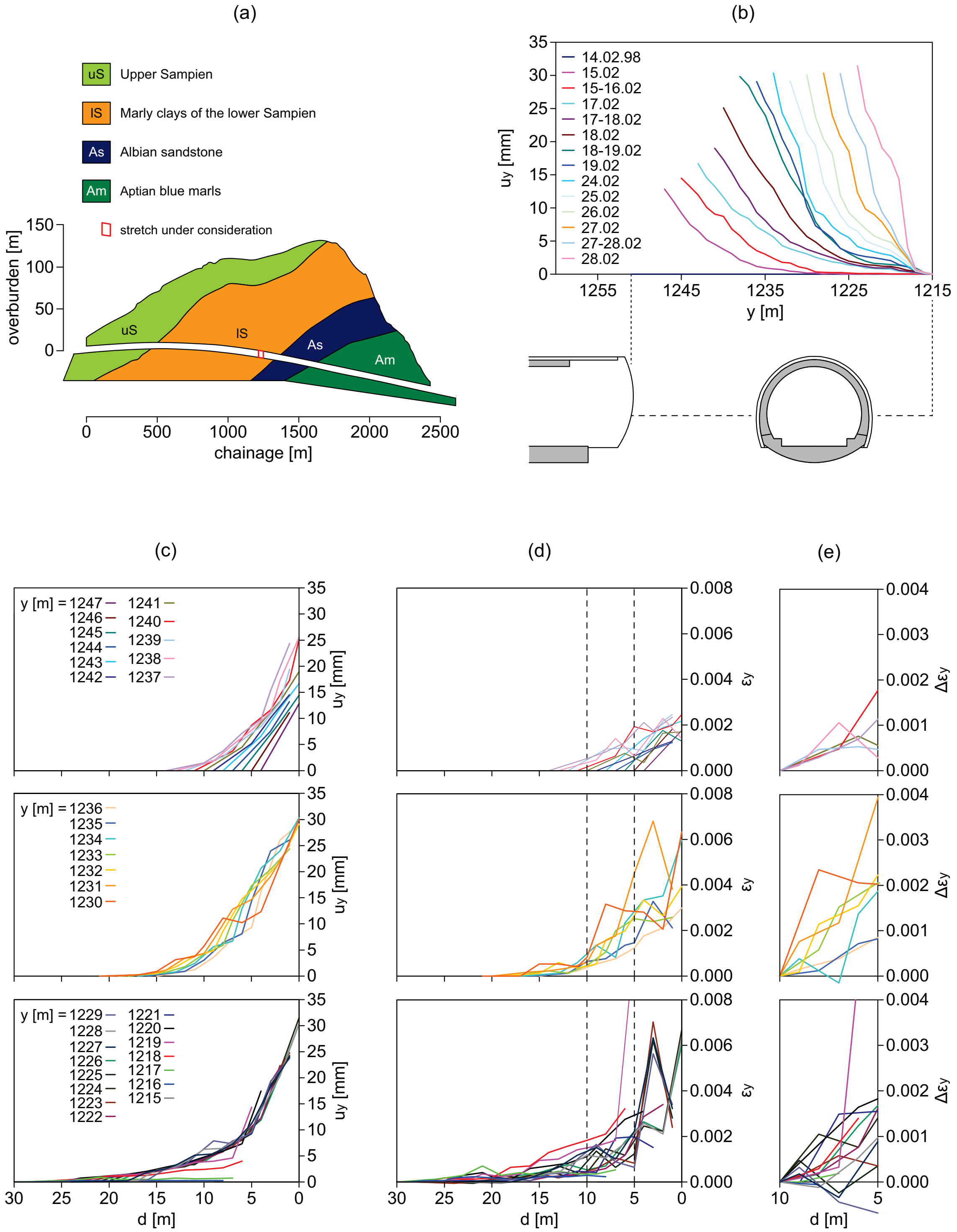

Fig. 4 a) Longitudinal geological profile of the Tartaiguille tunnel (after Wong and Trompille 2000) and tunnel stretch under consideration (rectangle); b) Axial displacement u_y as a function of the chainage y for different dates and positions of the face y_F (after Wong *et al.* 2000b) (the chainage of the first value of the extrusion u_y corresponds to the position of the face) as well as longitudinal and cross section of the tunnel (after Lunardi 1999); c) Influence line of the axial displacements u_y of the measuring points (the notation of the measuring points denotes their y-coordinates); d) Axial strain ε_y of the ground between the measuring points as a function of their distance to the face d; e) Influence line of the change in axial strain ε_y caused by the face approaching from a distance of 10 m to a distance of 5 m

As discussed in Section 3.2, the “fixed reference point”-effect can be avoided by analysing the axial strains ε_y and not the axial displacements u_y. Figure 4d shows the influence lines of the axial strain ε_y. Such an illustration makes it possible to incorporate the measuring points between chainage y = 1229 m and y = 1215 m (the lower diagram of Figure 4d) in the analysis.

The influence lines of Figure 4d show that the ground response to excavation is variable. The measuring points 1223, 1225, 1227, 1229 and 1231, for instance, show a high increase in the strain for the advance from 5 m to 3 m, and a subsequent decrease in the strain for the advance from 3 m to 1 m. This behaviour may be caused either by a heterogeneous rock structure (layers of different ground quality perpendicular to the tunnel axis) or by the effect of staggered face reinforcement. Both may cause the observed expansion and subsequent recompression of the ground.

An analysis of the change in strain $\Delta\varepsilon_y$ due to a specific face advance makes it possible to incorporate and compare all measuring points (cf. Section 3.2). The curves between the vertical dashed lines in Figure 4d define the strain portion generated during the face advance from d = 10 m to d = 5 m for every ground interval ahead of the face. By comparing these strain portions (Figure 4e), different behaviours of the core can be distinguished. The strain $\Delta\varepsilon_y$ developed during the face advance of 5 m amounts to about 0.001 for the intervals up to y = 1235 m. In the subsequent intervals y = 1234, 1233, 1232, 1230, 1226, 1224, 1222, 1221, 1220 and 1218 m, the strain increases to about 0.002. There seems to be a change either in ground quality or in support measures after chainage y = 1235 m, causing an increase in extrusion ahead of the face. Some of the intervals especially in the lower diagram of Figure 4e even show a decrease in strain due to a face advance (e.g. y = 1229 m). This behaviour may be caused, as already mentioned above, by rock structure heterogeneities or by the effect of staggered face reinforcement.

Raticosa tunnel

The Raticosa tunnel is part of the Bologna to Florence high-speed railway line, which crosses the Apennine range (Lunardi and Focaracci 1999). The tunnel has a length of about 10.5 km and the maximum overburden is about 500 m. The section under investigation is located near the northern portal and was excavated full face (A_F = 160 m^2) in 1998 (Figure 5a). The tunnel was excavated from the northern portal through a landslide area, formed of intensely tectonised clay shales (Bonini *et al.* 2009). The overburden ranged from a few meters to 100 m. The face was reinforced with 60 fibre-glass bolts, which had a length of 20 m and were installed every 10 m of face advance. After excavating, in steps of about 1.5 m, steel sets (at 1 m spacings) and shotcrete were applied. The final lining invert was cast within a distance of about one tunnel diameter from the face. The final concrete lining was completed in a distance of about 30 - 40 m behind the face. The extrusion of the face was monitored with a sliding micrometer of 30 m length. Only 6 extrusion measurements are available (including the zero reading).

Figure 5b shows the axial displacement profile assuming a fixed reference point as well as the longitudinal and cross section of the tunnel. A break from the 6th to the 15th July 1998 at face position 10 m and a subsequent face advance from 10 m to 12 m generated a major extrusion (Figure 5b). The extrusion probably developed over time during the standstill. Note, furthermore, that the subsequent face advance from 12 m to 15 m caused only very limited deformations. The installation of heavy face reinforcement during the break could be the reason for the limited axial displacements.

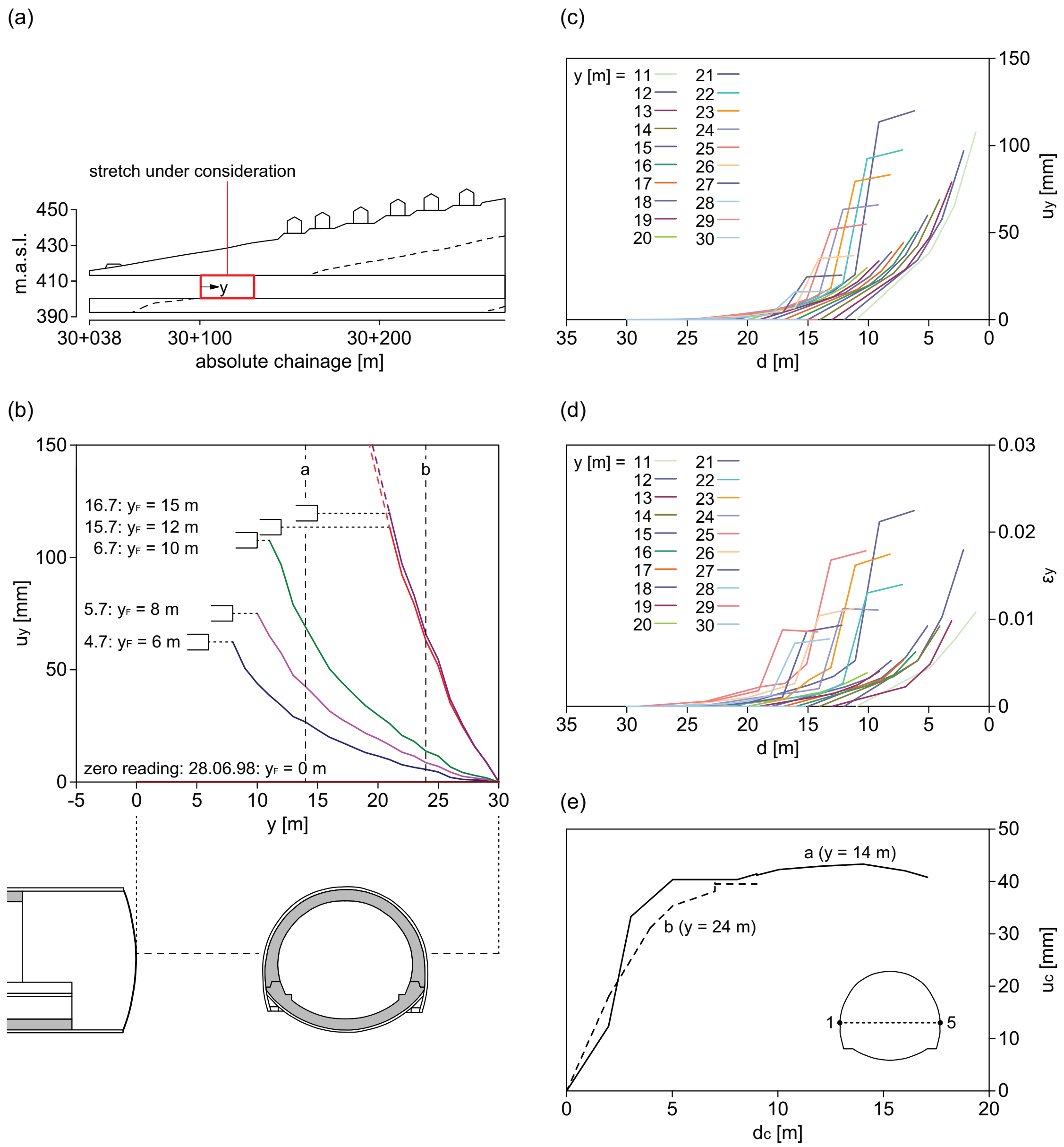

Fig. 5 a) Longitudinal geological profile of the Raticosa tunnel (after Lunardi and Focaracci 1999) with the tunnel stretch under consideration (rectangle); b) distribution of the axial displacement u_y as a function of the chainage y for different dates (and positions of the face y_F) (after Bonini *et al.* 2009) as well as longitudinal and cross section of the tunnel (after Boldini *et al.* 2004); c) Axial displacements u_y of the measuring points as a function of their distance to the face d; d) Influence lines of the axial strain ε_y (the notation of the intervals denotes the y-coordinate of their first points); e) Influence lines of convergences at the chainages 30+113 m (y = 14 m) and 30+123 m (y = 24 m)

The lack of information with regard to the executed sequence of face support installation makes it not possible to verify this conclusion.

According to the reading of the 4th July 1998 (face position at 6.1 m) the zone of influence is about 19 m (Figure 5b). The large zone of influence is evident also in Figure 5c, which shows the influence lines of the axial displacements u_y (assuming a fixed reference point). The total value of the extrusion u_y cannot be determined for most points, because the zero reading was done when the ground had already experienced deformations (note the influence zone extends up to 18 m – 19 m ahead of the face!) and because the records for the face advance after y_F = 14.8 m are missing.

According to the definition of Wong *et al.* (2000b) the usable length of this extensometer is reduced to zero. However, if we take account of the strains (instead of the displacements), more data can be used (cf. Section 3.2). Figure 5d shows the influence lines of the strains ε_y. A comparison of the increase in strains does not yield more information because there are no readings after face position of y_F = 15 m. A detailed interpretation of the data is very difficult because there are only a few readings. It is therefore possible to recognise only pronounced changes in extrusion.

The convergences were monitored at two cross sections (denoted by “a” and “b” in Figure 5b). Figure 5e shows the convergences u_c measured between the measuring points 1 and 5 at these two cross sections as a function of the distance from the face d_c. Both cross sections show approximately the same development of the convergences. The convergences stabilize (at about 40 mm only) after the installation of the invert (Bonini 2003). As shown later in Section 4 by means of numerical calculations, the extrusion does not provide any useful indication as to the convergence in case of stiff linings which are installed close to the face, because in such cases the convergences are almost independent of the ground quality.

Vasto tunnel

The Vasto tunnel is part of the railway line from Ancona to Bari. The tunnel has a length of about 6.2 km and maximum overburden of 135 m. The main part of the tunnel crosses complex formations consisting of a silty, clayey constitution, stratified with thin sandy intercalations and containing sizeable water bearing sand lenses. The excavation work began in 1983 and was stopped after several incidences in 1990. In 1992 the work continued with a new design concept, which also incorporated extrusion measurements. The tunnel was excavated full-face ($A_F \approx 120$ m^2). The face was reinforced by 55 fibre-glass bolts and horizontal jet-grouting was performed in advance around the future tunnel (Lunardi and Bindi 2004). A detailed description of the project can be found in Lunardi and Focaracci (1997).

Figure 6a shows the longitudinal profile of the tunnel and the approximate location of the monitored stretch. Both extrusion- and convergence- measurements are available for this tunnel. Figure 6b shows the cross section and the longitudinal section of the tunnel (including the axial sliding micrometer and the location of convergence measurements a, b, and c) and the extrusion profiles assuming a fixed reference point recorded during face advance. After the excavation passed chainage y = 3 m, the extrusion profiles show a considerable increase in displacement. Furthermore, it is remarkable that, on the one hand, the maximum extrusions of the first three recordings (the curves for y_F = 1, 2 or 3 m) are relatively small, but on the other hand the profiles indicate a very large influence zone of the face (extending up to 15 - 20 m ahead of the face). The large zone of influence can also be seen in Figure 6c, which shows the influence lines of the axial displacements u_y (assuming a fixed reference point). However, the influence lines of the axial strain ε_y indicate a much smaller influence zone (about 9 m, Figure 6d). A closer examination of the extrusion profiles confirms this conclusion (the distances of the measuring points far ahead of the face remain practically constant - the displacement profiles are practically horizontal). The difference between the zone of influence indicated by the displacements and by the strains is probably due to measuring inaccuracies.

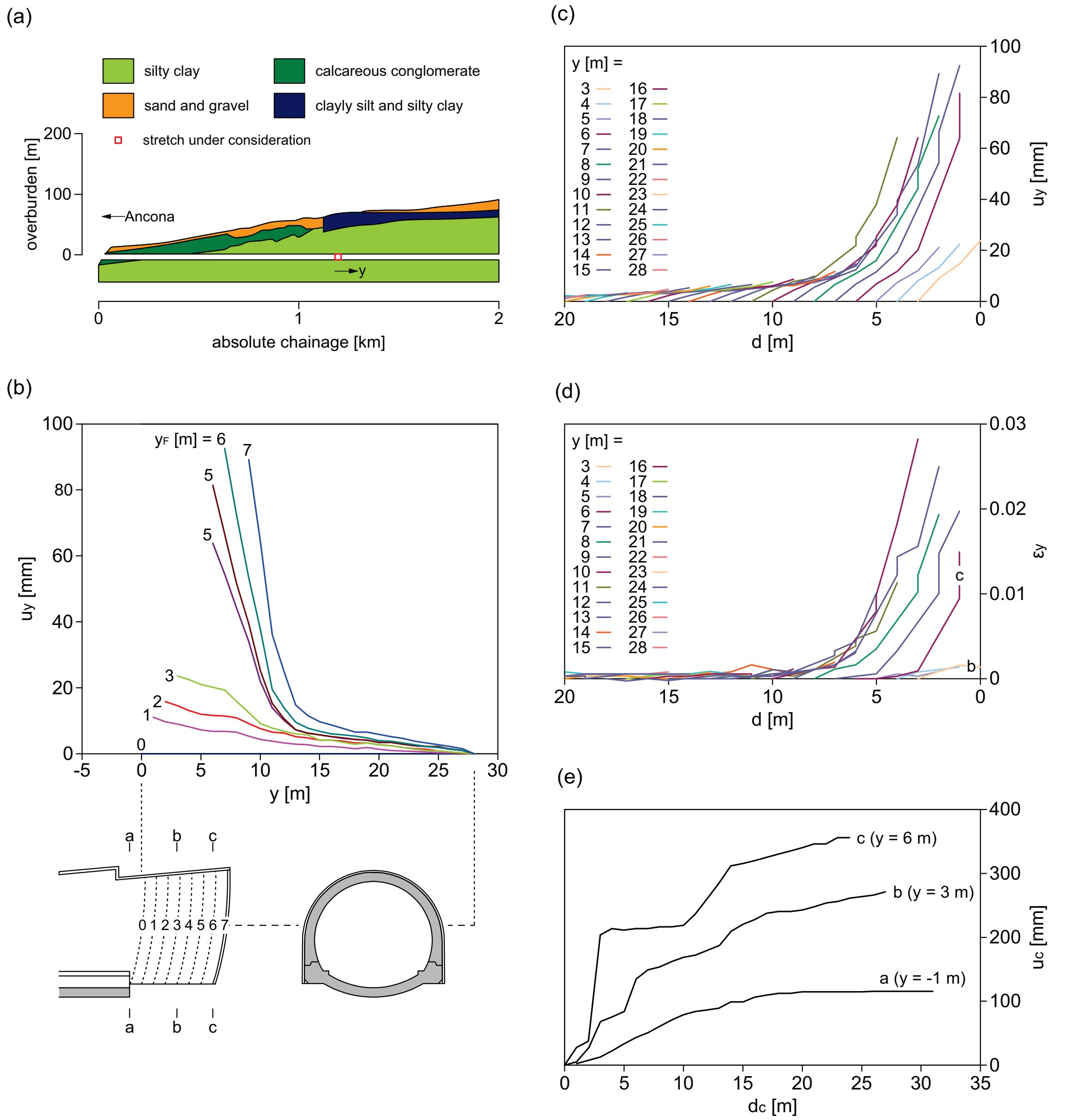

Fig. 6 a) Longitudinal geological profile of the Vasto tunnel (after Lunardi 2000) and stretch under consideration (rectangle); b) axial displacement u_y as a function of the chainage y for different positions of the face y_F (Lunardi and Focaracci 1997) as well as longitudinal and cross section of the tunnel (after Lunardi 2000); c) Influence lines of axial displacements u_y of a measuring point at chainage y; d) Influence lines of axial strain ε_y over the intervals between the measuring points at chainage y and (y + 1 m); e) Influence lines of convergences at the chainages y = -1, 3 and 6 m

The convergences were monitored at three cross sections (denoted by “a”, “b” and “c” in Figure 6b). Figure 6e shows the convergences u_c measured at these three cross sections as a function of the distance from the face. The convergences at the chainages y = 3 m (point b) and y = 6 m (point c) increased after the face passed chainage y = 8 m. According to Lunardi and Focaracci (1997), these results indicate that the face support reduces both the extrusion and the convergences. As shown later in Section 4 by means of numerical calculations, a lighter face support should lead theoretically to bigger extrusions (particularly in the case of a low overburden) but smaller convergences. The data documented in the literature is not sufficient for establishing the reason for the observed increase in convergences with certainty. The large convergences monitored (> 0.3 m) indicate that the lining was not installed immediately behind the face. An increase in the distance between the face and the lining installation (or a decreasing ground quality after chainage y = 8 m) would also lead to larger convergences.

4 Theoretical aspects

4.1 Introduction

The present section analyses the response of the core ahead of the face by means of numerical computations in order to understand better the observed behaviour, and to investigate whether there is a correlation between the extrusions and the convergences. The numerical analyses take into account the effects of support (face support, yielding support or stiff support) and ground properties (e.g. strength, deformability, rheology and heterogeneity). As a reference, the case of an unsupported tunnel crossing a homogeneous ground with time-independent behaviour will be discussed first.

4.2 An unsupported tunnel in homogeneous ground

4.2.1 Numerical model

For the numerical analysis of the deformation behaviour of the core ahead of the face, an axisymmetric model of a deep, unsupported, cylindrical tunnel crossing a homogeneous and isotropic ground which is subject to uniform and hydrostatic initial stress will be considered (Figure 7). The mechanical behaviour of the ground is modelled as linearly elastic and perfectly plastic according to the Mohr-Coulomb yield criterion, with a non-associated flow rule. The angle of dilatancy ψ was taken equal to φ – 20° for φ > 20° and to 0° for $\varphi \le$ 20° (cf. Vermeer and de Borst 1984). According to comparative calculations, the angle of dilatancy does not affect the relationship between the ex-

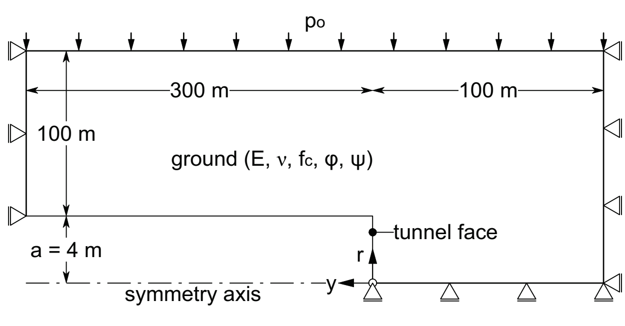

Fig. 7 Axisymmetric model and boundary conditions

Table 2 Model parameters

Parameter		Value
Initial stress	p_0	10 MPa
Tunnel radius	a	4 m
Ground		
Young's Modulus	E	1 GPa
Poisson's ratio	ν	0.3
Angle of internal friction	φ	variable
Dilatancy angle	ψ	φ - 20° for φ > 20°; 0° for $\varphi \le$ 20°
Uniaxial compressive strength	f_c	variable

trusions and the convergences significantly, because an increase of the angle of dilatancy will increase both the extrusions and the convergences. Table 2 summarizes the parameters of the model. The numerical solution of the axisymmetric tunnel problem has been obtained by means of the finite element method. The problem is solved numerically by the so-called "steady state method", a method introduced by Nguyen-Minh and Corbetta (1991) for efficiently solving problems with constant conditions in the tunnelling direction by considering a reference frame which is fixed to the advancing tunnel face. A comparison of the steady state method with the more widely used step-by-step method, which handles the advancing face by deactivating and activating the ground and support elements respectively, can be found in Cantieni and Anagnostou (2009a).

In order to save computation and data processing time, some general properties of the solutions of elasto-plastic tunnel problems will be taken into account in the numerical analyses. The displacement u of the boundary of an unsupported opening in linearly elastic (according to Hooke's law) and perfectly plastic ground (obeying the Mohr–Coulomb yield criterion and a non-associated flow rule) depends on the material constants of the ground (E, ν, f_c, ϕ, ψ), on the initial stress p_0 and on the problem geometry (in the present case the tunnel radius a of the cylindrical tunnel):

$$u = f_1\left(E, \nu, f_c, \phi, \psi, p_0, a\right) \quad . \tag{3}$$

The parameters can be reduced by means of a dimensional analysis and by normalizing the displacements by the reciprocal value of the Young's modulus E (c.f. Anagnostou and Kovári 1993):

$$\frac{uE}{ap_0} = f_2\left(\nu, \phi, \psi, \frac{f_c}{p_0}\right) \quad . \tag{4}$$

With reference to the spatial model of an advancing tunnel, both the radial displacements at the tunnel face $u_r(y_F)$ (Figure 1) and the final radial displacements far behind the face $u_r(\infty)$ can be expressed by Eq. 4:

$$\frac{u_r(y_F)E}{ap_0} = f_3\left(\nu, \phi, \psi, \frac{f_c}{p_0}\right) \quad , \tag{5}$$

$$\frac{u_r(\infty)E}{ap_0} = f_4\left(\nu, \phi, \psi, \frac{f_c}{p_0}\right) . \tag{6}$$

The convergence of the opening u_c is according to Eq. 5 and 6:

$$\frac{u_c}{ap_0}E = \frac{u_r(\infty) - u_r(y_F)}{ap_0}E = f_4 - f_3 = f_5\left(\nu, \phi, \psi, \frac{f_c}{p_0}\right) . \tag{7}$$

The axial displacement u_y at a location y can be expressed as:

$$\frac{u_y E}{ap_0} = f_6\left(\nu, \phi, \psi, \frac{f_c}{p_0}, \frac{y}{a}\right) . \tag{8}$$

The axial strains ε_y at the tunnel axis are obtained as:

$$\varepsilon_y = \frac{\partial u_y}{\partial y} = a\frac{p_0}{E}\frac{\partial f_6\left(\nu, \phi, \psi, \frac{f_c}{p_0}, \frac{y}{a}\right)}{\partial y} = \frac{p_0}{E} f_6\left(\nu, \phi, \psi, \frac{f_c}{p_0}, \frac{y}{a}\right) . \tag{9}$$

The change in axial strain $\Delta\varepsilon_y$ at any location due to a face advance of S can be expressed by a similar equation (cf. Figure 3b):

$$\Delta\varepsilon_y \frac{E}{p_0} = f_7\left(\nu, \phi, \psi, \frac{f_c}{p_0}, \frac{y}{a}, \frac{S}{a}\right) . \tag{10}$$

Figure 3 shows the longitudinal profiles of the displacement u_y, strain ε_y and strain increase $\Delta\varepsilon_y$ due to a face advance of S. The indexes A and B denote points on the tunnel axis. In homogeneous ground, the absolute position on the axial co-ordinate y is not relevant, and only the distance to the face d has to be considered. The expressions for the displacements and strains can thus be simplified to: $u_y(d)$, $\varepsilon_y(d)$ and $\Delta\varepsilon_y(d,S)$.

4.2.2 Numerical results

Deformed shape of the face

Figure 8a shows the curved shape of the deformed face for different normalized uniaxial compressive strengths f_c/p_0. As expected, the maximum extrusion appears in the centre of the face. Figure 8b shows that the extrusion of the face $\varepsilon_y(0)$ is about constant for uniaxial strengths higher than $0.8p_0$. The maximum extrusion increases strongly for uniaxial strengths lower than about $0.4p_0$.

Figure 8c shows the radial displacements of the tunnel boundary $u_c = u_r(\infty) - u_r(y_F)$ (cf. Figure 1) as a function of the normalized uniaxial strength f_c/p_0. The curve shows a similar development to Figure 8b with respect to the uniaxial compressive strength of the ground, thus suggesting a strong correlation between these two variables.

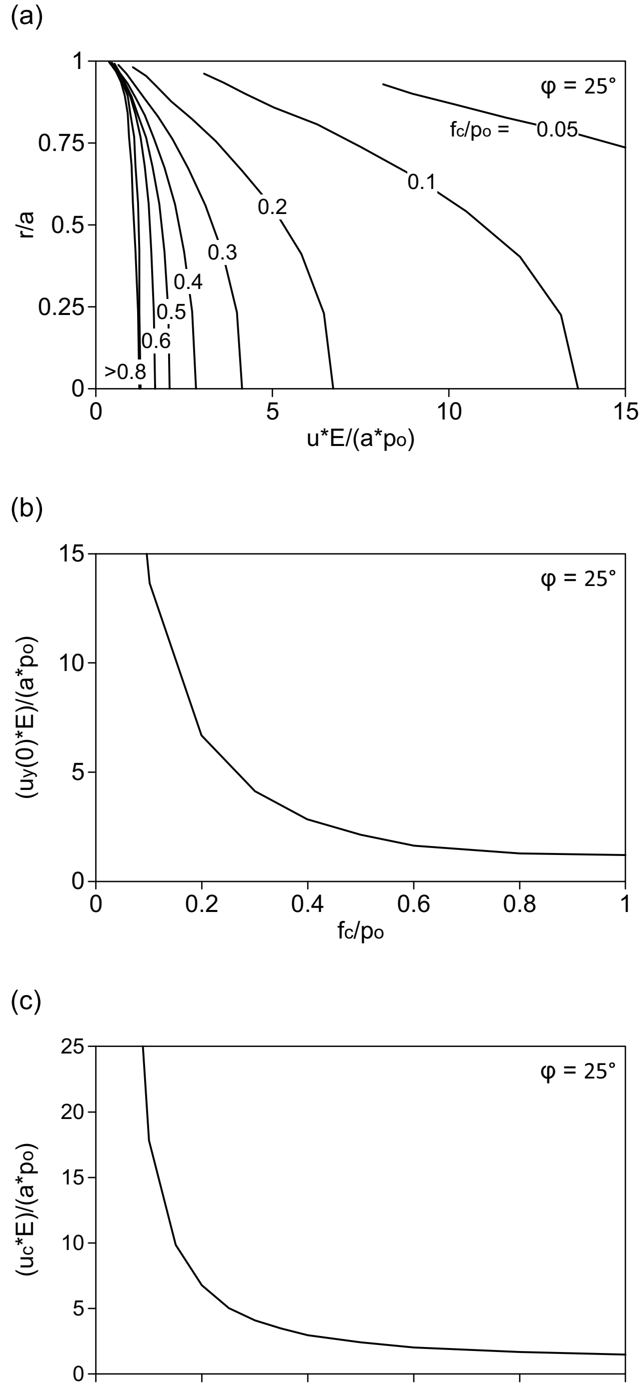

Fig. 8 Unsupported tunnel. a) Deformed shape of the face as a function of the normalized uniaxial compressive strength f_c/p_0; b) Normalized extrusion of the centre of the face $u_y(0)*E/(a*p_0)$ as a function of the normalized uniaxial strength f_c/p_0; c) Normalized convergences $u_c*E/(a*p_0)$ as a function of the normalized uniaxial strength f_c/p_0

Displacements and strains along the tunnel axis

Figure 9a shows the axial displacements $u_y(y)$ at the tunnel axis ahead of the face (extrusion profile) for different normalized uniaxial compressive strengths f_c/p_0. Both the magnitude of the displacements and the region ahead of the face influenced by the excavation increase with decreasing strength. Figure 9b shows the axial strains $\varepsilon_y(y)$ at the tunnel axis. The strain decreases with

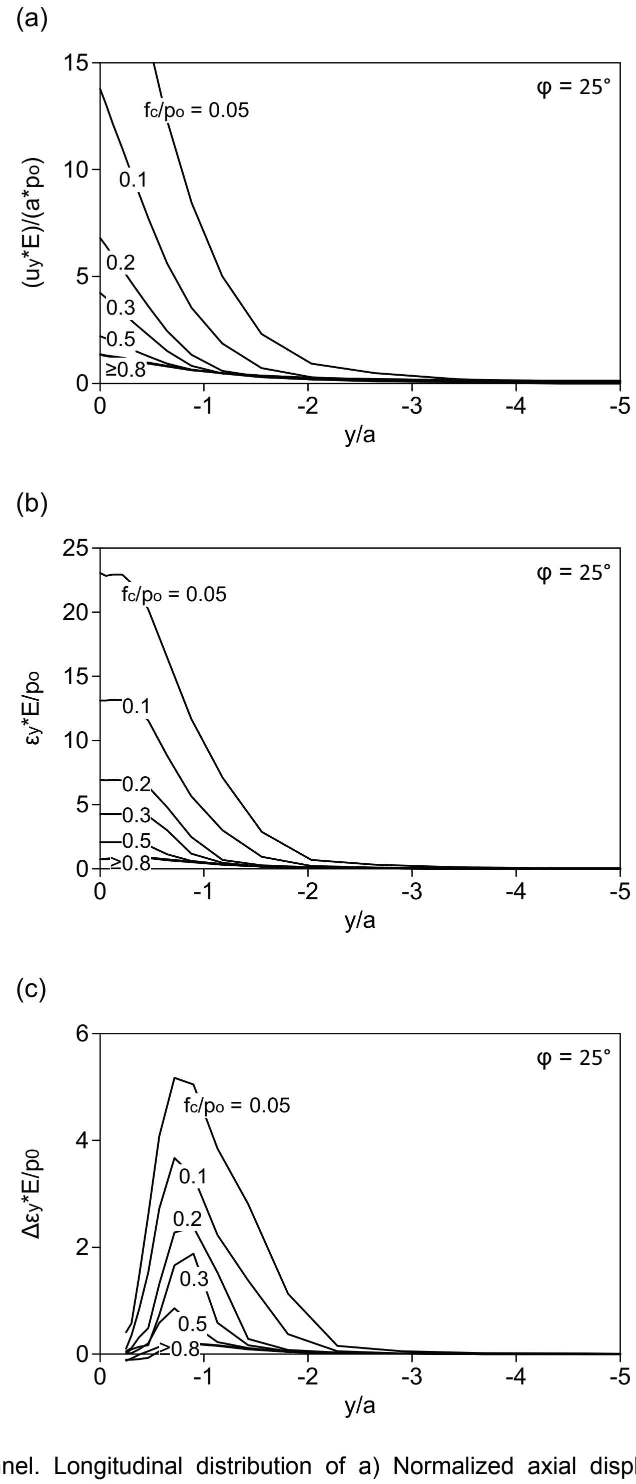

Fig. 9 Unsupported tunnel. Longitudinal distribution of a) Normalized axial displacements u_y*E/(a*p_0), b) strains ε_y*E/p_0 and c) increase of strain $\Delta\varepsilon_y(S)$*E/p_0 caused by a face advance of $S = a/4$

the distance y to the face. It is remarkable that the strain is constant in the region close to the face (y < 0.25a to 0.5a). This behaviour can be traced back to the arching effect ahead of the face (the centre of the face is not stressed by the surrounding ground). This behaviour also becomes evident when considering the increase in strain $\Delta\varepsilon_y(y)$ due to a face advance of S = 1 m (Figure 9c). The centre of the core, at a distance of a/4 ahead of the face, is not influenced significantly by the face advance. The biggest increase in strain occurs at a distance y of about 0.5a - a ahead of the face.

In homogeneous ground the extrusion profiles of Figure 9 are identical to the influence lines of the extrusion. The diagrams of Figure 9 can be read as influence lines by replacing the axial coordinate y with the distance to the face d.

Relationship between extrusion and convergences

The radial displacements occurring in the tunnel can be expressed by the tangential strain which develops at the tunnel boundary behind the tunnel face:

$$\varepsilon_{t,c} = \frac{u_r(\infty) - u_r(y_F)}{a} \quad , \qquad (11)$$

where $u_r(\infty)$ and $u_r(y_F)$ denote the final radial displacement of the ground occurring far behind the face and the radial displacement of the ground at the face, respectively.

Figure 10 shows the tangential strain $\varepsilon_{t,c}$ as a function of the axial strain at the centre of the face $\varepsilon_y(0)$ for different values of the normalized uniaxial compressive strength f_c/p_0 and of the friction angle ϕ. The conditions that lead to high axial strains at the face lead also to larger convergences of the tunnel (see Figures 8b and 8c). As the relationship is unique, prediction is theoretically possible. The dashed lines in Figure 10 show that most values are in the range of $\varepsilon_{t,c}/\varepsilon_y(0)$ = 1 to 2.

Figure 11a shows the ratio $\varepsilon_{t,c}/\varepsilon_y(0)$ as a function of the normalized uniaxial compressive strength f_c/p_0. Each curve clearly consists of four sections:

I $f_c/p_0 \geq 2$

II $0.8 < f_c/p_0 < 2$

III $0.3 < f_c/p_0 < 0.8$

IV $f_c/p_0 < 0.3$

Section I, which concerns high strength to initial stress ratios, concerns elastic behaviour, and is therefore characterized by a constant ratio $\varepsilon_{t,c}/\varepsilon_y(0)$ of about 1.75. When the uniaxial strength decreases to values lower than f_c/p_0 = 2, plastic yielding occurs around the tunnel, while the central portion of the core ahead of the face remains in the elastic domain as long as the ratio of f_c/p_0 is higher than 0.8 (Figure 11b). The axial strains thus remain approximately constant in section II, while the tangential strains increase with decreasing uniaxial strength. At f_c/p_0 ratios lower than f_c/p_0 = 0.8, the plastic zone comprises the entire core ahead of the face (Figure 11b). The extrusion of the core is then due mainly to the developing plastic strains, which increase with decreasing ground strength (section III). In section IV, the convergence to extrusion ratio increases rapidly with decreasing compressive strength. The reason is that for f_c/p_0 < 0.3 the plastic zone continues to increase in the radial direction around the tunnel but not ahead of the face (Figure 11b).

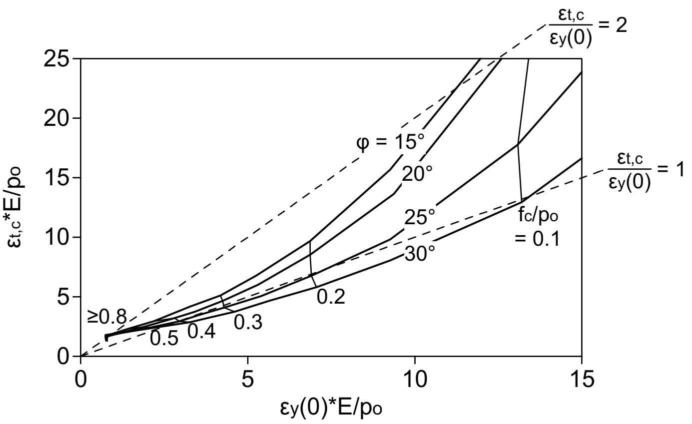

Fig. 10 Unsupported tunnel. Normalized tangential strain $\varepsilon_{t,c}$*E/p_0 over normalized axial strain at the centre of the face $\varepsilon_y(0)$*E/p_0

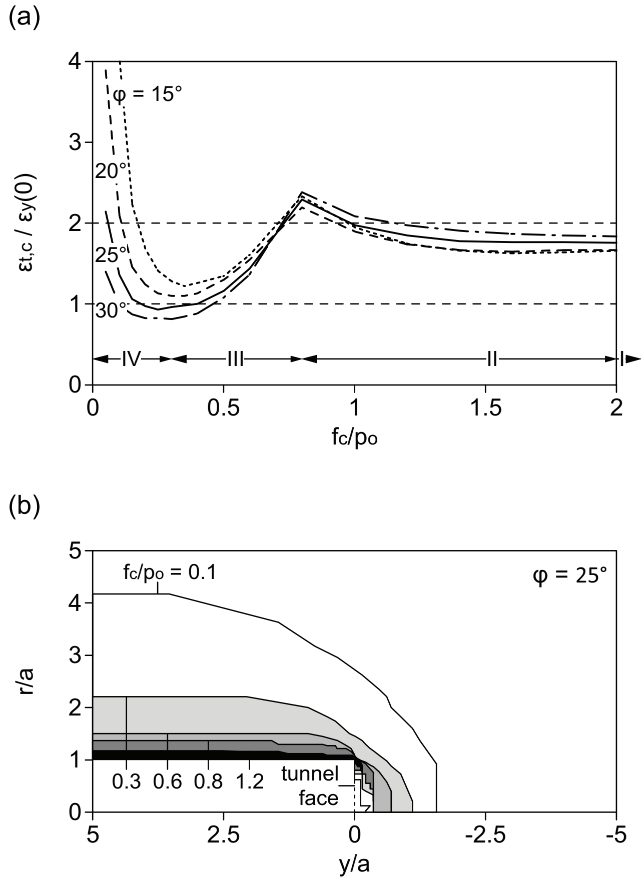

Fig. 11 Unsupported tunnel. a) Ratio of normalized convergence to axial strain as a function of the normalized uniaxial compressive strength f_c/p_0; b) Extent of the plastic zone

The parts mentioned above are similar to the cases distinguished by Panet (1995, 2009) using the stability coefficient $N = 2p_0/f_c$:

$f_c/p_0 > 1$	(N<2)	No plastic zone ahead of the tunnel face
$0.4 < f_c/p_0 < 1$	(2<N<5)	The plastic zone comprises only part of the tunnel face
$f_c/p_0 < 0.4$	(N>5)	Large plastic zone comprising the entire tunnel face

The dashed lines in Figure 11a also show that most cases have a ratio $\varepsilon_{t,c}/\varepsilon_y(0)$ between 1 and 2. Only in case of very poor ground does the ratio increase to over 3. The ratio of $\varepsilon_{t,c}/\varepsilon_y(0)$ = 1.5 proposed by Hoek (2001) is therefore a good approximation.

4.3 The effect of a yielding support

Under severe squeezing conditions, yielding supports are used to reduce the rock pressure on the lining. In the present section, the yielding support is modelled in a simplified way by assigning a constant pressure (which is taken to be equal to the yield pressure p_y of the support) on the tunnel boundary. For alternative models and a detailed analysis of the interaction of yielding supports with squeezing ground see Cantieni and Anagnostou (2009b).

By introducing the normalized yielding pressure p_y/p_0 as an additional parameter in Eq. 9 the axial strains of the ground at the tunnel axis can be expressed by the following function:

$$\varepsilon_y \frac{E}{p_0} = f_8\left(\nu, \phi, \psi, \frac{f_c}{p_0}, \frac{y}{a}, \frac{p_y}{p_0}\right) . \tag{12}$$

The numerical model is identical to the model of Figure 7, with the difference that the pressure p_y is applied as a boundary condition to the tunnel boundary (inset of Figure 12).

According to Figure 12, the higher the yield pressure p_y of the support, the lower will be the tangen-

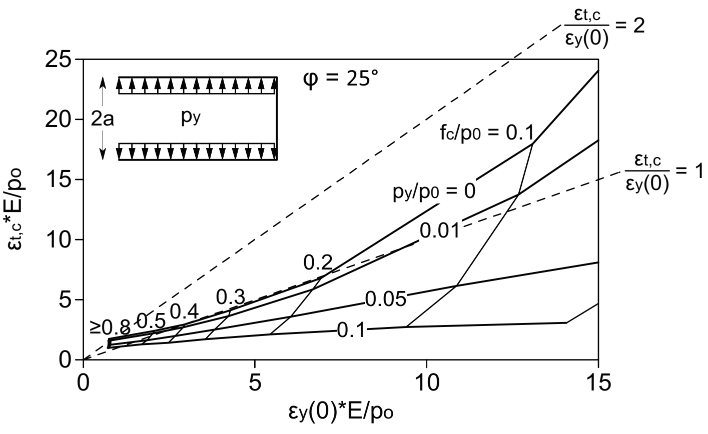

Fig. 12 Tunnel with yielding support. Normalized convergence $\varepsilon_{t,c}\, E/p_0$ over normalized axial strain at the centre of the face $\varepsilon_y(0)^*E/p_0$

tial strain $\varepsilon_{t,c}$ and the axial strain at the centre of the face $\varepsilon_y(0)$. The reduction in the tangential strain $\varepsilon_{t,c}$ is more pronounced. The curve flattens for increasing yield pressures p_y. At very high ratios of yield pressure to initial stress ($p_y > 0.1p_0$), the curve is so flat that the axial strains do not provide any indication as to the magnitude of the convergences. Such high p_y/p_0 - ratios are, however, feasible only in tunnels with overburdens lower than 100 m. The yield pressure of the support system applied in the squeezing section of the Sedrun Lot of the Gotthard Base Tunnel was equal to about $0.01p_0$. For such realistic p_y/p_0 – ratios, the normalized convergence $\varepsilon_{t,c}$ is approximately equal to the axial strain at the centre of the face $\varepsilon_y(0)$ (remember that, according to the last section, unsupported tunnels exhibit $\varepsilon_{t,c}/\varepsilon_y$-ratios between 1 and 2).

4.4 The effect of a stiff support

The stiff support is modelled as an elastic radial support with stiffness k. The radial stiffness k of the ring-shaped lining is equal to $E_L d/a^2$, where a, d, and E_L denote its radius, thickness, and Young's modulus, respectively. The longitudinal bending stiffness of the lining will not be taken into account. The resistance of the lining with the stiffness k is taken into account as a boundary condition of the model by imposing a radial pressure $p(y)$ which is proportional to the displacement of the lining at location y and depends therefore not only on the radial ground displacement $u_r(y)$ but also on its displacement $u_r(e)$ at the installation point ($y = e$) of the lining (Anagnostou 2007a):

$$p(y) = k(u_r(y) - u_r(e)) \quad \text{(for y > e).} \qquad (13)$$

The parameters k and e have to be considered in addition to the parameters of Eq. 5. The axial strains of the ground at the tunnel axis can thus be expressed as follows (c.f. Eq. 13):

$$\varepsilon_y \frac{E}{p_0} = f_9\left(\nu, \phi, \psi, \frac{f_c}{p_0}, \frac{y}{a}, \frac{e}{a}, \frac{a\,k}{E}\right) \qquad (14)$$

The numerical model is identical to the model of Figure 7, with the exception of the boundary condition of the tunnel boundary (Eq. 13).

Figures 13a and 13b show that the installation of a stiff support close to the face reduces the magnitude of the extrusion, but does not affect the extent of the region ahead of the face influenced by the excavation.

The presence of a lining predictably hinders the development of convergences considerably (Figure 13c). The closer the lining is installed to the face, the smaller will be the convergences. For linings which are installed very close to the face ($e < a$), the $\varepsilon_{t,c}$ versus ε_y the curves are so flat that the extrusion does not provide any useful indication as to the convergence.

4.5 The effect of face reinforcement

The presence of a face reinforcement was considered in a simplified manner by prescribing a uniform pressure on the face p_F (cf. Dias and Kastner 2005). The effect of face support was investigated only for the case of a stiff lining (see Section 4.4). As an additional parameter, the normalized face pressure p_F/p_0 must be taken into account in the parameters of Eq. 14:

$$\varepsilon_y \frac{E}{p_0} = f_{10}\left(\nu, \phi, \psi, \frac{f_c}{p_0}, \frac{y}{a}, \frac{e}{a}, \frac{a\,k}{E_R}, \frac{p_F}{p_0} \right) . \tag{15}$$

The numerical model is identical to the model of Figure 7 with the boundary conditions at the tunnel boundary and at the face according to the inset of Figure 14a. The analysis considers an unsup-

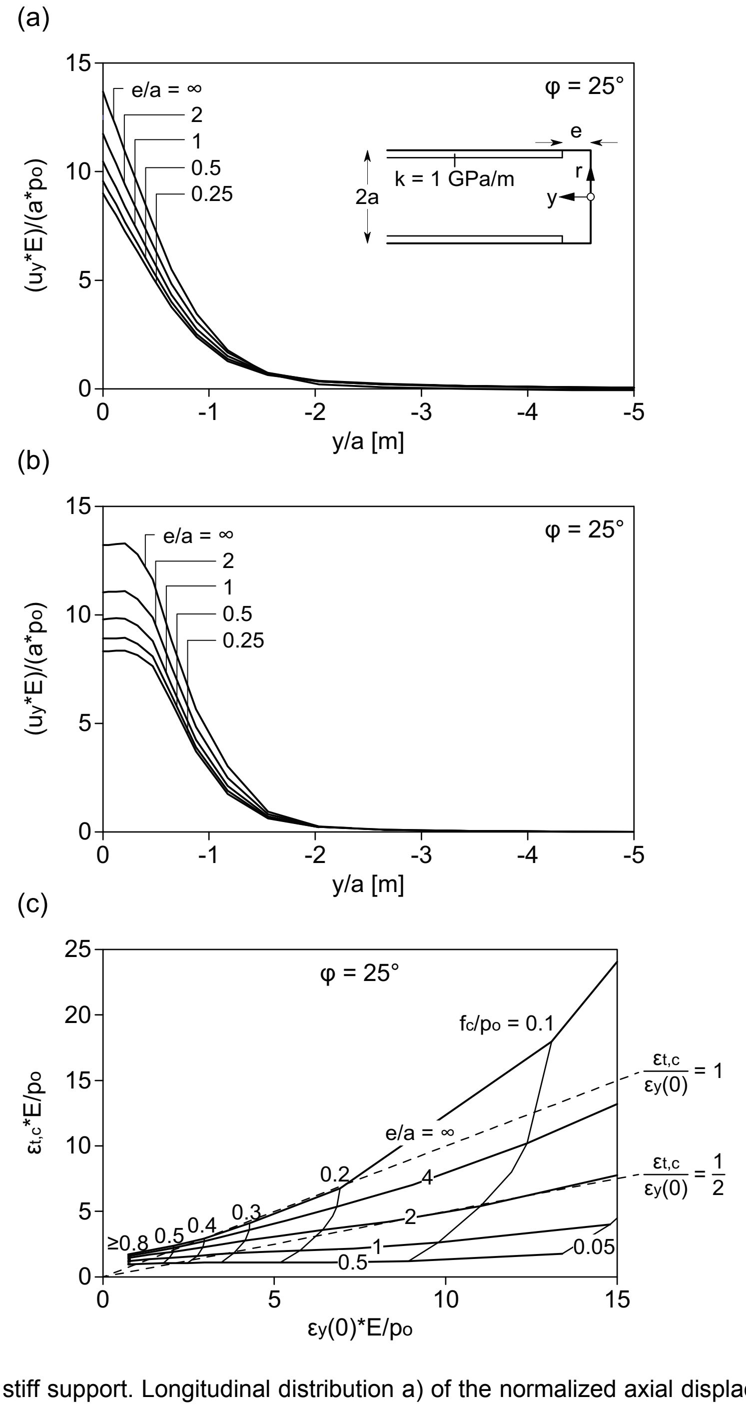

Fig. 13 Tunnel with stiff support. Longitudinal distribution a) of the normalized axial displacements u_y*E/(a*p_0) and b) of the strains ε_y*E/p_0; c) Normalized tangential strain $\varepsilon_{t,c}$*E/p_0 over normalized axial strain at the centre of the face $\varepsilon_y(0)$*E/p_0

ported length of $e = a/2$.

Figures 14a and 14b show that a high support pressure p_F leads to smaller extrusion, but does not affect the influence zone of the advancing face (which extends up to about one diameter ahead of the face). Figure 14c shows that for high face support pressures p_F (> 0.2 p_0), which, however, are

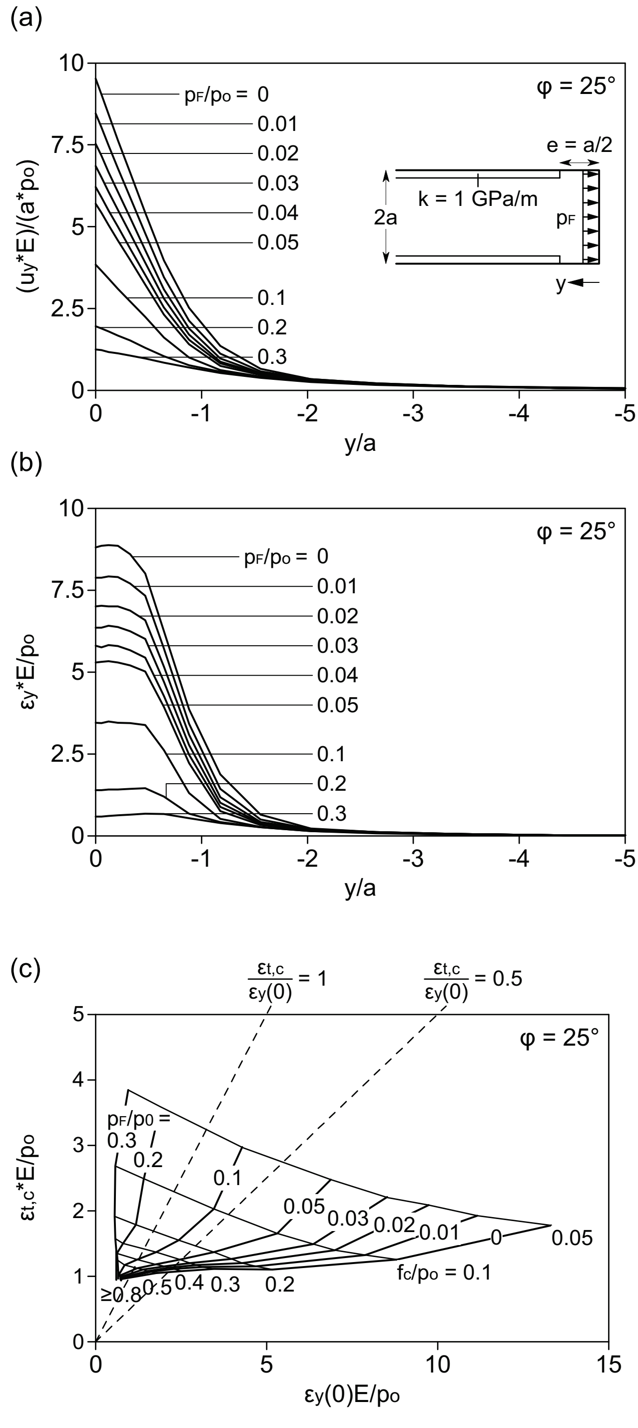

Fig. 14 Tunnel with stiff support and face support. Longitudinal distribution a) of the normalized axial displacements $u_y*E/(a*p_0)$ and b) of the strains ε_y*E/p_0; c) Normalized tangential strain $\varepsilon_{t,c}*E/p_0$ over normalized axial strain at the centre of the face $\varepsilon_y(0)*E/p_0$

feasible only in shallow tunnels, the extrusion of the face does not depend significantly on the ground strength and cannot be used as an indicator of ground quality. It is remarkable that the higher the face support pressure, the bigger will be the convergences developing over the unsupported span *e*.

4.6 The effect of ground rheology

4.6.1 Computational model

Squeezing ground often exhibits a pronouncedly time-dependent response to tunnelling. The deformations in a cavity may continue for several weeks or even months after excavation. As different time scales are relevant for the core extrusion (a short term phenomenon) and for the convergence (a long term phenomenon), it is interesting to investigate extent to which the rheological behaviour of the ground might influence the correlations between these two manifestations of squeezing behaviour.

This issue will be analysed here with the aid of transient stress analyses based on an axisymmetric model of an unsupported tunnel (Figure 15a). The tunnel advance is simulated with 60 excavation steps, each containing an instantaneous advance of s = 1 m, followed by a transient calculation that simulates a standstill period of 1 day. The overall advance rate is therefore v = 1 m/day. For the purpose of comparisons, the time-independent problem (zero viscosity) was also solved by the step-by-step method. The results are slightly different from those presented in Section 4.2.2, where the same problem was solved using the steady state method, which by definition assumes a continuous excavation, i.e. a round length s of zero (Cantieni and Anagnostou 2009a).

The time-dependency of the ground behaviour is considered according to the elasto-viscoplastic creep model after Madejski (1960), which introduces only one additional parameter to the parameters used in the preceding elasto-plastic computations. The micro-mechanical model consists of an elastic spring in series with a Bingham model (inset of Figure 15a). The strain rate $\dot{\varepsilon}_{ij}$ is resolved into an elastic and an inelastic part:

$$\dot{\varepsilon}_{ij} = \dot{\varepsilon}_{ij}^{e} + \dot{\varepsilon}_{ij}^{p} \quad . \tag{16}$$

The elastic part depends, according to Hooke's law, linearly on the stress rate, while the inelastic part $\dot{\varepsilon}_{ij}^{p}$, which represents combined viscous and plastic effects, reads according to the classic formulation of Perzyna (1966) as follows:

$$\frac{d\varepsilon_{ij}^{p}}{dt} = \frac{f}{\eta}\frac{\partial g}{\partial \sigma_{ij}} \quad , \tag{17}$$

where f, g and η denote the yield function, the plastic potential and the viscosity, respectively.

The calculations have been carried out for different values of the viscosity η. Table 2 shows the other model parameters.

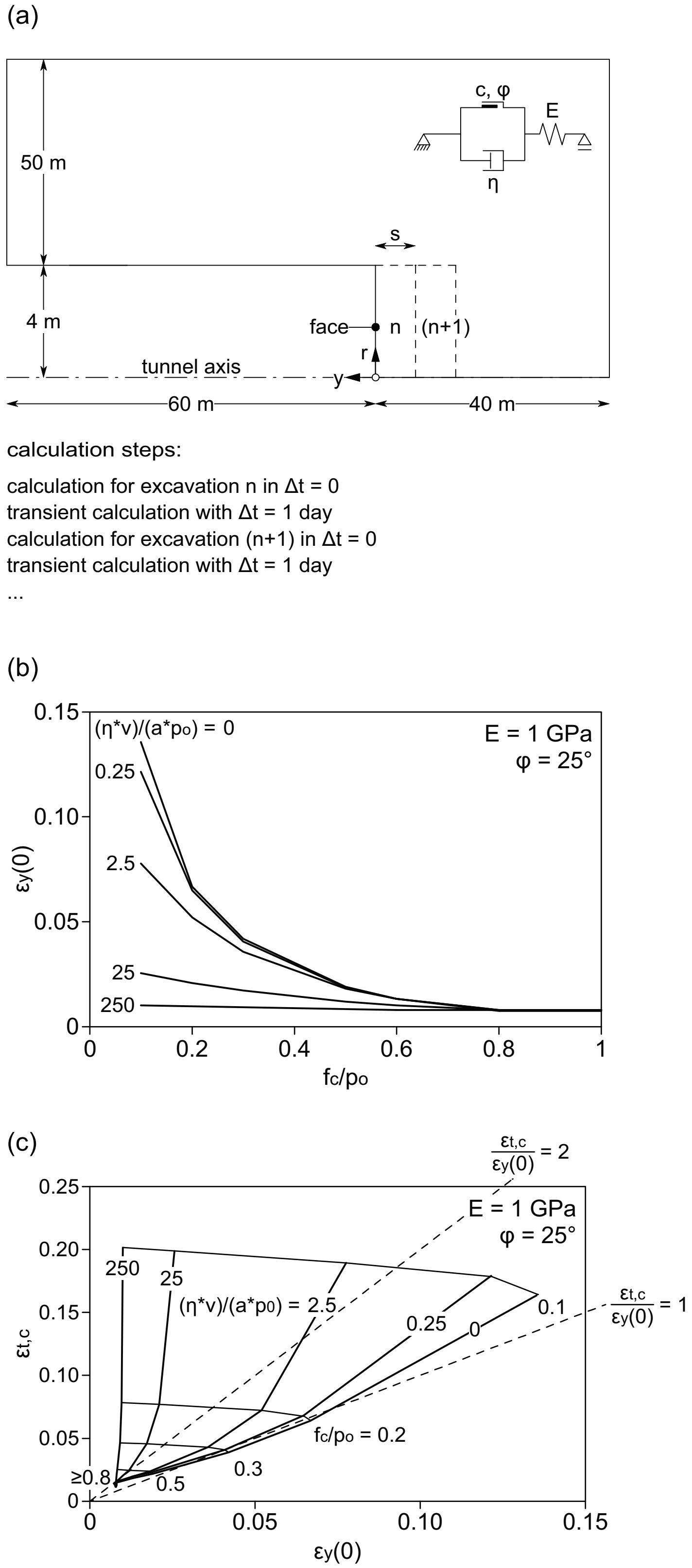

Fig. 15 a) Problem layout, boundary conditions of the step-by-step numerical model and sequence of the calculation steps (inset: micromechanical material model); b) Axial strains at the centre of the face $\varepsilon_y(0)$ as a function of the normalized uniaxial strength f_c/p_0; c) Tangential strain at the tunnel boundary $\varepsilon_{t,c}$ as a function of the axial strain at the centre of the face $\varepsilon_y(0)$, the normalized viscosity $\eta^*v/(a^*p_0)$ and the normalized uniaxial compressive strength f_c/σ_0

Due to the time dependency of the material behaviour, the displacements of the problem under consideration (Figure 15a) depend in general on the following parameters:

$$u = f_{11}\left(E, \nu, f_c, \phi, \psi, \eta, p_0, a, s, t\right) \ , \tag{18}$$

where s denotes the round length and t the time taken by each excavation round. By considering the gross advance v (= s/t) as an independent parameter instead of the round duration t and by performing a dimensional analysis, one obtains the following expression for the convergence u_c and for the axial strain ε_y at the face:

$$\frac{u_c}{a} = f_{12}\left(\nu, \phi, \psi, \frac{E}{p_0}, \frac{f_c}{p_0}, \frac{s}{a}, \frac{\eta\, v}{a\, p_0}\right) \ , \tag{19}$$

$$\varepsilon_y = f_{13}\left(\nu, \phi, \psi, \frac{E}{p_0}, \frac{f_c}{p_0}, \frac{s}{a}, \frac{\eta\, v}{a\, p_0}\right) \ . \tag{20}$$

According to these equations, the response of the model depends on the product of the advance rate v and the viscosity η (cf. Bernaud 1991). The effect of a high advance rate is equivalent to that of a high viscosity. In the borderline case of an "infinitely" rapid excavation, only elastic deformations will occur ahead of the advancing face.

4.6.2 Numerical results

Figure 15b shows the axial displacements of the centre of the face $u_y(0)$ immediately after the excavation step as a function of the normalized uniaxial compressive strength f_c/p_0 and of the dimensionless parameter $\eta v/ap_0$. The curve for $\eta v/ap_0 = 0$ applies to time-independent ground behaviour. The extrusion of the core is, particularly for low ground strengths, strongly influenced by the viscosity. Viscosity significantly reduces the axial strain at the face, because the development of the plastic strains needs more time than is temporarily available in the vicinity of the advancing tunnel face.

Figure 15c shows the tangential strains at the tunnel boundary $\varepsilon_{t,c}$ as a function of the axial strains at the face $\varepsilon_y(0)$:

- The viscosity η of the ground influences the convergence only slightly. The higher the viscosity, the greater will be the convergence. This is because the pre-deformation of the ground $u_r(y_F)$ is small when the viscosity is high, while the final total radial displacement of the ground developing far behind the face $u_r(\infty)$ is independent of the viscosity and the advance rate in the case of an unsupported tunnel (Bernaud 1991) and was therefore calculated with the time-independent plane strain closed-form solution of Anagnostou and Kovári (1993).
- As a consequence of the viscous behaviour (which is decisive mainly for the deformations ahead of the face) the ratios of convergence to axial displacement are in general higher than in the case of time-independent behaviour. The rule established in Section 4.2.2 (ratio $\varepsilon_{t,c}/\varepsilon_y$ = 1 – 2) is valid only if the dimensionless parameter $\eta v/(ap_0)$ is lower than about 2.5. In the case of a 400 m deep traffic tunnel (a = 5 m, p_0 = 10 MPa) and of a gross advance rate v of 2 m/d, this condition leads to η < 62500 kPa*day, which is typical for materials that respond within a few weeks (Cantieni and Anagnostou 2011).

At very high viscosities η and advance rates v, the axial strain at the face does not depend significantly on the uniaxial compressive strength f_c of the ground, because the strains developing ahead of the face are almost entirely elastic. In such cases it is impossible to predict the convergences of the opening on the basis of the observed extrusion. Consider, for instance, the curve $\eta v/(ap_0)$ = 250. The convergence $\varepsilon_{t,c}{}^*a$ varies between 0.05*a* and 0.20*a* for one and the same axial strain of about 0.01. Also the viscosity η itself represents a source of uncertainty. For an axial strain of 0.025, for example, the convergence may vary with a factor of about 7 for viscosities between $\eta v/(ap_0)$ = 2.5 and 25. Such inaccurate predictions are useless from the practical point of view.

In conclusion, if the ground behaviour is time-dependent, the fact that the core extrusion is low does not necessarily mean that the convergences will be small. On the other hand, large core extrusions are always associated with poor ground quality. One could also say that a large extrusion represents a sufficient, but not a necessary, condition for large convergences to occur.

4.7 Entering into a fault zone

4.7.1 Numerical Model

The present section investigates numerically the evolution of core extrusion and convergence when tunnel advance approaches and enters into an extended, lower quality fault zone, which strikes perpendicularly to the tunnel axis.

The purpose of the present analysis was to find if it is possible at least in principle to recognize a fault zone before entering into it on the basis of the observed extrusion, and if the magnitude of the extrusions provides a useful indication as to the magnitude of the later convergences. Similar numerical analyses have been carried out by (cf. Jeon *et al.* 2005), but these were investigating another question (the possibility of early fault identification on the basis of observed changes in the orientation of the displacement vectors).

The considered axisymmetric numerical model (Figure 16a) includes a transition zone between the competent rock and the fault zone, where the deformability and strength parameters decrease gradually (Figure 16b). The excavation was simulated step by step. The 200 m long tunnel was excavated in 100 steps, every excavation step having a length of s = 2 m. The calculations have been carried out using the parameters of Table 2 and the deformability and strength parameters of Figure 16b.

4.7.2 Results

Figure 17a shows the distribution of the axial strain ε_y along the tunnel axis for different positions y_F of the advancing face. The axial strain ahead of the face is similar for all of the excavation steps up to a point that is 4 m ahead of the first change in ground properties at y = 0. The shape of the next curve (y_F = -2 m) deviates from the preceding one. The strain 2 m to 3 m ahead of the face is sig-

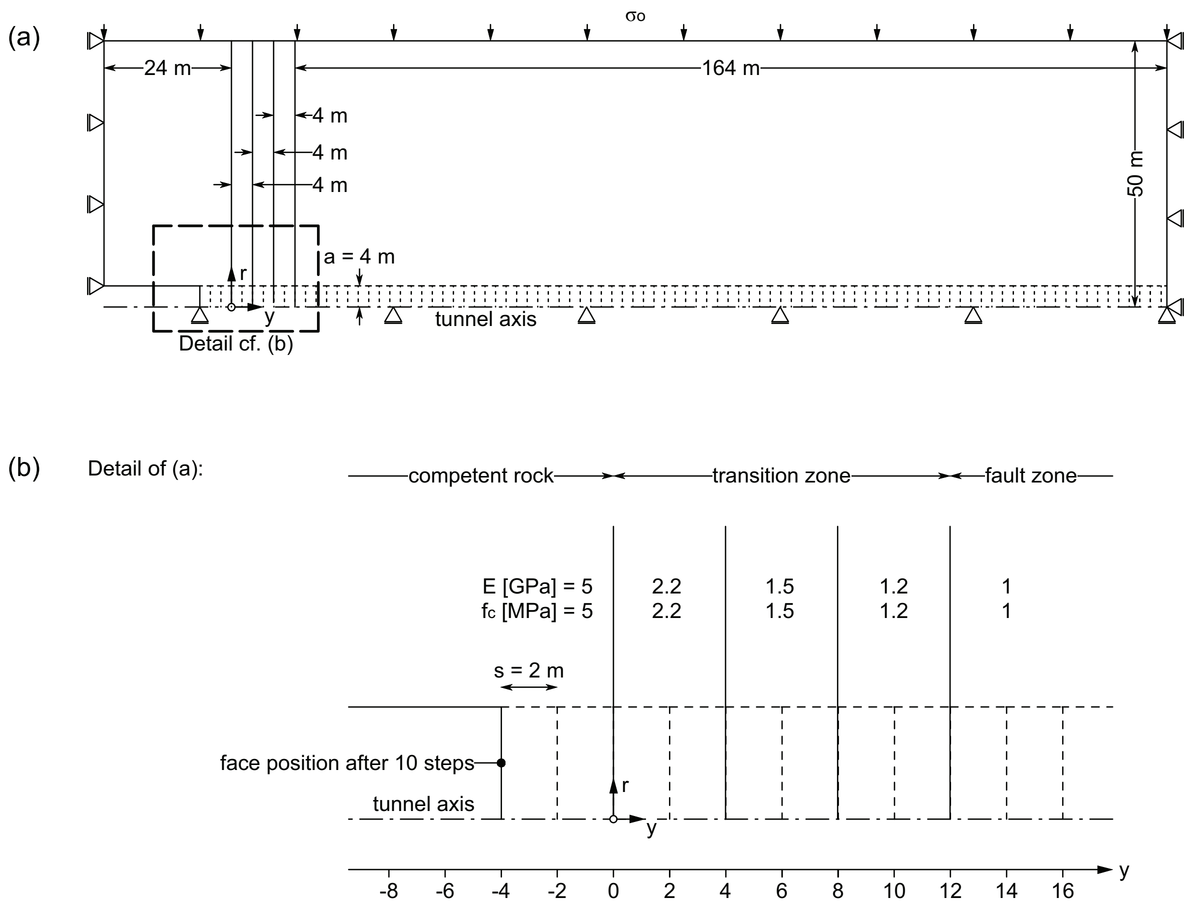

Fig. 16 Fault zone. a) Axisymmetric numerical step-by-step model and boundary conditions; b) Detail of the transition zone with a gradual decrease in the deformability and strength parameters, including the definition of the chainage *y* and of the strain intervals AB

nificantly higher than for preceding excavation steps. The strain ahead of the face increases continuously during the subsequent excavation steps.

Figure 17b shows the influence lines of the average axial strain $\varepsilon_{y,AB}$ for some selected intervals with a length of 0.5 m (every curve in Figure 17b applies to another interval AB, see inset of Figure 17b). The intervals starting before y_A = -2 m exhibit the same increase in strain for the approaching face. The influence zone of the excavation extends up to about 4 m ahead of the face. The interval starting at y_A = 0 (i.e. at the begin of the transition zone) shows a more pronounced increase of the strains, starting when the advancing face comes to within about 4 m of the interval. The proximate intervals all show a more pronounced increase in the strains again due to the approaching face. After passing the transition zone, the influence lines tend to show the same characteristics. The influence zone of the face increases from initially 4 m to 8 m.

Figure 17c shows the radial displacements u_c of selected "measuring" points on the tunnel boundary as a function of their distance from the face. The convergence increases with the advancing face. The maximum convergence increases continuously for the measuring points in the transition zone and in the first 50 m of the fault zone. The increase in the maximum convergences despite the uniform ground conditions prevailing within the fault zone is due to the so-called "wall-effect".

The wall-effect describes the stabilizing effect of competent ground on weak ground. The interface shear stresses between the competent and the weak ground reduce the deformations of the weak zone. The wall-effect was analysed by Kovári and Anagnostou (1995) for the borderline case of rigid competent rock and by Cantieni and Anagnostou (2007) for the case of competent rock having a

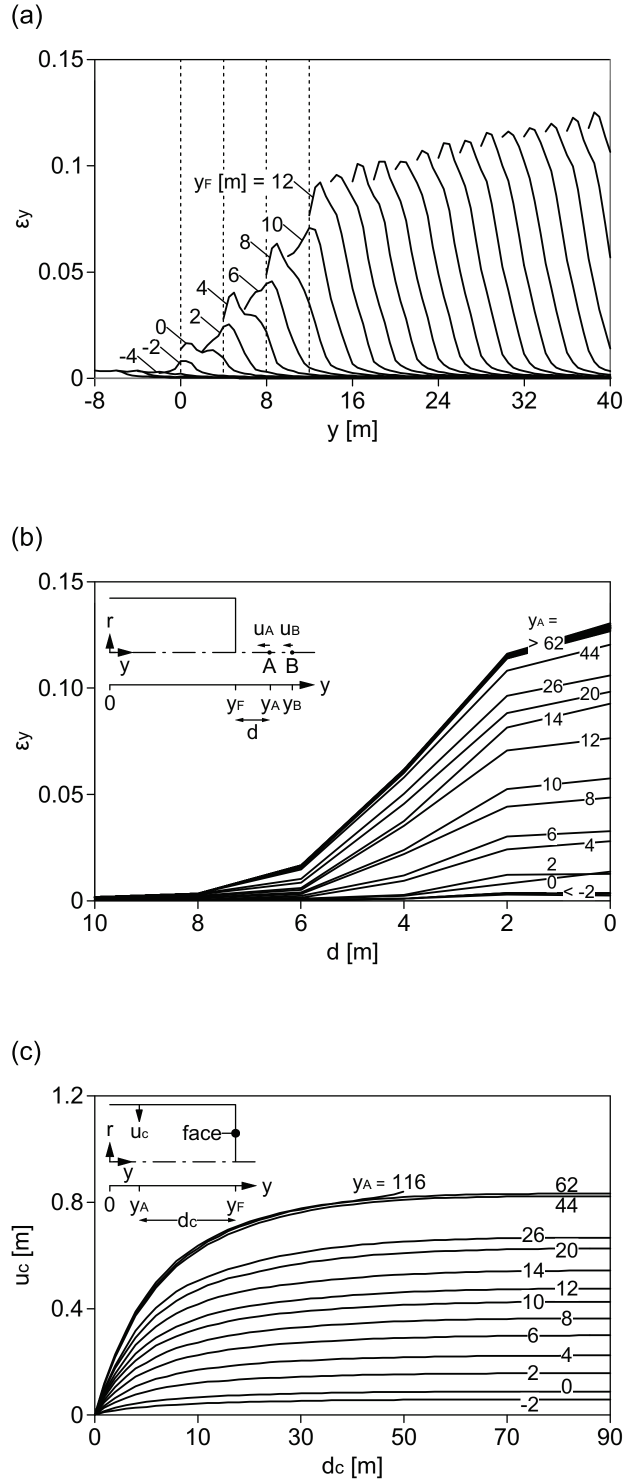

Fig. 17 a) Axial strain ε_y profiles for all face positions between y = -8 and 38 m; b) Influence lines of the axial strain ε_y; c) Influence lines of the radial displacements u_c of selected points on the tunnel boundary

elasto-plastic ground behaviour.

The influence lines of the extrusions and the convergences (Figures 17b and 17c) correlate with each other. Cross sections exhibiting large extrusions also experience high convergences after excavation. A fault zone can thus be detected by monitoring the extrusion of the core ahead of the face (unless the ground exhibits a markedly time-dependent behaviour, see last section).

In a last step, we investigate whether it is possible to predict the convergences (including all spatial effects associated with the fault zone) on the basis of the monitored extrusions, by applying the simple rule established in Section 4.2.2. (Section 4.2.2 showed for the case of homogeneous ground, that the ratio of the convergence $\varepsilon_{t,c}$ to the axial strain at the centre of the face $\varepsilon_y(0)$ is in most cases between 1 and 2.) Figure 18a compares the convergences u_c obtained by the numerical computation with the convergences which have been estimated on the basis of the extrusions assuming a ratio $\varepsilon_{t,c}/\varepsilon_y(0)$ of 1, 1.5 or 2. The diagram shows that the assumption of $\varepsilon_{t,c}/\varepsilon_y(0)$ = 1.5 leads to convergences which agree very well with the actual convergences. Figure 18b, where the tangential strains $\varepsilon_{t,c}$ are plotted against the axial strains at the face $\varepsilon_y(0)$, shows that most points are grouped in the vicinity of the line $\varepsilon_{t,c}/\varepsilon_y(0)$ = 1.5.

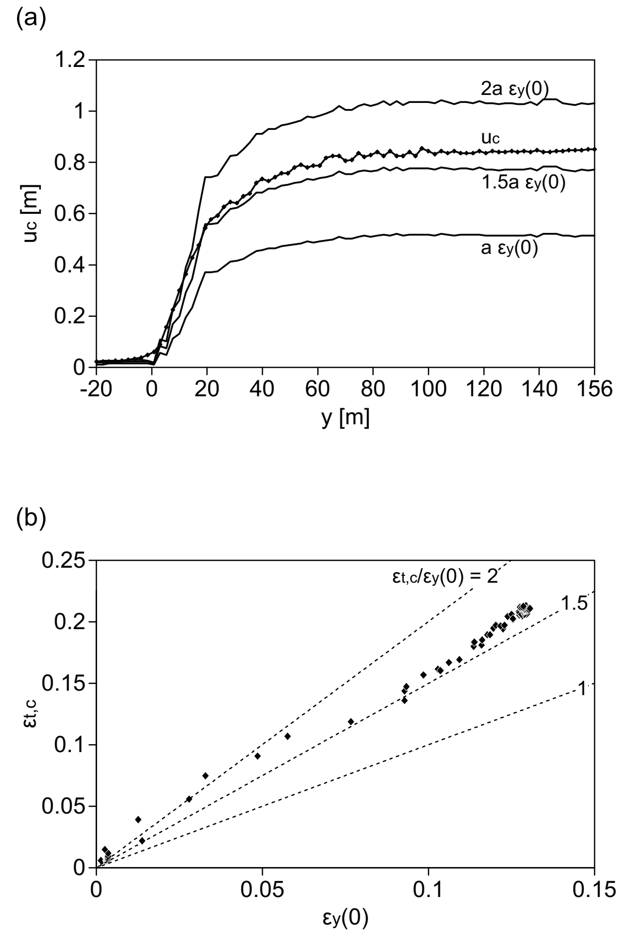

Fig. 18 a) Comparison of the ground convergences u_c (= $\varepsilon_{t,c}$*a) at chainage *y* with the convergences calculated on the basis of the face extrusions $\varepsilon_y(0)$ with the ratios $\varepsilon_{t,c}/\varepsilon_y(0)$ of 1, 1.5 and 2; b) Tangential strain $\varepsilon_{t,c}$ over axial strain at the centre of the face $\varepsilon_y(0)$ for all chainages *y* in the fault zone model

5 Gotthard Base Tunnel

5.1 Introduction

The present case history investigates the data monitored during the construction of the western tunnel of the new Gotthard Base Tunnel, which crosses the northern intermediate Tavetsch-formation (so-called TZM formation) and the adjacent Clavaniev zone (referred to as “CZ” in Figure 19). In this section of the tunnel, squeezing conditions had been expected from the planning phase. For this reason, the geological survey included an inclined, exploratory borehole SB 3.2, which was over 1700 m deep and which passed through the problematic series of rocks (Figure 19b). The core samples retrieved from the boring were used to carry out a laboratory testing programme in order to investigate the strength and deformation properties of the weakest zones. The testing program was carried out at the Institute for Geotechnical Engineering of the ETH Zurich (Vogelhuber 2007) and also continued during construction of the tunnels with rock samples retrieved by horizontal drillings performed from the tunnel face (Anagnostou *et al.* 2008).

The aim of the present case history is to investigate whether there is a correlation between the extrusion of the core and the convergences of the tunnel and, accordingly, if it would have been possible to predict the convergences with the monitored extrusions. The present case history will focus on two tunnel reaches. The first reach reaches from chainage 1690 m to chainage 1780 m of the western tube excavated northwards (NW tube). The second reach starts at chainage 1980 m and ends at chainage 2140 m of the NW tube (Figure 19b). In both reaches, the extrusion of the core has been monitored with a series of RH-extensometers (Thut *et al.* 2006).

5.2 Geology

The tunnel crosses the northern TZM formation and the Clavaniev zone for about 1150 m at a depth of 800 m (Figure 19b). The Clavaniev zone denotes the tectonically intensively sheared southern part of the Aar-massif between the Aar-massif and the TZM formation (cf. Schneider 1997). The Clavaniev zone was encountered over about 120 m at the end of the advance before entering into the competent rocks of the Aar-massif. Both, the TZM formation and the Clavaniev zone are characterized by alternating layers (having a thickness in the range of decimetres to decametres) of intact and more or less kakiritic gneisses, slates, and phyllites. The term “kakirite” denotes a broken or intensively sheared rock, which has lost a large part of its original strength (cf. Schneider 1997; Vogelhuber 2007). The orientation of the layers to the tunnel axis varies from perpendicular to parallel.

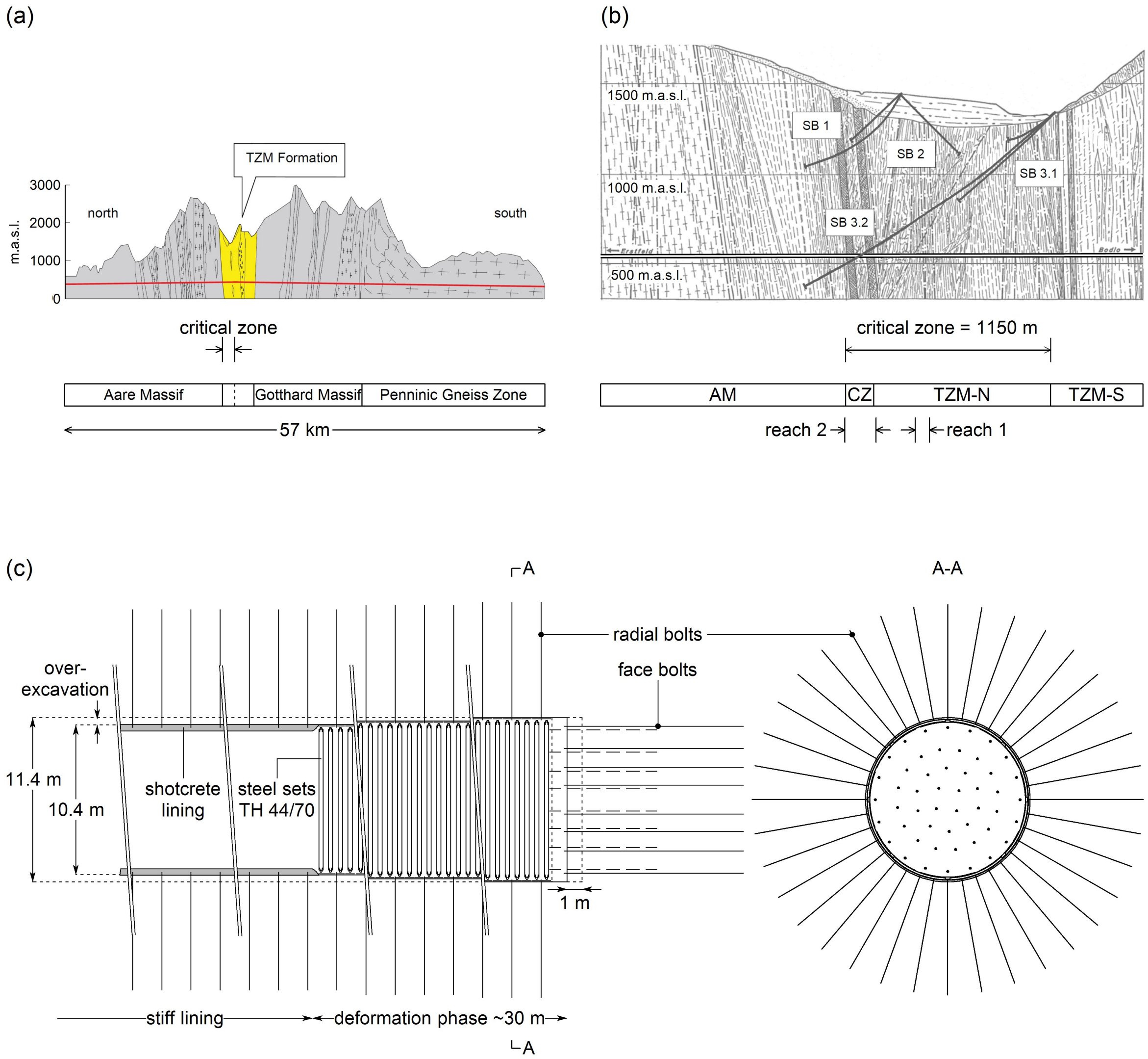

Fig. 19 a) Gotthard Base Tunnel: schematic representation of the longitudinal geological section with the squeezing TZM-Formation (after Kovári 2009); b) Detail of the TZM formation (after Vogelhuber 2007) showing the Aare massif (AM), the Clavaniev zone (CZ), the northern TZM formation (TZM-N), the southern TZM formation (TZM-S) and the two reaches under consideration; c) Longitudinal and cross section of the yielding support system realized in the northern TZM formation (after Ehrbar and Pfenninger 1999)

5.3 Construction method

The tunnel has been excavated full-face. Squeezing was tackled through a yielding support system consisting of two rings of sliding steel sets (TH 44/70) lying one upon the other and connected by friction loops (Ehrbar and Pfenninger 1999; Kovári *et al.* 2006; Kovári and Ehrbar 2008). Figure 19c shows the longitudinal and the cross section of the yielding support system. In the tunnel reaches under investigation, the radial over-excavation (which is required for accommodating the deformations) was either 0.5 m or 0.7 m, the cross section area A_F = 101 or 122 m^2, respectively, and the spacings of the steel sets 0.66 m or 0.5 m, respectively. Between 125 m and 190 m of radial bolts with a length of 8 m were installed per meter of the tunnel over the whole circumference.

The face was supported by about 50 to 60 bolts with a length of 12 m to 18 m and having an overlap of about 6 m. After the rate of convergence slowed down, a shotcrete ring of 0.5 m was applied (normally at a distance of about 30 m behind the face).

5.4 Monitoring

The core extrusion was monitored by 4 RH-extensometers in the first reach (TZM formation) and 7 RH-extensometers in the second reach (Clavaniev zone). The RH-extensometers were placed at the axis of the tunnel. They had a length of 24 m and overlapped 4 m to 8 m with the preceding ones. The position of the measuring head and the six measuring points of each extensometer with respect to the tunnel alignment are shown at the bottom of Figure 25.

The convergences of the opening were monitored optically with 5 or 7 points per cross section. The distance between the monitored cross sections was between 5 m and 20 m. The exact location and the number of monitored points per cross section along the tunnel alignment are shown at the bottom of Figure 25.

5.5 Data analysis

Primary data

Figures 20a and 20b show the primary data obtained by the RH-extensometers of reaches 1 and 2, respectively. The variation in the extrusion rate (note the wavelike shape of the curves in Figure 20) indicates that the ground exhibits a time-dependent behaviour. Every excavation step accelerates the development of the extrusions before they slow down until the next excavation step again accelerates the rate of deformations. The extrusions monitored consist of the time-independent extrusions due to the stress redistribution after each excavation step, and the time-dependent extrusions due to rock creep and consolidation processes. After an excavation step, the extrusions continue for several days. For instance, the last measuring point of extensometer 5 at chainage 2090 m of reach 2 shows the extrusion that developed at a distance of 4 m ahead of the face during a standstill of 30 days (curve B in Figure 20b). The extrusion rate is almost zero after 30 days and accelerates when the excavation is restarted. The measurements indicate that 95% of the final extrusion is reached after about 20 days. This indicates a viscosity η of about 10^4 to 10^5 kPa*day (cf. Cantieni and Anagnostou 2011).

In order to assess the behaviour of the ground along the tunnel it is necessary to compare deformations that occur under similar conditions and, more specifically, during the same period of time. As the duration of the advance halts was variable along the tunnel reaches, the comparability of the final extrusion values would be questionable. Therefore, the present analysis considers only the extrusions developing during the excavation round and the subsequent 10 hours. Figure 20c shows the way the extrusions have been determined from the example of the axial displacements.

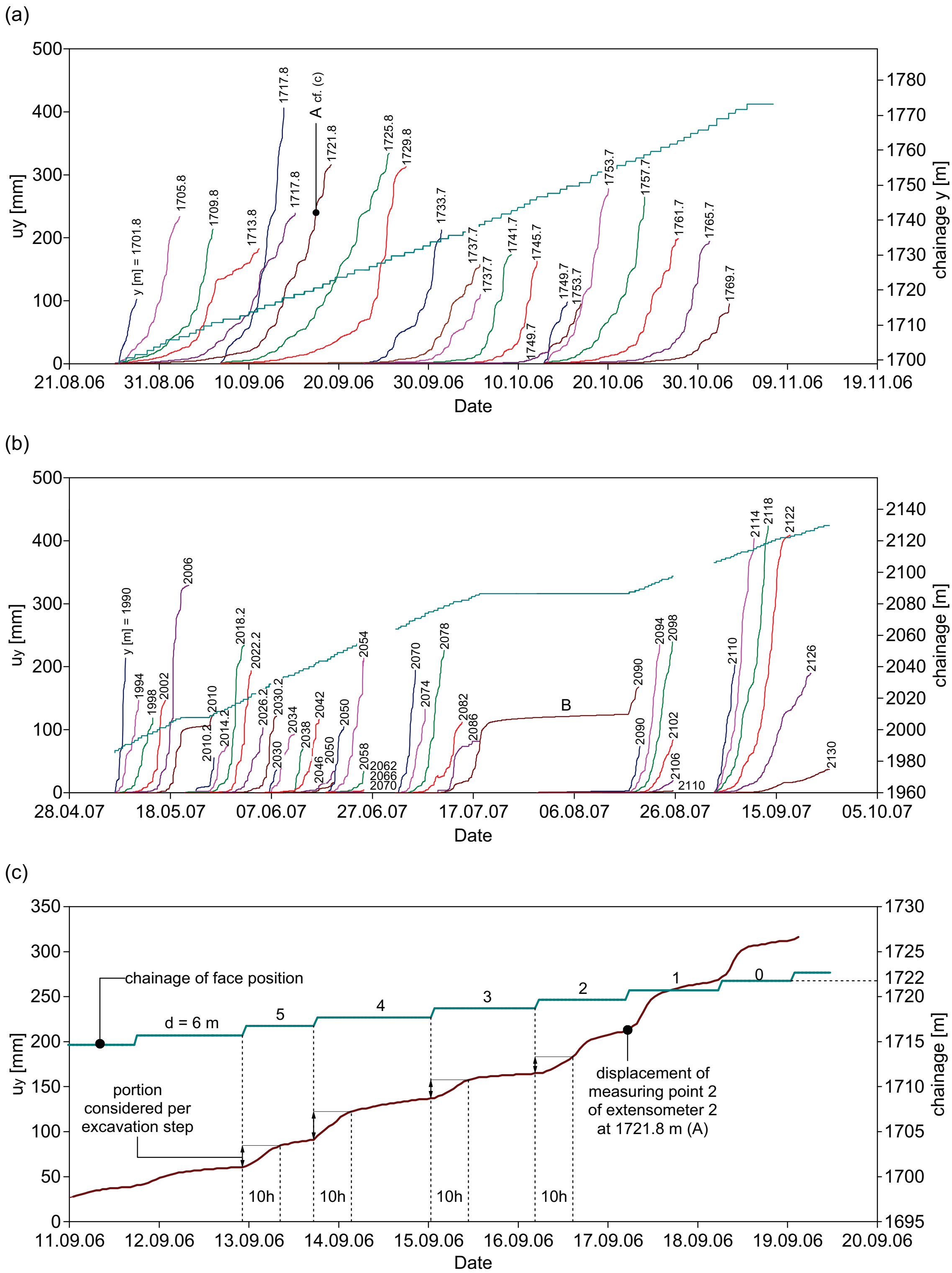

Fig. 20 a) Extrusions u_y over time for the measuring points of reach 1 of the NW tube; b) Extrusions u_y over time for the measuring points of reach 2 of the NW tube; c) Exemplary determination of the extrusions on the example of curve A of Fig. 20a

Influence lines

Due to the low spatial resolution of the monitored profile (the relatively small number of measuring points) and to the large number of readings, the most meaningful way to present the monitoring data is to plot influence lines.

Figures 21 and 22 show the influence lines of the axial strain ε_y (taking account of the extrusion generated by face advances and during the 10 hours following each advance) for all extensometers. The characteristics of the influence lines are similar for all extensometers. The observation that the strains increase continuously until d = 0, contradicts with the theoretical predictions, according to which the strain should not increase close to the advancing face (Figure 9b). The reason for the different behaviour is the length of the interval (4 m). The average strain over a 4 m long interval increases until the face reaches the interval (d = 0), even if the strain locally close to the face remained constant over the last meters.

Variations in the magnitude of the strain, as well as in the extent of the influence zone of the advancing face, indicate changes in the quality of the core ahead of the face (the support measures are assumed to be constant). Figure 21 shows the influence lines of the axial strain ε_y over tunnel reach 1. The last interval of extensometer 3 shows an increase (at about 11 m) in the strain earlier than the other intervals (at about 7 m) of the same extensometer. The influence lines of extensometer 4 confirm this trend.

Consider now the *maximum* strain, i.e. the strain developing up to the time point where the face reaches the first measuring point (d = 0). It is possible to distinguish 3 cases: Most measurements show maximum strains of 0.03. Exceptions with lower maximum strains are the interval 1709.8 m of extensometer 1, 1737.7 m of extensometer 3 and 1769.7 m of extensometer 4. The interval 1721.8 m of extensometer 1 shows a considerably higher maximum strain than all other intervals. The intervals 1713.8 m and 1717.8 m also seem to tend to such high values. But at d = 3 m the strain suddenly decreases with the approaching face. A decrease in strain indicates an axial recompression of the rock over the considered interval. This behaviour cannot be traced back to the effect of a heavier face support, because this effect is very small at the actual initial stress level (see curve $0.01p_0$ in Figure 14b). Besides measuring errors, this behaviour could be due to the presence of a very strong ground interlayer perpendicular to the tunnel axis, which hinders the axial deformation and thus recompresses the weak ground further away from the face.

Figure 22 shows the influence lines of the axial strain ε_y over tunnel reach 2. Extensometer 6 clearly shows that the influence zone of the considered intervals increases continuously. This observation provides an indication of decreasing ground quality (as shown later, the convergences also increase in this portion). Extensometers 3 and 4 appear to be in a more competent rock than the others. The influence zone of the face is considerably less extended (about 6 m) than in most of the other intervals of tunnel reach 2 (between 8 m and 12 m) and the extrusion values are also lower (2%). In the next section we will see that also the convergences are lower in this tunnel portion.

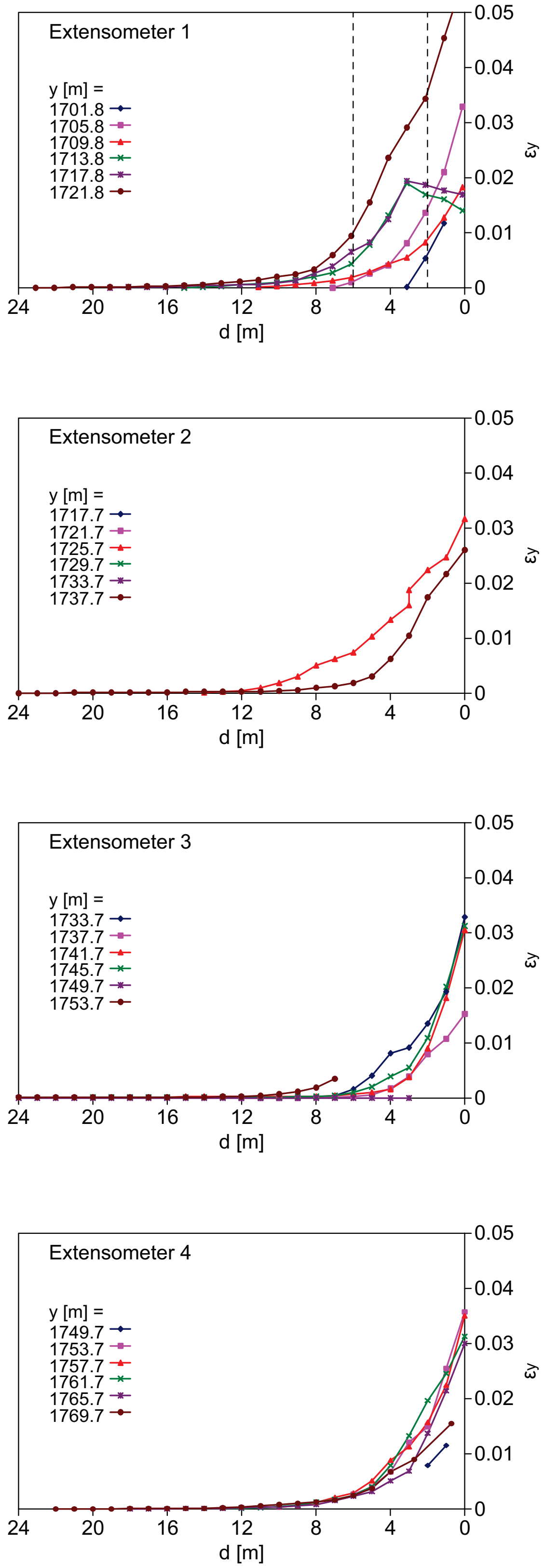

Fig. 21 Influence lines of axial strain ε_y for the intervals between the measuring points at chainage y and (y + 4 m) of extensometer 1 to 4 of reach 1

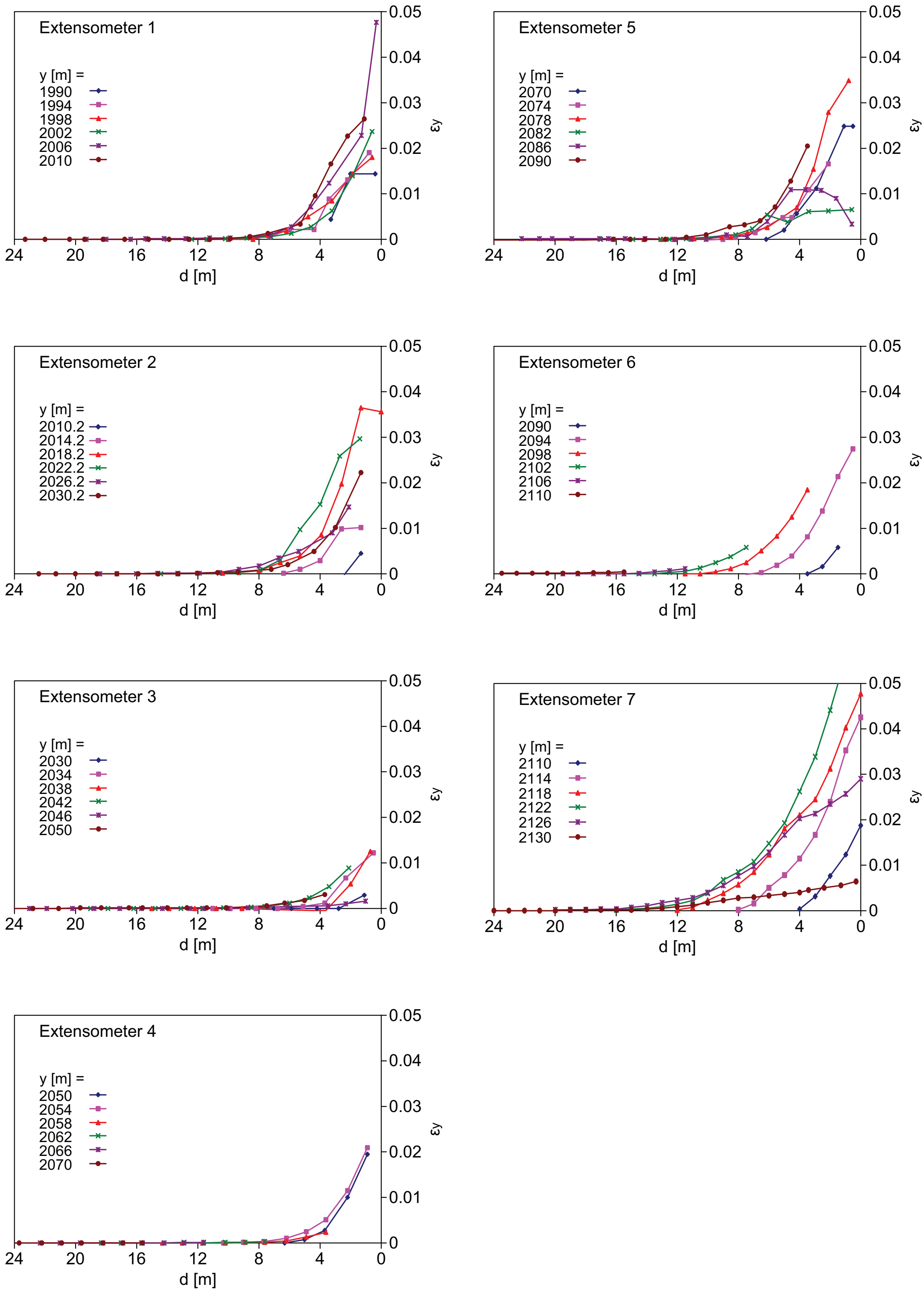

Fig. 22 Influence lines of axial strain ε_y for the intervals between the measuring points at chainage y and (y + 4 m) of extensometer 1 to 7 of reach 2

Extrusions vs. convergences

Subsequently, the longitudinal distribution of the extrusion will be compared with the distribution of the convergences. In order to obtain comparable values, the analysis considers as a measure of the extrusion the strain that develops due to the advance of the face from a distance of 6 m to a distance of 2 m in respect of each ground interval (see the strain portion between the vertical dashed lines in the diagram of extensometer 1 in Figure 21 and the upper part of Figure 23). The face advance specified above (from 6 m to 2 m behind the measuring point) was determined so that as many measuring points as possible could be used for the analysis.

The radial displacement of the tunnel crown will be used as a measure of the convergence. In order to get comparable values, the analysis takes account of only a specific portion of the monitored displacements, occurring due to a face advance of 25 m. More specifically, we consider the displacement that develops as the distance of the face to the monitoring section increases from 5 m to 30 m, see lower part Figure 23. This interval was chosen because the latest zero reading of a measuring point in the reaches under consideration was done about 5 m behind the face, and because the shotcrete ring is applied at a distance of about 30 m from the face. Figure 24 shows the radial displacements Δu_r of the crown for different cross sections as a function of their distance to the face d_c. Most of the curves of Figure 24 show convergences (in respect of a face advance from 5 m to 30 m ahead of the monitored point) of between 0.06 and 0.08 m.

Figure 25 shows the axial strain and the radial displacements of the crown along tunnel reaches 1 and 2. The figure includes only the measuring points which worked properly during the monitored face advance. (Some measuring points failed because the bar which connects the measuring point with the measuring head, was damaged by face bolt drillings.) In addition to the convergences and

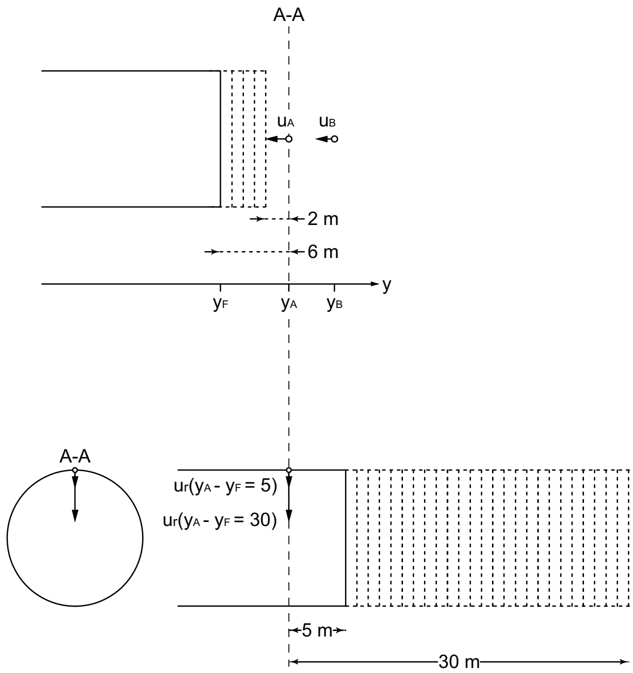

Fig. 23 Way of determining of the accumulated strain $\Delta\varepsilon_y$ ahead of the face for the advance of the face from 6 m to 2 m ahead of each measuring point and the radial displacements of the crown Δu_r of the tunnel generated due to a face advance of 25 m

extrusions, Figure 25 also illustrates information about the geology, construction method and monitoring setup. The convergences of tunnel reach 2 exhibit a weak correlation with the extrusions. The decrease in the convergences before reaching chainage 2050 m, and the subsequent increase in the convergences were indicated by a decrease and an increase in the extrusions. The change in convergences appeared even without a significant change in the geology, construction method or overburden. Also, the decrease and increase in convergences around chainage 2090 m are indicated by a decrease and a subsequent increase in the extrusions.

No correlation can be observed between the convergences and the extrusions in tunnel reach 1. The decrease in the convergences after chainage 1745 m could not be predicted by the extrusions. One reason for the non-correlation may be the arrangement of the monitoring stations. In alternating layers of weak and hard rock the variation in convergences can be significant even over short distances and can thus not be monitored completely if the distance between the monitoring stations

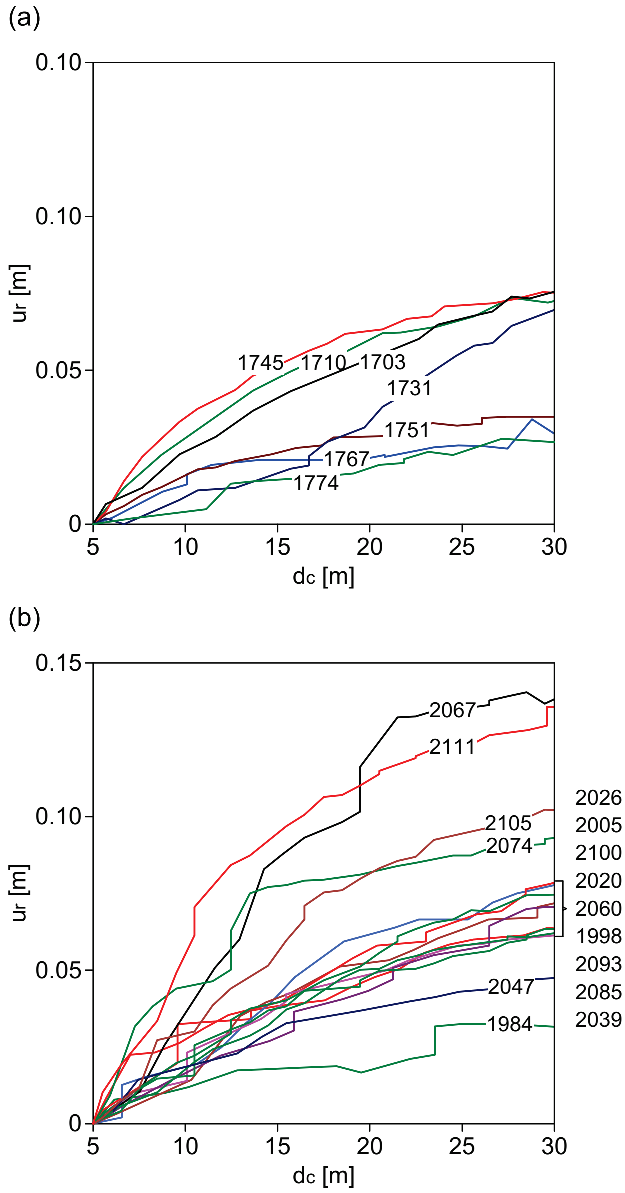

Fig. 24 a) Convergences as a function of the distance to the face d_c; a) for reach 1 and b) for reach 2

is large (Cantieni and Anagnostou 2007).

Figure 26 shows the normalized displacement of the tunnel crown ($\Delta\varepsilon_{t,c}$ = u_c/a) as a function of the axial strain $\Delta\varepsilon_y$ of the core for the two tunnel reaches. The points from tunnel reach 2 are roughly grouped around a slightly inclined straight line. Note that the deformations plotted in Figure 26 are not the total deformations, but only the deformations that developed due to the specific face ad-

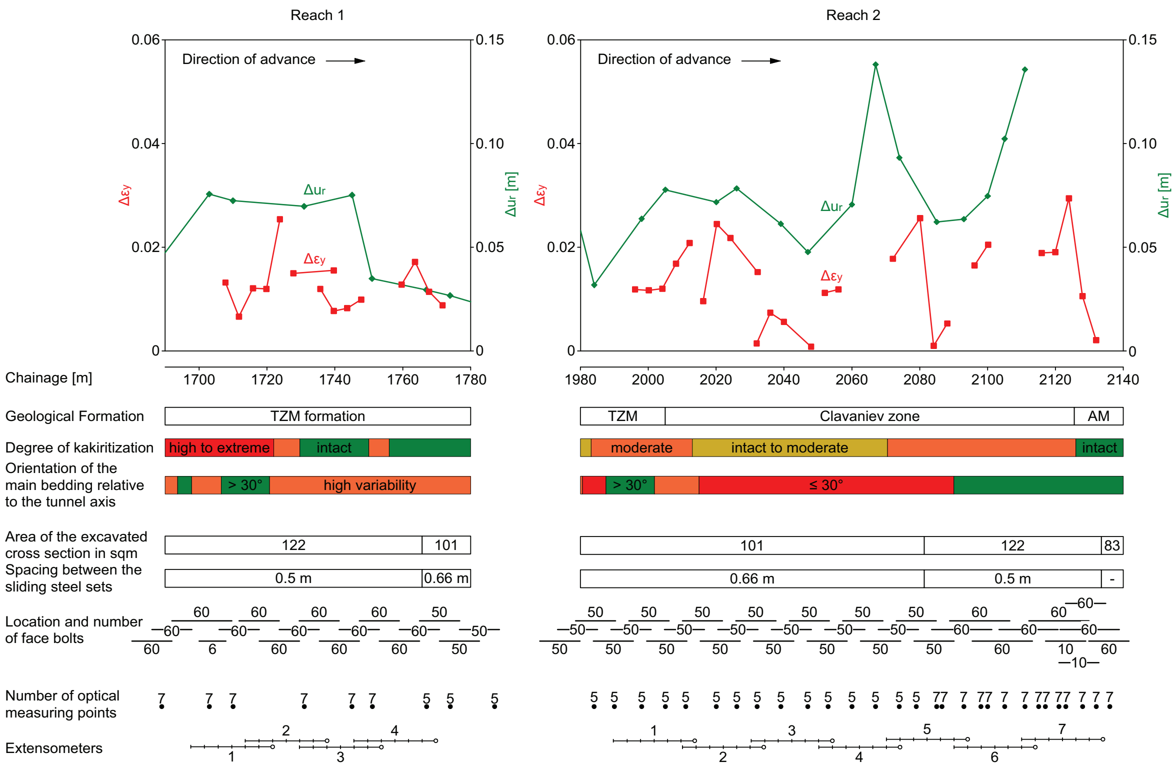

Fig. 25 Axial strain $\Delta\varepsilon_y$ and radial displacement Δu_r of the crown plotted along the alignment of reach 1 and 2, including information about the actual geology, the support measures applied and the monitoring setup

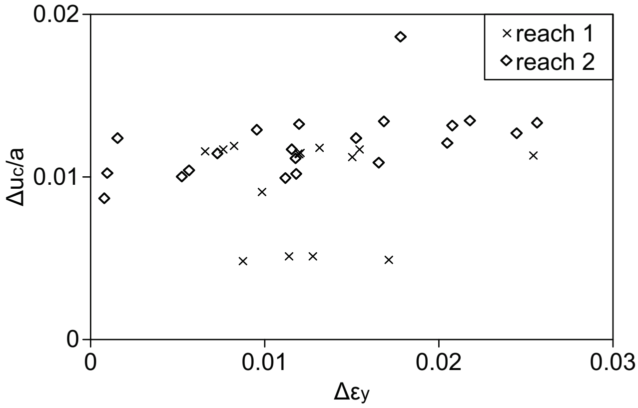

Fig. 26 Normalized displacement of the tunnel crown $\Delta u_c/a$ at the tunnel crown as a function of the axial strain $\Delta\varepsilon_y$ for reaches 1 and 2

vances mentioned above. For this reason, Figure 26 cannot be compared directly to the similar diagrams of Section 4, which consider the total deformations. A qualitative comparison is nevertheless possible. The relationship between the extrusions and the convergences is similar to the relationship between the numerical results for a yielding support shown in Figure 12 and for the stiff support shown in Figure 13, where the convergences do not vary significantly compared to the extrusions. This behaviour seems reasonable because the support system applied is a yielding support, which is set rigidly at a distance of about 30 m (e/a = 5) behind the face. Furthermore, the big variation in the extrusions indicates that the effect of the time-dependency of the ground and of the face support is of subordinate importance in the present case history (cf. Figures 14 and 15). For a ground viscosity η between 10^4 and 10^5 kPa*day, an advance rate of v = 1 m/day and an initial stress of p_0 = 20 MPa the normalized viscosity $\eta v/(ap_0)$ is between 0.08 and 0.8. According to Figure 15, such viscosities influence the extrusions only slightly.

6 Conclusions

The extrusion of the core is affected by ground quality, the initial stress state and the construction method. Stiff supports which are installed close to the face reduce the magnitude of the extrusions, as do yielding supports to a lesser extent. Face reinforcement also reduces the magnitude of extrusions. However, the effect of yielding supports and face support on extrusion is less pronounced in deep tunnels.

It is theoretically possible to predict ground response when the ground exhibits only a moderately time-dependent behaviour. The time-independent numerical analysis of tunnelling into a fault zone showed that the convergences can be estimated by means of extrusion measurements.

Pronounced time-dependent ground behaviour makes it very difficult to predict the ground response, because the extrusions are governed by short-term behaviour, while the final ground response is characterised by long-term behaviour. A large extrusion represents a sufficient, but not a necessary, condition for large convergences to occur.

The analysis of the extrusions by means of the axial strains instead of the axial displacements makes it possible to use a longer portion of the measuring device, because the error introduced by a non-fixed reference point can be avoided. It is possible to use an even longer portion of the measuring device if the increase in strains due to the specific face advance is analysed. Such an analysis is also independent of the deformations which the ground experiences before the installation of the measuring device.

The case history of the Gotthard Base Tunnel shows that there is only a weak correlation between the axial extrusions and the convergences of the tunnel.

Acknowledgments

The authors wish to thank the AlpTransit Gotthard AG, Switzerland for the high quality data provided from the tunnel advance of the Sedrun Lot and for the permission to use the data for this research. The authors also wish to thank to Mariacristina Bonini (Politecnico di Torino) for the supplementary information concerning the Raticosa tunnel.

References

Anagnostou, G. 2007a. Continuous tunnel excavation in a poro-elastoplastic medium. In: Pande, Pietruszczak (eds) Numerical Models in Geomechanics (NUMOG X), Rhodes, Greece, pp 183-188

Anagnostou, G. 2007b. Practical Consequences of the Time-Dependency of Ground Behavior for Tunneling. In: Traylor MT, Townsend JW (eds) Rapid Excavation and Tunneling Conference, Toronto, pp 255-265

Anagnostou, G., Kovári, K. 1993. Significant parameters in elastoplastic analysis of underground openings. Journal of Geotechnical Engineering 119 (3):401-418

Anagnostou, G., Kovári, K. 2005. Tunnelling through geological fault zones. In: International symposium on design, construction and operation of long tunnels, Taipei, pp 509-520

Anagnostou, G., Pimentel, E., Cantieni, L. 2008. Report on behalf of AlpTransit AG: Felsmechanische Laborversuche Los 378 - Schlussbericht - AlpTransit Gotthard Basistunnel, Teilabschnitt Sedrun. ETH Zurich, Institute for Geotechnical Engineering, Chair of Underground Construction, Zurich, Switzerland

Barla, G. 2005. Large size tunnels excavated full face in difficult conditions. In: Löw (ed) Geologie und Geotechnik der Basistunnels am Gotthard und am Lötschberg, Zurich, pp 275-286

Barla, G. 2009. Oral Communication 7th Mai 2009. Zürich

Barla, G., Barla, M. 2004. Discussion on the full face method. Felsbau 22 (4):26-30

Barla, G., Barla, M., Bonini, M. 2004. Characterisation of Italian Clay Shales for Tunnel Design. Int J Rock Mech Min Sci 41 (3):CD-ROM - Proceedings of SINOROCK2004 Symposium

Bernaud, D. 1991. Tunnels profonds dans les milieux viscoplastiques: approches expérimentale et numérique. PhD Thesis, Ecole Nationale des Ponts et Chaussées, Paris, France

Bernaud, D., Maghous, S., Buhan, P.D., Couto, E. 2009. A numerical approach for design of bolt-supported tunnels regarded as homogenized structures. Tunnelling and Underground Space Technology 24:533-546

Boldini, D., Graziani, A., Ribacchi, R. 2004. Raticosa Tunnel, Italy: Characterization of Tectonized Clay-Shale and Analysis of Monitoring Data and Face Stability. Soils and Foundations 44 (1):57-69

Bonini, M. 2003. Mechanical behaviour of Clay-Shales (Argille Scagliose) and implications on the design of tunnels. Ph.D. Thesis, Politecnico di Torino, Torino, Italy

Bonini, M., Debernardi, D., Barla, M., Barla, G. 2009. The Mechanical Behaviour of Clay Shales and Implications on the Design of Tunnels. Rock Mechanics and Rock Engineering 42 (2):361-388. doi:10.1007/s00603-007-0147-6

Cantieni, L., Anagnostou, G. 2007. On the variability of squeezing in tunneling. In: Ribeiro e Sousa L, Olalla C, Grossmann NF (eds) 11th Congress of the International Society for Rock Mechanics, Lisbon, pp 983-986

Cantieni, L., Anagnostou, G. 2009a. The effect of the stress path on squeezing behaviour in tunnelling. Rock Mechanics and Rock Engineering 42 (2):289–318. doi:10.1007/s00603-008-0018-9

Cantieni, L., Anagnostou, G. 2009b. The interaction between yielding supports and squeezing ground. Tunneling and Underground Space Technology 24 (3):309-322. doi:10.1016/j.tust.2008.10.001

Cantieni, L., Anagnostou, G. 2011. On a Paradox of Elasto-Plastic Tunnel Analysis. Rock Mechanics and Rock Engineering 44:129-147. doi:10.1007/s00603-010-0126-1

Cosciotti, L., Fazio, A.L., Boldini, D., Graziani, A. 2001. Simplified behavior models of tunnel faces supported by shotcrete and bolts. In: al Ae (ed) Modern Tunneling Science and Technology, pp 407-412

De Biase, A., Grandori, R., Bertola, P., Scialpi, M. 2009. Gibe II Tunnel Project - Ethiopia: 40 Bars of Mud Acting on the TBM “Special Designs and Measures Implemented to Face One of the Most Difficult Events in the History of Tunneling”. In: Almeraris G, Mariucci B (eds) Rapid Excavation and Tunneling Conference, Las Vegas, Nevada, pp 151–170

Dias, D., Kastner, R. 2005. Modélisation numérique de l'apport du renforcement par boulannage du front de taille des tunnels. Can Geotech J 45:1656-1674. doi:10.1139/T05-086

Eclaircy-Caudron, S., Dias, D., Kastner, R. 2009. Displacements and stresses induced by a tunnel excavation: Case of Bois de Peu (France). In: Ng HL (ed) Geotechnical Aspects of Underground Construction in Soft Ground, Shanghai, China, pp 373-379

Egger, P. 1980. Deformation at the face of the heading and determination of the cohesion of the rock mass. Underground Space 4:313-318

Ehrbar, H., Pfenninger, I. 1999. Umsetzung der Geologie in technische Massnahmen im Tavetscher Zwischenmassiv Nord. In: Vorerkundung und Prognose der Basistunnels am Gotthard und am Lötschberg, Symposium Geologie Alptransit, Zurich, Switzerland, pp 381-394

Ghaboussi, J., Gioda, G. 1977. On the Time-Dependent Effects in Advancing Tunnels. International Journal for Numerical and Analytical Methods in Geomechanics 1:249-269

Hoek, E. 2001. Big Tunnels in Bad Rock. Journal of Geotechnical and Geoenvironmental Engineering 127 (9):726-740

Jeon, J.S., Martin, C.D., Chan, D.H., Kim, J.S. 2004. Predicting ground conditions ahead of the tunnel face by vector orientation analysis. Tunnelling and Underground Space Technology 20:344-355

Kovári, K. 1998. Tunnelling in Squeezing Rock. Tunnel 5:12-31

Kovári, K. 2009. Design Methods with Yielding Support in Squeezing and Swelling Rocks. In: World Tunnel Congress, Budapest, Hungary

Kovári, K., Amstad, C., Koppel, H. 1979. New Developments in the Instrumentation of Underground Openings. In: Proc. of the 4th Rapid Excavation and Tunnelling Conference, Atlanta, USA

Kovári, K., Anagnostou, G. 1995. The ground response curve in tunnelling through short fault zones. In: Fujii T (ed) 8th Congress of the International Society for Rock Mechanics, Tokyo, pp 611-614

Kovári, K., Ehrbar, H. 2008. Gotthard Basistunnel, Teilabschnitt Sedrun - Die druckhaften Strecken im TZM Nord: Projektierung und Realisierung. In: Swiss Tunnel Congress, Luzern, pp 39-47

Kovári, K., Ehrbar, H., Theiler, A. 2006. Druckhafte Strecken im TZM Nord: Projekt und bisherige Erfahrungen. In: Löw (ed) Geologie und Geotechnik der Basistunnels, Zürich, pp 239-252

Kovári, K., Lunardi, P. 2000. On the Observational Method in Tunneling. In: GeoEng2000, Melbourne

Lee, K.M., Rowe, R.K. 1990. Finite Element Modelling of the Three-Dimensional Ground Deformations due to Tunnelling in Soft Cohesive Soils: Part 2 - Results. Computers and Geotechnics 10:111-138

Lunardi, G., Gatti, M. 2010. Tunnel Monitoring System – A Contribution for the Preparation of Guidelines. In: ITA-AITES World Tunnel Congress 2010 - Tunnel Vision Towards 2020, Vancouver, Canada

Lunardi, P. 1995. L'importanza del precontenimento del cavo in relazione ai nuovi orientamenti in tema di progetto e costruzione di gallerie. Gallerie e Grandi Opere Sotterranee Marzo (45):16-37

Lunardi, P. 1998. The influence of the rigidity of the advance core on the safety of the tunnel excavations. Tunnel 8:32-44

Lunardi, P. 1999. La galleria "Tartaiguille", ovvero l'applicazione dell'approccio ADECO-RS per la realizzazione di un tunnel "impossibile". Gallerie e Grandi Opere Sotterranee 58 (agosto 1999):65-77

Lunardi, P. 2000. The design and construction of tunnels using the approach based on the analysis of controlled deformation in rocks and solis. Tunnels & Tunnelling International *special supplement, ADECO-RS approach* (May)

Lunardi, P. 2008. Design and construction of tunnels: analysis of controlled deformation in rocks and soils (ADECO-RS). Springer, Berlin Heidelberg. doi:10.1007/978-3-540-73875-6

Lunardi, P., Bindi, R. 2004. The Evolution of Reinforcement of the Advance Core Using Fibre-Glass Elements. Felsbau 22 (4):8-19

Lunardi, P., Cassani, G., Tanzini, M. 2009. Lo scavo di gallerie di grandi dimensioni nei terreni a grana fine e strutturalmente complessi. Gallerie e Grandi Opere Sotterranee 92 (dicembre):47-60

Lunardi, P., Focaracci, A. 1997. Aspetti Progettuali e construttivi della galleria "Vasto". Strade & Construzioni (Agosto 97):72-88

Lunardi, P., Focaracci, A. 1999. The Bologna to Florence high speed railwa line: Progress of underground. In: al. Ae (ed) Challenges for the 21st Century, Oslo, Norway

Madejski, J. 1960. Theory of non-stationary plasticity explained on the example of thick-walled spherical reservoir loaded with internal pressure. Archiwum Mechaniki Stosowanej 5/6 (12):775-787

Mair, R.J. 2008. Tunnelling and geotechnics: new horizons. Géotechnique 58 (9):695-736. doi:10.1680/geot.2008.58.9.695

Myer, L.R., Brekke, T.L., Dare, C.T., Dill, R.B., Korbin, G.E. 1981. An Investigation of Stand-up Time of Tunnels in Squeezing Ground. In: Rapid Excavation and Tunnelling Conference, San Francisco, California, pp 1415-1433

Nguyen-Minh, D., Corbetta, F. 1991. New calculation methods for lined tunnels including the effect of the front face. In: 7th Congress of the ISRM, Achen, pp 1334-1338

Oreste, P., Peila, D., Pelizza, S. 2004. Face Reinforcement in Deep Tunnels. Felsbau 22 (4):20-25

Panet, M. 1995. Le calcul des tunnels par la méthode convergence-confinement. Presses de l'école nationale des ponts et chaussées, Paris, France

Panet, M. 2009. Ground behaviour at the tunnel face. In: The evolution of design and construction approaches in the field of underground projects - Rocksoil S.p.A. 30th anniversary conference, Milan

Paulus, M. 1998. Le tunnel de Tartaiguille. Travaux 742 (May)

Peila, D. 1994. A theoretical study of reinforcement influence on the stability of a tunnel face. Geotechnical and Geological Engineering 12:145-168

Pellet, F., Roosefid, M., Deleruyelle, F. 2009. On the 3D numerical modelling of the time-dependent development of the damage zone around underground galleries during and after excavation. Tunnelling and Underground Space Technology 24 (2009):665-674

Perzyna, P. 1966. Fundamental Problems in Viscoplasticity. *Advances in Applied Mechanics* 9:243-377

Ramoni, M., Anagnostou, G. 2010. Tunnel boring machines under squeezing conditions. Tunnelling and Underground Space Technology 25:139–157

Rossi, P.P. 1995. Il ruolo del monitoraggio negli interventi di miglioramento e rinforzo dei terreni e delle rocce. In: XIX Conegno Nazionale dell’Associazione Geotechnica Italiana, Pavia, Italy

Russo, G., Repetto, L., Piraud, J., Laviguerie, R. 2009. Back-analysis of the extreme squeezing conditions in the exploratory aid to the Lyon-Turin base tunnel. In: Rock Engineering in Difficult Conditions, Toronto , ON, Canada

Schneider, T.R. 1997. Behandlung der Störzonen beim Projekt des Gotthard Basistunnels. Felsbau 15 (6):489-495

Sellner, P. 2000. Prediction of Displacements in Tunnelling. Ph.D. thesis, University of Technology, Graz, Austria

Steindorfer, A. 1998. Short term Prediction of Rock Mass Behaviour in Tunnelling by advanced analysis of displacement monitoring data. Gruppe Geotechnik Graz, Riedmüller, Schubert, Semprich (eds), Heft 1. Graz, Austria

Steiner, P. 2007. Displacement measurements ahead of a tunnel face using the RH Extensometer. In: FMGM 2007: Seventh International Symposium on Field Measurements in Geomechanics

Steiner, P., Yeatman, R. 2009. New instruments improve site characterization with time based measurements. In: Vrkljan (ed) EUROCK 2009 - Rock Engineering in Difficult Ground Conditions - Soft Rocks and Karst, Dubrovnik, pp 577-582

Sulem, J., Panet, M., Guenot, A. 1987. Closure analysis in deep tunnels. International Journal for Rock Mechanics and Mining Science 24 (3):145-154

Thut, A., Nateropp, D., Steiner, P., Stolz, M. 2006. Tunnelling in Squeezing Rock - Yielding Elements and Face Control. In: 8th Int. Conference on Tunnel Construction and Underground Structures, Ljubljana

Trompille, V. 2003. Etude expérimentale et théorique du comportement d'un tunnel renforcé par boulonnage frontal. PhD Thesis, Ecole National des Travaux Publics de l'Etat, Lyon, France

Vermeer, P.A., de Borst, R. 1984. Non-associated Plasticity for Soils, Concrete and Rock. Heron 29 (3):1-64

Vogelhuber, M. 2007. Der Einfluss des Porenwasserdrucks auf das mechanische Verhalten kakiritisierter Gesteine. PhD Thesis, ETH Zurich, Zurich, Switzerland

Wong, H., Subrin, D., Dias, D. 2000a. Extrusion movements of a tunnel head reinforced by finite length bolts - a closed-form solution using homogenization approach. International Journal for Numerical and Analytical Methods in Geomechanics 24:533-565

Wong, H., Trompille, V. 2000. Displacement Behaviour of a Bold-Reinforcement Tunnel Face with Finite Ground-Bolt Bond Strength: Analytical and Numerical Approaches, In Situ Data. In: GeoEng 2000, Melbourne

Wong, H., Trompille, V., Dias, D. 2004. Extrusion analysis of a bolt-reinforced tunnel face with finite ground-bold bond strength. Can Geotech J 41:326-341. doi:10.1139/T03-084

Wong, H., Trompille, V., Subrin, D. 2000b. Tunnel face reinforcement by longitudinal bolts: Analytical model and in situ data. In: Miyazaki F (ed) Geotechnical Aspects of Underground Construction in Soft Ground, Kusakabe, pp 457-463

CONCLUSIONS AND OUTLOOK

Conclusions and Outlook

Three-dimensional and axially symmetric computational models produce more reliable results than plane strain models which take account only of a cross section of the tunnel. The use of plane strain models is essential, however, because they allow a rapid assessment to be made of the ground behaviour with the little information available in the preliminary design stages and, of course, also because they are less costly. However, when using such models one should always be aware of their inherent limitations.

Part I of the thesis showed that, in the case of elasto-plastic material behaviour, an axisymmetric model that takes into account the sequence of excavation and lining installation will always lead to ground response points above the plane strain ground response. This is due to the inability of the plane strain model to map the radial stress reversal that follows the installation of the lining. The convergence–confinement method, even in combination with advanced methods of pre-deformation estimation, underestimates the ground pressure and deformation, particularly for stiff linings, long unsupported spans, and heavily squeezing ground with highly non-linear material behaviour. The inherent weakness of any plane strain analysis is that it cannot reproduce at one and the same time both the deformations and the pressures. This is relevant from the design standpoint, particularly for heavily squeezing conditions that require a yielding support in combination with an over-excavation: in this case, one needs reliable estimates of the deformations that must occur in order for the squeezing pressure to be reduced to a pre-defined, technically manageable level. In cases where the question of deformation is of secondary importance, however, a plane strain analysis in combination with an implicit method of pre-deformation estimation will suffice. For support completion close to the face, the differences in the ground pressures obtained by the different methods of analysis are not important from a practical point of view.

Part II investigated an important practical consequence of the Part I results. Part II showed that an analysis of the interaction between ground and yielding support that takes into account the stress history of the ground leads to conclusions which are qualitatively different from those obtained through plane strain analysis. The ground pressure developing far behind the tunnel face in a heavily squeezing ground depends considerably on the amount of support resistance during the yielding phase. The higher the yield pressure of the support, the lower will be the final load. A targeted reduction in ground pressure can be achieved not only by installing a support that is able to accommodate a larger deformation (which is a well-known principle), but also through selecting a support that yields at a higher pressure. Furthermore, a high yield pressure reduces the risk of a violation of the clearance profile and increases safety levels in terms of roof instabilities (loosening) during the deformation phase.

These results are important from the standpoint of conceptual design, even if the range of potential project conditions, design criteria and technological constraints does not allow us to make generalizations about structural solutions for dealing with squeezing ground. Some basic design issues are illustrated through the use of practical examples. Additionally, the nomograms presented in Part II contribute to the decision-making process, as they make it possible to produce a quick assessment of different supports and of their sensitivity with respect to variations in geology.

Part III investigated a paradox of elasto-plastic tunnel analysis. The computational models commonly used for tunnel design predict that under certain conditions (i.e. support from a stiff lining near to the tunnel face, weak ground, high initial stress) the load developing upon the lining will increase with the strength of the ground. Such behaviour deserves to be called a paradox because it is clearly contrary to what one would expect on the basis both of intuition and tunnelling experience. The reason for this counter-intuitive behaviour is the stress relief which takes place in the ground ahead of the face and which is more pronounced in the case of a low strength ground. The decisive simplifying modelling assumptions, i.e. the assumptions which cause the difference between model behaviour and actual behaviour, are related: (i), to the rheological behaviour of the ground (which is usually neglected in design computations, but is particularly important in the case of overstressed ground, limiting the extent of stress relief ahead of the face); and, (ii), to the stiffness of the support system, which may - due to the nature of the construction procedures - be considerably lower than it is assumed to be in the design calculations. By taking into account the two main effects mentioned above in the design computations, it is possible to eliminate the paradoxical model behaviour.

Part IV showed that the frequently observed phenomenon of squeezing variability can be traced back to heterogeneities of the ground on different scales and with respect both to its mechanical and to its hydraulic characteristics. In the case of a heterogeneous ground structure, the results of numerical calculations indicate that even relatively thin competent rock interlayers may have a pronounced stabilizing effect.

Part V showed that the extrusions of the core ahead of the tunnel face are affected by ground quality, the initial stress state and also by the construction method. Stiff supports, which are installed close to the face, and to a lesser extent also yielding supports, reduce the magnitude of the extrusions. Face reinforcement also reduces the magnitude of extrusions. However, the effect of yielding supports and face supports on the extrusion is limited in deep tunnels. A prediction of the ground response is theoretically possible in ground with a moderate time-dependent behaviour. The time-independent numerical analysis of tunnelling into a fault zone showed that the convergences can be estimated by means of the extrusion measurements. Pronounced time-dependent ground behaviour makes it very difficult to predict the ground response, however, because the extrusions are governed by the short-term behaviour, while the final ground response is characterised by the long-term behaviour. One can say that large extrusions represent a sufficient, but not necessary condition for large convergences of the profile. The analysis of the extrusions by means of the axial strains instead of the axial deformations allows us to use a longer portion of the measuring line, because the error introduced by the displacement of the reference point can be avoided. An even longer portion of the measuring device may be used if the increase in strains due to a specific face advance is analysed. Such an analysis is additionally independent of the deformations which the ground experiences before the installation of the measuring device. It is shown by means of case histories that there is a weak correlation between the axial extrusions and the convergences of the tunnel.

The findings of the present thesis illustrate the uncertainties (both quantitative and qualitative) that exist in all computational models - even in the very familiar and well established ones - and emphasize the importance of a careful interpretation of the computational results and of a critical review of the underlying modelling assumptions. The scientific discussion initiated by Li (2009) and the response by Cantieni and Anagnostou (2009) highlighted the importance of the findings of the present thesis, because it showed that the notion of a ground response curve and the method of characteristic lines are deeply entrenched in conceptual thinking and that the differences between the plane strain model and the spatial models are not fully understood either in engineering practice or in the theoretical field.

There are still a number of open questions concerning ground response in squeezing ground which merit further investigation.

The first group of open questions concerns the constitutive models of the ground. Most of the numerical analyses of the thesis have been made with the assumption of a linearly elastic, perfectly plastic constitutive model. This assumption may oversimplify the constitutive behaviour of some squeezing rocks but it is, however, the most common model used in engineering practice. Vogelhuber (2007) showed, for instance, that the mechanical behaviour under triaxial testing conditions of the rocks encountered in the squeezing section of the Sedrun Lot of the Gotthard Base Tunnel corresponds well with a linearly elastic and perfectly plastic behaviour. On the other hand, the triaxial tests performed with samples from the planed Gibraltar tunnel area show a completely different behaviour (cf. Anagnostou 2008 and Anagnostou *et al.* 2010c). The determination of advanced constitutive models for such rocks is currently under investigation at the ETH Zurich, as well as the examination of basic aspects of the ground response to tunnelling when incorporating advanced constitutive models.

The time-dependency of ground behaviour was handled by using an elasto-viscoplastic constitutive model. The next step is to investigate either the effect of consolidation or the effect of consolidation in combination with creep in order to understand their effect on the deformations and stresses in the vicinity of the face and on the final equilibrium reached far behind the face. Investigations in this field have been carried out by Ramoni and Anagnostou (2010) with respect to the effect of consolidation on TBM shield loading.

Squeezing ground is associated with large displacements and strains. The Cauchy small strain assumption, which is normally used in the finite element method, is not valid for such high strains (>10%). An investigation into the effects of large strain approaches on the ground response by means of spatial computations would help to improve our knowledge of the interaction between supports and squeezing ground.

A further open question concerns the constitutive model of the shotcrete. The shotcrete applied in squeezing ground experiences high deformations before reaching its final strength. The response of young shotcrete to a high strain rate and the effect of such a loading on the final properties of the shotcrete merit an in-depth experimental investigation.

Another important open question concerns the face stability of deep tunnels. The mechanism behind face instability in deep tunnels is still not well understood. A failure mechanism which reaches the ground surface (often used in shallow tunnels) seems not to be appropriate for deep tunnels. The investigation of face stability by means of second order mechanisms seems to be a more appropriate approach. Also, the time-dependency of face stability (often defined by the so-called "stand-up time") requires an in-depth investigation for both creeping ground and low-permeability water-bearing ground. Initial investigations into face stability in water-bearing ground, with an emphasis on the effects of advance drainage, have been carried out within the framework of the assessments for the Lake Mead No 3 intake tunnel in Nevada, USA (Anagnostou *et al.* 2010a and

2010b). Further investigations are in progress at the ETH Zurich into the static effects, feasibility and execution of drainage in tunnelling.

References

Anagnostou, G. 2009. Some rock mechanics aspects of subaqueous tunnels. Keynote Lecture EUROCK 2009 - Rock Engineering in Difficult Ground Conditions and Karst, Dubrovnik, Croatia

Anagnostou, G., Cantieni, L., Nicola, A., Ramoni, M. 2010a. Face stability assessment for the Lake Mead No 3 Intake Tunnel. Tunnel vision towards 2020, ITA World Tunnel Congress 2010, Vancouver, Canada

Anagnostou, G., Cantieni, L., Nicola, A., Ramoni, M. 2010b. Lake Mead No 3 Intake Tunnel – Geotechnical aspects of TBM operation. Tunnelling: Sustainable Infrastructure, North American Tunnelling Conference, Portland, pp 125-135

Anagnostou, G., Pimentel, E., Cantieni, L. 2010c. Report on behalf of SECEG SA, Madrid, Spain and SNED, Rabat, Morocco: Gibraltar strait fixed link - Tunnel project: Experimental investigations on the strength and deformability of Breccia material - Report Nr. 7. ETH Zurich, Institute for Geotechnical Engineering, Chair of Underground Construction, Zurich, Switzerland

Cantieni, L., Anagnostou, G. 2009. Response by the Authors to C.C. Li’s discussion of the paper "The interaction between yielding supports and squeezing ground” by L. Cantieni and G. Anagnostou [Tunnelling and Underground Space Technology 24 (2009) 309–322]. Tunnelling and Underground Space Technology 24 (6):741–743

Li, C.C. 2009. Discussion of the paper ‘‘The interaction between yielding supports and squeezing ground” by L. Cantieni and G. Anagnostou [Tunnelling and Underground Space Technology 24 (2009) 309–322]. Tunnelling and Underground Space Technology. 24 (6): 739-740

Ramoni, M., Anagnostou, G. 2009. The Effect of Consolidation on TBM Shield Loading in Water-Bearing Squeezing Ground. Rock Mechanics and Rock Engineering. 44(1): 63-83

Vogelhuber, M. 2007. Der Einfluss des Porenwasserdrucks auf das mechanische Verhalten kakiritisierter Gesteine. PhD Thesis, ETH Zurich, Switzerland

Curriculum Vitae

Personal data

First name	Linard
Family name	Cantieni
Date of birth	10.05.1979
Place of birth	Chur, Switzerland
Citizen of	Donat, Switzerland
Nationality	Swiss

Education

2005–2011	Ph.D. thesis at the ETH Zurich, Switzerland under the supervision of Prof. Dr. G. Anagnostou
2005	Diploma in civil engineering (equivalent with MSc)
1999–2005	Study of civil engineering at the ETH Zurich, Switzerland
1999	High School Diploma
1995–1999	High School at the EMS Schiers, Switzerland

Work experience

Since 2005	Research assistant at the ETH Zurich (activities: research, consulting, teaching)